Copper - Gold Exploration in the Middleback Ranges; Source(s) of Fluids and Metals.

Thesis submitted by

Ben Cave BSc. (UofA)

October, 25th 2010.

In partial fulfilment of the requirements for the degree of Bachelor of Science with Honours in the Centre for Tectonics, Resources and Exploration, Department of Geology and Geosciences, School of Earth and Environmental Sciences, University of Adelaide, South Australia.

ben.cave@student.adelaide.edu.au

TABLE OF CONTENTS

ABSTRACT

The Moola Prospect of the Middleback Ranges, South Australia is an epigenetic, hypothermal copper-gold prospect that displays several clear genetic affinities with IOCG deposits/prospects in the Gawler Craton, although from this study alone classification of the mineralisation is imprudent. A broad study on the mineral paragenesis and geochemistry of the deposit was carried out on a single drill core provided by OneSteel, the holder of the tenement encompassing the Moola Prospect. The mineralisation, characterised by pyrite + chalcopyrite, hematite and magnetite, is hosted by the Palaeoproterozoic metavolcanic / volcaniclastic, Myola Volcanics and an unnamed, undated fine-grained microgranite that intrudes the Myola Volcanics. This unnamed, undated microgranite, displays geochemical and petrological similarities with the Myola Volcanics from which it's thought to be partial derived from its anatexis; likely being a Wertigo Granite equivalent. Four alteration assemblages were observed in the Moola Prospect drill core and placed into the following paragenic sequence; Na (Ca-Fe) characterised by the formation of albite; sericite replacing K-feldspar and plagioclase and alteration increasing towards sericite veining; chlorite with alteration increasing towards chlorite-mica±epidote veins; late stage quartz, quartz-carbonate, carbonate flooding, that hosts mineralisation. Ore mineral paragenesis occurs in an overlapping sequence; the first mineral precipitated was magnetite that was later extensively martitised, with hematite followed by pyrite and minor heamatite + pyrite, pyrite + chalcopyrite, then chalcopyrite. Later supergene alteration altered the chalcopyrite to native copper and malachite. Sphalerite precipitation couldn't be constrained from petrological evidence alone. Iron oxide and sulphide chemistry, and sulphur isotopes from the sulphides support this paragenesis, and constrains precipitation of sphalerite between the pyrite only and chalcopyrite only phases. Iron oxide chemistry also revealed the presence of illmentite in the core, however could only constrain illmentite precipitation as, coeval to after haematite precipitation. Sulphur isotopes revealed evidence for an additional late stage pyrite precipitation, after the chalcopyrite only phase. Bulk rock composition was quite variable with some altered samples showing strong enrichments of Fe_2O_3, SiO_2, CaO, K_2O, Na_2O SO_3, MnO, P_2O_5 and MgO. Strong enrichment of CaO and/or SiO_2 in some of the altered samples, but not others, suggests that the quartz-carbonate alteration represented by this geochemical signature is sporadic in nature. Depletion in SiO_2 in some of the altered samples could also represent the consumption of silica during the Na-Ca-Fe alteration event. Enrichment of SO_3 in the altered samples likely directly represents alteration related to the precipitation of sulphide ore minerals. Trace element and rare earth element compositional changes from alteration shows enrichments of Cu, U, Pb, Li, B, Mn and V likely relating to alteration associated with mineralisation. εNd (1590Ma) values of the Moola Prospect together with εNd (1590Ma) versus whole rock Cu concentration and Co: Ni ratios of pyrite, indicates a crustal derived, with minor mantle input for the sources of metals. Sulphur isotopes and trace element whole rock geochemistry indicates a primitive/ magmatic fluid source is responsible for alteration and/ or mineralisation.

1. INTRODUCTION

The Moola Prospect is located on the northeastern edge of the Eyre Peninsula, approximately 60 kilometers southwest of Whyalla, South Australia, within the historic Iron Ore mining district the Middleback Ranges (Figs. 1, 2). The Middleback Ranges consist of Palaeoproterozoic rocks interleaved with mid to late Archaean basement which is overlain or intruded by Mesoproterozoic rocks. This region has been the focus of recent exploration drilling by OneSteel targeting iron oxide-copper-gold (IOCG) style mineralisation in their Middleback tenements.

The Middleback area contains several major crustal scale structures running approximately north south, thought to be splays of the Kalanjala Shear Zone (KSZ). These structures are associated with small historical workings of the Cu-Bi Murninnie Mine and several small Cu-Au prospects in the region. The Moola Prospect mineralisation is hosted within a sequence of volcanics, thought to be the Palaeoproterozoic Myola Volcanics. The Myola Volcanics has very limited previous work published on them, in regards to geochemistry, alteration within the region, isotopic signatures.

No information is available on the nature and paragenesis of the mineralisation and sources of fluids and metals at the Moola Prospect. The relationship to other deposits in the broader region is also unknown, with the Moonta-Wallaroo Cu-Au mines and the large IOCGs of the northeastern Gawler Craton possibly having genetic affinities to the Moola Prospect. There is considerable scope to investigate these properties and compare this prospect to known IOCG mineralisation in the Gawler Craton, to assess the nature of the deposit and fertility of the region for IOCG mineralisation.

Since the discovery of the world class Olympic Dam deposit in 1975 and subsequent classification of it as a new class of deposit; termed iron oxide-copper-gold (IOCG), IOCG deposits have been a major focus for exploration in many regions of the world including the Gawler Craton due to the promising size and grades of larger deposits.

The IOCG group of deposits, were initially defined following the discovery of the Olympic Dam deposit, and have since been used to describe a broad range of deposit styles with many authors (Williams *et al.* 2005; Groves *et al.* 2010) arguing that the term IOCG has been used to liberally to include several low Ti iron oxide-associated deposits i.e. iron oxide (P-rich), iron oxide (F- and REE- rich), Fe or Cu-Au skarn, high-grade iron oxide Au ± Cu, carbonate-hosted (Cu-, REE, and F-rich), and IOCG sensu stricto deposits (Groves *et al.* 2010).

Iron oxide copper gold deposits of the Gawler Craton are characterised by their extensive polymetallic enrichment consisting primarily of Cu, Au, Ag, U and REE, which are hosted within hydrothermal breccias, vein stockworks, and disseminations under strong structural control (Hitzman 2000; Hitzman & Valenta 2005; Corriveau 2006). Extensive hydrothermal alteration halo's, associated with this style of mineralisation consists of focussed potassic, hydrolytic and iron oxide alteration with a larger regional sodic-calcic footprint (Skirrow *et al.* 2002; Barton & Johnson 2004). The Gawler Craton IOCG deposits are commonly, spatially and temporally associated with the Mesoproterozoic Hiltaba Suite granitoids, which is an extensive series of granitoids that is often cited as the source of metals and fluids in proximal deposits (Ferris *et al.* 2002; Pollard 2006; Cerlienco 2009). The ore bearing fluids of IOCG deposits are generally highly saline, being of meteoric, metamorphic or magmatic origin (Barton & Johnson 2004). The host rock is variable, and is not a defining characteristic of these deposits, although it does determine in part the chemistry and mineralogy produced by hydrothermal activity (Hitzman *et al.* 1992). Numerous models for tectonic setting are proposed for this broad class of deposit (Hitzman 2000; Skirrow 2008).

The Gawler Craton has been the focus of exploration for IOCG style mineralisation in South Australia since the discovery of the world-class Olympic Dam deposit. This has led to the discovery of the Prominent Hill deposit, as well as many prospective and sub economic IOCG occurrences throughout the Olympic Cu-Au province including Oak Dam, Emmie Bluff, Carrapateena, Acropolis, Hillside and Punt Hill prospects (Bastrakov *et al.* 2007; Cerlienco 2009). These discoveries, have led to an increased interest in targeted IOCG exploration along the eastern edge of the Gawler Craton known as the Olympic Cu-Au province.

Several historic small, high-grade copper mines and prospects occur around the Middleback area. This coupled with large favourable structures and the presences of Hiltaba suite granitoids has led to the initial stages of IOCG exploration by OneSteel Ltd in their Middleback tenements. Previous base metals exploration programs (including IOCG style mineralisation) have been conducted in the region by several mining companies.

1.2 Geological Setting

The OneSteel Moola Cu-Au Prospect is located on the eastern edge of the Gawler Craton, which has experienced several phases of continental rifting and collisions since the late Achaean (2560-2500Ma) (Hand *et al*. 2007). The Gawler Craton can be subdivided into a number of tectonic sub-domains on the basis of structure and tectono-stratigraphic history (Hand *et al*. 2007). With the Moola Prospect lying within the Olympic Cu-Au province, which includes part of the Olympic Domain (Fig. 3), as well as part of the Mt Woods Inlier, Cleve Domain, Spencer Domain and Gawler Range Volcanics Domain (Skirrow *et al*. 2002). Within these provinces are two operating mines of IOCG deposits, the world class Olympic Dam deposit and the Prominent Hill deposit, along with a several other prospective IOCG occurrences including Wirrda Well, Oak Dam, Emmie Bluff, Carrapateena, Acropolis, Hillside and Punt Hill deposits (Fairclough 2005; Bastrakov *et al.* 2007; Belperio *et al.* 2007; Cerlienco. 2009).

1.3 Project aims

This project was undertaken in cooperation with One Steel and was aimed at increasing the knowledge basis of both the local geology and the nature of copper ± gold mineralisation at the Moola Prospect, in particular the source(s) of fluid and metals associated with mineralisation and is based on a single diamond drill hole (ML001) completed by OneSteel in late November 2009.

This project was one of two projects on the mineralisation at the Moola Prospect with the other project (Jones 2010) aimed at determining the conditions of mineralisation/ alteration.

The fundamental issues to be addressed in this project were to classify the host rock type, alteration and nature of ore minerals, with an attempt on placing them into a paragenetic sequence. Additional investigations aimed to characterise possible sources for metals and fluids of the identified mineralisation and alteration. This information was used to compare the Moola Prospect mineralisation to other IOCG deposits and prospects within the Gawler Craton.

This was achieved by employing the following techniques:

- Radiogenic (Sm-Nd, Sr/Sr)
- Stable isotope (d34S)
- Whole rock geochemistry (major, trace and REE)
- Reflect and transmitted light microscopy
- Electron Probe Microanalysis (sulphides and oxides)

1.4 Topography and Vegetation

The Moola drill hole (ML001) was sunk into a relatively featureless red- brown plain dominated by Quaternary thin red-brown sand and clay soil veneers over locally exposed Ripon Calcrete, as well as fluviatile gravels, sands and clays of modern drainage channel sediments (Fig. 4). No outcrop of the host lithology was present at the site of the drill hole. The area is cut by a major paleochannel that drains from the Middleback Ranges eastwards towards the Spencer Gulf. Vegetation in the area was quite sparse, with bluebush and saltbush covering plains with local sheoak, myall and mallee.

1.5 Stratigraphy

1.5.1 MESOARCHAEAN

Prior to the work of Fraser *et al*. (2010) the oldest lithological units of the Gawler Craton were late Archaean to early Palaeoproterozoic in age, although some authors (Creaser & Fanning 1993; Daly & Fanning, 1993) inferred the existence of Mesoarchaean lithologies at depth in the Gawler Craton. Fraser *et al*. (2010) recently revealed an early Mesoarchaean age (≈3150Ma) for the Cooyerdoo Granite orthogneiss using U-Pb SHRIMP zircon ages and Sm-Nd isotopic techniques.

The Cooyerdoo Granite is located on the eastern side of the Middleback Ranges, south of Iron Knob and sporadically outcrops across a region of 20 km by 7km. Fraser *et al.* (2010) have used the granites' geophysical properties i.e. low magnetic and gravity signatures to suggest that the Mesoarchaean extends ≈30 km further south beneath the southern Middleback Range on the Middleback 1:100 000 map sheet and at a regional scale is enclosed by the significantly younger Middleback Subgroup banded iron formations and Myola Volcanics.

The relationship between the Cooyerdoo Granite and adjacent rocks is unclear, due to the rarity of exposed contacts as well as the lack of work completed on this unit. However Fraser *et al.* (2010) postulates that a highly weathered, schistose granite in sheared contact with iron rich and dolomitic members of the Middleback Subgroup may be a sheared equivalent of the Cooyerdoo although no geochronological work has been attempted on this unit.

1.5.2 MESOARCHAEAN- PALAEOPROTEROZOIC

Underlying the Palaeoproterozoic Hutchison Group metasediments of the Cleve Sub-domain on the southern Eyre Peninsula, are Archaean to very early Palaeoproterozoic gneissic basement units known as the Sleaford Complex and in the Cowell area by the Miltalie Gneiss (Thomson 1980; Parker *et al.* 1988). Equivalents of these units were thought to extend north- eastward of the Kalinjala Shear Zone (KSZ). However the identification of the Mesoarchaean Cooyerdoo granite by Fraser *et al.* (2010) further complicates this, as the relationship between the Hutchison Group metasediments and the Cooyerdoo granite is unclear, with Fraser speculating that the metasedimentary Middleback Subgroup (Hutchison Group) unconformably overlies the Mesoarchaean Cooyerdoo granite

The Sleaford Complex

The Sleaford Complex is a highly metamorphosed supracrustal sequence of paragneisses and orthogneisses, comprised of the Carnot Gneisses, Wangary Gneiss and the Dutton Suite which were deformed during the Sleaford Orogeny (ca. 2440 Ma), (Fanning *et al.* 1981; Daly & Fanning 1993; Curtis 2007).

The Carnot Gneisses comprises granulite facies paragneiss and orthogneiss. The paragneiss is dominated by finely layered garnet gneiss and lesser biotite - garnet gneiss, cordierite - garnet gneiss and leucogneiss, with the orthogneiss consisting of basic gneiss, augen gneiss and crosscutting pegmatites (Schwarz et al. 2005; Curtis 2007). The Wangary Gneiss is a massive to compositionally layered paragneiss and orthogneiss that has experiencing metamorphism to amphibolite facies (Parker *et al*. 1985; Schwarz 2003; Curtis 2007). The Dutton Suite is a suite of igneous rocks that were emplaced during the late stages of the Sleaford Orogeny, and includes the Coulta Granodiorite, Kiana Granite, Whidbey Granite and other undifferentiated granitoids (Daly & Fanning 1993; Schwarz 2003; Curtis 2007).

The Miltalie Gneiss

The Miltalie Gneiss is a migmatitic granitic medium to coarse-grained gneiss, which contains pegmatitic segregations and structurally concordant amphibolite sills or deformed dykes (Parker *et al.* 1993; Curtis 2007).

The Miltalie Gneiss structurally underlies the Warrow Quartzite (Hutchison Group) adjacent to the Plug Range and thus has been interpreted as underlying the Hutchison Group, and possibly intrudes the Sleaford Complex (Parker 1981; Parker & Lemon 1982; Curtis 2007).

1.5.3 PALAEOPROTEROZOIC

Middleback Subgroup

The Middleback Subgroup (Hutchison Group) of metasediments is composed of a mixed sequence of chemical and clastic sediments and outcrops in the low north-south trending Middleback Ranges. The Middleback Subgroup has been differentiated into a basal Warrow Quartzite, the Middleback Subgroup that comprises of the Katunga Dolomite, Lower Middleback Jaspilite, Cook Gap Schist and Upper Middleback Jaspilite, and the Yadnarie Schist (Parker & Lemon 1982).

The deposition of the Hutchison Group/ Middleback Subgroup is interpreted as to have taken place on a

passive continental margin, orientated approximately north–south; Parker & Lemon (1982) also suggest a deepening of the basin towards the east.

The overlying carbonate and BIF units are interpreted to represent a shallow marine to intertidal depositional environment with sediments dominated by chemical sediments with little or no clastic contribution (Parker 1983; Curtis 2007). Both the Cook Gap Schist and Yadnarie Schist are interpreted to represent a transgression from a shallow marine/ intertidal depositional environment into a deeper marine environment with an increased influx of clastic sediments.

It should be noted that the historical correlation between the iron rich chemical/ clastic metasediments of the Middleback Subgroup and the Hutchison Group i.e. Parker & Lemon (1982) has been recently been questioned (Szpunar *et al.* 2007; Barovich *et al.* 2008) and is currently being reviewed (Fraser *et al.* 2010).

Myola Volcanics

The Myola Volcanics are a sequence of deformed metamorphosed (upper greenschist – lower amphibolite facies (Parker *et al.* 1993)) felsic bimodal volcanics and fine-grained gneisses, outcropping east of the Middleback Ranges. U-Pb isotopic analysis of zircon grains from a rhyolite unit of the Myola Volcanics gives a crystallisation age of 1791±4 Ma (Fanning *et al.* 1988). The type section of the Myola Volcanics is located east of Iron Baron, where they comprise interbanded porphryritic rhyolite and rhyodacite (?), fine-grained felsic and hornblende-bearing gneisses and fine-grained amphibolite.

Broadview Schist

The Broadview schist is a sequence comprised of deformed schists, quartzites and interlayered amphibolites.

The contact between the Broadview Schist and the Myola Volcanics is not exposed, therefore the stratigraphic relationship between the two units is uncertain, and the Myola Volcanics may underlie, overlie or be interbedded with the Broadview Schist (Parker *et al.* 1993; Curtis 2007).

Wertigo Granite

Intruding into the Myola Volcanics, but may also be partially derived from anatexis of the Myola Volcanics is the massive, pink to grey migmatoid granite the ≈1820ma Wertigo granite, that belongs to the igneous and undifferentiated metamorphic and tectonic units known as the Lincoln Complex; these units were formed during the Kimban Orogeny (Parker 1988).

The McGregor Volcanics

The McGregor Volcanics are a sequence of weakly deformed, bimodal volcanics that unconformably overly the Broadview Schists, and consist of acidic, welded and ash flow tuffs derived from melting of a lower crustal source and basaltic lava flows derived from a mantle source (Giles et al. 1980). The McGregor Volcanics are steeply inclined and outcrop in the Moonabie Range, sandwiched between the Moonabie Formation and intrusive Charleston Granite (Parker *et al*. 1988). They have been dated using U-Pb isotopic analysis of zircon grains as being extruded approximately 1740 Ma (Fanning *et al.* 1986).

Moonabie Formation

Interlayered within the McGregor Volcanics, but mostly overlying is the Moonabie Formation, which consists of volcaniclastic grits containing a mixture of acid volcanic and chert clasts in an immature matrix, indicating that the Moonabie Formation was formed by the rapid erosion of the underlying volcanic pile. The Moonabie formation also contains local thin heavy mineral beds.

1.5.4 MESOPROTEROZOIC

The Corunna Conglomerate and other Mesoproterozoic units in this region record a change in the tectonic development of the Gawler Craton. From the highly deformed, dominantly marine metasediments to relatively undeformed, dominantly non-marine, continental derived sediments.

Corunna Conglomerate

Unconformably overlying the Moonabie Formation and McGregor Volcanics is the Corunna Conglomerate, which represents an intracontinental, shallow water sedimentary sequence consisting of the basal conglomerate, Nilgenee Member and the Cowleds Member.

The basal conglomerate contains boulders of the McGregor Volcanics and Moonabie Formation, with clasts grading into pebbles and boulders derived mostly from the Hutchison Group of metasediments and the Broadview Schist with abundant quartzite clasts.

Overlying, the basal conglomerate is the Nilgenee Member, which consists of heavy mineral sandstones and minor red siltstones, inter-fingered with massive talus breccias (the Cowleds Member). The Cowleds Member contains abundant fragments of fine-grained mylonite, coarsening towards the east and was likely deposited off an ancient escarpment (Giles *et al.* 1980)

Charleston Granite

Intruding into the McGregor Volcanics, Moonabie Formation and Corunna Conglomerate along the southwestern margin of the Moonabie Range, is the Charleston Granite. This granite belongs to the Roxby Sub-Group of Hiltaba suite granitoids. The Charleston Granite is massive, homogeneous, undeformed megacrystic granite that is interpreted to form a pluton approximately 15 km in diameter. The Roxby Sub-Group granites are associated with numerous IOCG deposits in the Gawler Craton, such as Olympic Dam (Johnson & Cross 1995), Moonta- Wallaroo (Conor 1996) and prospects Hillside (Cerlienco. 2009), Acropolis, Wirrda Well, Emmie Bluff, Oak Dam and Murdie (Gow *et al.*1994)

The Charleston Granite has been dated using U–Pb isotopes in zircons as having a magmatic crystallisation age of 1585±5 Ma (Creaser & Fanning 1993). Some zircons exhibit significantly older ages i.e. ~1780, ~1970 and >3150 Ma, and together with other isotope work (neodymium) show the presence of an older crust, which has been interpreted as the Charleston Granites being derived from the recycling of Archaean and Palaeoproterozoic crust.

Gawler Range Volcanics

Several northwest trending rhyolite dykes are observed to the west of Iron Baron, these rhyolite dykes are believed to be dykes related to the eruption of the Gawler Range Volcanics (GRV) (Parker 1988).

These dykes termed the GRV Felsic Dykes are massive, pink, porphryritic rhyolite dykes containing abundant K-feldspar and quartz phenocrysts. These dykes intrude syntectonic granite west of the Middleback Range (Parker 1988).

The Pandurra Formation

The Pandurra Formation unconformably overlies the deformed Moonabie Formation at Mount Laura near Whyalla (Nixon 1975; Drexel 1976; Parker 1981) and shows a rapid facies change from conglomerates to haematitic siltstones, representing a transition from a high-energy environment to low energy environment. Miles (Miles 1954) interpreted this as representing a deepening in depositional environment of an ancient graben deepening rapidly northeast of Whyalla into the Cariewerloo Basin.

1.6 Structural Setting

Based on evidence largely gathered in the southern and southwestern Eyre Peninsula, the Middleback Range region underwent two major deformational events during possible times of mineralisation; The Kimban Orogeny and the Wartakan Event (Fig. 5).

The Kimban Orogeny is the dominant deformational event in the Middleback Range area, with evidence of deformation and metamorphism associated with the Kimban Orogeny being observed in all units from the metasedimentary Hutchison Group units to just prior to the deposition of the Corunna Conglomerate. (Parker 1988)

The Kimban Orogeny according to Parker (1993) was initiated between ≈1850-1845Ma and continued intermittently through to ≈1710Ma. This orogenic event is characterised by three major phases in the Cleve-Cowell area, these being D_1, D_2 and D_3.

D_1 was recognised in the Cleve-Cowell area in all units of the ?Sleaford Complex, Miltalie Gniess, Hutchison Group and earliest units of the Lincoln Complex (Parker 1988). The D_1 event is recognised in the

Hutchison Group as layers of parallel fabric defined by mineral elongation and preferred alignment of mica and sillimanite. D_1 however hasn't been recognised in the Middleback Ranges.

D_2 was an east-west compressional event that caused major folding in the Middleback Ranges, The D_2 event like the D_1 event occurred at upper amphibolite facies conditions, and caused major isoclinal folding within the region (Parker 1988; Parker 1993).

D_3 like the D_2 was an east-west compressional event that occurred along a similar axis to the D_2 event; however D_3 was a retrograde event occurring at upper greenschist facies. The D_3 event is attributed to the formation of major north-south trending shear zones and mylonite belts in the region, including the Kalinjala shear zone (KSZ) (Parker 1988; Parker 1993). Splays of which are thought to be the major north-south trending features observed in aeromagnetic data of the study area. Also attributed to the D_3 event is the formation of open regional scale folds (Parker & Lemon 1982)

The Wartaken Event was a north-south compressional event within the region, estimated by Parker *et al.* (1993) to have occurred approximately between 1500-1450Ma. This north-south compressional event resulted in north-easterly and north-westerly cross faulting, as well as minor kink banding and shears (Parker 1988).

1.7 Copper Mineralisation in the Area

The Moola Prospect is situated within the highly prospective IOCG metallogenic belt, termed the Olympic Cu-Au-(U) province (Skirrow *et al*. 2002; Skirrow *et al*. 2006). This province contains the Olympic Dam, Prominent Hill, Mount Gunson, Moonta and Wallaroo Proterozoic IOCG deposits, as well as numerous IOCG prospects.

Iron oxide copper gold deposits have become highly prospective targets in the Gawler Craton due to the size of the larger deposits, the giant Olympic Dam deposit (9.8 Bt at 0.87% Cu, 0.28 kg/t U3O8, 0.31 g/t Au, 1.5 g/t Ag) and world class Prominent Hill (189.7Mt @ 1.32% Cu, 0.5g/t Au, 3.1 g/t Ag) (PIRSA 2010), with numerous companies exploring the region.

The Moola Prospect and its surrounding areas has previously been explored for IOCG style mineralisation by Eagle Bay Resources, Merritt Mining, BHP, REX Minerals, Helix, Minotaur etc. with several prospects being identified i.e. Moola, Highway, Princess, Myall Creek and Lake Gilles, in addition to the historic Murninnie Mine (Fig. 6).

The Moola Prospect together with the Highway and Princess Prospects were identified by Helix by calcrete sampling which showed copper/gold/base metal anomalism around the Myola Prospect, with subsequent RAB and RC drilling on the Moola grid confirmed broad intercepts of low-grade copper and gold mineralisation, with the best intercept at the Moola Prospect being 12m@1.2% Cu (Helix 1994). Limited information is available for the other prospects, with iron oxide mineralisation and alteration associated with IOCG being noted but not discussed in detail.

The historic Murninnie Mine is located approximately 35 Kms south west of Whyalla and was discovered in the early 1860's, and developed to a depth of 52m. Although records of production are sporadic, total production from the mine is thought to be in the order of several thousand tonnes of high-grade copper ore, with variable bismuth, gold and silver content. Mineralisation at the Murninnie Mine is exposed along strike over a distance of approximately 400m, with mineralisation contained within steeply dipping multiple lode systems in fractured zones of granitoid and metasedimentary rocks of the Hutchison group rocks. Primary Industries and Resources South Australia (PIRSA) records from the record of mines summary card of 1901, show one parcel of ore from the mine totalled 60 tons of ore containing 10% Cu and 5% Bi, with another parcel being 15 tons of 10 % Cu with no Bi. Hand specimens tested by Australasia Gold Ltd from mine spoil and underground lodes yielded peak assay values of 7.7% Cu, 3.8 ppm Au, 2.4% Bi and 10ppm Ag. The Murninnie Mine mineralisation displays evidence of a number of characteristics defined by Ferris *et al.* (2002) and Hitzman (2000) to be associated with IOCG deposits i.e. Multiple intrusions of a Hiltaba aged granite, strong structural controls (mineralisation along strike with north-south trending Murninnie Scarp), haematitic, potassic and calcic alteration.

Another style of copper mineralisation prominent within the area is syngenetic unconformity-related Cu mineralisation, with the historic Pandurra and Point Lowly copper mines and Myall Creek copper prospect being located within the area (Fig. 6).

The historic Pandurra copper mine is located approximately 40km northwest of Whyalla, with old mine working consisting of thirty pits that extend for approximately 400m. There is no recorded production for these

workings and probably were worked during the late nineteenth century (Jones 1970; Curtis 2007). Mineralisation consists of secondary copper (malachite, azurite and chrysocolla) and manganese minerals, localised along the unconformity and faulted contact between the Tapley Hill formation and the Pandurra formation (Curtis 2007).

The historic Point Lowly copper mine is located approximately 35km north-east of Whyalla and like the Pandurra copper mine consists of multiple working with no recorded production (Mason 1980; Curtis 2007). Copper mineralisation occurs within quartz veined, sheared and intercalated volcanics and siltstones within the fault zone and along the unconformable contact between the Beda Volcanics and Tapley Hill formation (Curtis 2007)

The Myall Creek copper prospect is located approximately 50km north east of Whyalla, and was discovered by Australian Selection and Sims Metals in 1975 (Curtis 2007). Mineralisation at the Myall Creek prospect consists of low-grade copper sulphides, with lesser zinc and lead. Mineralisation is hosted with the basal units of the Tapley Hill formation, which locally unconformably overlies a sequence of Beda Volcanics, Blacky Point formation and Pandurra formation that is deformed by north south trending steeply dipping faults (Mason 1980; Curtis 2007).

Peak assay results from drill hole SAU-20 yielded the following values; Cu 1.45%, Zn 0.43%, Pb 0.13% and Ag 43ppm (Curtis 2007).

2. METHODOLOGY

2.1 Field work

Due to the mineralisation being blind, with sparse outcrop of the host rock in the region little information about the mineralised rock units could be gained from fieldwork. Surface samples of the different rock types of the Myola Volcanics were collected as unaltered standards for petrology and geochemistry.

2.2 Petrography

Representative samples of each host rock, alteration types and multiple examples of mineralisation were sampled for the production of thin/ polished thick sections and polished blocks by Pontifex Petrographic Services Ltd. These were used for the identification of minerals/ assemblages and nature of mineralisation/ paragenesis with thin sections investigated using a transmitted light microscope, polished thick sections with both transmitted and reflected light and polished block with reflected light microscope.

2.3 Whole rock geochemistry

Fifteen Samples in total were prepared for major, trace and rare earth element XRF analysis, with a collective seven samples collected by John Parker for PIRSA in the seventies and by myself in April 2010 from the type example of Myola Volcanics some 2.2 km northeast of the Moola Prospect. The additional eight samples were collected from OneSteel drill core, with the aim to best represent the major lithological units of altered Myola Volcanics.
Both outcrop samples and drill core samples were used to demonstrate the transition from relatively unaltered? Myola Volcanics (outcrop) to their heavily altered equivalents (drill core). Descriptions of the samples are in Appendix A. All samples were crushed in a steel jaw crusher and milled in a tungsten carbide mill to produce a fine powder.

2.3.1 MAJOR ELEMENT ANALYSIS

The samples were dried in an oven at 110°C for over two hours to remove absorbed moisture.
The samples were then weighed into ceramic crucibles and ignited overnight in a furnace at 960°C and weighed again to yield the Loss on Ignition (LOI) values. This LOI comprises; organic material, CO_2 from carbonate minerals, H_2O+ (water in combination with the crystal structure), and possibly S, Cl and other volatiles.

A nominally 1g of the ignited material was then accurately weighed with 4g of flux (commercially available as type 12:22, comprising 35.3% lithium tetraborate and 64.7% lithium metaborate). The sample-flux mixture was fused for eight minutes using a propane-oxygen flame, at a temperature of approximately 1150°C, using Pt-Au crucibles, and cast into a preheated mould to produce a glass disc suitable for analysis (Stanley, *pers comm.*, 2010).

Samples were analysed with a Philips PW 1480 X-ray Fluorescence (XRF) Spectrometer, using an analysis program calibrated against several international and local Standard Reference Materials (SRM's). A dual-anode (Sc-Mo) X-ray tube was used, operating at 40kV, 75mA (Stanley. *pers comm*. 2010).

2.3.2 TRACE ELEMENT ANALYSIS

Approximately 5-10g of sample powder was mixed with nominally 0.5ml of binder solution (Poly Vinyl Alcohol) and pressed to form a 30 mm diameter pellet. This was allowed to dry in air and was heated for a further 1 to 2 hours in a 60°C oven to ensure that the pellet was completely dry before analysis.

Samples were analysed using a Philips PW 1480 XRF Spectrometer, using several analysis programs covering suites of from 1 to 7 trace elements, with conditions optimised for the elements being analysed. The programs were calibrated against many (30 or more) local and international SRM's. The dual-anode Sc-Mo tube (operated at sufficient voltage to excite the Mo) and an Au tube were used for the analyses. Matrix corrections are made using either the Compton Scatter peak, or mass absorption coefficients calculated from the major element data (Stanley, *pers comm*. 2010).

2.3.3 RARE EARTH ELEMENT ANALYSIS

Rare Earth Element (REE) analyses were conducted at Adelaide Microscopy after whole rock samples had been dissolved in high pressure/ high temperature vessels (bombs). High-pressure bombs were used as previous geochemical work on the Myola Volcanics showed high concentrations of zirconium which is usually, hosted in high-pressure minerals i.e. Zircons.
Approximately 50mg of sample powder was weighed into Bombs. To the 50mg of sample 2mL of 7M nitric acid (HNO3) and 4mL 50% hydrofluoric acid (HF) was added and placed on the hotplate at 140°C, the sample/ acid solution was evaporate to dryness on a hotplate at 140°C with an extra couple of mls of 7M HNO3 added just before dryness to promote the formation of nitrates in favour of fluorites.

The dissolution is then repeated by adding 2mL 7M HNO3 and 4mL 50% HF to the bombs, the bombs were then placed in an oven at 190°C for 2 days. The solutions were then evaporated to dryness on a hotplate at 140°C with an extra couple of mls of 7M HNO3 added just before dryness to promote the formation of nitrates in favour of fluorites.6mL of 7M HNO3 was then added and the bombs placed in an oven at 150°C overnight and evaporated to dryness on a hotplate at 140C.

The samples were then diluted to give a final solution concentration of up to ~.1% Total dissolved solids (TDS)and no more than this as is required for analysis when using solution ICPMS i.e. 50mg sample and a thousand times dilution factor, yields TDS= .1% (and < .1% when silicon is lost as SiF_4 during evaporations, thus meeting the requirement.)

The samples were analysed using solution inductively coupled plasma mass spectrometry (ICP-MS), using an analysis program calibrated against a couple of commercially produced standards materials (SRM's). Samples were analysed covering a whole range of light and heavy Rare Earth Elements (REE) and trace elements. Some elements (Ti, Sb, Zr, Ag, Sn, Te and Nb) where excluded from the final data as they weren't in the commercially produced standard and therefore gave spurious data, concentrations of tungsten and cobalt were also removed from the dataset as a result of contamination of the samples arising from a wearing of the tungsten carbide mill during sample grinding.

2.4 Radiogenic Isotopes

Eight core samples of altered rocks were selected for Nd, Sm and Sr isotope whole rock analysis. These samples were taken from a variety of depths and different lithologies, as well different alteration intensities and copper mineralisation, to try and best characterise the radiogenic isotope values/ variation of the systems due to alteration/ mineralisation, with an increase in alteration/ mineralisation expected to show an increased mafic signature.

All samples were crushed in a steel jaw crusher and milled in a tungsten carbide mill to produce a fine powder.

2.4.1 NEODYMIUM, SAMARIUM AND STRONTIUM ISOTOPES

Neodymium, Samarium and Strontium isotopes analyses were undertaken at the University of Adelaide after samples had been dissolved in high pressure/ high temperature vessels (bombs) and spiked, the dissolution

process was similar to that for the REE differing however in sample size and the addition of a Sm-Nd spike (Bruce, *pers comm.*., 2010) .

After dissolution, evaporation and centrifugation of the samples the final stage of preparation was the separation of Sm-Nd and Sr in each sample, which is achieved by running the sample through Biorad PolyPrep columns with 2ml AG50W X8 200-400 mesh Biorad cation exchange. The Sm and Nd are separated using the Sm-Nd columns (2ml Teflon powder impregnated with HDEHP). The neodymium and samarium samples were loaded onto Rhenium and Tantalum ribbons and run on the mass spectrometer (MAT262) at the University of Adelaide. The strontium was loaded onto Rhenium and Tantalum ribbons on filaments and run on the mass spectrometer at the University of Adelaide.

2.5 Electron Probe Micro Analysis of sulphides and oxides

Electron Micro Probe analysis were used to determine major and trace element compositions of the alteration and mineralisation assemblages. Analysis was undertaken at Adelaide Microscopy at the University of Adelaide using the Cameca SX51 Microprobe. For the microprobe a voltage of 15kVand beam current of 20 nA were used.

2.6 Sulphur Isotopes

Sulphur Isotopes ($\delta 34S$) were conducted on selected sulphide samples (chalcopyrite and pyrite) from the core at a range of different depths, analysed by the Institute of Geological and Nuclear Sciences Limited (New Zealand) by weighing out the samples (prepared by Ryan Jones; Jones 2010) into duplicate tin capsules with an equal amount of V_2O_5, then run on a EuroVector Elemental Analyser connected to a GVI IsoPrime mass spectrometer with the results of the duplicates being averaged, results are reported with respect to Canyon Diablo Troilite (CDT)

3. CORE LOGGING

A study of the major host rocks, alteration styles and mineralisation was conducted upon diamond drill core obtained from OneSteel, diamond drill hole (ML001).
ML001 reached a depth of 249.4m of which the first 14.4m no core was obtained. The remaining 235m was cored and used for this study. Mineralisation is observed from 72.4m to the end of the hole (EOH)

3.1 Lithologies

Three lithologies dominate the 235m of Moola diamond drill core below the zone of weathering (55.7m), with a further three lithologies recognised in the core.

The three predominating lithologies are the porphryritic rhyolites (Figs. 5f, 5j) quartz -feldspar ± hornblende gneisses (Figs. 5d, 5k) and rhyodacite (Figs. 5h, 5I, 5l), with the minor lithologies being massive amphibolites (Figs. 5a, 5b), microgranites (Fig. 5b, 5c, 5d) and the weathered volcanics/ volcaniclastic unit (Fig. 5g).

The porphryritic rhyolites are fine to coarse-grained massive pink/ brownish pink bands consisting of phenocrysts of plagioclase, quartz and potassium feldspar with minor grey/ dark grey plagioclase quartz bands.

The quartz -feldspar ± hornblende gneisses, are almost identical mineralogically to the porphryritic rhyolites, however can be distinguished by their development of a strong gneissic fabric defined by interlayered pink bands of elongate potassium feldspar, quartz and plagioclase and dark grey bands of elongated quartz and feldspar.

The rhyodacite member is a blue/green well foliated dense rock with fine white bands consisting of plagioclase and quartz, and red/ pink alteration bands, as well as minor bands of the porphryritic rhyolite. The rhyodacite unit starts as a massive unit at 198.35 and continues until at least the EOH.

Interbedded with the porphryritic rhyolites and the quartz -feldspar ± hornblende gneisses are; minor, concordant, strongly magnetic green-black fine grained massive amphibolites.

From 176.28 – 198.35m occurs a zone of slightly to highly weathered light green to green/ grey felsic volcanic to volcaniclastic unit.

This sequence of rocks, hosting mineralisation at the Moola Prospect is assumed to belong to the 1791± 4 Ma (Fanning *et al* 1988) Myola Volcanics.

The above lithologies (excluding the Felsic volcanic to volcaniclastic unit) are observed in the core to be intruded by undifferentiated veinlets of light pink K-feldspar-quartz-plagioclase-micaceous microgranite to pegmatite, this pegmatitic/microgranite intrusion likely represents the intrusion of either a Wertigo granite or Charleston granite equivalent.

3.2 Alteration

Alteration identified in the Moola core was both intense and prevalent, with an initial log suggesting distinct zoning. In total six types of alteration were distinguished and are listed in order of intensity;

- Chlorite
- Sericite
- Na-Ca-Fe (Albite)
- Carbonate veining
- Silicification and quartz veining
- Epidote

Chloritic alteration is the most prevailing type and prevalent type of alteration in the core, and was commonly spatially associated with carbonate and quartz veining and serecite with rare epidote alteration (Figs. 5e, 5k, 5l). Chlorite alteration intensifies towards small ≈ 1 cm veinlets of chlorite-mica ± epidote veinlets.

Sericite alteration was prevailing throughout the core (Figs. 5e, 5j, 5k), although being difficult to recognise in the rhyodacite unit due to its dark colour. Serecite alteration was visible in the gneiss's, rhyolite and granites as yellow pseudomorphs of plagioclase and K-feldspar.

Sodic (Calcic-Iron) (Na-Ca-Fe) alteration was prevalent throughout the core in the form of albitisation of K-Feldspar and plagioclase; however it was much more intense or noticeable in the upper felsic units of the core (i.e. microgranite, felsic gneisses and rhyolites)

Carbonate Alteration was most prevailing at depth especially within the rhyodacite unit (Figs. 5I, 5h). This likely reflects a lithological control on this type of alteration, moving up in the core into the felsic volcanics, the carbonate alteration gradually changes to a quartz carbonate alteration.

Multiple stages of carbonate/ quartz-carbonate veining can be identified throughout the core and from a very basic paragenesis the carbonate/ quartz-carbonate veins appear to be late stage alteration and mineralisation.

Silicic alteration, like carbonate alteration, appears to be late stage and possibly an equivalent to the carbonate alteration, with veins of quartz moving down the core transition into quartz-carbonate veining, and was not found in the deeper section of the core (Figs. 5d, 5e, 5j, 5k, 5m, 5n). This alteration graduation likely represents a lithological control on alteration.

Multiple generations of quartz veining occur throughout the core with at least two distinguishable generations, those being the milky quartz veins and the clear quartz veins. With the milky quartz veins sometimes forming crackle style veining in the clear quartz veins, both the milky quartz and clear quartz generation contain mineralisation.

All or at least some of these late stage carbonate and quartz veins are coeval with the precipitation of chalcopyrite and pyrite.

Also within the core was epidote alteration although not being nearly as prevalent or prevailing as the other forms of alteration. Epidote alteration was observed in the rhyodacite unit in an association with sericite and chlorite alteration, this restricted style of alteration likely represents a lithological control on the epidote alteration.

3.3 Mineralisation

Mineralisation was observed sporadically in the Moola core from 72.4 m to 249.4m (E.O.H); with mineralisation largely hosted in small to large veinlets (Figs. 5d, 5k, 5I, 5n) but was also found in small (up 20cm) brecciated zones (Fig. 5j). Disseminated mineralisation of the country rock was not observed.

The mineralisation was hosted in multiple generations of overprinted quartz, quartz-carbonate and carbonate veins, ranging from millimetre sized veinlets to centimetre sized veins, with primary mineralisation consisting of chalcopyrite (Figs. 5j, 5k, 5i) and pyrite (Figs. 5m, 5n). Along with chalcopyrite and pyrite, small veins of haematite (Fig. 5a) occur sporadically, as do veins of an unidentified manganese oxide above the weathering base.

A zone of supergene enrichment was developed over 15.85m (178.35 – 194.2m) of the core and this zone likely represents secondary alteration of sulphide minerals in a fault zone by an oxidized fluid. This zone occurs in a light green/ white to green grey moderately to strongly weather felsic volcaniclastic rock. Contained within the supergene zone were secondary copper minerals such as native copper and malachite (Fig. 5g), these secondary copper minerals occur in multiple, overprinting veinlets as well as infill textures in the vuggy felsic volcanics.

4 RESULTS

4.1 Petrography

A full petrographic report of polished and thin sections can be found in Appendix A.

4.1.1 HOST ROCKS

Granite

Undifferentiated veinlets of granite were observed intruding the rhyolite, rhyodacite, amphibolite and felsic gneisses host lithologies.

This granite can be grouped by grain size into two distinct units: i) fine-medium grained (Figs. 5n, 5m) and ii) medium-coarse grained granites (Figs. 5b, 5c, 5d). The medium-coarse grained is the most common variety. Both varieties have a similar mineralogy and appearance, and were most probably derived from the same source with the medium-coarse grained granite developing large crystals.

The least altered sample of granite observed was a fine to medium grained K-feldspar-quartz-plagioclase-micaceous-sodic amphibole micrograinte (Fig. 7a), which has undergone sericite and sodic alteration.

The granite matrix is dominated by quartz and plagioclase, with large ≈ 5-20 mm subhedral to anhedral crystals of K-feldspar and plagioclase and at a lesser extent muscovite. Petrographic study has shown the approximate composition to be 35% quartz, 23% sericite, 20% K-feldspar, 15% plagioclase feldspar, 5% opaques and 2% muscovite. Amphibole, in the form of a sodic amphibole, is also present within the granite, but is relatively rare.

Plagioclase occurs as subhedral to anhedral grains ranging in size from the aphatic groundmass to 20 mm in size. The phenocrysts of plagioclase were characterised by a varying degree of sericite alteration, from crystals exhibiting minor alteration to crystals almost entirely pseudomorphed by sericite (Fig. 7a). The phenocrysts of plagioclase often exhibit polysynthetic twinning (albite) as well as containing inclusions of magmatic muscovite.

Quartz occurs in the granites along with plagioclase as the aphatic groundmass (Fig. 7a).

Potassium-Feldspar occurs as approximately 1-12mm subhedral to anhedral grains. The K-Feldspar is relatively unaltered (some minor sericite alteration observed) and commonly exhibits tartan twinning (microcline) (Fig. 7a), some grains contain inclusions of the sericite altered plagioclase and quartz.

Muscovite occurs as euhedral to subhedral strongly deformed, locally kinked lathes approximately 0.1-4mm in size. The muscovite was deflected around the highly sericite altered plagioclase, and is thought to be magmatic in origin.

Amphibole was assumed, from thin section, as being a sodic amphibole. The amphibole occurs as 0.4-1.5mm euhedral to subhedral grains that exhibit a pleochroism from pink to dark green (Fig. 7a).

The appearance of these granites can be quite variable as the increase in intensity of alteration changes the colour of the granite from a light pink to a green/yellow rock (sericite +chlorite ± epidote alteration) although the granitic texture was largely preserved. The granite generally displays a subtle foliation.

Volcanics

Five different types of volcanic/ volcaniclastic rocks were recognised in the diamond drill core (ML001), these being rhyolite, quartz-feldspar± hornblende gneisses, amphibolite, rhyodactite and volcaniclastics.

The rhyolite unit along with the felsic gneisses and rhyodactite were the most important (volume wise) host rocks.

Rhyolite

The rhyolite was generally fine-grained with the matrix dominated by quartz and plagioclase (being pseudomorphed by sericite), and contains phenocrysts (Figs. 7b, 7j) of potassium feldspar, plagioclase, lesser quartz, and opaques.

Petrographic study has shown the approximate composition to be 45% quartz,15% K-feldspar, 15% sericite, 13% chlorite, 5% plagioclase feldspar, 5% opaques and 2% muscovite. Perthite, was also present within the granite, but was relatively rare.

Plagioclase occurs in the groundmass and as phenocrysts, and occurs as subhedral to anhedral grains ranging in size from the aphatic groundmass plagioclase to 1.5mm in size. The groundmass plagioclase displays mild to pervasive sericite alteration. The porphryritic phenocrysts also display a mild to pervasive sericite alteration, with some of the phenocyrsts being completely pseudomorphed by sericite. Some of the more mildly sericite altered plagioclase exhibits polysynthetic twinning (albite).

Quartz occurs in the rhyolite along with plagioclase as a recrystalised aphatic groundmass, and as subhedral to anhedral porphryritic phenocrysts 0.2 mm in size (Figs. 7b, 7j).

Potassium-Feldspar, in the rhyolites occurs as approximately 1-5 mm subhedral to anhedral porphryritic phenocrysts. The K-Feldspar was pervasively sericite altered to the degree from mildly altered to completely replaced, the milder altered crystals of K-feldspar often exhibit tartan twinning (microcline).

Muscovite occurs as euhedral to subhedral strongly deformed, locally kinked lathes approximately 0.05- 2 mm in size, intergrown with chlorite (Fig. 7b). The kinked lathes of muscovite are magmatic in origin with the muscovite intergrowth much finer in grain size and intergrown with chlorite to form a fabric in a preferred orientation.

Chlorite was assumed, from thin section, as being an iron rich variety, due to its deep blue colour in some samples. The chlorite occurs as 0.05- 0.2 mm euhedral to subhedral, elongated platy grains, which intergrows with muscovite, opaques and quartz to form a fabric in a preferred orientation. Chlorite and the non-magmatic muscovite wrap around phenocrysts of highly sericite altered plagioclase and K-feldspar.

Like the granites the appearance of the rhyolite can be quite variable with the intensity of alteration changing the colour of the rhyolite from a light to dark brown pink to a green/yellow rock (sericite +chlorite ± epidote alteration) although the rhyolites texture was largely preserved. The rhyolite was mildly to well foliated in the core.

Gneisses

The quartz-feldspar± hornblende (QFH) gneisses were fine-grained with the matrix dominated by aphatic to fine grained recrystalised quartz and plagioclase, and contains phenocrysts. The phenocrysts commonly compose of potassium feldspar, plagioclase, lesser quartz, and opaques (Fig. 7c).

Petrographic study has shown the approximate composition to be 35% quartz, 25% sericite, 20% plagioclase feldspar, 14% K-feldspar, 5% opaques and 1% muscovite, Perthite, was also present within the QFH gneisses, but was relatively rare.

Plagioclase occurs in the groundmass and as phenocrysts, and occurs as subhedral to anhedral grains ranging in size from the aphatic groundmass plagioclase to 0.7 mm in size. The groundmass plagioclase displays mild to pervasive sericite alteration (Fig. 7c). The phenocyrsts also display a mild to pervasive sericite alteration, with some of the phenocyrsts being completely pseudomorphed by sericite. Some of the more mildly sericite altered plagioclase's exhibit polysynthetic twinning (albite).

Quartz occurs in the rhyolite along with plagioclase as recrystalised aphatic to fine grained groundmass, and subhedral to anhedral phenocrysts 0.2 mm in size (Fig. 7c).

Potassium-Feldspar, in the rhyolites occurs as approximately 0.2-1.0 mm subhedral to anhedral phenocrysts. The K-Feldspar was pervasively sericite altered to the degree from mildly altered to completely replaced, the milder altered crystals of K-feldspar often exhibit tartan twinning (microcline).

Muscovite occurs as euhedral to subhedral strongly deformed, locally kinked lathes approximately 0.1mm in size, as well as in fine veinlets.

Chlorite was found in some of the slides, but as the chlorite was a product of alteration the sample with no chlorite was selected to describe the host rock. Chlorite in the other sample was similar to that of the rhyolites in that it's assumed, from thin section, as being an iron rich chlorite. The chlorite occurs as 0.05-0.2mm euhedral to subhedral, elongated platy grains, which intergrows with muscovite, opaques and quartz to form a fabric in a preferred orientation (Fig. 7c).

Like the granites and rhyolites the appearance of the QFH gneisses can be quite variable with the intensity of alteration changing the colour of the QFH gneisses from a interlayered pink and dark grey banded rock to a green/yellow and grey banded rock (sericite +chlorite ± epidote alteration) although the QFH gneisses texture was preserved. The QFH gneiss was strongly foliated and lineated.

The origin of these gneisses is uncertain with cases for them being either volcanic or sedimentary in origin being made (Parker *et al.* 1988; Curtis 2007).

Amphibolites

The amphibolites were fine-grained, with their fabric being defined by anhedral to subhedral laths of chlorite and sericite with finer grained quartz and plagioclase, and contain phenocrysts (Fig. 5d). The phenocrysts were commonly composed of opaques and in the upper parts of the core were hornblende (Fig. 7d).

Petrographic study has shown the approximate composition to be 38 % chlorite, 30% sericite, 20% quartz, 5% opaques 5% plagioclase feldspar, 1% monazite and 1% zircon. Biotite, was also present? within the amphibolite, but was relatively rare.

Sericite occurs as pseudomorphs of plagioclase, which it has completely replaced. The sericite occurs as subhedral to anhedral grains approximately ≈0.1mm in size. As previously stated sericite represents the complete replacement of plagioclase by sericite.

Quartz makes up the fabric in the amphibolites along with plagioclase (serecite), chlorite. Quartz occurs as fine grained subhedral to anhedral grains ≈0.1 mm in size, the quartz exhibits undulosed extinction.

The amphibolites matrix was dominated by chlorite, chlorite occurs as, 0.02-4mm euhedral to subhedral, elongated platy grains, and were interpreted as being an iron rich chlorite. The chlorite wraps around the oxides and feldspars (now altered to sericite) and aligns in a preferential orientation, to define a foliation. The chlorite was observed replacing the amphiboles (hornblendes) in the upper depths of the core (Fig. 7d).

Amphibole was assumed, from thin section, to be hornblende and occurs as 0.1-0.3mm anhedral grains (Fig. 7d) and was restricted to the least altered sections of core (Fig. 7d). Hornblende was observed being replaced by an assumed iron rich chlorite.

The amphibolites appearance within the core changes little and was observed within the drill core as being a blue/green well foliated dense rock.

The origin of these amphibolites, have been suggested from their textures to be derived from either fine-grained dolerites or coarse-grained basalts (Parker *et al.* 1988; Curtis 2007).

Rhyodacites

The rhyodactite were fine-grained, holocrystalline rocks, commonly displaying a gneissic texture, these bands, were dominated by, quartz with lesser chlorite, and iron oxides with lesser quartz (Figs. 7f, 7g, 7i, 7l).

Petrographic study has shown the approximate composition to be 40 % chlorite, 20% plagioclase feldspar, 20% opaque, 5-20% sericite, 15% quartz and 1-5 % K-feldspar. Epidote, perthite, calcite, muscovite, monazite was also present within the rhyodacite, but was relatively rare.

Plagioclase occurs both in the groundmass along with quartz, in the quartz plagioclase bands, and as phenocyrsts. The groundmass plagioclase occurs as subhedral to euhedral grains ranging in size from the aphatic groundmass plagioclase to 0.1mm in size (Figs. 7f, 7g, 7i, 7l). The plagioclase phenocyrsts display mild to

pervasive sericite alteration, with some of the phenocyrsts being completely pseudomorphed by sericite. Some of the more mildly sericite altered plagioclase's exhibit polysynthetic twinning (albite) (Fig. 7i).

Quartz occurs in the rhyodactite along with the quartz-plagioclase banding and oxide-quartz banding, The quartz occurs as fine euhedral to subhedral grains groundmass ≈0.01-0.05mm in size(Figs. 7k, 7l).

Chlorite occurs as, 0.01-1.0mm euhedral to subhedral, elongated platy grains, and from thin section, as being an iron rich variety, due to its deep blue to purple colour (Fig. 7g). The chlorite wraps around the highly sericite altered plagioclase feldspars and along with oxides aligns in a preferential orientation, to define a foliation.

Opaques occur as anhedral elongated grains, and from reflected light microscopy was composed of magnetite with haematite alteration, like the chlorite the oxides aligns in a preferred orientation, to define a foliation (Fig. 7f, 7g, 7i, 7l).

Like the amphibolites, the rhyodactite appearance within the core changes little and was observed within the drill core as being a dark blue/ black well foliated dense rock.

Volcaniclastics

Due to the high degree of weathering and porosity of the volcaniclastics unit, the thin section made of this lithology was chosen on competency and not based on a representative sample; the petrography from hand specimen examination revealed the volcaniclastics unit was a light green/ white to green grey fine to medium grained, porous, moderately to strongly weathered, felsic volcaniclastic rock, containing coarse lithic fragments.

Thin section examination of the volcaniclastic unit revealed it was composed of fine grained quartz and sericite and very fine grained chlorite, that was highly weathered (Fig. 7e).

Quartz occurs as fine euhedral to subhedral grains groundmass ≈0.01-0.05mm in size and commonly has fine grained sericite inclusions.

Plagioclase occurs in the groundmass and as phenocrysts, and occurs as subhedral to anhedral grains ranging in size from the aphatic groundmass plagioclase to 0.3 mm in size. Both the groundmass plagioclase and phenocrysts of plagioclase display mild to pervasive sericite alteration, with some of the phenocyrsts being completely pseudomorphed by sericite. Some of the more mildly sericite altered plagioclase's exhibit polysynthetic twinning (albite).

Quartz veins ranging and form a cross cutting network across the sample which was comprised of medium to course grained quartz.

4.1.2 ALTERATION

Hydrothermal alteration of the host rocks was both intense and prevalent. The relative timing of some of the alteration events was difficult to constrain, namely due to multiple stages and overprinting nature of some of the alteration events and the limited amount of core observed. Alteration types are listed below in assumed chronological order.

Sodic (Calcic-Iron) alteration was prevalent throughout the core in the form of albitisation of K-Feldspar and plagioclase; however it was much more intense or noticeable in the upper felsic units of the core (i.e. microgranite, felsic gneisses and rhyolites) and is thought to represent the earliest stage of alteration. The characteristic mineral of this type of alteration was the sodic plagioclase, the albite end member.

The albite dominantly occurs as subhedral to anhedral, 0.1-12 mm phenocyrsts that often display a mild to pervasive sericite alteration (Fig. 7i), with some of the phenocyrsts being completely pseudomorphed by sericite.

Sericite alteration like the albite alteration was one of the most prevalent and prevailing types of alteration in the core, although more easily observed in the upper parts of the core, transmitted light microscopy has revealed sericite to be abundant in the lower section (rhyodacite) of the core as well.

Sericite alteration was observed as a mild to complete replacement of plagioclase and K-feldspar, with some of the mildly altered plagioclase exhibiting polysynthetic twinning (albite) (Figs. 7a, 7b, 7c, 7i, 7l). Sericite phenocrysts were controlled by the size of feldspartoids it's replacing, and ranges between aphatic and 20mm subhedral to anhedral phenocrysts. Small veinlets of sericite were observed within some thin sections (Fig. 7j) with serecite alteration increasing towards these veinlets.

Chlorite alteration (chlorite-mica ± epidote) was observed in all slides and similar to sericite and Na (Ca-Fe) alteration was highly prevalent and prevailing throughout the entire core and was commonly spatially associated with carbonate and quartz veining and serecite with rare epidote alteration.

Chlorite in many slides was extensive, with chlorite making up to 45% percent of minerals in some slides. Chlorite occurs as, .01 to 1.0mm euhedral to subhedral, elongated platy grains, and from thin section, and was thought to be an iron rich variety (Figs. 7c, 7f, 7d, 7g). The chlorite wraps around the highly sericite altered plagioclase feldspars and along with oxides aligns in a preferential orientation, to define a foliation (Fig. 7c, 7f, 7d, 7g).

Small veinlets (≈ 1 cm) of chlorite-mica ± epidote were observed within some thin section with chlorite alteration increasing towards these veinlets (Fig. 7k).

Epidote alteration was observed in the RJ014 (Fig. 7l) in the rhyodacite unit in an association with sericite and chlorite alteration, this restricted style of alteration likely represent a lithological control on the epidote alteration

The quartz-carbonate veining was sporadic within the core, and characterised by abundant multiple overprinting generations of carbonate, quartz-carbonate, quartz veining. The quartz carbonate veining shows a zonation, with the deeper rhyodacite unit containing veins almost entirely consisting of carbonate (Fig. 7g), moving up in the core transitions to quartz-carbonate veins and in the upper parts of the core (rhyolites, felsic gneiss and unnamed granite) was almost entirely consists of quartz (Fig. 7h) . This reflects a lithological control on this type of alteration, with carbonate alteration largely confined to the rhyodacite units and quartz alteration being confined to the felsic units, with a quartz- carbonate transition zone occurring between them.

Crackle style veining, was recognised in some of the thin sections.

The carbonate species were assumed from transmitted light microscopy to be calcite, and occur as subhedral to euhedral crystals.

These quartz-carbonate veining were one of the last stage of alteration that these rock have undergone, with the term late stage carbonate-silica flooding applying well to them.

All or at least some of these late stage carbonate veins were coeval with the precipitation of chalcopyrite and pyrite.

4.1.3 MYOLA VOLCANICS

A full petrographic report of the Myola Volcanics, thin sections can be found in Appendix B.

Petrologically the PIRSA thin sections of the Myola Volcanics type location, approximately 2.2km north east of the Moola Prospect, were very similar to thin sections of the gneisses, rhyolites and amphibolites from the Moola Prospect.

The Myola Volcanics type location was observed to differ from that of the Moola Prospect in alteration prevalence, with alteration being observed at a less pervasive level in the Myola Volcanics type location slides. Alteration styles present were sericite, Na Ca- (Fe) and epidote alteration, with minor Chloritic alteration.

Sericite and Na Ca- (Fe) alteration like in the Moola Prospect was prevalent and prevailing, epidote alteration unlike at the Moola Prospect was a dominant type of alteration in these slides. Chlorite alteration was a very minor style of alteration and was largely confined to thin chlorite veins.

Hornblende unlike in the Moola Prospect core was relatively abundant, which likely reflects that chlorite alteration plays a minor role here, as it was observed in slide of the Moola Prospect core consuming hornblende.

4.1.4 ORE PETROGRAPHY

Reflected light microscopy was carried out on the polished sections of Moola Core with the following ore minerals recognised; magnetite, haematite, chalcopyrite, pyrite, sphalerite.

Magnetite

Magnetite was observed in abundant quantities in RJ002 and RJ015, with trace amounts occurring in all other polished blocks. The magnetite forms fine 0.01 to 2 mm sized euhedral to subhedral, equigranular crystals to elongated lathes that display an alignment parallel to the fabric of the rock (Fig. 8a).

Magnetite was commonly observed as brown/grey to dark grey crystals, all magnetite displays a degree of martititsation along veins, fractures and the rim to haematite (Fig. 8a). The martititsation was mild to pervasive, with degree of martititsation increasing towards thin haematite veins (Fig. 8b).

Haematite

Haematite was present in all the polished blocks in large quantities > 10 % total composition, with haematite present as four distinct forms; haematite veins, haematite martititsation of magnetite, radiating haematite needles and haematite growth on the rim of pyrites.

Haematite veins were observed in RJ002 and RJ011 as small veinlets ≈1mm wide (Fig. 8f), comprised of massive mint green coloured haematite and minor gangue. Gangue minerals also form an infill texture in minor fracture in the haematite.

Martitised haematite, is a psedumorph of the predating magnetite minerals and subsequently displays the same crystallographic features i.e. 0.01 to 2mm sized euhedral to subhedral equigranular crystals to elongated lathes that display an alignment parallel to the fabric of the rock (Fig. 8a). The martititsed haematite was mint green in colour, but can also be light grey/green; with martititsation ranging from mild to pervasive, martititsed haematite was observed in all polished blocks.

Radiating haematite was observed in RJ006 and RJ002 as thin 0.01 to 1mm mint green radiating needles of haematite, these needles show no affinity for alignment and dominate RJ006 making up to 50% of the 0.7mm wide quartz ± carbonate vein (Fig. 8b).

In RJ006 and RJ008 small growths of mint green haematite occurs on the rims of a few pyrite crystals, and occurs as small 0.01-.05mm anhedral crystals (Fig. 8c).

These four distinct haematite groups appear to have been precipitated at the same time, or at least overlapping

Pyrite

Pyrite was commonly observed in most polished sections, and forms fine 0.01 to 2 mm sized euhedral to subhedral equigranular crystals (Figs. 8c, 8d). Pyrite was commonly found in a close relationship with chalcopyrite (Figs. 8c, 8d), and like chalcopyrite, pyrite mineralisation was confined within quartz/ quartz-carbonate / carbonate veins. Pyrite colour varies between polished blocks from cream to yellow crystals. Pyrite crystals were often intergrown with other pyrite crystals, with pyrite crystal commonly being mildly fractured with minor pitting and commonly contains inclusions of gangue, haematite (martitised) and chalcopyrite. Pyrite crystals were observed growing around radiating haematite (Fig. 8b). Also in RJ006 pyrite shows growth of haematite on their rims (Fig. 8c). Pyrite was not observed with any noticeable zonation

Chalcopyrite

Chalcopyrite was common in most polished blocks, and forms fine 0.01 to massive <3cm sized euhedral to anhedral equigranular crystals (Figs. 8c, 8d, 8e, 8g).

Chalcopyrite mineralisation was in a close relationship with pyrite (Figs. 8c, 8d), and was confined within quartz/ quartz- carbonate/ carbonate veins, and displays quite variability in colour from a cream yellow to deep metallic yellow-gold.

Chalcopyrite commonly contains inclusions of martititsed haematite, haematite rim growth pyrite, magnetite, pyrite, sphalerite and gangue. Chalcopyrite commonly displays a moderate degree of fracturing

(Figs. 8d, 8e); with chalcopyrite cut by fine veins 0.1 to 1 mm of gangue exhibits a higher level of fracturing. Chalcopyrite was also characterised by moderate small 0.01mm pits. Chalcopyrite commonly forms infill textures in pyrite fractures (Fig. 8c).

Sphalerite

Sphalerite was recognised in RJ008 and RJ015, as small subhedral to anhedral equigranular 0.1 to 0.2mm dark grey crystals, enclosed exclusive within chalcopyrite crystals (Fig. 8e). The sphalerite exhibits chalcopyrite emulsion textures, precipitating chalcopyrite within itself as small 0.01mm crystals (Fig. 8e).

Native Copper

Native copper was observed in RJ009 as highly altered fine 0.1- 2mm subhedral to anhedral equigranular crystals (Fig. 8h), and native copper occurrence was coincidental with quartz/ quartz- carbonate/ carbonate veins, in addition to forming an infill texture in vuggs.

Paragenetic sequence

From these petrological observations a paragenetic sequence of ore mineral precipitation was inferred. The determination of this paragenesis was complicated, with multiple generations of some minerals. As such this paragenesis should be treated with caution, as it has been developed from observations from one drill hole.

The first mineral precipitated was magnetite. The second mineral was hematite, which was observed in a close relationship with magnetite with haematite often causing extensive martititsation of the magnetite along veins, fractures and the rims (Fig. 8a).

Pyrite was then precipitated together with minor haematite. This is evidenced by hematite growth on the outside of some pyrite crystals, all encased by later massive chalcopyrite growth (Fig. 8c).

Sphalerite precipitation was hard to constrain from only petrographic evidence, and was thought to have been precipitated either before or after pyrite ± haematite precipitation.

The hydrothermal system then moved to precipitate pyrite only, later moving to co-precipitate pyrite with the chalcopyrite showing infilling textures in and around pyrite crystals (Fig. 8c). Sphalerite could have also been precipitated here.

Later supergene alteration in the interpreted fault zone altered the chalcopyrite to native copper, malachite. This alteration was observed as being the last stage of ore mineralisation/alteration in ML001. No gold or uranium minerals were observed in the core.

4.2 Whole rock geochemistry

Whole rock analyses of the Myola Volcanics from drill core and hand specimen are presented in tables 1, 2 and 3. The field samples collected from the Myola Volcanics were used in this study as an unaltered reference baseline, to illustrate the relative depletion and enrichment of elements during alteration.

Caution should be taken with the interpretation of these results, as a low sample population has been used and implied element depletion or enrichment could be within normal rock variability.

4.2.1 MAJOR ELEMENTS

Unaltered and/or altered versions of the known host rocks of the Moola Prospect are shown in Table 1 with Figure 9 graphically showing their compositions.

Major element whole rock analyses show that geochemically the unaltered samples of the Myola Volcanics (rhyolites and quartz feldspar gneisses) were quite similar with a composition (%) of $SiO_2 \approx 72$, $Al_2O3 \approx 12.5$ $Fe_2O3 \approx 4$, $K_2O \approx 4$, $Na_2O \approx 3$, $TiO_2 \approx 0.5$, $MnO \approx 0.5$, $MgO \approx 0.1$, $CaO \approx 0.75$, $P_2O_5 \approx 0.05$, $SO_3 \approx .01$ being common. In contrast, the altered samples show a high degree of variability of their major elements with

approximate composition (%) values of 50-80 SiO2, 9-15 Al_2O_3, 1-16 Fe_2O_3, 0.5-5 MgO, 0.5-5 CaO, 0.5-4 Na_2O, 2-6 K_2O, .15-2.7 TiO_2, and 0.01-0.3 SO_3.

The compositional variability of the amphibolites was low and is probably within the range of normal variability of the composition of this rock type.

The rhyodacites show a high degree of geochemical variability, but as unaltered versions of the rhyodacite weren't found in the field these results cannot be compared to an unaltered version to illustrate enrichment/ depletion of elements. However these results do indicate the variability of enrichment and depletion of elements within this system, with composition of the two samples approximately varying 9% in SiO_2, 3% Al_2O_3, Fe_2O3 7%, MgO 3% CaO 2% K_2O 2% and TiO_2 1%.

Major element composition of the altered granite is similar to granitoid rocks, having a slightly elevated SiO_2 75.23% and a slight depletion in Fe_2O_3, however this can be attributed to alteration.

4.2.2 TRACE ELEMENTS

Trace element analyses of the unaltered and altered versions of the Myola Volcanics (Fig. 10) show the trace element content as being at overall low for that of crustal rocks, the Myola Volcanics show a distinct decrease from the large ion lithophile elements (LILE) to the high field strength elements (HFS). The uranium and potassium levels were observed as being elevated in most samples.

The compositional variability of trace elements of altered and unaltered Myola Volcanics show how some elements were distinctly enriched in the altered samples whilst others were depleted with an enrichment in U and Pb, and a depletion of Ba, Zr, Sr, Nb, La, Sm, Gd and Y (Fig. 10).

4.2.3 RARE EARTH ELEMENTS

Rare Earth Element (REE) data obtained from analyses of unaltered and altered samples of the Myola Volcanics are presented in a spidergram normalised against the REE concentration of chondrite meteorites (Boynton 1984) (Fig. 11).

Overall, the REE spidergram has a relatively flat pattern, with the unaltered samples having a mild enrichment in REE's ($\sum$ REE = 96.73- 642.64) exemplified by average REE concentrations of La=68.62, Ce= 163.62, Pr= 16.08 and Nd 58.87. REE enrichment also shows a distinct decrease from the light REE's to the heavy REE's (ave LaN/YbN=5.37, ave LaN/SmN= 3.31), with the heavy REE's having a very flat trend (EuN/YbN=0.89). All samples show a negative Eu anomaly. Slight disturbances of the Ce values illustrate the redox sensitivity of this element and may suggest fluctuation of fO_2 during the alteration process

The REE plot (Fig. 11) shows a very distinct, decrease in REE content between the altered and unaltered samples, with the altered samples being significantly depleted in REE's compared with the unaltered samples.

4.2.4 COMPOSITIONAL CHANGES DURING ALTERATION AND MINERALISATION

Due to relative changes of elements in ppm or percent during alteration and mineralisation a difficultly of quantifying compositional changes during alteration arises. As the enrichment of one element i.e. SiO_2 during silicification automatically results in a relative or apparent depletion of the unchanged (immobile) elements (Grant 1986; Baumgartner & Olsen 1995).

Isocon diagrams are a suitable way to envisage the relative compositional changes by plotting the composition(s) of altered rocks against the composition of the least altered sample of the same lithology (Grant 1986). Figures 12.1, 12.2 and 12.3 show the isocon plots for major element and figures 13.1, 13.2 and 13.3 show the isocon plots for trace and rare earth elements of the Moola Prospect mineralisation.

In these plots elements that were relatively enriched in the altered samples plot above the 1:1 median line, whilst elements that were relatively depleted plot below this line.

Major elements

Alteration of the Myola Volcanics rhyolite unit at the Moola Prospect (Fig. 12.1) shows distinct enrichment of CaO, MgO, MnO, and depletion in Fe_2O_3 and TiO_2.

The quartz-feldspar gneisses (Fig. 12.2) show a large variability of elements concentration of the altered samples, although they generally show enrichment in SO_3, MnO, P_2O_5 and MgO, and depletion in CaO, Na_2O and K_2O.

The amphibolites (Fig. 12.3) show little variability in major element composition and only an increase in SO_3 should be looked as being the only enrichment/depletion outside of possible rock variability.

Major element compositional changes during alteration and mineralisation of the three lithologies displayed in the isochon diagrams show, the altered samples tend to be enriched in SO_3, MnO, P_2O_5 and MgO, and depleted in the following elements; with Fe_2O_3, SiO_2, CaO, K_2O and Na_2O showing a high degree of variability in the altered samples.

Trace elements and Rare Earth Elements

Alteration of the Myola Volcanics rhyolite unit at the Moola Prospect (Fig. 13.1) shows distinct enrichment of Bi, Li, B, Ni, V, U, Pb, Rb, Cu, Mn and depletions in Ba, Ga, Zr, Y, Th, As and all the REE's.

The quartz-feldspar gneisses (Fig. 13.2) show a large variability of trace and rare earth element concentrations of the altered samples, although they generally show enrichment in Mn, Cu, Ni, Cr, Li, B, V, and a depletion in Ba, Ga, Zr, Y, Th, As and all the REE's.

The amphibolites (Fig. 13.3) show little variability in trace and rare earth element composition and only Bi, Cu, Pb, Li and U should be looked as enrichments outside possible rock composition variation.

Overall, across these three different lithologies it can be observed that, altered samples tend to be enriched in Bi, Cu, Pb, Li, U, Mn, Ni, Cr, B, V, Rb, and depleted in the following elements; Ba, Ga, Zr, Y, Th, As and all the REE's.

Alteration of the selected samples shows a distinct enrichment of copper greater than an order of magnitude, in addition to U, Bi, Li, B, Zn, Mn, Ni and Pb which likely represents the geochemical signature of the mineralising system.

4.3 Sulphur Isotopes

Sulphur isotopes are commonly used for the determination of the source for sulphur, which is commonly used to define the source(s) of mineralising fluids. Two major reservoirs of sulfur on the Earth exist that have uniform sulfur isotopic compositions: the mantle, which has δ34S of ~0 and in which sulfur is primarily present in reduced form, and modern seawater, which has δ34S of +20 and in which sulfur is present as SO_4^{2-} δ34S in sedimentary, metamorphic, and igneous rocks of the continental crust may have δ34S that is both greater and smaller than these values. All of these can be sources of sulfide in ores, and further fractionation may occur during transport and deposition of sulfides. Thus the sulfur isotope geochemistry of sulfide ores is remarkably complex. (White 2001)

Samples for sulphur isotope analysis were obtained for sulphides (chalcopyrite and pyrite) from the ML001 core (Table. 5, Figure 14).

The sulphides have a δ34S range of –10.5 to -1.2 ‰ with a mean of ≈ -7.8 ‰. The bulk of the values fall between -8 and -9 ‰. The chalcopyrite has a range of –10.5 to -5.4% with a mean of –8.41% whereas; the pyrite has a range of –8.0 to -1.2% with a mean of –5.7%.

4.4 Radiogenic Isotopes

One of these samples (MC004) was omitted as it produced spurious results, which has been attributed to an analytical error.

4.4.1 NEODYMIUM (Nd) AND SAMARIUM (Sm)

Previous work by Johnson & McCulloch (1995), Gleason *et al.* (2000) and Skirrow *et al.* (2007) has shown Sm-Nd isotopes in REE-IOCG hydrothermal systems, can act as effective tracers.

Neodymium and samarium results are presented in table 6 and 8, the neodymium ratio 143/144 of the samples have a range from 0.51134 to 0.51193 with a mean of 0.51169. The samarium to neodymium ratio 147/144 has a range from 0.10449 to 0.14664 with a mean of 0.12923. Both the neodymium ratio 143/144 and the samarium to neodymium ratio 147/144 give εNd (T_0) values ranging from -25.21872 to -13.83376 with a mean of -18.47472.

4.4.2 STRONTIUM (Sr)

The measured strontium isotopic ratios ($^{87}Sr/^{86}Sr$) have a range from 0.750298 to 1.585981 (Table. 7). This range is highly variable, with $^{87}Sr/^{86}Sr$ values being highly fractionated. Fractionations of the $^{87}Sr/^{86}Sr$ ratio results from a distortion of the Rb/Sr system, where ^{87}Sr is selectively taken up, ^{87}Sr is the daughter product of the decay or ^{87}Rb isotope, hence selective mobilisation of ^{87}Rb is a viable means to generate anomalous $^{87}Sr/^{86}Sr$ ratios.

4.5 Electron Probe Micro Analysis

Six polished sections were selected for Electron Probe Micro Analysis. These samples were selected from a range of different depths and lithologies, to provide insight into the compositional variation of the sulphides (pyrite, chalcopyrite and sphalerite) and the iron oxides (magnetite and haematite).

4.5.1 SULPHIDES

Sixteen elements were analysed (S, Fe, Cu, Zn, P, V, Mn, Co, Ni, As, Mo, Ag, Cd, Sb, Pb and Bi) in pyrite, chalcopyrite and sphalerite grains, with the electron microprobe. Due to technical difficulties experienced by the electron microprobe, in which one of the wavelength-dispersive spectrometers became increasingly defocused during the analyses thus rendering the elements Cu, Fe, and Zn as unreliable and could not be used in comparison against any of the other elements. The blocks were reanalysed to gain the composition Cu, Fe, Zn and S, so they could be compared against one another, but due to time constraints associated with the electron microprobe booking only these four elements were re-examined.

Electron Probe Micro Analysis (EPMA) of sulphide mineral species backs up petrological observations, that chalcopyrite, pyrite and sphalerite mineral species were present within the diamond drill core.

<u>Major elements</u>

Major element compositions of the sulphides display variation within all major elements (table 9.2) with figures 15.1, 15.2, 15.3 and 15.4 graphically showing this variation.

Chalcopyrite composition exhibits this variation with major element compositions (w %) showing sulphur ranging from 31.28 to 35.58 with an average of 34.73, iron 27.42 to 35.50 with an average of 29.63 and copper 27.42 to 36.82 with an average of 34.61.

These results when compared to the ideal chalcopyrite composition (S= 34.94, Fe= 30.43 and Cu= 34.63), show a large variation in sulphur content of chalcopyrite with both undersaturated and oversaturated varieties being present, iron also showed a large degree of variation from ideal chalcopyrite composition with both

undersaturated and oversaturated varieties being present. Copper also displays this variance from ideal copper values, with both undersaturated and oversaturated varieties being present.

Pyrite major element composition (w %) shows sulphur content ranging from 51.74 to 54.28 with an average of 53.48, iron 45.16 to 47.51.

These results when compared to the ideal pyrite composition (S= 53.45 and Fe= 46.55), shows pyrite at Moola Prospect ranges from being as slightly undersatured in both sulphur and slightly oversaturated in iron, to being slightly oversaturated in both sulphur and slightly undersaturated in iron. Copper content ranges from being concordant with ideal pyrite to being oversaturated.

Sphalerite major element compositions (w %) shows zinc ranging from 55.20 to 65.88 with an average of 61.33, sulphur 32.84 to 33.48 with an average of 33.25, iron 0.95 to 4.62 with an average of 2.57 and copper 0.62 to 5.20 with an average of 2.25.

These results when compared to the ideal sphalerite composition (Zn= 64.06, S= 33.06, Fe= 2.88 and Cu= 0), Zn values of the probed sphalerite, shows sphalerite commonly was largely undersaturated, with only a couple of probed sphalerite points being slightly oversaturated. Sulphur and iron values reveal that both sulphur and iron under and oversaturated varieties were present. All copper values were elevated against ideal sphalerite composition, with up 5.20 W % being recorded.

Trace elements

Trace element composition of the sulphides (chalcopyrite, pyrite and sphalerite), show distinct differences when compared to each other (e.g. Pyrite compared with chalcopyrite). Trace element data is presented in table 9.1, and figure 16 were trace element compositions have been plotted against sulphur (W %).

Chalcopyrite trace element content, when compared to pyrite shows that chalcopyrite was relatively enriched in P,V, Mn and Cd, and depleted in Co and As.

Sphalerite compositions when compared to average chalcopyrite shows, that sphalerite displays a close geochemical enrichment signature to chalcopyrite.

Pyrite compositions when compared to sphalerite compositions shows, that Pyrite was relatively enriched in Co, Pb and Bi and depleted in V and Cd.

Overall chalcopyrite composition shows large variation in its composition, with maximum chalcopyrite compositions showing large enrichment in some of the chalcopyrite in the following elements; As (1244ppm), Mo (2233ppm), Ag (1667ppm), Cd (1190 ppm), Pb (3177ppm) and Bi (3022ppm).

Sphalerite composition shows large enrichment in Mo, Cd, Pb and Bi with max values of 2257,1190, 1694, 1559 ppm respectively.

Pyrite trace element content shows significant variation, with maximum values for pyrite compositions showing large enrichment with some of the pyrite showing enrichments in the following elements; Co (1.1 wt %), Ni (1297ppm), As (5159ppm), Mo (1568, Ag (1115ppm), Pb (2616ppm) and Bi (4086ppm).

4.5.2 IRON OXIDES

Sixteen elements (O, Mg, S, Ti, V, Cr, Mn, Fe, Co, Ni, Cu, Zn, As, Ce, Pb and Bi) were analysed in magnetite and haematite grains, with the electron probe. The technical difficulties experienced with the sulphides were not encountered in the iron oxide analysis.

Electron Probe Micro Analysis of iron oxides species confirms petrological observations, that haematite and magnetite were present with an emphasis on determining their relationship with mineralisation/ alteration; in addition ilmenite has been identified, indicating Ti mobility during the mineralising event.

Major elements

Major element compositions of the iron oxides shows variation within all major elements (table 10) with figure 17 graphically showing this variation.

Haematite composition exhibits this variation with major element compositions (w %) with iron ranging from 62.34 to 68.58 with an average of 65.62 and oxygen from 27.27 to 29.49 with an average of 28.61. These results when compared to the ideal haematite composition (Fe= 69.94 and O= 30.06), show an undersaturation of both Fe and O when compared to all haematite points.

Magnetite major element compositions (w %) ranges in Fe from 65.34 to 70.11 with an average of 68.49 and oxygen ranging from 28.96 to 31.34 with an average of 29.94. These results when compared to the ideal magnetite composition (Fe=72.36 and O=27.64), show an undersaturation of iron and oversaturation of oxygen.

Ilmenite major element compositions (w %) shows a large range in titanium 23.69 to 40.69 with an average of 34.93, iron 11.90 to 40.69 with an average of 25.76, and oxygen 32.64 to 35.87 with an average of 34.45. These results when compared to the ideal ilmenite composition (Fe=36.81, O=31.63 and Ti=31.56), displays an undersaturation of iron and an oversaturation of titanium and oxygen in regards to their average composition. Min and max values of ilmenite, shows some ilmenite was grossly under saturated in titanium and iron in some data points and grossly oversaturated in others. Oxygen values reveal that oxygen was oversaturated in all ilmenite. Ilmenite shows a strong correlation (solid solution) between Fe and Ti.

Trace elements

Trace element composition of the Iron oxides (haematite, magnetite and ilmenite), shows distinct difference in trace element concentration when compared to the other iron oxides (e.g. Haematite compared with magnetite). Trace element data is presented in table 10, and in figures 18.1 and 18.2 were trace element data was plotted against Fe and O (W%).

Haematite's composition when compared to magnetite compositions shows that haematite was heavily enriched in V and Cu, with some points showing enrichment in Mg, Mn and Pb.

Magnetite compositions when compared to haematite, shows magnetite was relatively enriched in S, but a significant overlap was present with haematite. One data point shows a large enrichment in Co, but this was not representative as most values were below detection limit.

Ilmenite trace element compositions were highly variable, but when compared to haematite and magnetite, shows ilmenite was relative to depleted in regard to most trace elements with notable sporadic element enrichment of Zn and Cr.

Overall haematite was highly enriched in Ti, Mg and V with max values of Ti (8271ppm), Mg (3404ppm), V (5060ppm) with notable enrichment of Ni, Cu, As, Pb and Bi with max values of 730, 1007, 1036, 1834 and1964ppm respectively.

Magnetite trace element composition was also highly enrichment with max concentration of the following elements; Ti (4.96W %), Mg (1155ppm), Co (719ppm), Ni (630ppm), As (1035ppm) and Bi (1914ppm).

Ilmenite trace element composition shows enrichment in the max concentration in the following elements; Mg (1144ppm), V (1730ppm), Ni (815ppm), Zn (1632ppm), As (874ppm), Pb (985ppm) and Bi (1914ppm).

Trace element compositions show haematite and ilmenite share a lot of enrichment elements although ilmenite enrichment was a lot lower the exception being a couple points containing very high levels of zinc, these shared enrichments could indicate a relationship between the two.

Magnetite and haematite can be differentiated from each of as haematite contains larger concentrations of Mg, V, Cu and Pb.

5 INTERPRETATIONS OF RESULTS

5.1 Host rocks

The host rocks at the Moola Prospect, are a sequence of deformed and metamorphosed (greenschist to amphibolite facies); volcanic, magmatic and sedimentary (?) rocks.

Petrography of the Moola Prospect diamond drill core yielded six-host rock types; of these three dominate the core. The host rock types listed in order of most dominate to least dominate rock type in ML001 was as follows; porphryritic rhyolite, quartz-feldspar ±hornblende gneisses, rhyodacite, volcaniclastics, granite and amphibolite.

This sequence of rocks (excluding the granite) was petrologically similar to the Myola Volcanics of which they were presumed to belong to.

Whole rock major element analyses of host rock types, shows alteration can be both prevailing and sporadic, with the least altered samples being geochemically very similar to the Myola Volcanics. This coupled with the petrological similarities strongly suggests that the host rock type for mineralisation at the Moola Prospect is in fact as originally presumed the Myola Volcanics.

Trace element compositions of the volcanics were typical for within plate volcanism, with REE analyses displaying a mild enrichment of REE and especially LREE when compared to CHUR; this suggests derivation from a lower crustal melting, which is concordant with work previously completed on the Myola Volcanics by Parker *et al*. (1988) and fits with Giles & Betts (2006) proposed tectonic setting of the region during the Kimban Orogeny (When the Myola Volcanics were erupted).

Petrology and trace element composition of the granite shows similarities with the rhyolite unit within the core, which likely indicates an association between the two, with the granite possibly being derived from the anatexis of the rhyolite.

The ratio of $^{143}Nd/^{144}Nd$ in the altered samples as previously stated has a range from 0.51134 to 0.51193 with a mean of 0.51169. When this range was compared with the present-day chondritic $^{143}Nd/^{144}Nd$ ratio value of 0.512638, it was observed that the altered sample range was lower than that of the chondritic value (approximately equivalent to the bulk earth) of neodymium ($^{143}Nd/^{144}Nd$). The lower $^{143}Nd/^{144}Nd$ ratio values for the Moola Prospect mineralisation imply an evolved crustal setting for the analysed rocks or their precursors.

The samarium to neodymium ratio 147/144 has a range from 0.10449 to 0.14664 with a mean of 0.12923. Both the neodymium ratio 143/144 and the samarium to neodymium ratio 147/144 give εNd (T_0) values ranging from -25.21872 to -13.83376 with a mean of -18.47472.

The$^{147}Sm/^{144}Nd$ ratio values for the samples range from 0.10449 to 0.14664 with a mean of 0.12923. These and $^{143}Nd/^{144}Nd$ values can be used to calculate the approximate crustal residence time/ the approximate timing separation of the protolith from a possible crustal (chondritic) source (TCHUR) occurred. The calculated CHUR model ages for the samples range between 1958 to 2710Ma with an average separation age of 2185Ma. This variation in CHUR ages of the samples was quite large, and can be explained by the amphibolite (MC005) being separated earlier than the granite, and the other Myola Volcanic units. Classifying the amphibolite separately, it has a CHUR model age of 2710Ma; this classification also changes the range and average of the other Myola Volcanics, with the new range minus the amphibolite being between 1958 to 2131Ma with an average of 2056Ma (Fig. 20).

Calculating the age of possible mantle separation of the protolith, assuming a slightly more complex evolution (TDM?), reveals an age range from 2489 to 2628Ma with an average of 2530Ma for the samples minus the amphibolite, with the amphibolite giving a TDM age of 3134Ma.

Volcanics and granite samples show very close TDM and CHUR times further add to weight to the granite being derived from the anatexis of the volcanics, which suggests that the unnamed/ undated granite belongs to or was an equivalent of the Wertigo granite.

5.2 Alteration

Six alteration types have been documented and previously described from thin section and core observations, and subsequently placed in a paragenic order (Fig. 19).

Chlorite, albite and sericite alteration were volumetrically the most important types of alteration observed within the core, these alteration styles were also recognised in PIRSA thin sections of the Myola Volcanics type location approximately 2.2 km away. This indicates that a large Na (Ca-Fe), serecite, chlorite alteration halo exists around the Moola Prospect. Epidote alteration was also present in the PIRSA thin sections were it was present as a prevalent and prevailing style of alteration.

Sodic (Calcic-Iron) alteration was prevalent throughout the core in the form of albitisation of K-Feldspar and plagioclase.

Serecite alteration was widespread and characterised by serecite replacement of plagioclase and K-feldspar, sericite alteration was observed as a mild to complete replacement of plagioclase and K-feldspar with sericite alteration increasing towards small veinlets of sericite.

Chlorite alteration was the most prevalent and prevailing type of alteration throughout the entire core, and was commonly spatially associated with carbonate and quartz veining, and serecite with rare epidote alteration, with alteration increasing towards small chlorite veinlets.

Epidote was a very minor form of alteration at the Moola Prospect and was only observed in one slide in an association with both sericite and chlorite alteration in the Rhyodacite unit, this may represent a lithological control.

Quartz-carbonate veining economically was the most important type of alteration at the Moola Prospect as several stages of this multistage late carbonate/quartz flooding event, was mineralised. Quartz-carbonate veining was both prevalent and sporadic within the core, and shows a distinct, probably lithologically controlled zonation, from carbonate veining in the rhyodacite unit to quartz dominated veining in the more felsic units (rhyolites, felsic gneiss and unnamed granite), with a transitional zone in-between with quartz-carbonate veining.

Whole rock analyses of the unaltered and altered Myola Volcanics rock samples, provides a geochemical signature for some of the alteration styles observed in thin section and hand specimen, in addition to providing information about the scale at which some of these alteration styles operated at.

From major element data it can be interpreted that the alteration styles can be highly variable, with geochemical data of the Myola Volcanics showing a strong enrichment of Fe_2O_3, SiO_2, CaO, K_2O, Na_2O SO_3, MnO, P_2O_5 and MgO in some of the altered samples (Figs. 12.1, 12.2, 12.3). An enrichment of MgO in the altered samples likely represent the prevalent and prevailing chlorite-mica ± epidote style of alteration, with the strong enrichment of MgO being related to the high proportion of chlorite observed in thin section petrography of the altered host rocks.

Strong enrichment of CaO and/or SiO_2 in some of the altered samples but not others (Figs. 12.1, 12.2, 12.3), suggests that the quartz-carbonate alteration represented by this geochemical signature was sporadic in nature, which was of little surprise when observing the narrow, irregular veinlet of quatz-carbonte in the core. Depletion in SiO_2 in some of the altered samples could also represent the consumption of silica during the Na-Ca-Fe alteration event, that lead to the production of albite from mica and the anorthite component of plagioclase.

The common enrichment of SO_3 in the altered samples likely directly represents, alteration related to the precipitation of sulphide ore minerals. Alteration of the host rocks directly related to ore mineral precipitation can also be observed in figures 13.1, 13.2 and 13.3 with trace element enrichments of Cu, U, and Pb.

Unaltered samples also show geochemical evidence of some of the types of alteration namely Na-Ca-Fe (albite), sericite, chlorite-mica ± epidote which is concordant with field descriptions and thin section petrography, this indicates these alteration styles occur on a broad scale with the altered samples being collected some 2.2 km away from the Moola Prospect.

One of the most distinct geochemical patterns within this alteration system was the order of magnitude depletion of the rare earth elements in the altered Myola Volcanics. Other elements depleted within the system were Ba, Ga, Zr, Y, Th and As.

Barium can be present in K-feldspar and in the accessory mineral barite, both of which can be a major sink for REE. K-feldspar was usually one of the first minerals affected by Na-Ca alteration, this destruction of K-feldspar and/ or the destruction of barite could account for the depletion of Ba and REE element in the altered samples. Both Ba and REE were depleted by an order of magnitude and when Ba concentrations from unaltered to altered samples were plotted against the ∑REE it shows a strong correlation (Fig. 21), providing evidence that REE and Ba moved together in the system, and were possibly hosted within barite and/or K-feldspar.

In addition to petrological and geochemical results, strontium isotopic ratio's implies a "disturbed" Sr system, which was a common feature in strongly altered rock, especially for alkali (K) alteration which can drastically and selectively change the Sr and Rb content of a given rock. These results of the Sr isotope analysis confirm intense and most likely multiple alkali alteration occurred around the Moola Prospect. An indication of the affinity of the mineralising system cannot be inferred from the classic plot of εNd versus $^{87}Sr/^{86}Sr$, as the $^{87}Sr/^{86}Sr$ ratio was so highly fractionated that they do not plot in the area of field.

5.3 Mineralisation and ore paragenesis

Mineralisation at the Moola Prospect consists of the sulphide minerals; chalcopyrite, pyrite and minor sphalerite, and the iron oxides; magnetite, haematite and ilmenite. All sulphides show variation in major element composition with sulphur, iron, copper and zinc, undersaturations and oversaturations present.

Precipitation of these ore minerals, based on petrography was thought to have occurred during chlorite/epidote/carbonate/silicification alteration event(s). Mineralisation consists of sulphides (chalcopyrite, pyrite and sphalerite) and iron oxides (magnetite, haematite and ilmenite), with the iron oxides being disseminate and vein hosted, and the sulphides being hosted in narrow quartz, quartz-carbonate, carbonate veins.

These host veins have been analysed for fluid inclusions and coupled with Ti-quartz thermoboratary (Jones 2010) have given the conditions for mineralisation, with mineralisation taking place at ≈560 – 570°C at ≈5-6.8 Kbars.

Electron Probe Micro Analysis (EPMA) of sulphides show distinct compositional differences between sulphide species, these differences can be used to gives an insight in ore paragneiss.

High levels of copper in the sphalerite 0.62 to 5.20 W % when compared to ideal sphalerite composition shows a large enrichment of copper, which was observed under a microscope as chalcopyrite exsolutions in the sphalerite. This exsolution of chalcopyrite in the sphalerite can be interpreted as sphalerite precipitation occurring from a copper rich fluid, possibly just prior/ to coeval with chalcopyrite precipitation.

Copper concentration in pyrite shows a continuous increase of copper from below detection limit levels to 20091ppm copper (Fig. 22). This can be interpreted as pyrite growth being active before and until at least the time of the influx of the copper rich fluid into the system and precipitation of chalcopyrite, this is concordant with petrological observations that described pyrite forming before and coeval with the precipitation of chalcopyrite.

Sulphur isotopes (Fig. 14) further indicate at least two generations of pyrites with $\delta^{34}S$ (CDT) showing two distinct groups at -1 and -8 CDT, although the -1 CDT value is only one analysis it might represent a last stage of sulphide mineralisation, a stage not previously recognised from petrography. Lighter sulphur is preferentially taken up in the earlier stages of mineralisation as it was kinetically favoured in the initial hydrothermal system leaving the last stage with heavier sulphur isotopes. The highest frequency of $\delta^{34}S$ values of both chalcopyrite and pyrite occurs from -9 to -8. This adds further weight to precipitation of chalcopyrite and pyrite being coeval, or at least overlapping.

Electron Probe Micro Analyses of iron oxides shows magnetite and haematite compositions differ from one another in that haematite contains larger concentrations of Mg, V, Cu and Pb, and magnetite contains higher concentrations of Co. The higher levels of Cu in haematite indicate haematite formed closer to the copper mineralising event, which fits petrological observation placing haematite precipitation just prior to copper mineralisation

Electron Probe Micro Analyses of Trace element compositions in haematite and ilmenite shows that the two share a lot of composition similarities, with ilmenite's major difference being a larger enrichment of Zn. This

could represent ilmenite forming as a product of the alteration of haematite or that the two were precipitated coevally / near coevally.

Sulphur isotopes and EPMA were almost concordant with petrological observations, with the addition of a late stage pyrite mineralisation.

From petrological, EPMA and sulphur isotopes an ore paragenisis (Fig. 23) was developed to best describe ore mineral precipitation in the Moola Prospect diamond drill core ML001.

5.4 Sources of fluids

Sulphur isotope values are commonly used to gain an insight into the sources of fluid(s) associated with mineralisation, as well as showing ?any evolution of the hydrothermal system.

Analyses of Moola Prospect sulphur isotopes shows one distinct population for pyrite and chalcopyrite δ34S values within the Moola prospect, with one outlier (-1.2‰). This sulphur isotope distribution is typical for an evolving hydrothermal system where lighter sulphur is fractionated from the source into the fluid phase and incorporated into the crystal matrix first as is kinetically favoured. As the system evolves and the lighter sulphur is preferentially removed from the source, the fluid increasingly fractionates the heavier sulphur and thus the heavier isotope signature is observed in precipitates.

The Moola Prospect mineralisation was largely concordant with ore paragenesis of chalcopyrite and pyrite being co- precipitates or at least overlapping; however the heavy pyrite value (-1.2‰) was not explained by the ore paragenesis. The overall range of sulphur isotope values from -10.5 to -1.2‰ this indicates the source of sulphur was rather primitive and largely falls within Eldridge & Dantic (1994) δ34S range for Olympic Dam (Fig. 18), possibly indicating a magmatic fluid source.

Further evidence for a primitive or magmatic source can be ascertained from the whole rock trace element geochemistry with distinct enrichments of Li, B and V (Figs. 13.1, 13.2, 13.3). Enrichments of these elements imply a mantle source or in at least part a mantle influence in the fluid responsible for alteration and/ or mineralisation.

5.5 Source(s) of metals

Following the work of Johnson & McCulloch (1995), Gleason *et al.* (2000) and Skirrow *et al.* (2007) in proving the effectiveness of Sm-Nd isotopes as tracers in REE-rich iron oxide hydrothermal systems and the work Ridley & Diamond (2000) the isotopic composition of hydrothermal precipitates ultimately reflect prior isotopic exchanges between rock and fluid along fluid pathways. In the case of the Sm-Nd isotope system, mantle-derived rocks generally show primitive initial Nd isotope signature, whereas crustally derived rocks tend to have more evolved isotopic compositions and lower Nd contents (Skirrow *et al.* 2007).

Epsilon Nd (1590Ma) values are used within the Gawler Craton to allow comparison between IOCG deposits and Prospects of the area, the altered Myola Volcanics εNd (1590Ma) values range from -5.98 to -2.63 with an average of -4.05, and a value of -7.27 for the amphibolite (Table. 8). These values indicates a crustal, with possibly minor mantle input as the origin for the mineralising system and when compared against Johnson & McCulloch (1995) values of εNd (1590) for Olympic Dam show similarities, however Olympic Dam displays higher εNd (1590) values, ranging from -0.3 to -4.9 with an average at -2.7, indicating a higher mantle affinity of the metal source for Olympic Dam (Fig. 21).

Following the work of Johnson & McCulloch (1995) and Skirrow *et al* (2007), the εNd (1590) values were plotted against whole rock copper concentration in the altered host rocks, which produced a positive correlation between Cu and εNd (1590) as shown in figure 25.

This positive correlation can be interpreted as copper and neodymium being co-transported in the same hydrothermal fluid(s), and indicate a crustal derived evolved source with possible minor mantle input for neodymium and copper.

Cobalt : Nickel ratios in ore minerals have been used in many studies of ore genesis (Carstens 1941; Hegemann 1943; Gavelin & Gatinelson 1947; Hawley & Nichol 1961; Bajwah *et al.* 1987; Monterio *et al.* 2008) to discriminate between submarine exhalative, magmatic, sedimentary and hydrothermal origin. Pyrite is considered as being the most reliable indicator in ore genesis (Bralia *et al.* 1979; Mookherjee & Philip 1979; Bajwah, Seccombe & Offier 1987). Monterio *et al.* (2008) produced a Co: Ni ratio diagram depicting these

fields. Pyrite Co and Ni concentrations from the Moola Prospect have been plotted onto modified version of this figure (Fig. 26). Moola Prospect pyrite composition Co : Ni ratios range from below 0.01 to 121, however the majority of Co : Ni ratios were between 1 to 10, which plots the majority of pyrite's Co, Ni concentrations around and/or in the volcanogenic, hydrothermal and magmatic fields, possibly showing a mixed metal source with magmatic input. Three of the Co: Ni ratio's plotted in the sedimentary field, however no petrological evidence was found for sedimentary pyrite in ore microscopy.

6. DISCUSSION

6.1 IOCG alteration in the Gawler Craton

Iron oxide Cu-Au deposits are formed under diverse geological environments and in a range of different host rock types. Source fluid chemistry variability is evident from enrichment of different minor elements associations between deposits and from fluid inclusion studies. This high degree of variability in the fundamentals of deposits produces the many different alteration assemblages observed in IOCG provinces (Mark, Williams 2000).

The Moola Prospect Cu mineralisation displays some of the alteration assemblages commonly associated with IOCG deposits in the Gawler Craton, and other IOCG provinces. Two of the four-principle alteration mineral assemblage recognised in the Olympic Province (Skirrow *et al* 2002; Skirrow *et al* 2007; Skirrow *et al* 2008) were recognised in the Moola Prospect diamond core.

Albite-actinolite±magnetite (Williams 2008), Sodic-calcic (Barton & Johnson, 1996), or Na-Ca-Fe alteration is described in many of the IOCG provinces globally, including the Gawler Craton (Barton & Johnson 1996; Hitzman 2000; Williams *et al*.. 2005; Skirrow 2008).

Albite-actinolite±magnetite alteration style was present in the Moola Prospect diamond drill core and was described in this paper as Na-Ca-(Fe) albite alteration.

The albite-actinolite±magnetite alteration assemblage as described by Williams (2008) differs from the Na-Ca-(Fe) albite alteration style observed in the Moola Prospect diamond drill core in that no actinolite was observed. Also whether the magnetite observed in the core was part of this assemblage is unclear, however petrological and geochemical data indicate the magnetite was precipitated before the major sulphide mineralising event, therefore magnetite mineralisation could have occurred in the Moola core during this alteration event.

This style of alteration is often observed as a kilometre-scale regional alteration (Skirrow *et al.* 2008), which it was around the Moola Prospect evident from geochemical and petrological observation of the Myola Volcanics in the core and at their type location.

The main mineralisation assemblage associated with IOCG deposits in the Olympic Domain is the haematite-sericite -chlorite-carbonate ± Fe & Cu sulphides, ± U and REE bearing minerals (Skirrow et al. 2008, Cerlienco, 2009). This assemblage is observed as the main mineralisation assemblage at Olympic Dam, Prominent Hill and Emmie Bluff, which suggests this style of alteration, is temporally associated with IOCG style mineralisation (Bastrakov *et al.* 2007; Cerlienco 2009)

In the Moola drill core the main alteration event associated with the mineralisation was the quartz-carbonate veining, which was concurrent with the sericite and chlorite-mica-epidote alteration styles. These form a chlorite-sericite - (quartz-carbonate)-epidote alteration assemblage, which correlates well with the haematite-sericite -chlorite-carbonate alteration assemblage described by Skirrow *et al.* (2008). These two alteration assemblages differ markedly, with the Moola alteration assemblage significantly lacking in haematite.

Fluid inclusion analysis and quartz-Ti thermobarometry of these quartz-carbonate veins (Jones 2010) associated with the chlorite-sericite - (quartz-carbonate)-epidote alteration assemblage have yielded a high temperature (560-570 C) deep crustal alteration for this alteration assemblage.

The absence of the biotite-magnetite alteration assemblage was noted, which is commonly observed in the Olympic Domain, and represents a focused potassic alteration.

One of the striking differences from other IOCG deposits of the Gawler Craton with the Moola Prospect was the severe lack of iron oxides with depletion of total Fe_2O_3 of most altered rocks observed in core, however sporadic mild Fe2O3 enrichment was also observed in the core.

6.2 Alteration geochemistry of IOCG deposits and fertility of the region

Literature on the elemental changes due to alteration associated with IOCG deposits within the Gawler Craton is sparse. In general IOCG's exhibit a high variability in Cu: Au ratios and display no single consistent minor element association however IOCG's in the Gawler Craton are commonly associated with enrichments of F, Ba, LREE, U, Co and Mo in some cases to economic levels. The Moola Prospect displays order of magnitude depletion in REE and Ba, and sporadic enrichment of U up to approximately an order of magnitude, with minor enrichments in Ni, Zn and Pb. As previously stated the Fe_2O_3 values for the Moola core was low in comparision to other Gawler Craton IOCG deposits, which are characterised by large enrichments of Fe_2O_3.

Sulphur isotopes and εNd values are commonly used to compare differences in the IOCG deposits of the Gawler Craton and other IOCG provinces. With sulphur isotope analysis of various locations in the Olympic Cu-Au Province, showing Olympic Dam has a lighter sulphur isotopes signature (-10 to -5 ‰) than many of the other barren or sub economic prospects (~ -5 to 10 ‰ CDT).

Values from the Moola Prospect displays a δ34S range from –10.5 to -1.2 ‰ (Fig. 24) with a mean of ≈ -7.8 ‰, this places the Moola Prospect around the same isotopic range as Olympic Dam with the exception of the significant outlier one same with a value of -1.2‰,

Difference in sulphur isotope signatures is thought to relate to differences in the fluid sources, with Olympic Dam thought to have a larger fluid input from mantle derived origin than the sub economic prospects. The source of mineralising fluids at the Moola Prospect is thought to be like that at Olympic Dam being from a mantle-derived origin, albeit at a much lower level.

Epsilon Nd (1590Ma) values are commonly used within the Gawler Craton to allow comparison between IOCG deposits and Prospects of the area, the altered Myola Volcanics εNd (1590Ma) values range from -6.46 to -2.63 with an average of -4.05 and -7.27 for the amphibolite. These values indicates a crustal, with possibly minor mantle input as the origin for the mineralising system and when compared against Johnson & McCulloch (1995) values of εNd (1590) for Olympic Dam show similarities, however Olympic Dam displays higher εNd (1590) values, ranging from -0.3 to -4.9 with an average at -2.7, possibly indicating a higher input of metal from a mantle source for Olympic Dam.

Skirrow et al (2007) has provided a model for the classification of IOCG prospects, based on εNd (1590) and δ34S values the prospects are divided into barren/ minor Cu and major deposit, with major deposits having a major mantle input and barren/ minor Cu having a crustal/ local source. The Moola prospect under Skirrow *et al.* (2007) classification (Fig. 24), shows the Moola prospect lies in-between the major and minor/ barren deposits, which is concordant with the sources of metal showing evidence for a mixed source with limited mantle input.

Epsilon Nd(1590Ma), Co : Ni ratios of pyrites and Cu V εNd(1590Ma) indicates the source for metals of the mineralisation was from a evolved crustal source with a minor to mild mantle input. εNd (1590Ma) values fall within the ranges for both major and minor deposits/ barren.

Mineralising fluid temperature data in the Olympic Province is limited, however Bastrakov (2007) calculating a range of mineralising fluids from 250 and 800°C for several of the sub economic prospects in the region. The Olympic Dam deposit displays a decrease in temperature from 400°C to 200°C as the fluid moved from precipitating magnetite to hematite (Oreskes & Einaudi 1992). Limited research has investigated any possible correlations between mineralising fluid temperatures and ore grade (Cerlienco 2009). The temperature range of the Moola Prospect was determined by Jones (2010) with a median temperature range between 560-570ºC, putting the Moola Prospect within the temperature range of the other Gawler Craton deposits.

7 CONCLUSION

The Moola Cu-Au Prospect broadly fits with some of the geological and mineralogical framework of other IOCG deposits of the Gawler Craton.

This research established and described several essential parameters of the mineralisation. These include host rock lithology, alteration paragenesis, ore paragenesis, bulk rock geochemistry, sulphide and iron oxide geochemistry and radiogenic isotope signatures.

The host rock lithology was confirmed to be a sequence of the Myola Volcanics with the addition of an

unnamed/ undated pink fine to medium grained K-feldspar-quartz-plagioclase-micaceous± sodic amphibole granite likely derived from the anatexis of the Myola Volcanics.

Ore microscopy identified and paragenetically defined the ore mineralogy, with chalcopyrite, pyrite, sphalerite, haematite, magnetite and ilmenite being present as primary mineralologies. Later supergene alteration in the interpreted fault zone altered the chalcopyrite species into native copper and malachite. These minerals were then placed into a sequence thought to best describe the ore paragenesis of drill hole ML001 (Fig. 23).

Radiogenic isotope signatures provide insight into fluid and metal source for the Moola Prospect mineralisation, with δ34S data indicating a primitive/ magmatic fluid source, with sulphur isotope values largely fall within Eldridge's (1994) δ34S range for Olympic Dam.

Epsilon Nd(1590Ma), Co : Ni ratios of pyrites and Cu V's εNd(1590Ma) indicates the metals source as being an evolved crustal source with a minor to mild mantle input. εNd (1590Ma) values fall within the ranges for both major and minor deposits/ barren.

The similarity in geological setting, alteration mineralogy and isotope geochemistry links the Moola Prospect with other IOCGs of the Olympic Domain.

Whether the Moola Prospect is an IOCG style mineralisation is still unclear, as although it has several similarities with IOCG deposits in the Olympic Domain such as geological setting, alteration mineralogy and isotope geochemistry, it lacks some of the important elemental characteristics of IOCG deposits i.e. low Fe_2O3 content and its large depletion in Ba and REE.

ACKNOWLEDGEMENTS

Firstly, I would like to thank my supervisor Andreas Schmidt Mumm for his guidance and support throughout the year, in both the field and laboratory. OneSteel for both funding this research, as well as provided invaluable support in the field, in particular Geoff Johnson and Chris Wilcox. Angus Netting at Adelaide Microscopy for his tutorials and guidance in the use of the Electron Probe, Ben Wade and Aoife McFadden for carrying out my Solution-ICPMS analysis's, as well as John Stanley who both guided me through various devices within the university and carried out XRF analysis. David Bruce for his guidance and technical assistance in relation to analytical procedures and the subtleties of radiogenic isotope work. David and Keryn Groom at PIRSA'a Glenside Drillcore Storage Facility, who managed to *rediscover* rock samples for me, Marc Davies (PIRSA) for tracking down thin sections of the Myola Volcanics and subsequent petrological report. I would also like to thank Ryan Jones who worked on this project with me, and the entire Honours class of 2010 for making this year so enjoyable.

REFERENCES

AUSTRALASIACONSOLIDATED LTD. 1999. Eyre Peninsula, South Australia - *Murninnie Project*. Online <http://www.australasiaconsolidated.com.au/html/eyrepen.htm>

BAJWAH Z.U., SECOMBE P.K. & OFFLER R. 1987. Trace element distribution, Co:Ni ratios and genesis of the Big Cadia iron–copper deposit, New South Wales, Australia, *Mineralium Deposita* **22**, pp. 292–300.

BAROVICH K., SZPUNAR M., HAND M., JAGODZINSKI E. 2008. Depositional age and provenance of the Paleoproterozoic Hutchison Group, southern Gawler Craton, South Australia. *Geological Society of Australia Abstracts*, 50–51.

BARTON M. D. & JOHNSON D. A. 1996. Evaporitic source model for igneous-related Fe oxide–(REE–Cu–Au–U) mineralization. *Geology* **24**:259–262

BARTON M. D. & JOHNSON D. A. 2004. Footprints of Fe-oxide(-Cu-Au) systems. *SEG 2004: Predictive Mineral Discovery Under Cover. Centre for Global Metallogeny, Special Publication* **33**, 112-116.

BASTRAKOV E.N., SKIRROW R.G., Davidson G.J. 2007. Fluid evolution and origins of iron oxide Cu-Au prospects in the Olympic Dam district, Gawler craton, South Australia: *ECONOMIC GEOLOGY*, **102**, p. 1415–1440.

BAUMGARTNER L.P & OLSEN S.N. 1995. A least-squares approach to mass transport calculations using the isocon method. *Economic Geology.* **90**, pp. 1261–1270.

BELPERIO A., FLINT R. & FREEMAN H. 2007. Prominent Hill: A hematite-dominated, iron oxide copper-gold system. *Economic Geology*. **102**, 1499-1510.

BETTS P.G., GILES D. 2006. The 1800–1100Ma tectonic evolution of Australia. *Precambrian Research* **144**, 92–125.

BOYNTON W. V. 1984. Cosmochemistry of the rare earth elements: meteorite studies. *In: Henderson P. ed. Rare Earth Element Geochemistry*, pp. 63-114. Elsevier, Amsterdam.

BRALIA A, SABATINI G. & TROJA F. 1979. A revaluation of the Co/Ni ratio in pyrite as a geochemical tool in ore genesis problems. *Miner. Deposita* **14**, pp. 353–374.

CARSTENS C. W.1943. Über den Co-Ni-Gehalt norwegischer Schwefelkiesvorkommen. *Kgl. Norske Videnskab. Selskabs, Forh*. **15**, 165-168.

CERLIENCO B. 2009. Geological Setting and alteration characteristics of the Hillside Mineralizing System, Yorke Peninsula. Geology and Geophysics. Adelaide, University of Adelaide. B Sc. (hons), (unpublished).

CONOR C. H. H. 1996. Curnamona, Moonta and Cloncurry: Common styles of alteration and mineralization linked by the Diamantina Orogen.

CORRIVEAU L. 2006. Iron Oxide Copper-Gold (±Ag ±Nb ±REE ±U) Deposits: A Canadian Perspective. *Mineral Deposits of Canada: Deposit Synthesis*. Geological Survey of Canada.

CREASER R.A., FANNING C.M. 1993. A U–Pb zircon study of the Mesoproterozoic Charleston Granite, Gawler Craton, South Australia. *Australian Journal of Earth Sciences* **40**, 519–526.

CURTIS S. 2007. *The geology and mineral potential of the Port Augusta area, eastern Gawler Craton. South Australia*. Department of Primary Industries and Resources. Report Book 2007/6.

DALY S.J., FANNING C.M. 1993. Archaean. In: Drexel, J.F., Preiss, W.V., Parker, A.J. (Eds.). The Geology of South Australia, vol. 1, *The Precambrian. Geological Survey of South Australia*, Bulletin **54**.

DREXEL J.F. 1976. *The geology of Mt Laura, Whyalla, South Australia. South Australia*. Department of Mines. Report Book, **76/146**.

ELDRIDGE CS. & DANTI K. 1994. Low sulfur isotope rates; high gold values; a closer look at the Olympic Dam Deposit via SHRIMP Abstract with Programs, *Geological Society of America* **26**:498–499

FAIRCLOUGH M. 2005. Geological and metallogenic setting of the Carrapateena FeO-Cu-Au prospect - a PACE success story. *MESA Journal* **38**, 4-7.

FANNING C.M., BLISSETT A.H., FLINT R.B., LUDWIG K.R., PARKER A.J. 1986. A refined geological history for the southern Gawler Craton through U–Pb zircon dating of acid volcanics, and correlations with northern Australia. In: *8th Australian Geological Convention, Adelaide, 1986*. Geological Society of Australia. Abstracts, **15**:67-68.

FANNING C.M., FLINT R.B., PARKER A.J., LUDWIG K.R., BLISSETT A.H. 1988. Refined Proterozoic evolution of the Gawler Craton, South Australia, through U–Pb zircon geochronology. *Precambrian Research* **40/41,** 363–386.

FANNING C.M., OLIVER R.L. & Cooper, J.A. 1981. The Carnot Gneisses, southernmost Eyre Peninsula. South Australia. *Geological Survey. Quarterly Geological Notes*, **80**:7-12.

FERRIS G. M., SCHWARZ M. P. & HEITHERSAY P. 2002. The Geological Framework, Distribution and Controls Of Fe-Oxide-Cu-Au Mineralisation In The Gawler Craton, South Australia. Part I - Geological And Tectonic Framework. In: Porter T. M. ed. *Hydrothermal Iron Oxide Copper-Gold & Related Deposits: A Global Perspective 2 PGC Publishing*, Adelaide.

FERRIS G.M. & SCHWARZ M.P. 2003. Proterozoic gold province of the central Gawler craton: *MESA Journal*, **30**, p. 4–12

FRASER G., MCAVANEY S., NEUMANN N., SZPUNAR M. & REID A. 2010. Discovery of early Mesoarchean crust in the eastern Gawler Craton, South Australia. *Precambrian Research* Volume **179**, Issues 1-4, May 2010, Pages 1-21

GAVELIN S. & GABRIELSON O. 1947. : Spectrochemical investigations of sulphide minerals from the ores of the Skellefte» district. *Sveriges Geol. Undersoka* **41**, 1-45.

GILES C.W. 1977. Rock units in the Gawler Range Volcanics, Lake Everard area, South Australia. *Geological Survey of South Australia, Quarterly Geological Notes*, **61**.

GILES C.W., GOODE A.D.T. & LEMON N.M. 1980. Middle Proterozoic volcanism and sedimentation in the Moonabie area. In: Parker, A.J. (Compiler), *Symposium on the Gawler Craton, 11 December 1979. Geological Society of Australia. Journal*, **27**:53.

BETTS P G & GILES D. 2006. The 1800-1100 Ma tectonic evolution of Australia, *Precambrian Research*, 144, p.92-125.

GLEASON J.D., MARIKOS M.A., BARTON M.D. & JOHNSON D.A. 2000. Neodymium isotopic study of rare earth element sources and mobility in hydrothermal Fe oxide (Fe-P-REE) systems: *Geochimica et Cosmochimica Acta*, **64**, p. 1059–1068.

GOW P.A., WALL V.J., OLIVER N.H.S. & VALENTA R.K. 1994. Proterozoic iron oxide (Cu-U-Au-REE) deposits: Further evidence of hydrothermal origins: *Geology*, v. **22**, p. 633-636.
GRANT J.A. 1986. The Isocon diagram—a simple solution to Gresens' equation for metasomatic alteration, *Economic Geology* **81** (8), 1976–1982

GROVES D.I., BIERLEIN F.P., MEINERT L.D. & HITZMAN M.W. 2010. Iron Oxide Copper-Gold (IOCG) Deposits through Earth History: Implications for Origin, Lithospheric Setting, and Distinction from Other Epigenetic Iron Oxide Deposits. *Economic Geology; May 2010*; v. **105**; no. 3; p. 641-654; DOI: 10.2113/econgeo.105.3.641
HAND M., REID A. & JAGODZINSKI L. 2007. Tectonic framework and evolution of the Gawler craton, southern Australia. *Economic Geology* **102**, 1377-1395.
HAWLEY J.E. & NICHOL I. 1961. Trace elements in pyrite, pyrrhotite and chalcopyrite of different ores. *Economic Geology*. **56** pp. 467–487.

HEGEMANN F. 1943. Die geochemische Bedeutung von Kobalt und Nickel in Pyrite. *Z. Angew. Mineral*. **4**, 122-239
HELIX LTD. 1994. Annual Report Exploration License EL 2763 Middleback Ranges: for period 1st January 1994 to 31st December 1994 (unpublished).
HELIX LTD. 2001. Annual Report Exploration License EL 2763 Middleback Ranges: for period 1st January 2001 to 31st December 2001((unpublished).
HITZMAN M. W. & VALENTA R. K. 2005. Uranium in iron oxide-copper-gold (IOCG) systems. *Economic Geology* **100**, 1657-1661.
HITZMAN M. W. 2000. Iron Oxide-Cu-Au Deposits: What, Where, When, and Why. In: Porter T. M. ed. *Hydrothermal Iron Oxide Copper-Gold & Related Deposits: A Global Perspective*, pp. 9-25. 1, Adelaide.
HITZMAN M. W., ORESKES N. & EINAUDI M. T. 1992. Geological characteristics and tectonic setting of Proterozoic iron-oxide (Cu-U-Au-REE) deposits. *Precambrian Research* **58**, 241-287.
JOHNSON J.P. & Cross K.C. 1995. U-Pb geochronological constraints on the genesis of the Olympic Dam Cu-U-Au-Ag deposit, South Australia: *Economic Geology*, v. **90**, p. 1046-1063.
JOHNSON J.P. & MCCULLOCH M.T. 1995. Sources of mineralising fluids for the Olympic Dam deposit (South Australia): Sm-Nd isotopic constraints. Chemical Geology **121**, 177-199.
JONES M.T. 1970. Summary Report on the Pandurra Prospect, S.M.L. 204, South Australia. Department of Mines and Energy. Open File Envelope 01174. (unpublished).
JONES R. 2010. Cu Mineralisation in the Middleback Ranges: Conditions of Mineralisation. Geology and Geophysics. Adelaide, University of Adelaide. B Sc. (hons), (unpublished).
MARK G. & FOSTER D.R.W. 2000. Magmatic-hydrothermal albite-actinolite-apatite-rich rocks from the Cloncurry district, NW Queensland, Australia: *Lithos*, v. **51**, p. 223-245.

MASON M.G. 1980. Myall Creek Copper Prospect. Mineral Resources Review, 151:58-64.
MILES K.R. 1954. The geology and iron ore resources of the Middleback Range area. South Australia. *Geological Survey*. Bulletin, **33**.
MONTEIRO L.V.S., XAVIER R.P., HITZMAN M.W., JOHNSON C.A., CARVALHO E.R., SOUZA FILHO C.R. & TORRESI I. 2008. Spatial and temporal zoning of hydrothermal alteration and mineralization in the Sossego iron oxide–copper–gold deposit, Carajás Mineral Province, Brazil: paragenesis and stable isotope constraints, *Mineralium Deposita* **43**, pp. 129–159
MOOKHERJEE A., PHILLIP R. 1979. Distribution of copper, cobalt and nickel in ores and host-rocks, Ingladhal, Karnataka, India. *Mineral. Deposita* **14**, 33-55
NIXON L.G.B. 1975. The stratigraphy and structure of the Moonabie Formation at Mount Laura, South Australia. South Australia. *Geological Survey. Quarterly Geological Notes*, **56**:10-12.
ORESKES N. & EINAUDI M. T. 1992. Origin of hydrothermal fluids at Olympic Dam; preliminary results from fluid inclusions and stable isotopes. *Economic Geology* **87**, 64-90.
PARKER A.J. 1981. *Structural and metamorphic controls on the origin of nephrite jade near Cowell, South Australia. South Australia*. Department of Mines and Energy. Report Book, **81**/114
PARKER A.J. 1983. *Precambrian correlation of the Lake Superior region, North America, and the Gawler Craton. South Australia.* Department of Mines and Energy. Report Book, **83**/80.
PARKER A.J. 1993. Paleoproterozoic. In: Drexel, J.F., Preiss, W.V. Parker, A.J. (Eds.). *The geology of South Australia*, vol. **1**. The Precambrian. Geological Survey of South Australia, Bulletin 54.
PARKER A.J., FANNING C.M., FLINT R.B. 1985. Geology. In: Twidale, C.R., Tyler, M.J., Davies, M. (Eds.), *Natural History of Eyre Peninsula.* Royal Society of South Australia, pp. 21–55.
PARKER A.J., FANNING C.M., FLINT R.B., MARTIN A.R. & RANKIN L.R. 1988. *Archaean–Early Proterozoic granitoids, metasediments and mylonites of southern Eyre Peninsula, South Australia*. Geological Society of Australia. Specialist Group in Tectonics and Structural Geology. Field Guide Series, 2.
PARKER A.J.& LEMON N.M. 1982. *Reconstruction of the Early Proterozoic stratigraphy of the Gawler Craton, South Australia.* Journal of the Geological Society of Australia **29**, 221–238.
PIRSA. 2010. South Australia's Major Operating Mines and Mineral Development Projects Resource Estimates and Production Statistics. Online
<http://www.minerals.pir.sa.gov.au/__data/assets/pdf_file/0003/69312/000_resourcestable4.pdf?
POLLARD P. J. 2006. An intrusion-related origin for Cu-Au mineralization in iron oxide-copper-gold (IOGG) provinces. *Mineralium Deposita* **41**, 179-187.
RIDLEY J.R. & DIAMOND L.W. 2000. Fluid chemistry of orogenic lode gold deposits and implications for genetic models: *Economic geology*, **95**, p. 141–162.
SKIRROW R. G. 2008. '*Hematite-group' IOCG±U ore systems: Tectonic settings, hydrothermal characteristics, and Cu-Au and U mineralizing processes. Exploring for Iron Oxide Copper-Gold Deposits: Canada and Global Analogues Shortcourse Notes*, GAC-MAC-SEG-SGA 2008, Quebec City, 29-30th May 2008 X. Geological Association of Canada.

SKIRROW R. G., BASTRAKOV E. N., DAVIDSON G. J., RAYMOND O. L. & HEITHERSAY P. 2002. The Geological Framework, Distribution and Controls of Fe-oxide Cu-Au Mineralisation in the Gawler Craton, South Australia. Part II - Alteration and Mineralisation. In: Porter T. M. ed. *Hydrothermal Iron Oxide Copper-Gold & Related Deposits: A Global Perspective*, pp. 33-47. 2 PGC Publishing, Adelaide.

SKIRROW R.G., BASTRAKOV E.N., BAROVICH K, FRASER G.L, CREASER R.A., FANNING C.M., RAYMOND O.L. & DAVIDSON G.J. 2007. Timing of iron oxide Cu-Au-(U) hydrothermal activity and Nd isotope constraints on metal sources in the Gawler craton, South Australia: Economic geology, v. **102**, p. 1441–1470.

SKIRROW R.G., FAIRCLOUGH M.C., BUDD A.R., LYONS P., RAYMOND O., MILLIGAN P., BASTRAKOV E., FRASER G., HIGHET L., HOLM O. & Williams N. 2006. *Iron oxide Cu-Au (-U) potential map of the Gawler craton, South Australia:* Geoscience Australia, Canberra, 1:500 000 scale, 1st ed.
www.ga.gov.au/minerals/research/regional/gawler/gaw_mapgis.jsp.

SUN S.S. 1980. Lead isotopic study of young volcanic rocks from mid ocean ridges, ocean islands and island arcs. *Phil. Trans. Royal Soc. Lond.*, **A297**, 409–45.

SCHWARZ. M.P., MORRIS B.J., SHEARD M.J., FERRIS G.M., DALY S.J. & Davies M.B. 2005. Chapter 4:Gawler Craton, *In: South Australian mineral explorers guide*, PIRSA

SZPUNAR M., HAND M., BAROVICH K., JAGODZINSKI E. 2007. Age and Provenance of the Paleoproterozoic Hutchison Group, southern Gawler Craton, South Australia. Deformation in the Desert, Specialist Group in Tectonics and Structural Geology, Geological Society of Australia, abstracts

THOMSON B.P. (COMPLIER) 1980. Geological map of South Australia. South Australia. Geological Survey. Maps of South Australia Series, 1:1 000 000.

VASSALLO J. J. & WILSON J. L. 2001. Structural repetition of the Hutchison Group metasediments, Eyre Peninsula, South Australia. *Australian Journal of Earth Sciences*, **48**: 331–345. doi: 10.1046/j.1440-0952.2001.00859.

White, W. M. 2001. Geochemistry. J. H. U. Press.

WILLIAMS P.J., BARTON M.D., JOHNSON D.A., FONTBOTE L., HALLER A., MARK G., OLIVER N.H.S., MARSCHIK R. 2005. Iron oxide copper–gold deposits: geology, space–time distribution, and possible modes of origin. *Economic Geology* **100**, pp 371–406

Figures

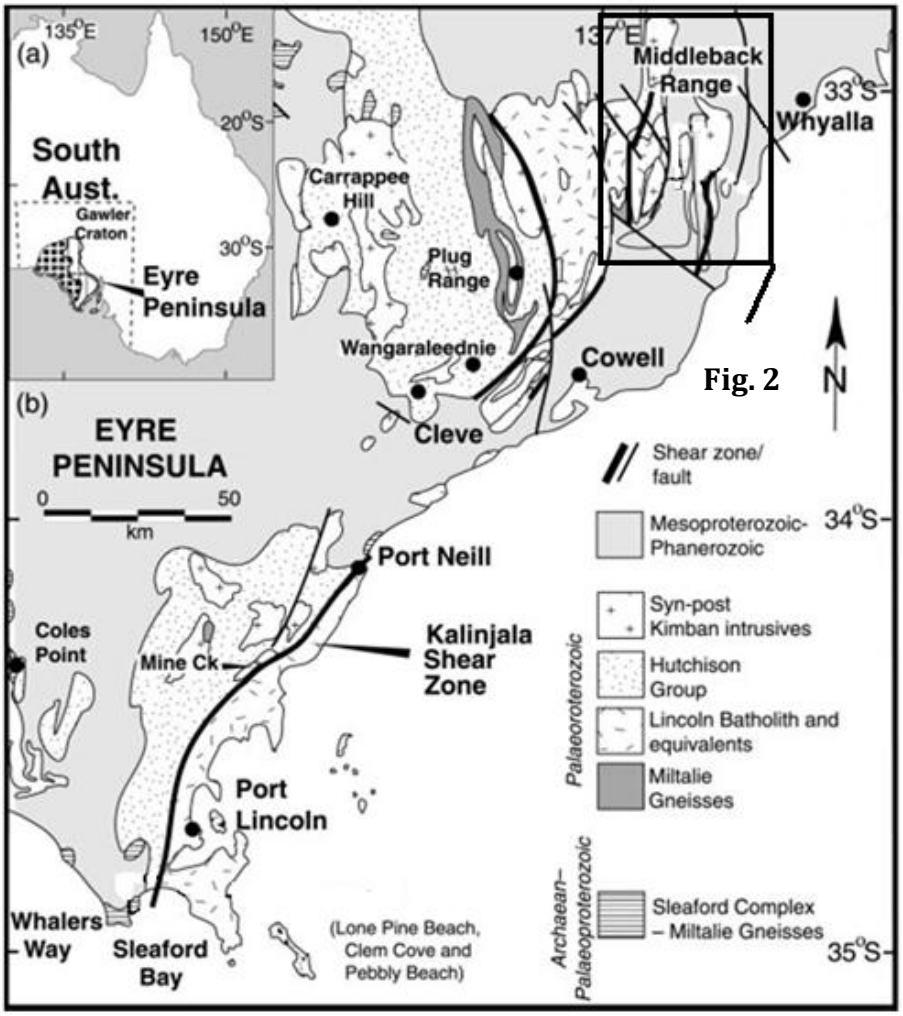

Figure 1: (a) Eyre Peninsula and Gawler Craton, South Australia.Eyre Peninsula consists of Archaean–Palaeoproterozoic basement in the west (stippled) and younger Palaeoproterozoic sequences in the east .(b) Outline of the main structural elements of Eyre Peninsula (after Parker 1993) modified from Vassallo and Wilson (2001)

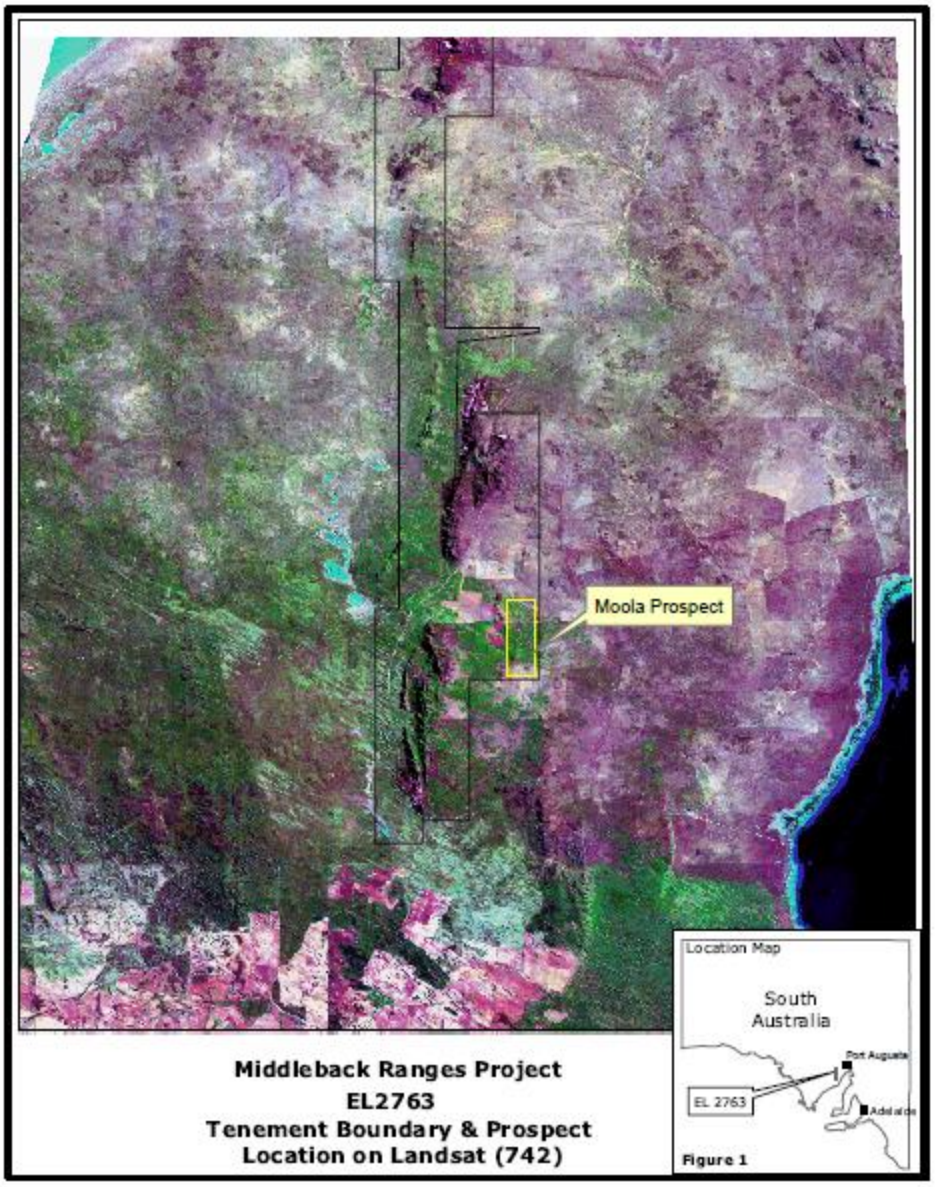

Figure 2: Southern Middleback Ranges with Moola Prospect. Modified from Helix 2001

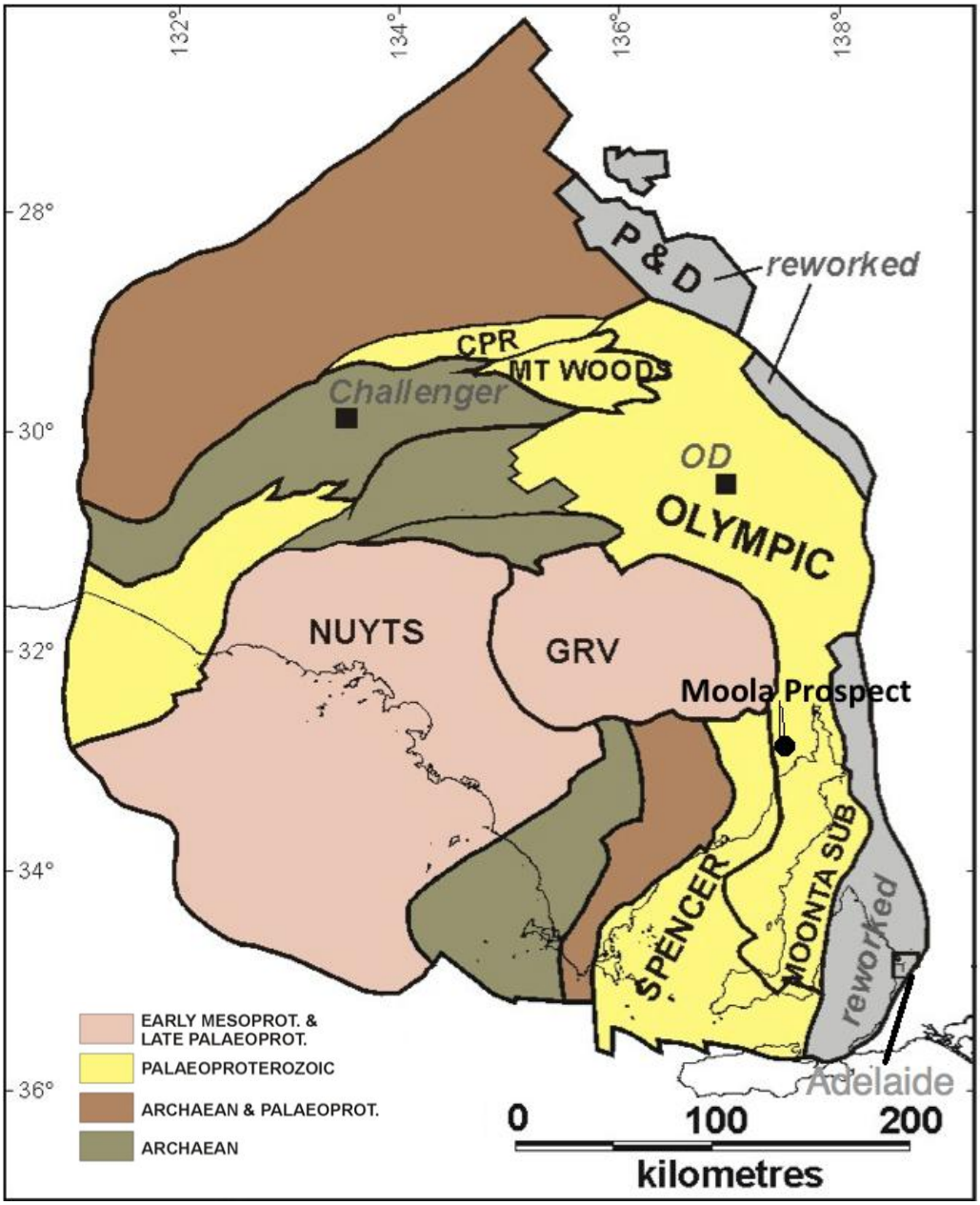

Figure 3: Geological provinces of the Gawler Craton, with the location of the Challanger gold mine, Olympic Dam IOCG and the Moola Prospect modified from Ferris et al. (2002).

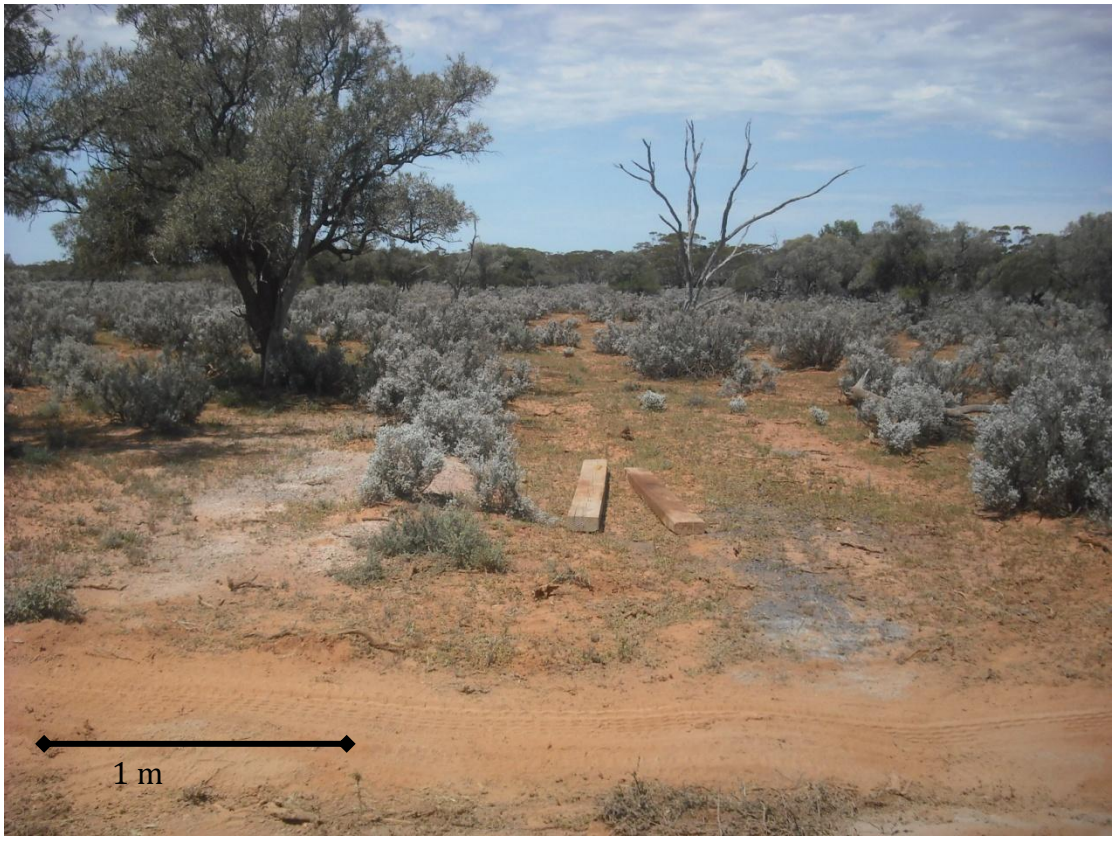

Figure 4: Topography and vegetation around diamond drill hole ML001, thin red-brown quaternary sands and clays cover locally exposed Ripon Calcrete, as well as fluviatile gravels, sands and clays of modern drainage channel sediments. Vegetation in the area can be seen as quite sparse, with bluebush and saltbush covering plains with local sheoak, myall and mallee trees.


(a
Failed
10 cm
(b
10 cm
(c
10 cm
(d)
7 cm
(e
10 cm
(f)
5 cm
(g)
10 cm
(h
1 m

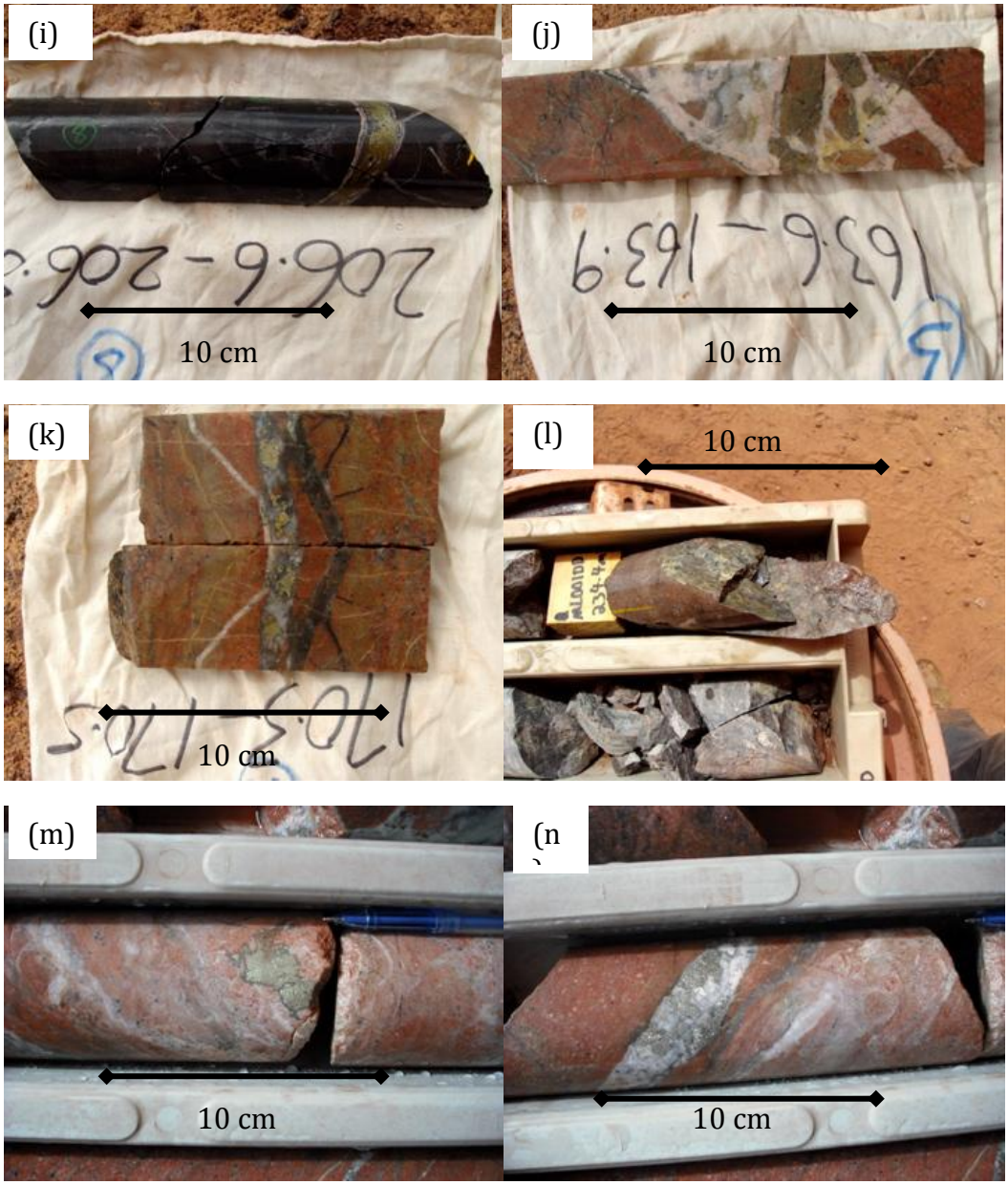

Figure 5: (a) Fine grained black grey, weathered, moderately magnetic amphibolite, with small haematite veins (depth 65.25m). (b) Fine grained black grey, strongly magnetic amphibolite, in sharp contact with medium to coarse microgranite (114.7m). (c) medium to coarse micro grained pink brown microgranite (143.1m). (d) Medium grained pink micro granite, with small quartz veins (136.93m). (e) Highly sericite and chlorite altered fined grained felsic banded quartz feldspar gneiss (171.4m). (f) Fine grained pink rhyolite, cut by multiple fine 1-2mm quartz veins (131.4m). (g) Slightly to moderately weathered light green to green/ grey felsic fine to medium grained volcanic to volcaniclastic unit (189.5m). (h) Dark grey/ black fine graine rhyodacite, with highly deformed flow banding? (214.87m). (i) Dark grey/ black fine grained rhyodacite with a large (1-2 cm) carbonate vein dominated by chalcopyrite mineralisation (206.6m). (j) Brecciated zone in fine to medium grained pink rhyolite, brecciated zone contains carbonate- quartz infill and angular to sub angular sericite altered rhyolite and sulphides, later carbonate quartz veining cuts the breciation with chalcopyrite precipitation (163.6m). (k) Highly sericite and chlorite altered fined grained felsic banded quartz feldspar gneiss containing multiple generations of quartz-carbonate veining, with one being mineralised with chalcopyrite (170.3m). (l) Chlorite alteration on rhyodacite joint. (234.4m). (m) Highly Silicic/ carbonate altered rhyolite?/ microgranite, with clotty pyrite infill. (n) Pink medium grain microgranite with prominent (2-3cm) quartz carbonate vein (with pyrite), and multiple finer quartz carbonate veins leading to silicic/ carbonate alteration

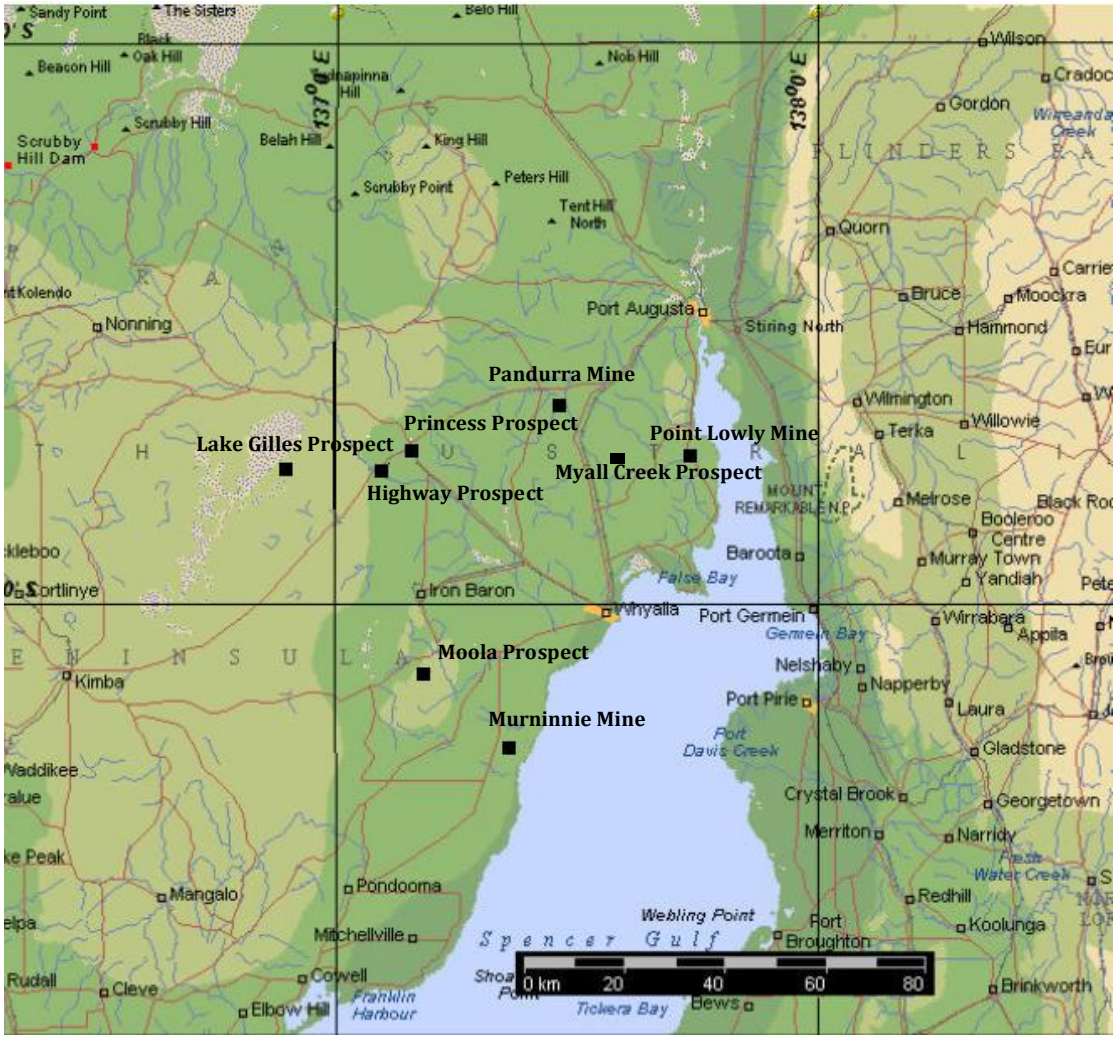

Figure 6: Locations of copper mineralisation around the Middleback Ranges/ Whyalla area. Modified from Helix (2001).

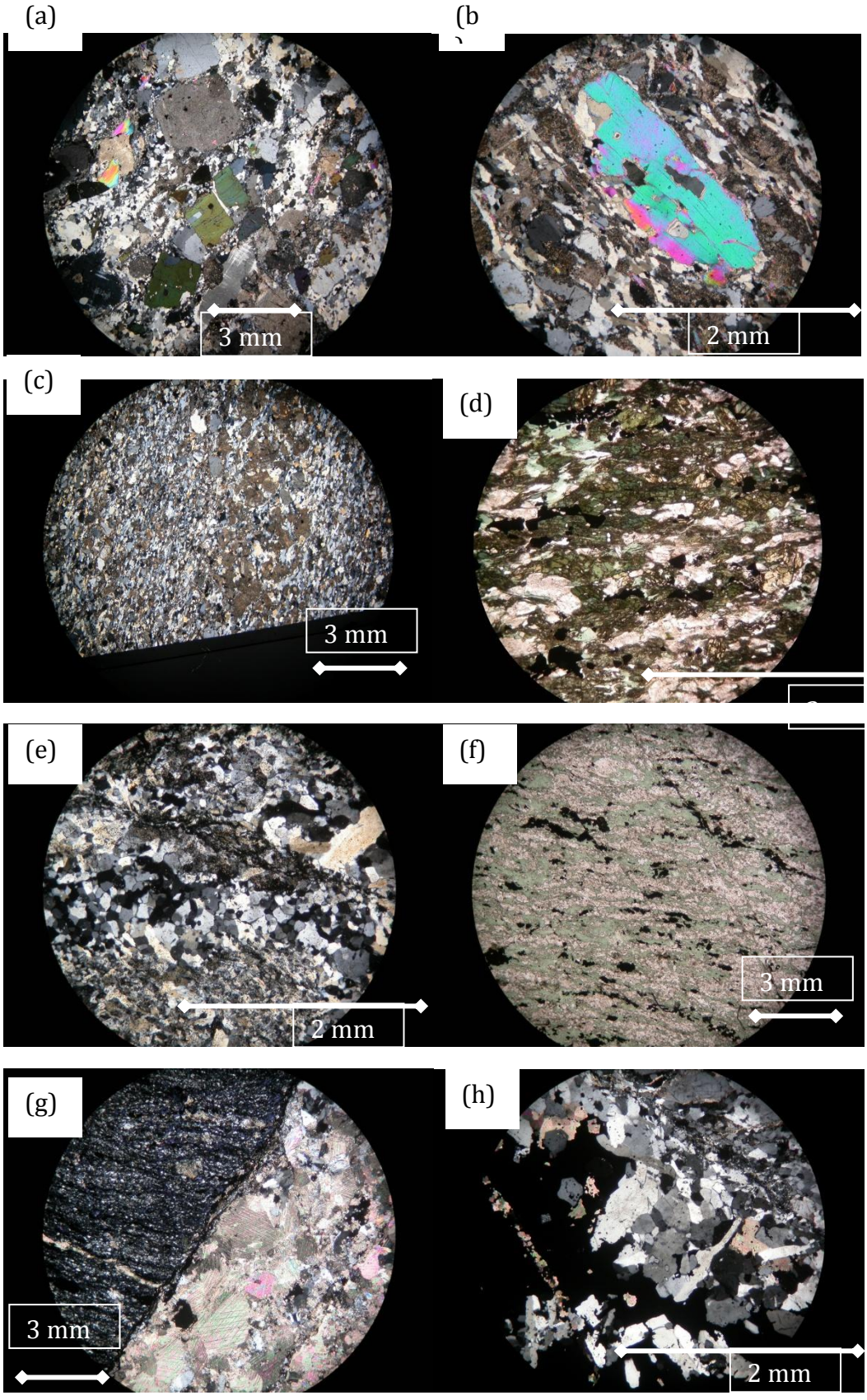
(a)
3 mm
(b
2 mm
(c)
3 mm
(d)
(e)
2 mm
(f)
3 mm
(g)
3 mm
(h)
2 mm

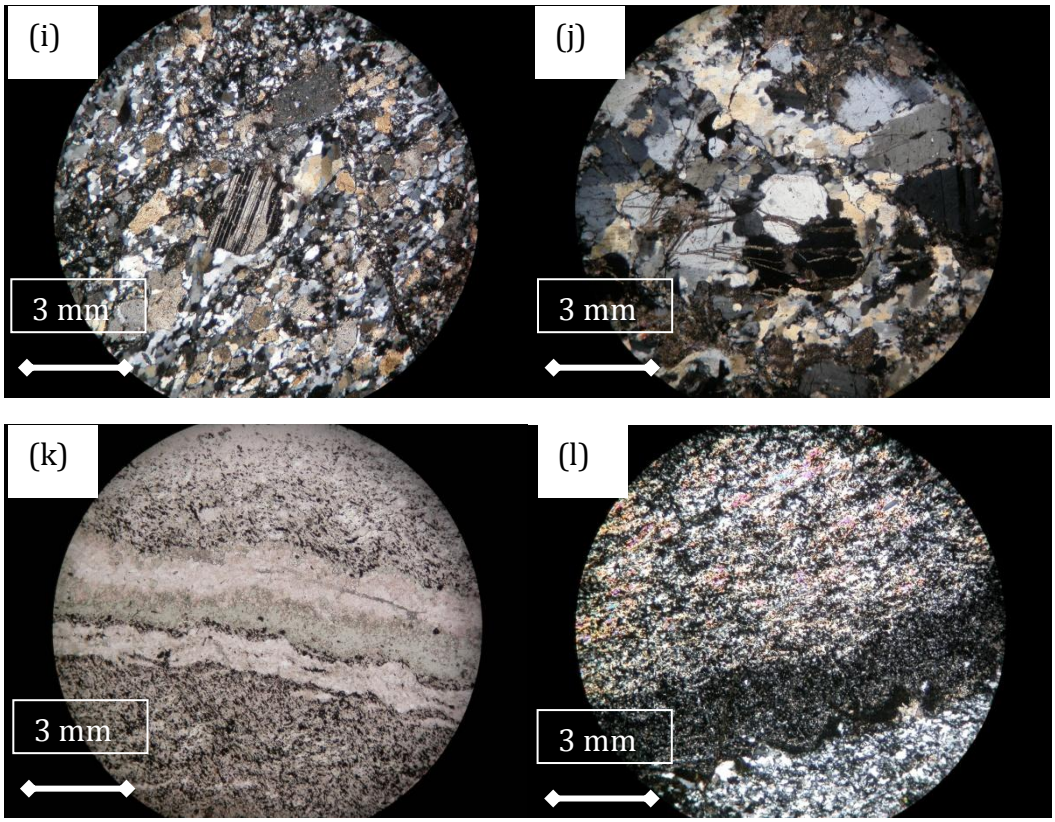

Figure 7: (a) OS004 (microgranite)- fine grained groundmass of plagioclase, sericite altered plagioclase and quartz with large phenocryst of magmatic muscovite, K-feldspar, sodic amphibole, plagioclase and sericite altered plagioclase. (b) RJ006 (rhyolite) - fine grained groundmass of plagioclase, sericite altered plagioclase and quartz, with phenocrysts of plagioclase (albite), sericite altered plagioclase and K-feldspar. (c) OS003 (felsic gneiss) - fine grained groundmass consisting of recrystallised quartz, plagioclase and sericite altered plagioclase, with larger pseudomorphed phenocrysts of plagioclase replaced by sericite. (d) RJ002 (amphibolite)- fine groundmass of plagioclase quartz and sericite altered plagioclase, with large lathes of oxides, plagioclase, sericite altered plagioclase, quartz, hornblende and chlorite (chlorite is observed replacing hornblende) defining the fabric of the rock. (e) RJ009 (volcaniclastic) - fine grained groundmass of plagioclase, sericite altered plagioclase, altered chlorite? and quartz, with phenocrysts of plagioclase, sericite altered plagioclase and k-feldspar, contains abundant quartz veining. (f) RJ010 (rhyodacite)- fine groundmass of plagioclase quartz and sericite altered plagioclase, with large lathes of oxides, plagioclase, sericite altered plagioclase, quartz and chlorite defining the fabric of the rock. (g) RJ012 (rhyodacite with carbonate-quartz vein) fine groundmass of plagioclase quartz and sericite altered plagioclase, with large lathes of oxides, plagioclase, sericite altered plagioclase, quartz and chlorite defining the fabric of the rock cut by large mineralised (chalcopyrite) carbonate-quartz vein. (h) RJ008 (vein) quartz vein hosting significant amount of mineralization, both pyrite and chalcopyrite, housed within felsic volcanic unit. (i) OS001 (rhyodacite)- fine grained groundmass consisting of recrystallised quartz, plagioclase and sericite altered plagioclase, with larger pseudomorphed phenocrysts of plagioclase replaced by sericite, mildly sericite altered albite and K-feldspar. (j) RJ008 (rhyolite)- fine grained groundmass of plagioclase, sericite altered plagioclase and quartz, with phenocrysts of plagioclase (albite), sericite altered plagioclase and K-feldspar. Phenocyrsts of plagioclase are fragmented by fine sericite veins. (k) RJ014 (rhyodacite)- fine grained flow banded? rhyodacite with chlorite cutting parallel with quartz banding. (l) RJ014 (rhyodacite)- fine groundmass of plagioclase quartz and sericite altered plagioclase, with large lathes of oxides, plagioclase, sericite altered plagioclase, quartz and chlorite defining the fabric of the rock, minor epidote alteration is observed in this slide in association with chlorite and sericite.

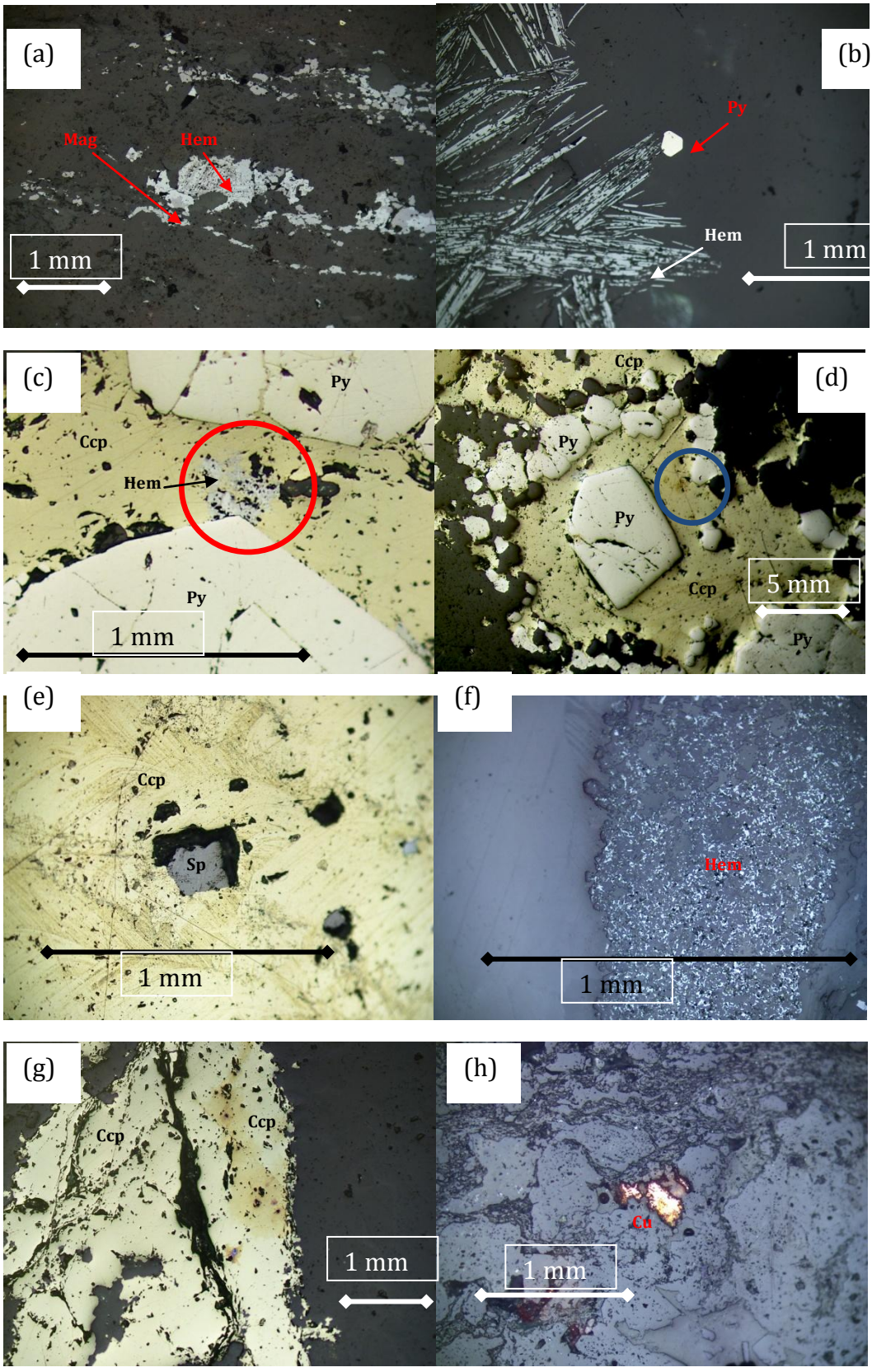

Figure 8: (a) (RJ015 rhyodacite) Martitisation of magnetite by haematite. Martititsation occurs along fractures and the rims

of the magnetite. (b) (RJ006 rhyolite) Mint green radiating needles of haematite with small euhedral equigranular crystal of pyrite growing around one of the needles. (c) RJ008 (rhyolite) Haematie growth on the out rim of pyrite (circled in red). Pyrite display high level of fracturing infilled with chalcopyrite (d)) RJ008 (rhyolite)- euhedral equant crystal of

pyrite surrounded by chalcopyrite, other pyrite display intergrowth with each other. Chalcopyrite and pyrite are obsevered as being moderate to slightly fractured with pyrite having minor pitting and chalcopyrite major pitting. Chalcopyrite also displays alteration along at least on of the fractures (circled in blue). (e)) RJ008 (rhyolite)- small subhedral equant crystal of sphalerite enclosed by chalcopyrite. Sphalerite exhibits chalcopyrite emulsion textures, precipitating chalcopyrite within itself as small ≈0.01mm crystals. Chalcopyrite is moderately pitted and fractured. (f) RJ002 (amphibolite)- thin 0.2-0.5mm wide veins of gangue, with tiny .01-.02mm grains of mint green haematite. Martitisation of magnetite increases in intensity towards these veins. (g) In RJ004 chalcopyrite is moderately fractured, highly pitted and exhibits alteration (note alteration is focused around fractures/ pits).

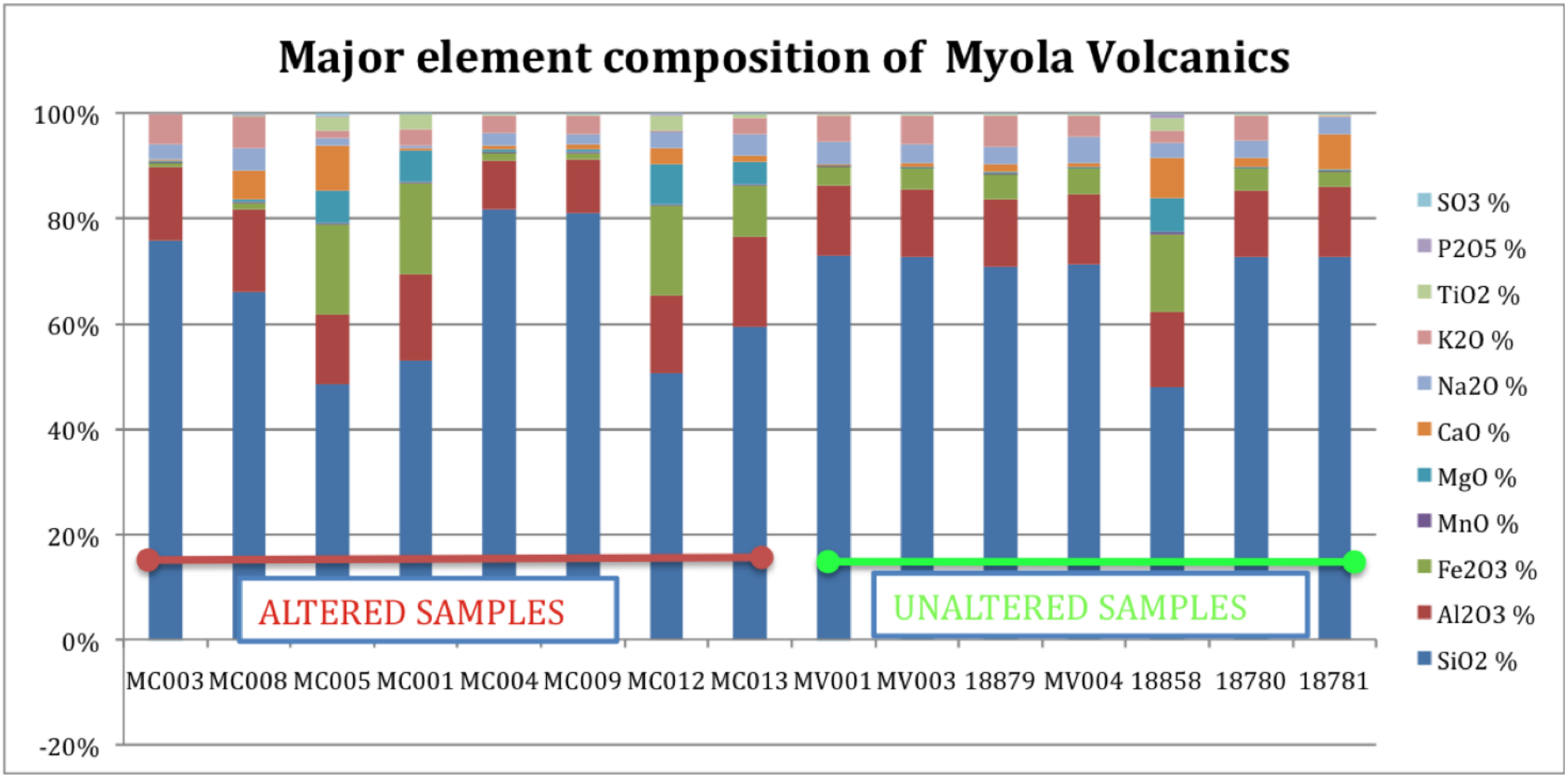

Figure 9: Major element composition of the Myola Volcanics samples. MC003- altered unnamed granite; MC008- altered rhyolite; MC005- altered amphibolite; MC001- altered quartz feldspar gneiss; MC004- altered quartz feldspar gneiss; MC009- altered quartz feldspar gneiss; MC012- altered rhyodacite; MC013- altered rhyodacite; MV001- unaltered rhyolite; MV003- unaltered rhyolite; 18879- unaltered rhyolite; MV004- unaltered rhyolite; 18858- unaltered amphibolite; 18780- unaltered quartz feldspar gneiss; 18781- unaltered quartz feldspar gneiss.

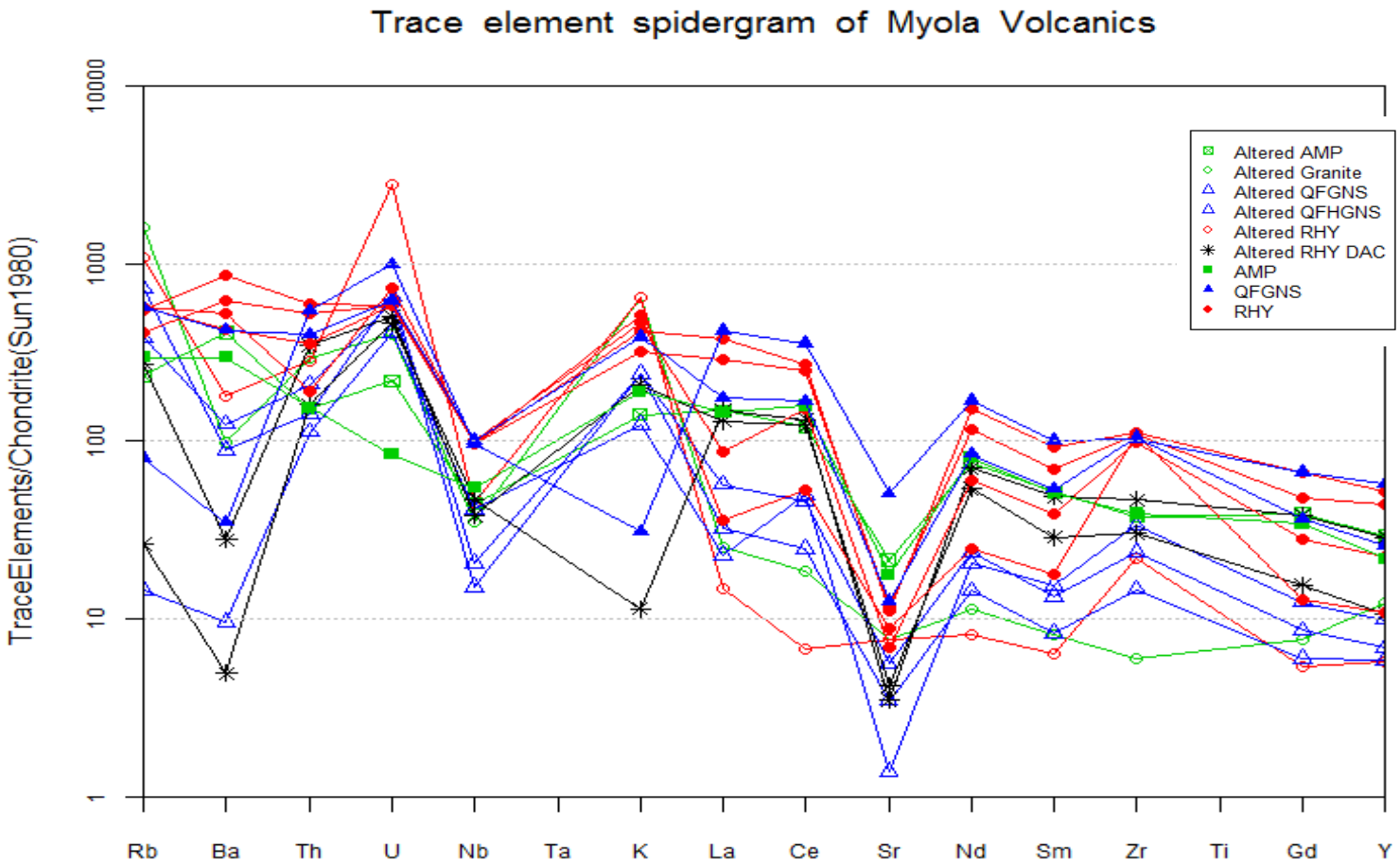

Figure 10: Trace and rare earth elements normalised to chondrite (Sun 1980) and plotted in a spidergram sample lithologies displayed in the key.

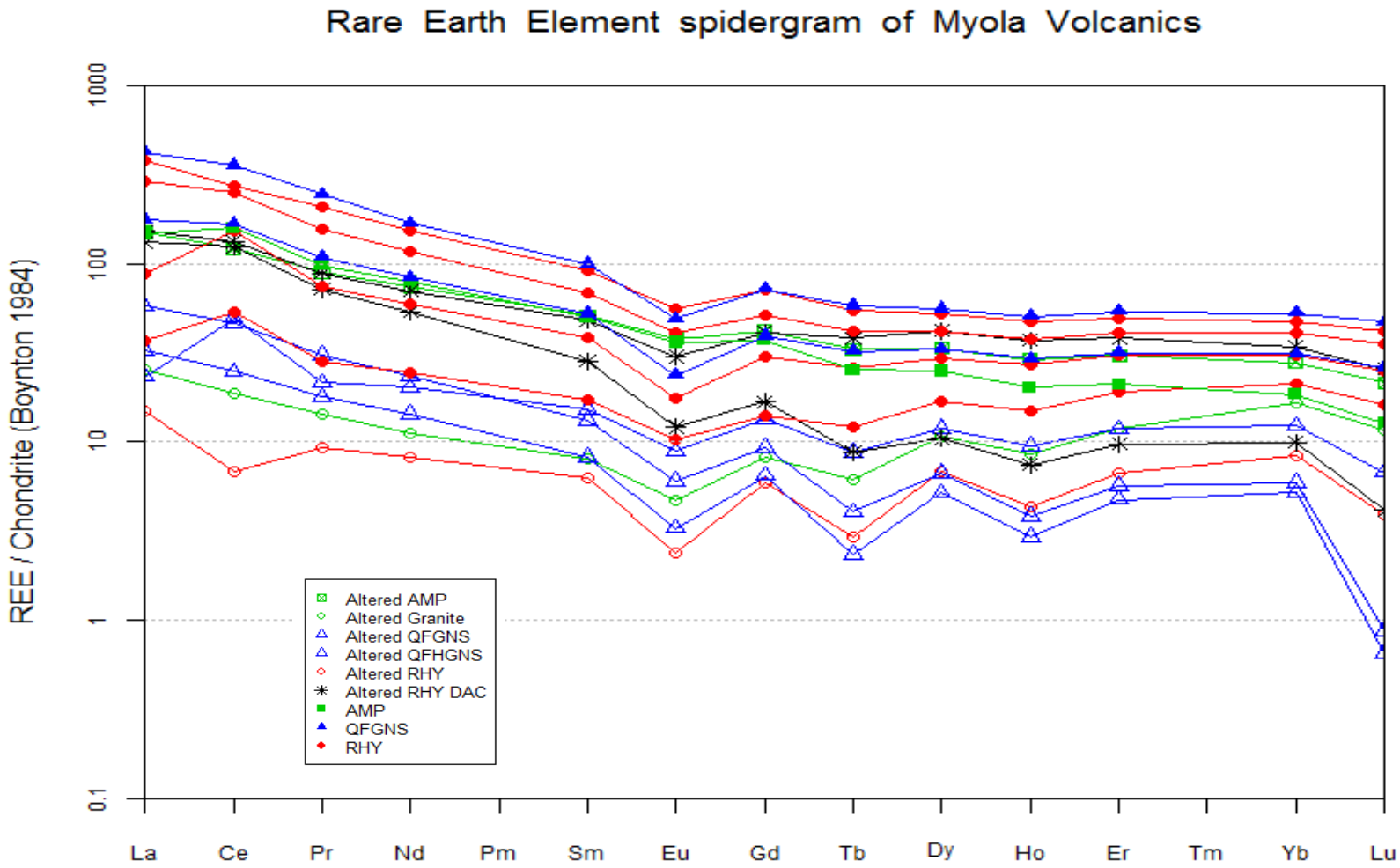

Figure 11: Rare Earth Elements normalised to chondrite (Boynton 1984) plotted in a spidergram.

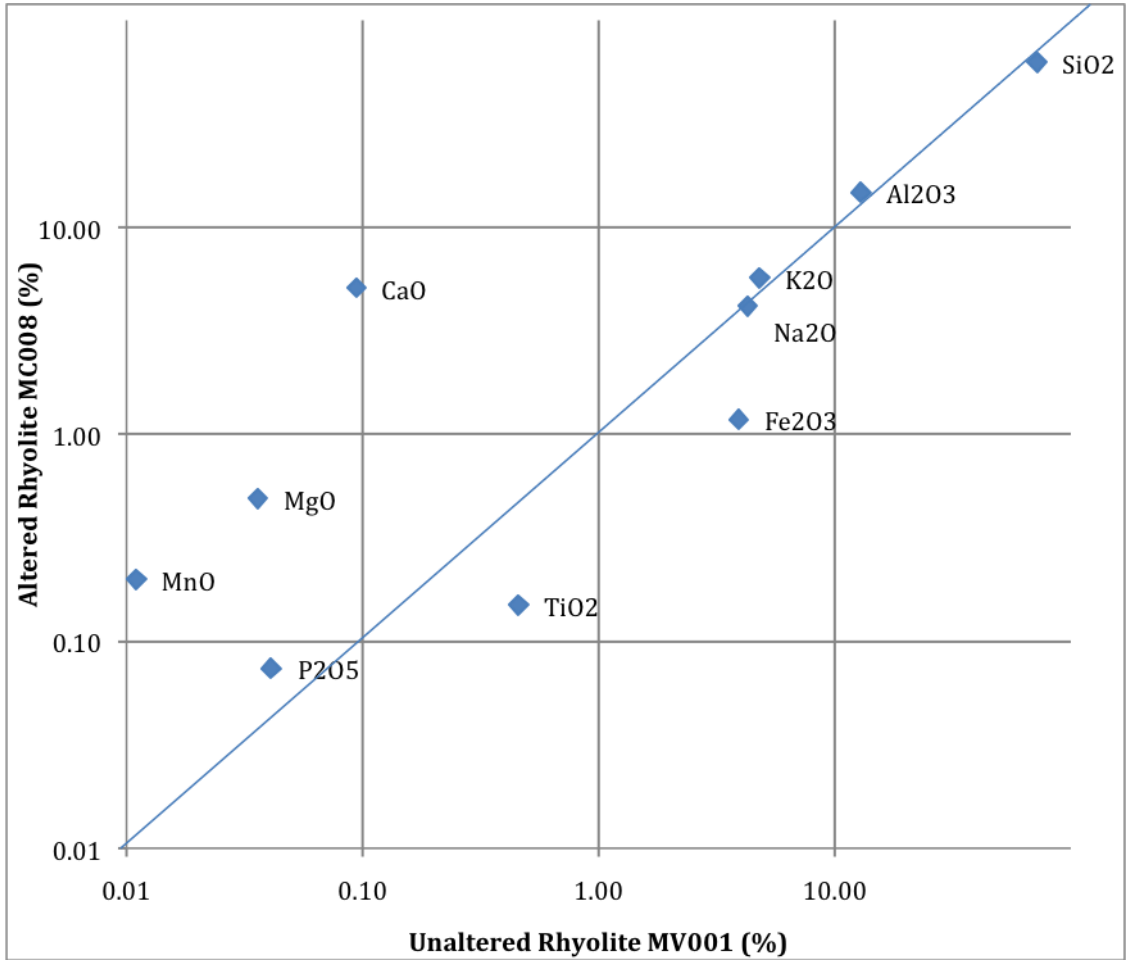

Figure 12.1: Isocon plot, showing relative major element enrichments and depletions in composition, of the rhyolites.

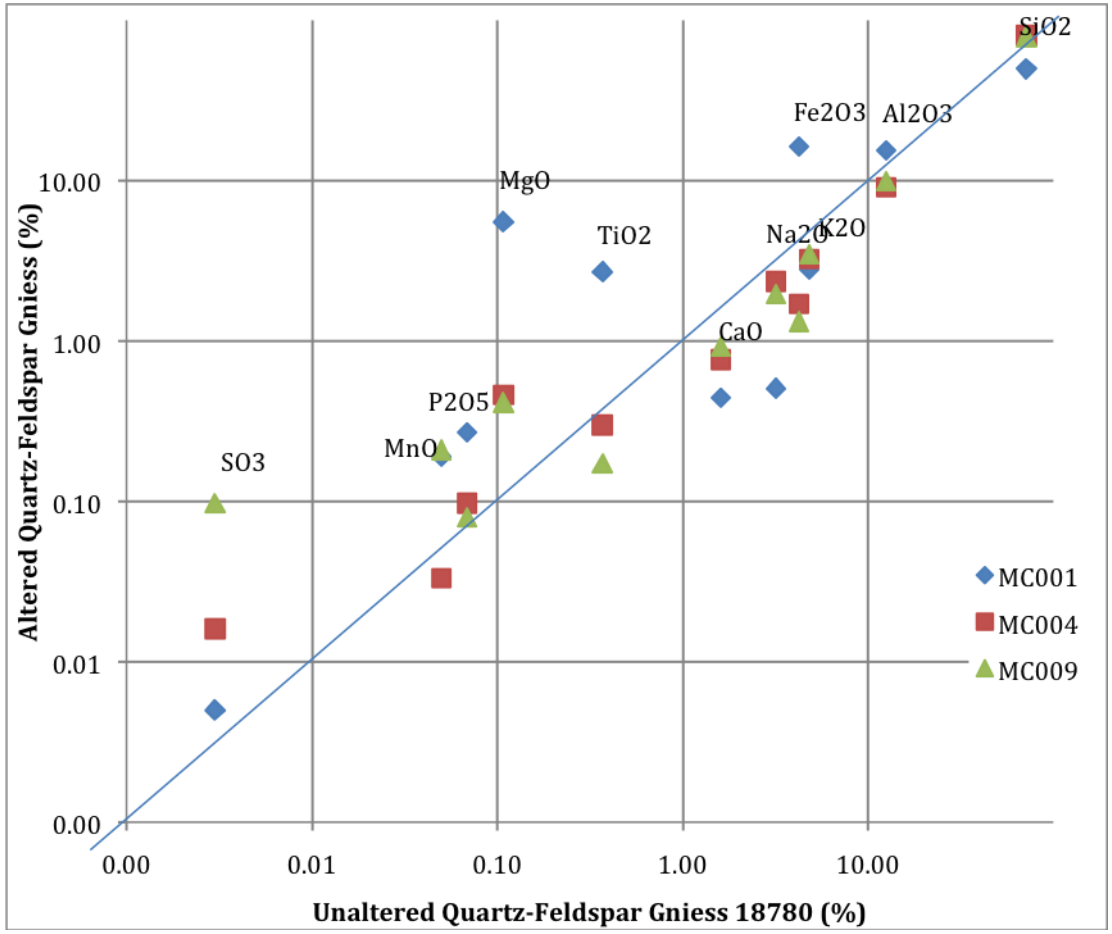

Figure 12.2: Isocon plot, showing relative major element enrichments and depletions in composition, of the quartz- feldspar gneisses.

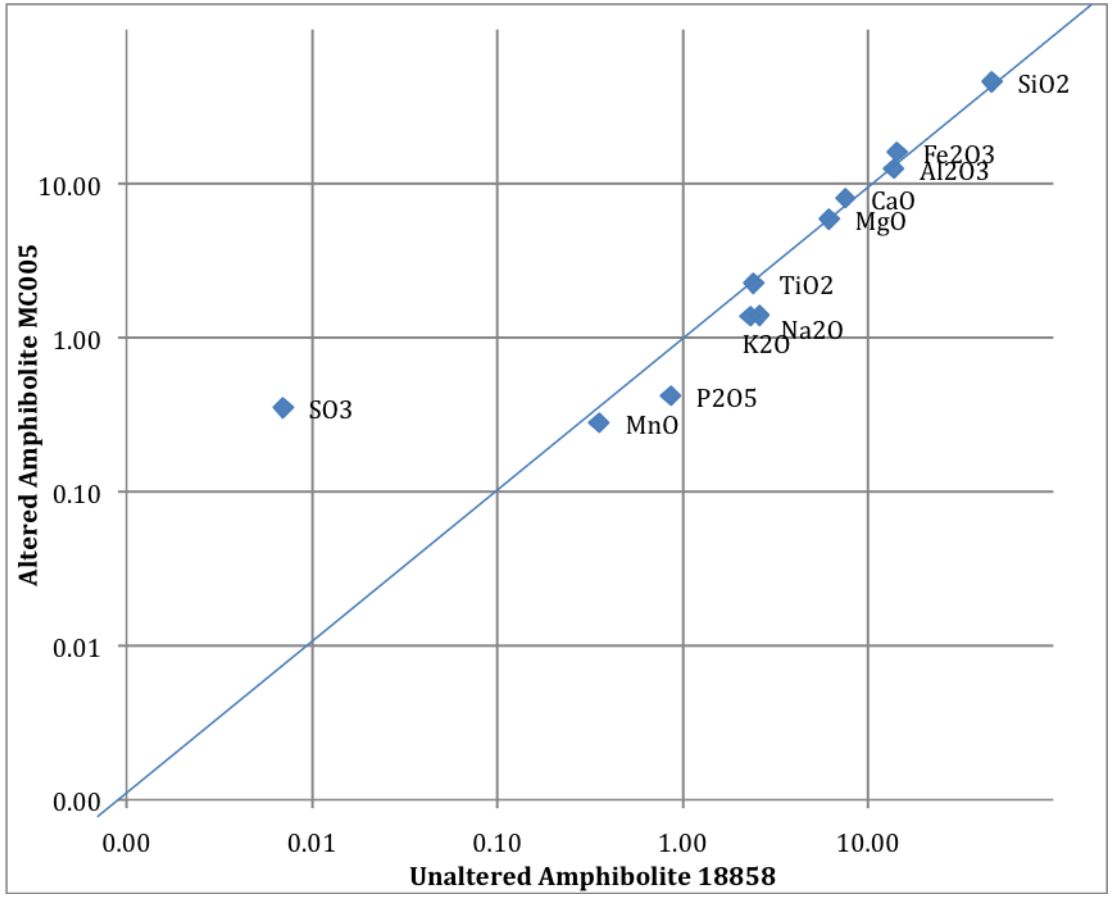

Figure 12.3: Isocon plot, showing relative major element enrichments and depletions in composition, of the amphibolites.

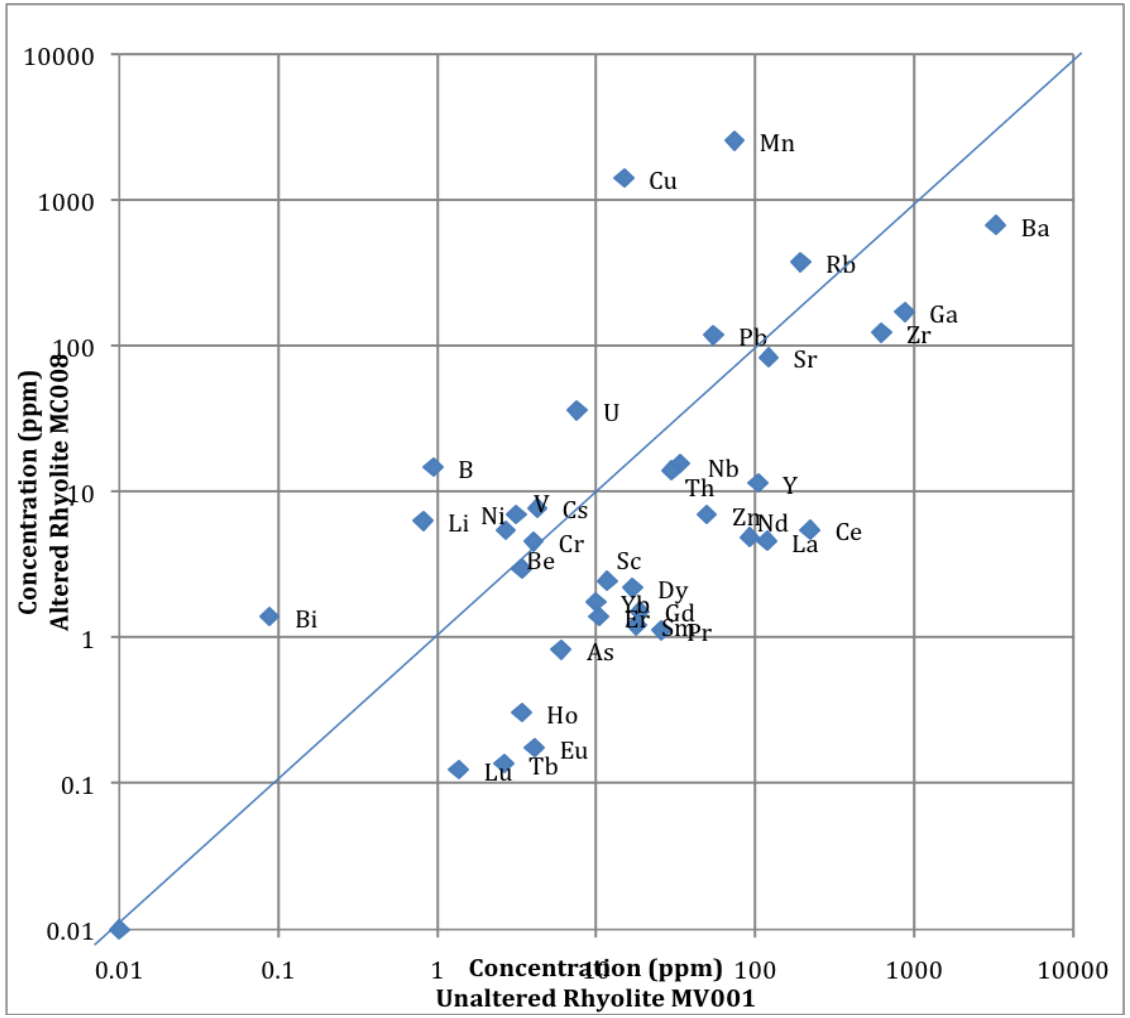

Figure 13.1: Isocon plot, showing relative trace and rare earth element enrichments and depletions in composition, of the rhyolites.

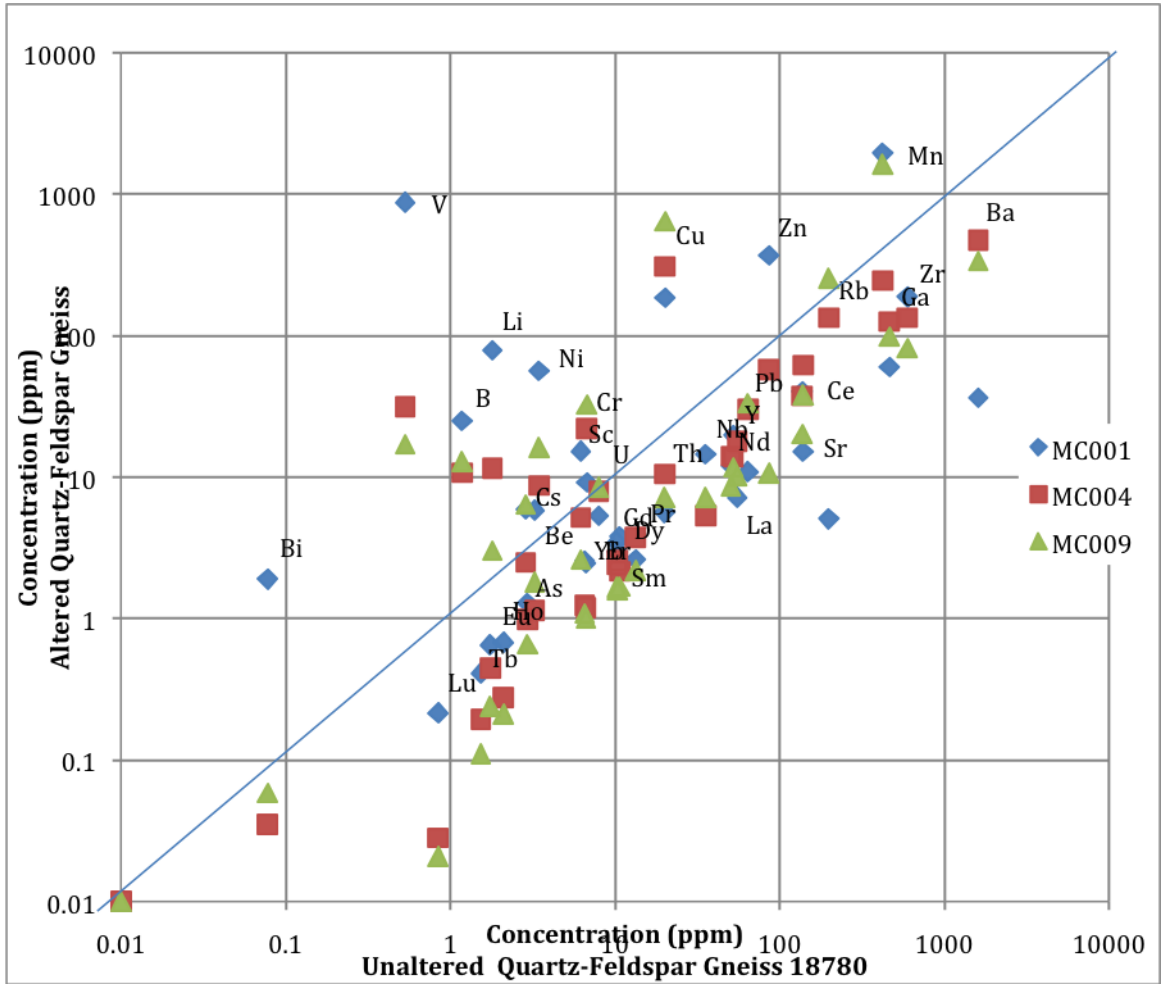

Figure 13.2: Isocon plot, showing relative trace and rare earth element enrichments and depletions in composition, of the quartz- feldspar gneisses.

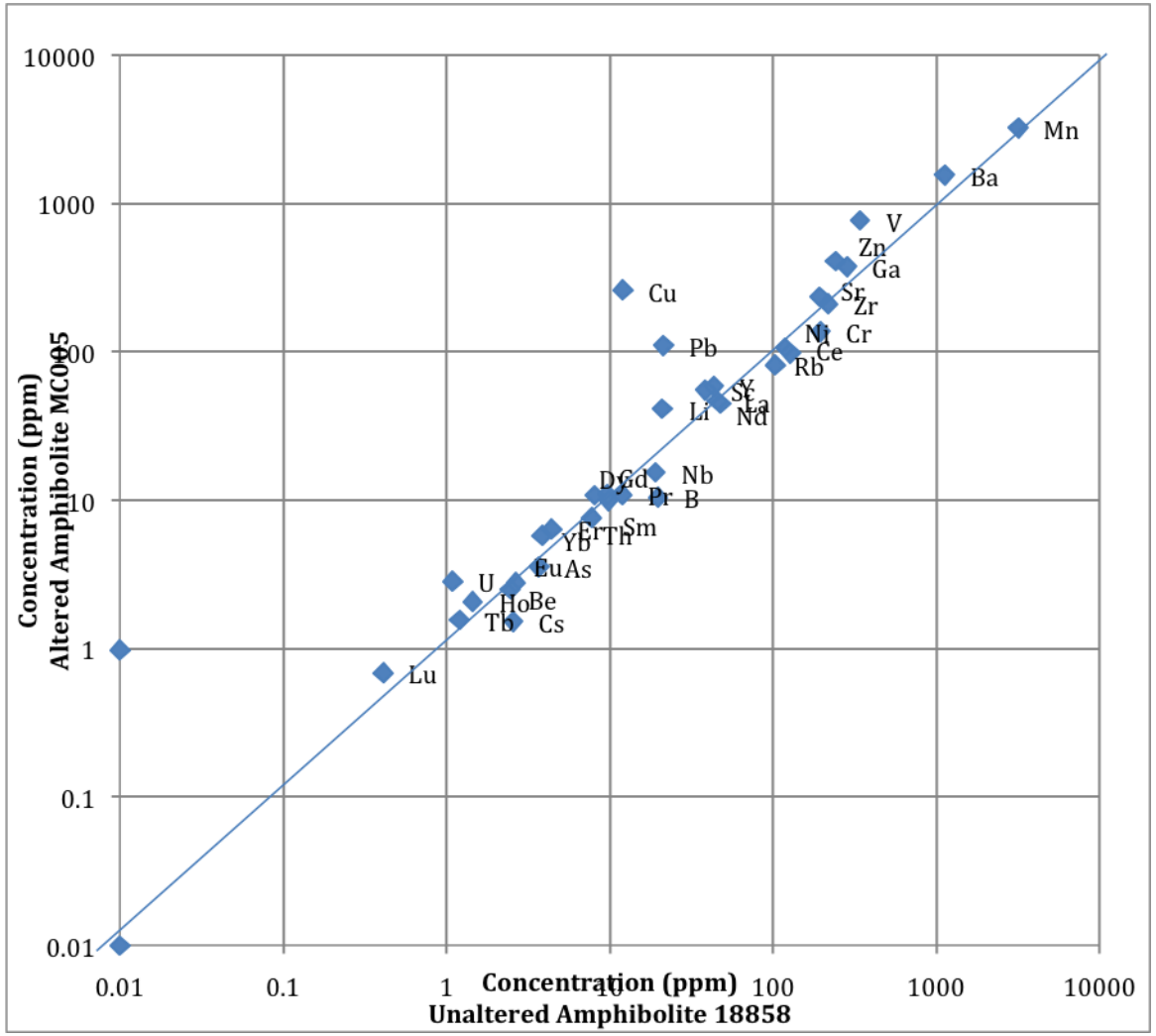

Figure 13.3: Isocon plot, showing relative trace and rare earth element enrichments and depletions in composition, of the amphibolites.

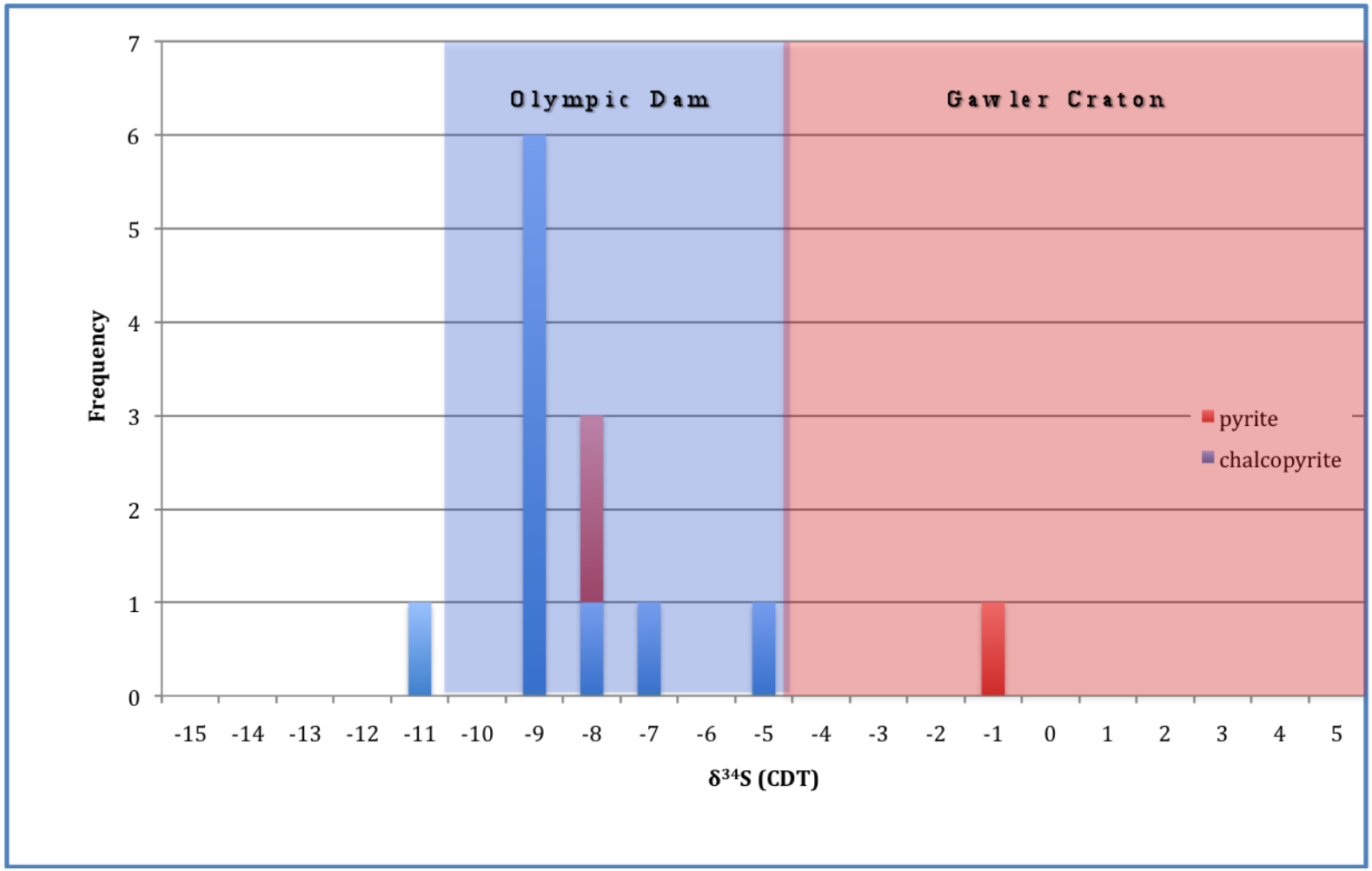

Figure 14: Sulphur isotope data of chalcopyrite and pyrite from the Moola Prospect. Also shown are S-isotope data from Eldridge & Danti (1994) for Olympic Dam (blue field) and Skirrow et al. (2006) for the Gawler Craton (red field).

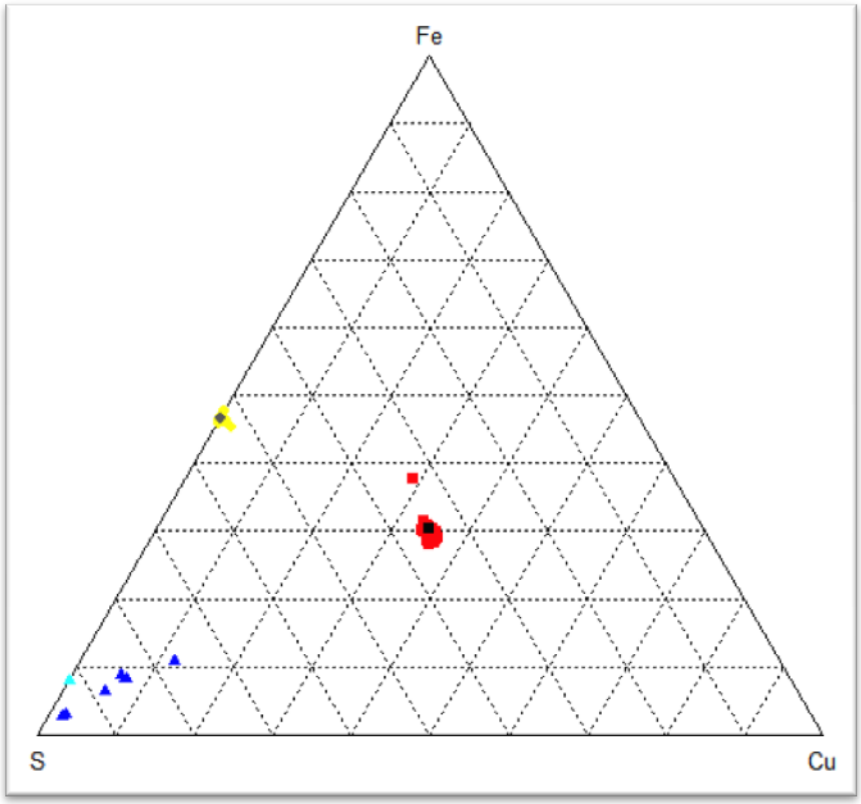

Figure 15.1: S, Fe and Cu saturation in chalcopyrite, pyrite and sphalerite

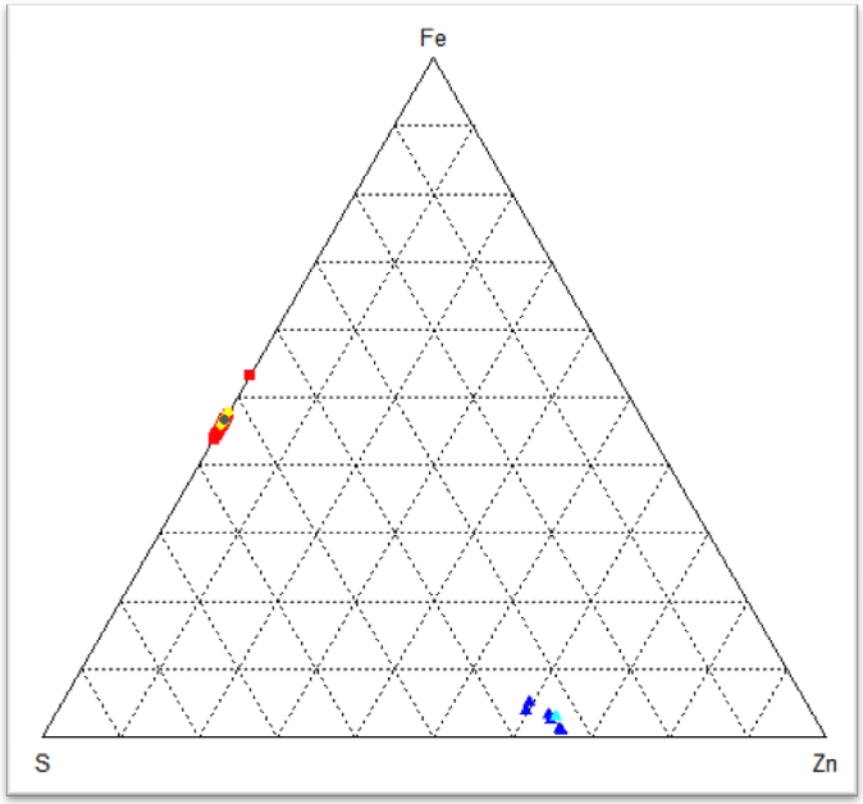

Figure 15.2: S, Fe and Zn saturation in chalcopyrite, pyrite and sphalerite

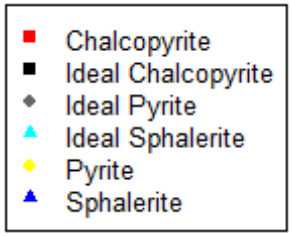

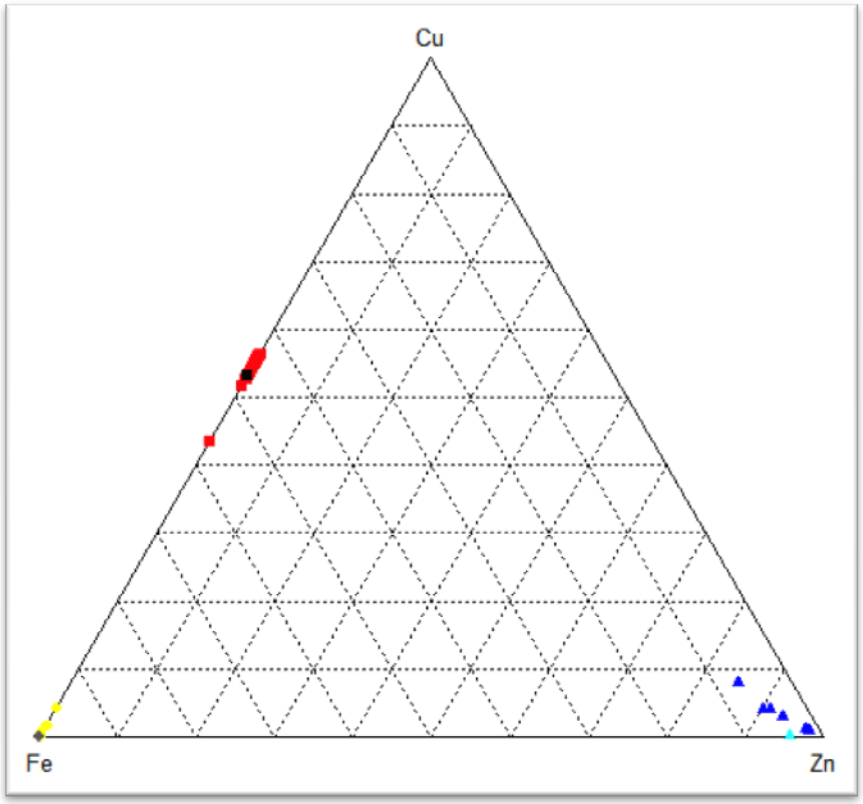

Figure 15.3: Fe, Cu and Zn saturation in chalcopyrite, pyrite and sphalerite

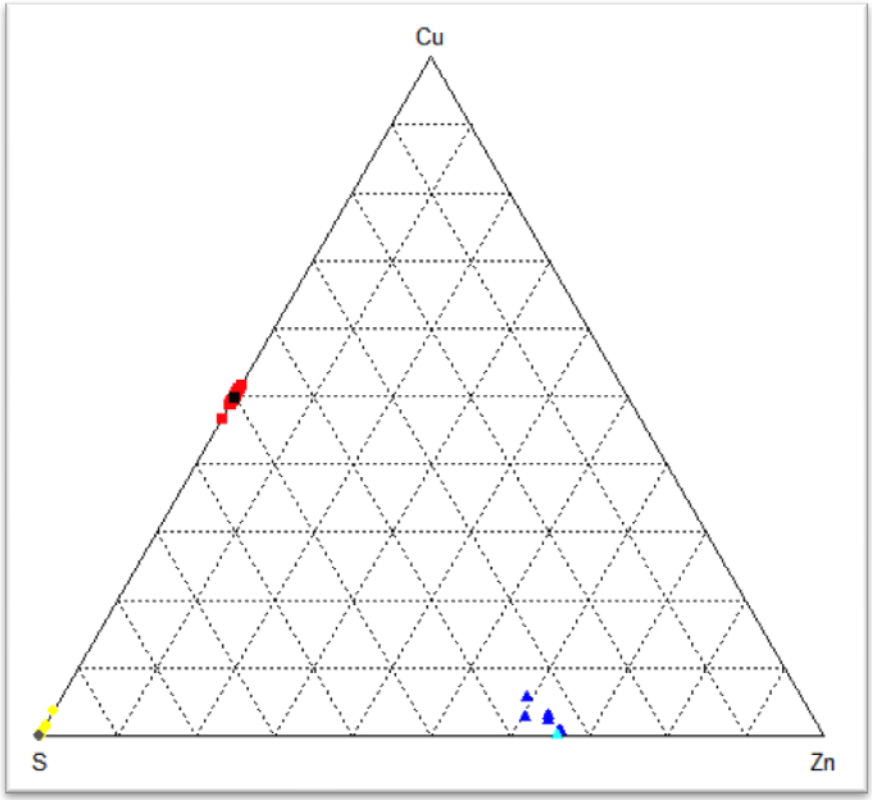

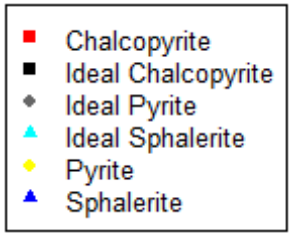

Figure 15.4: S, Cu and Zn saturation in chalcopyrite, pyrite and sphalerite

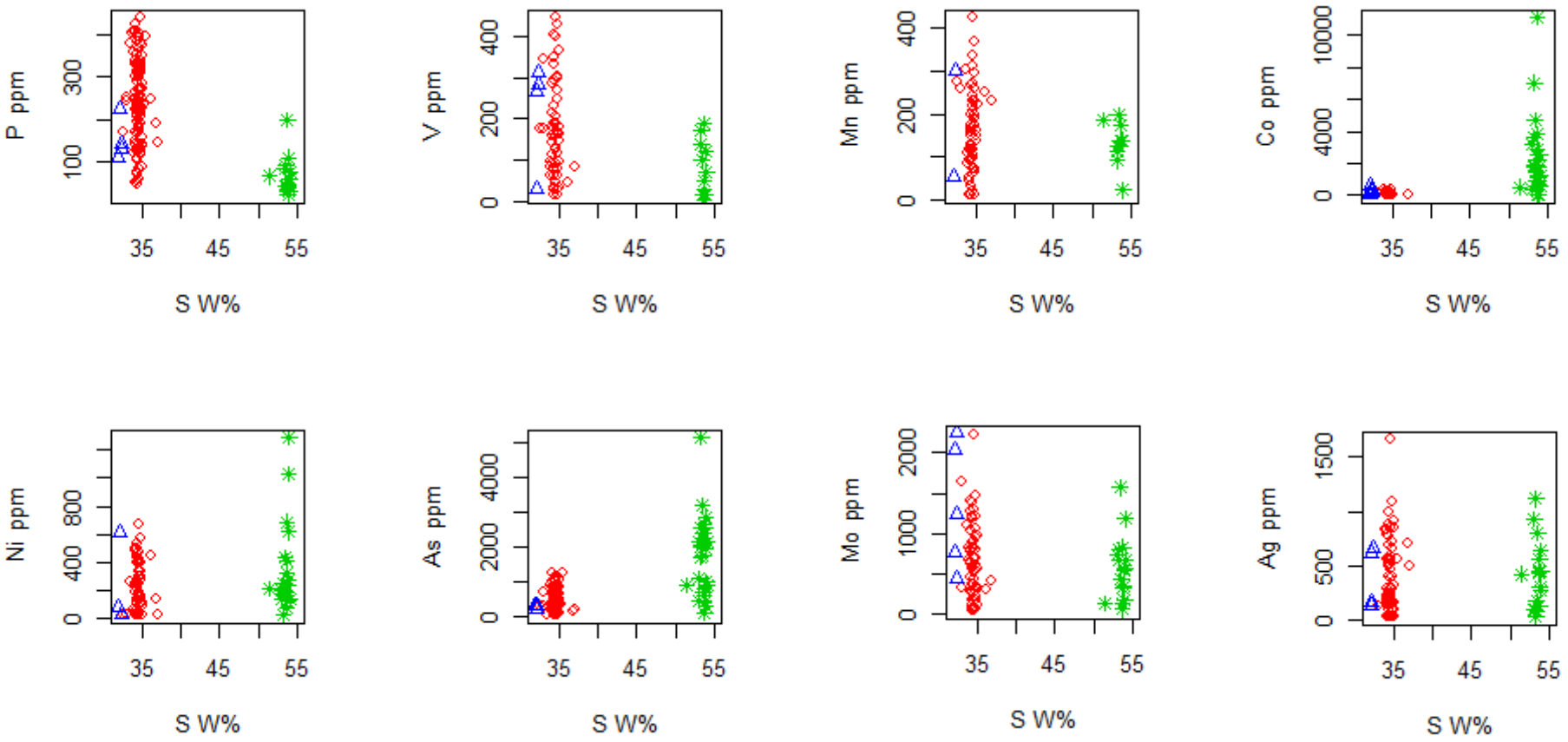
P ppm
100
300
35
45
55
S W%
V ppm
0
200
400
35
45
55
S W%
Mn ppm
0
200
400
35
45
55
S W%
Co ppm
0
4000
10000
35
45
55
S W%
Ni ppm
0
400
800
35
45
55
S W%
As ppm
0
2000
4000
35
45
55
S W%
Mo ppm
0
1000
2000
35
45
55
S W%
Ag ppm
0
500
1500
35
45
55
S W%

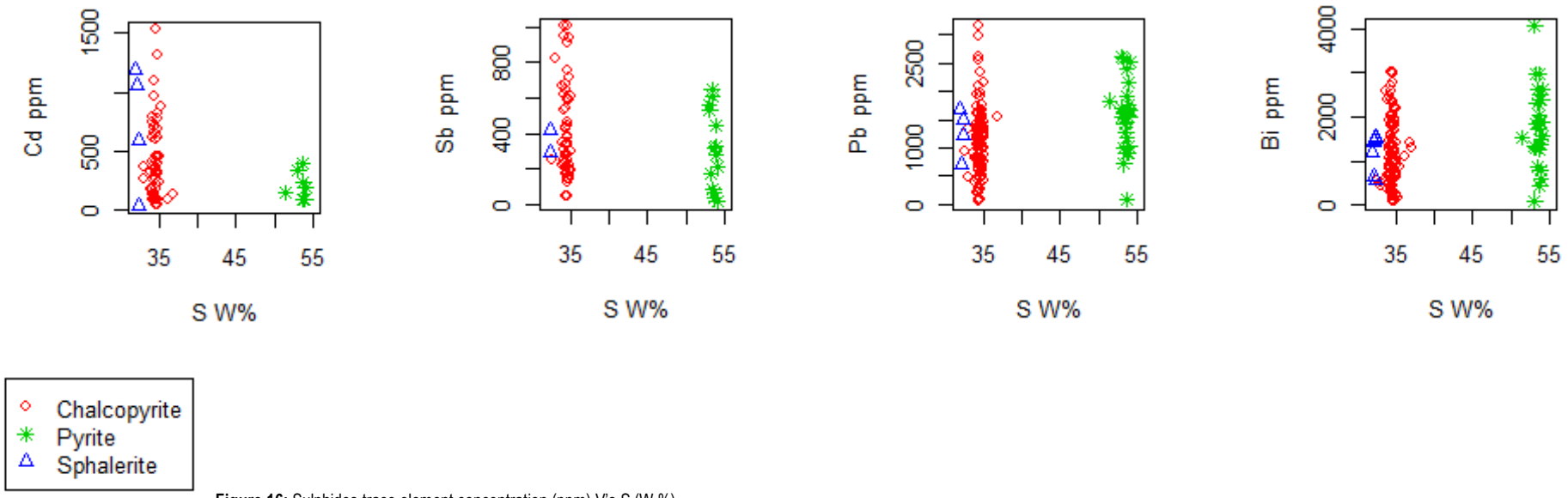

Figure 16: Sulphides trace element concentration (ppm) V's S (W %)

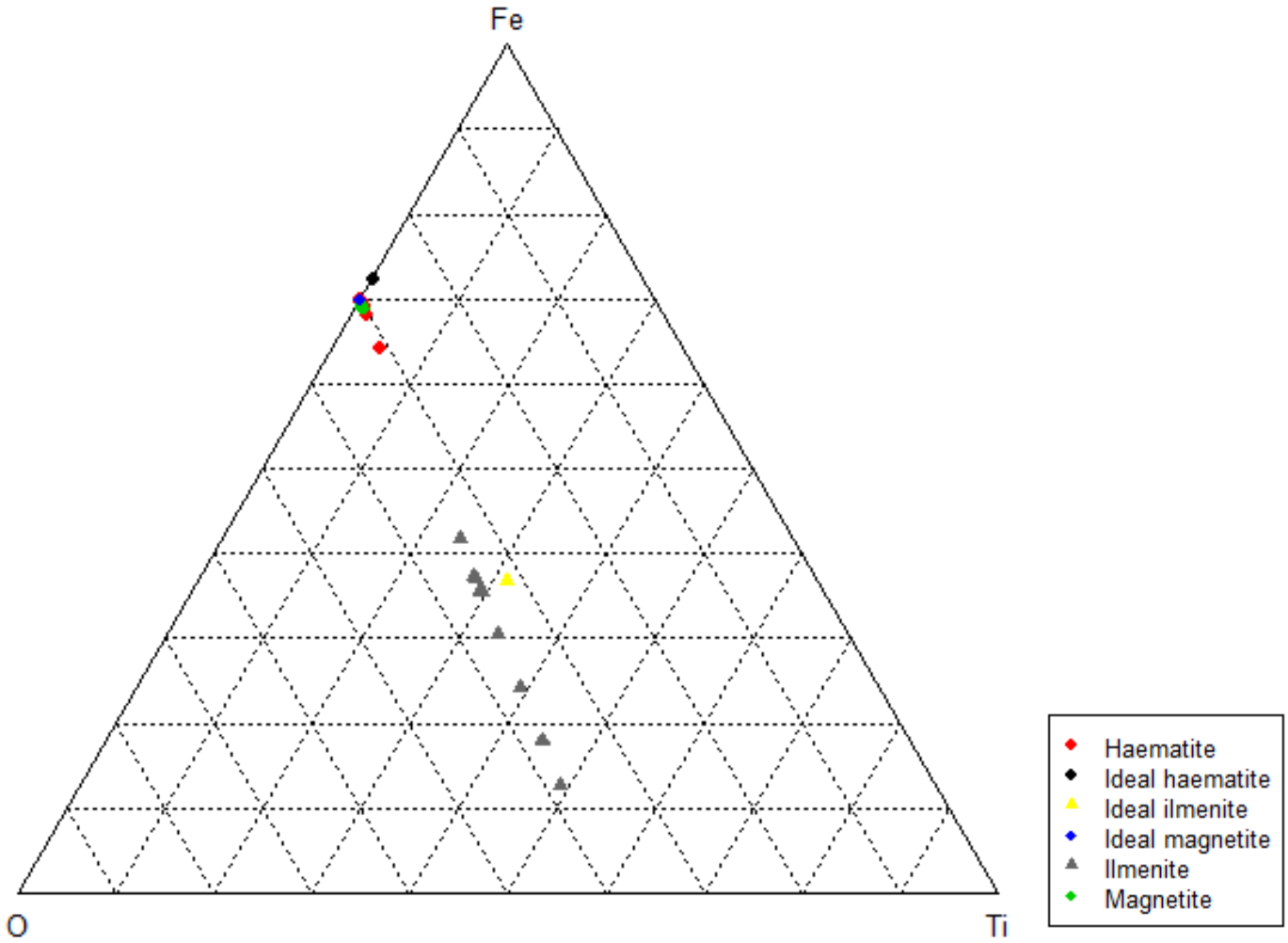

Figure 17: Fe, O and Ti saturation in Mawson Prospect iron oxides

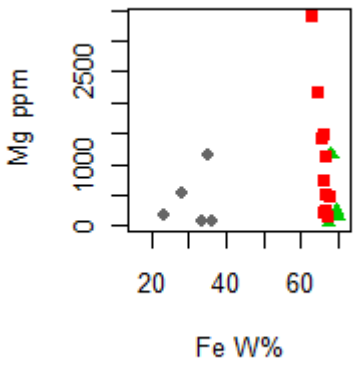
Mg ppm
0
1000
2500
20
40
60
Fe W%

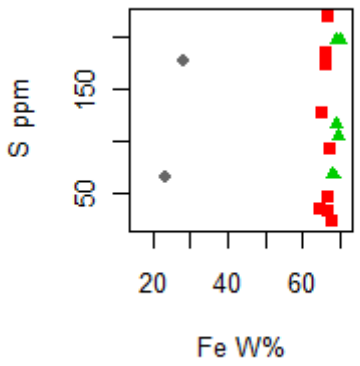
S ppm
50
150
20
40
60
Fe W%

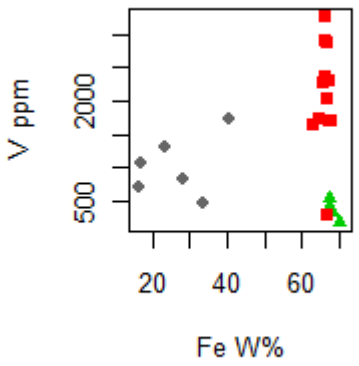
V ppm
500
2000
20
40
60
Fe W%

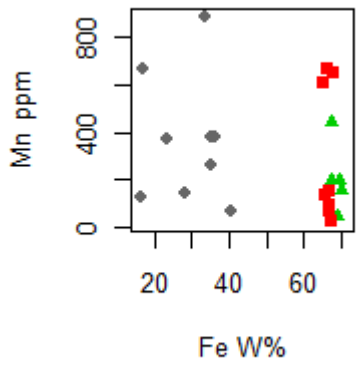
Mn ppm
0
400
800
20
40
60
Fe W%

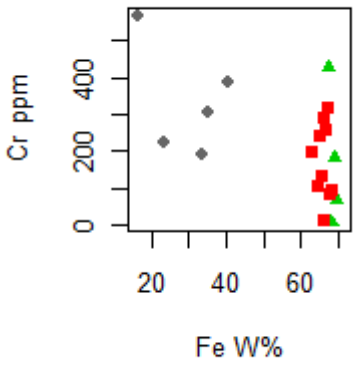
Cr ppm
0
200
400
20
40
60
Fe W%

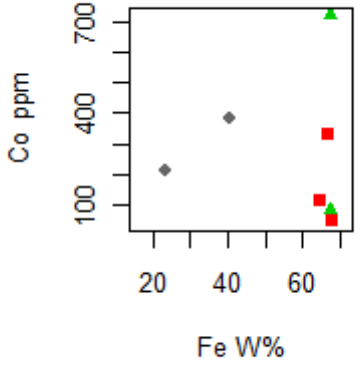
Co ppm
100
400
700
20
40
60
Fe W%

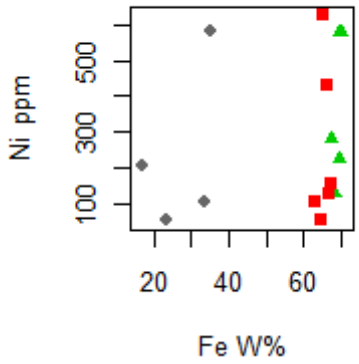
Ni ppm
100
300
500
20
40
60
Fe W%

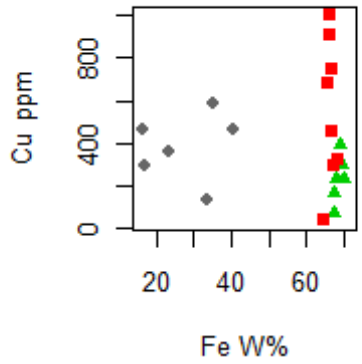
Cu ppm
0
400
800
20
40
60
Fe W%

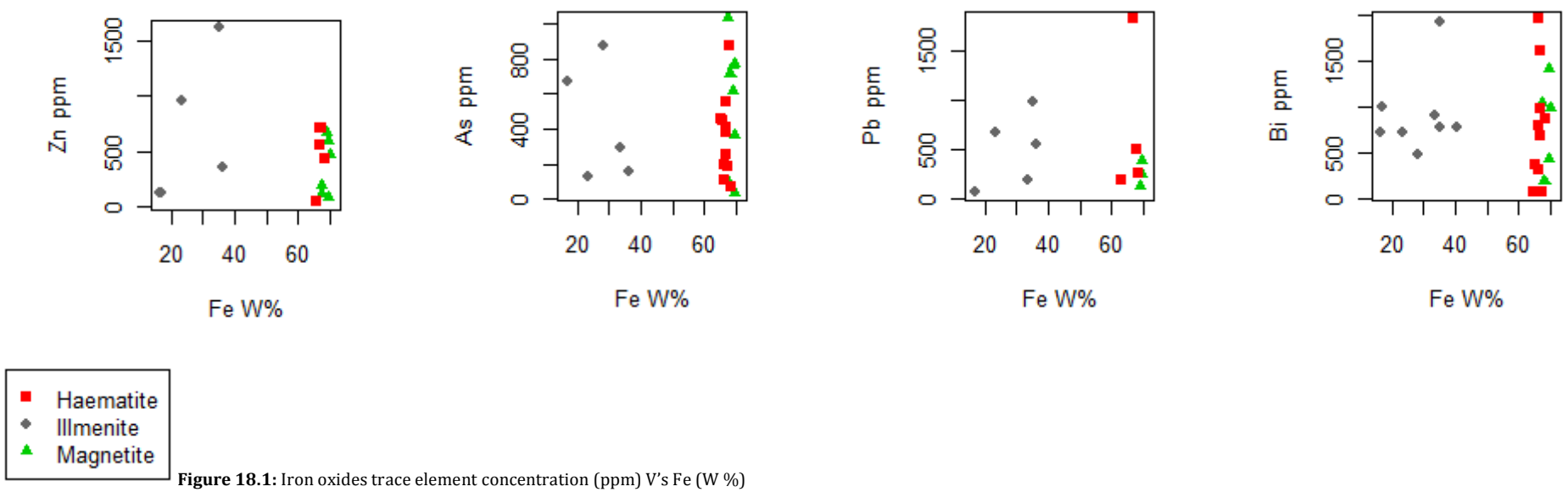

Figure 18.1: Iron oxides trace element concentration (ppm) V's Fe (W %)

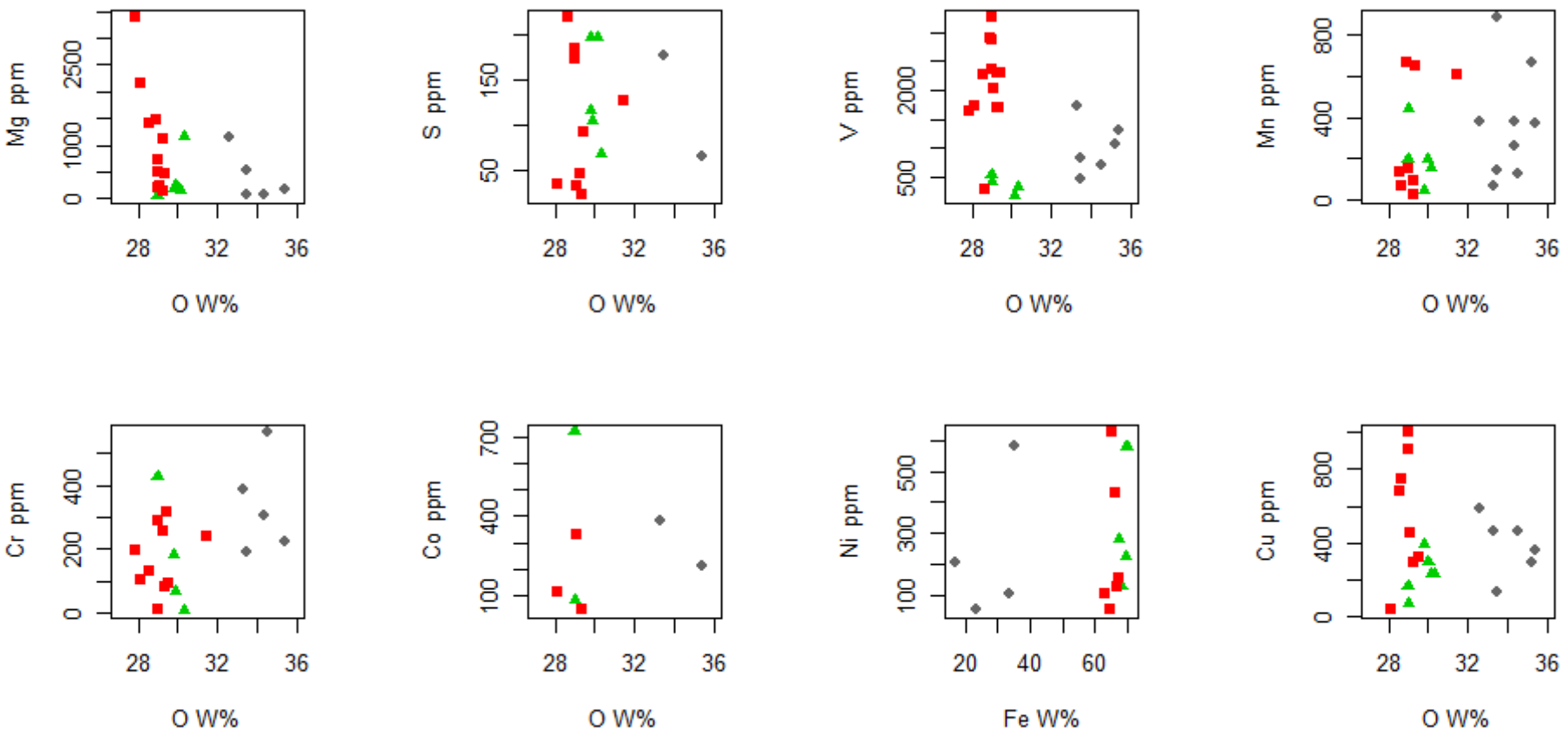
Mg ppm
0
1000
2500
28
32
36
O W%
S ppm
50
150
28
32
36
O W%
V ppm
500
2000
28
32
36
O W%
Mn ppm
0
400
800
28
32
36
O W%
Cr ppm
0
200
400
28
32
36
O W%
Co ppm
100
400
700
28
32
36
O W%
Ni ppm
100
300
500
20
40
60
Fe W%
Cu ppm
0
400
800
28
32
36
O W%

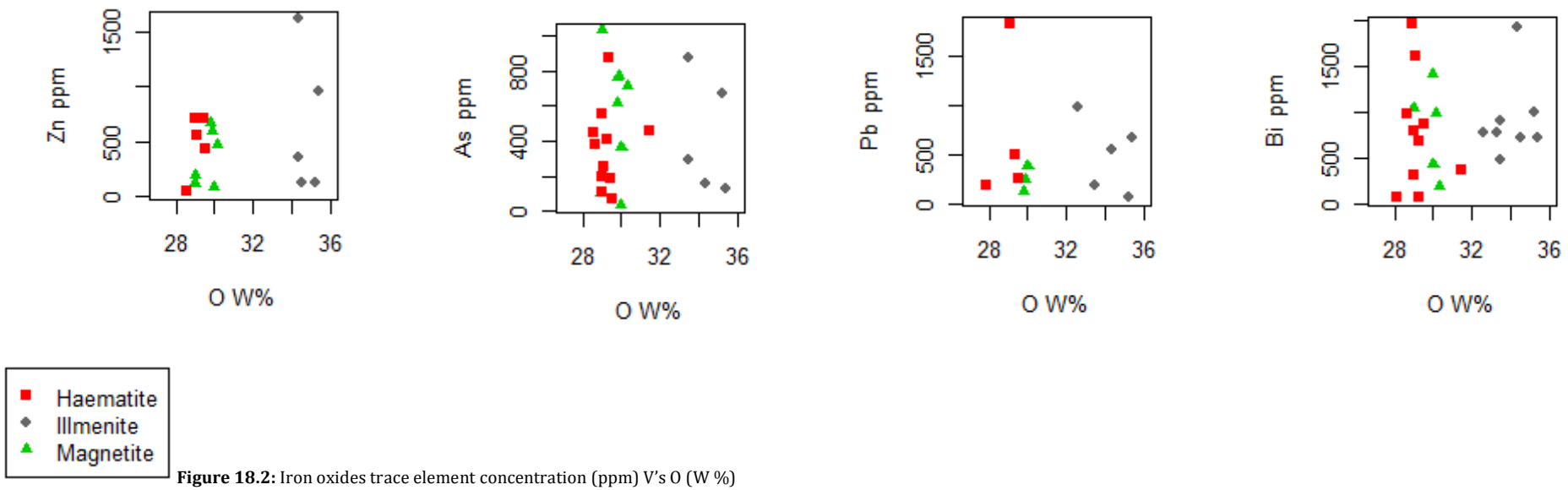

Figure 18.2: Iron oxides trace element concentration (ppm) V's O (W %)

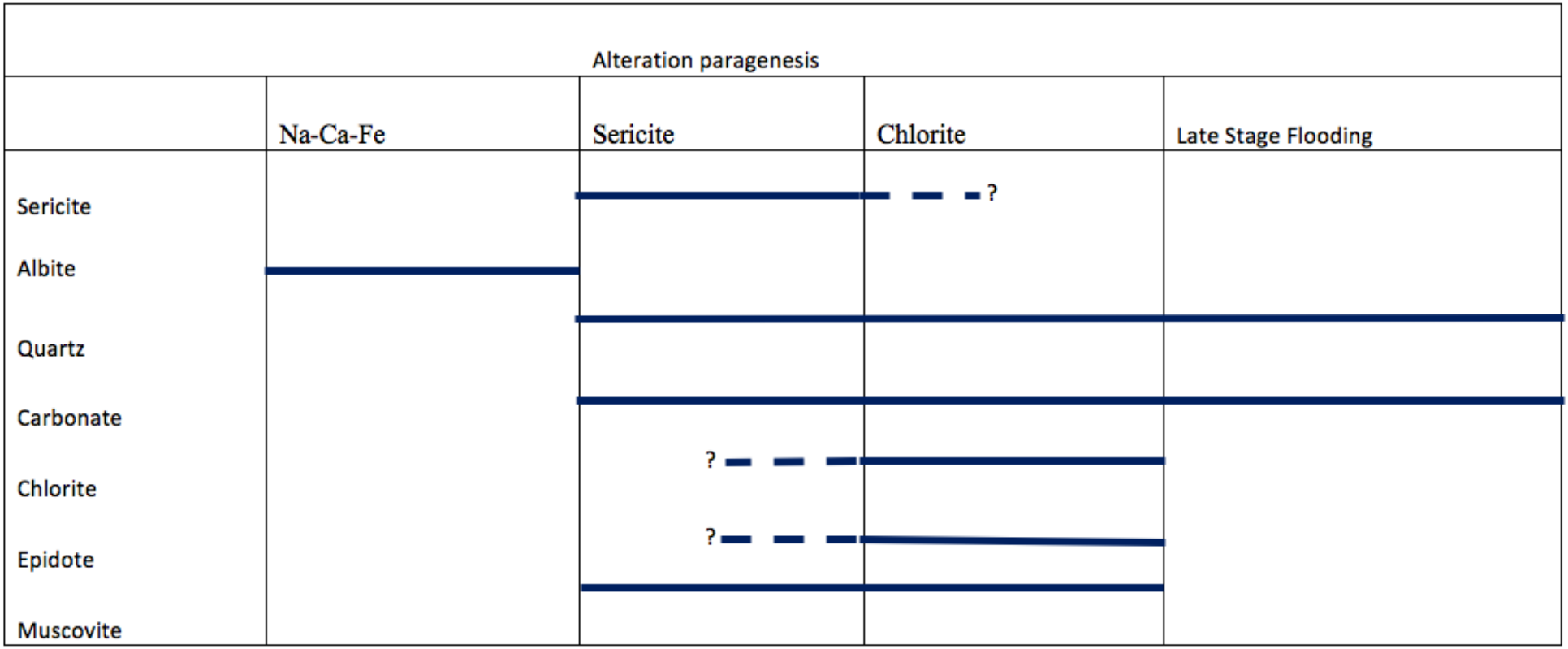

Figure 19: Paragenic sequence of minerals in observed alteration styles.

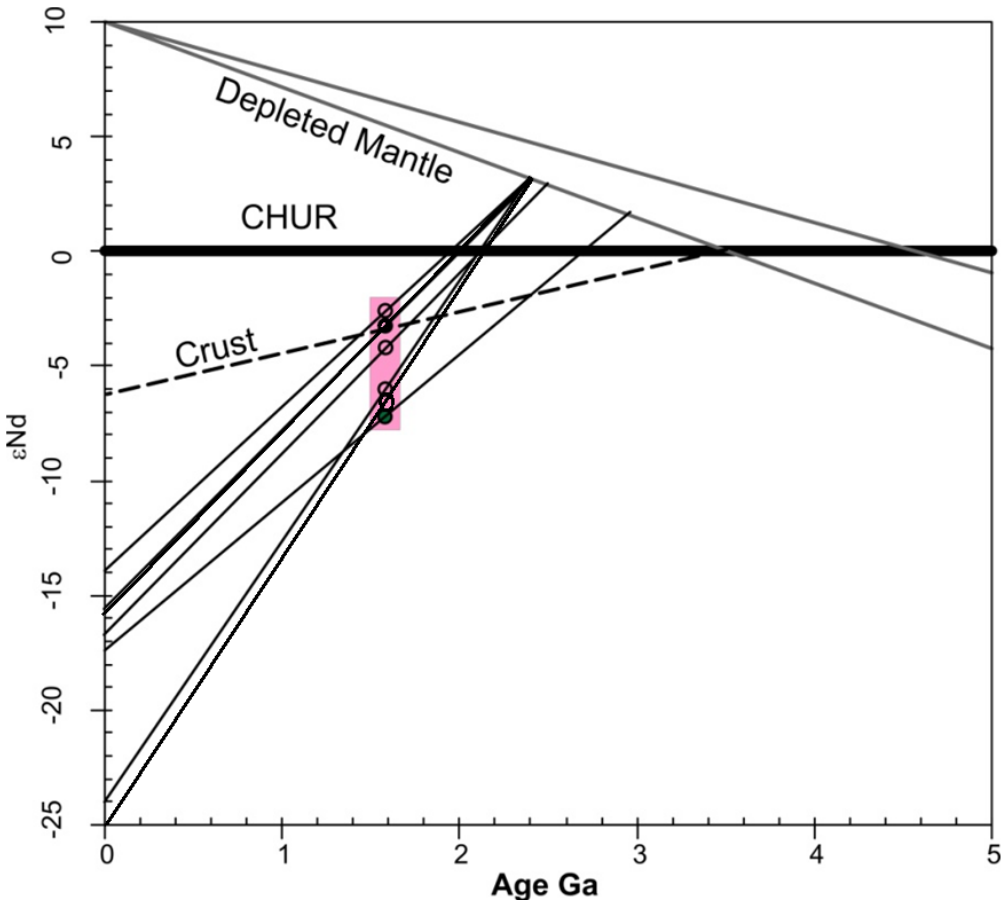

Figure 20: εNd interpretation of the Sm/Nd analysis of Moola Prospect mineralised rock samples (red Box with circles.

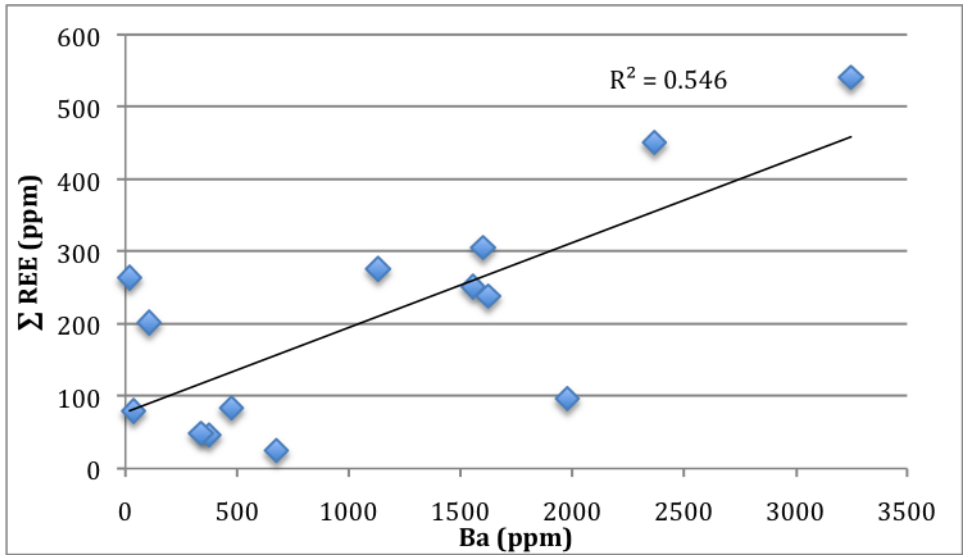

Figure 21: Binary plot of ∑REE against Ba ppm.

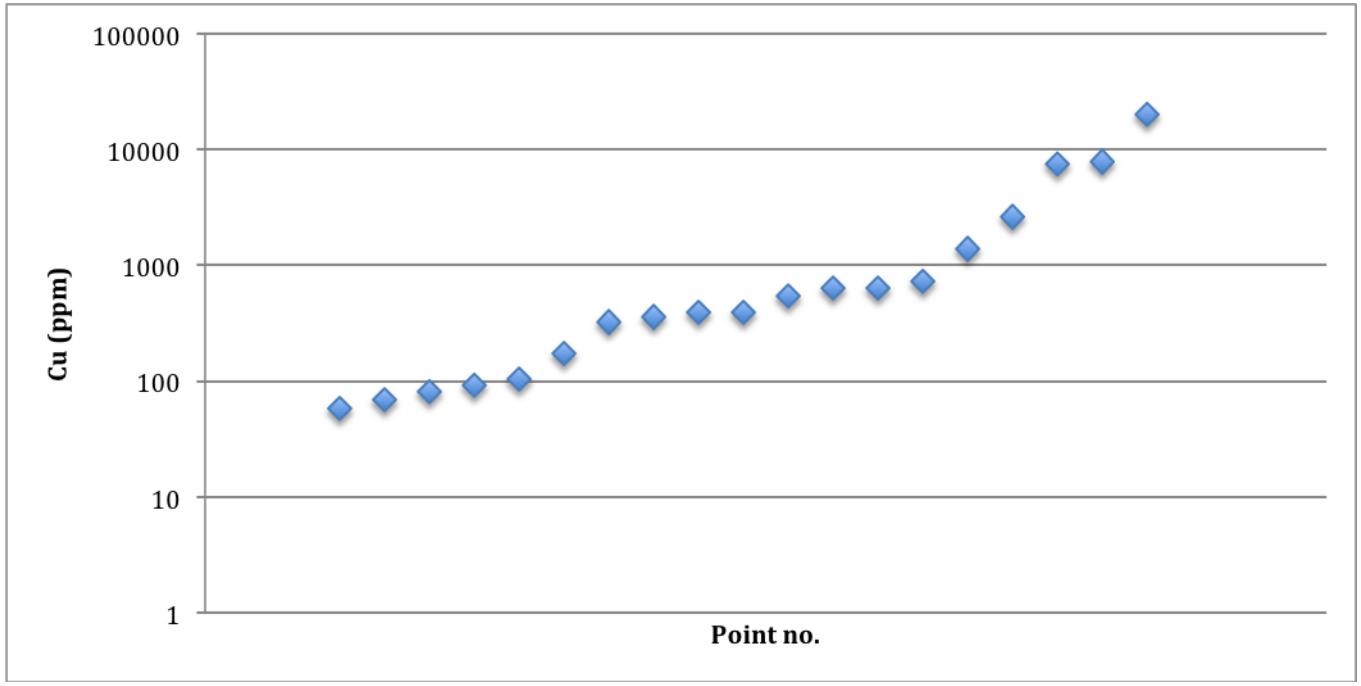

Figure 22: Copper concentration in pyrite arranged from lowest to highest concentration

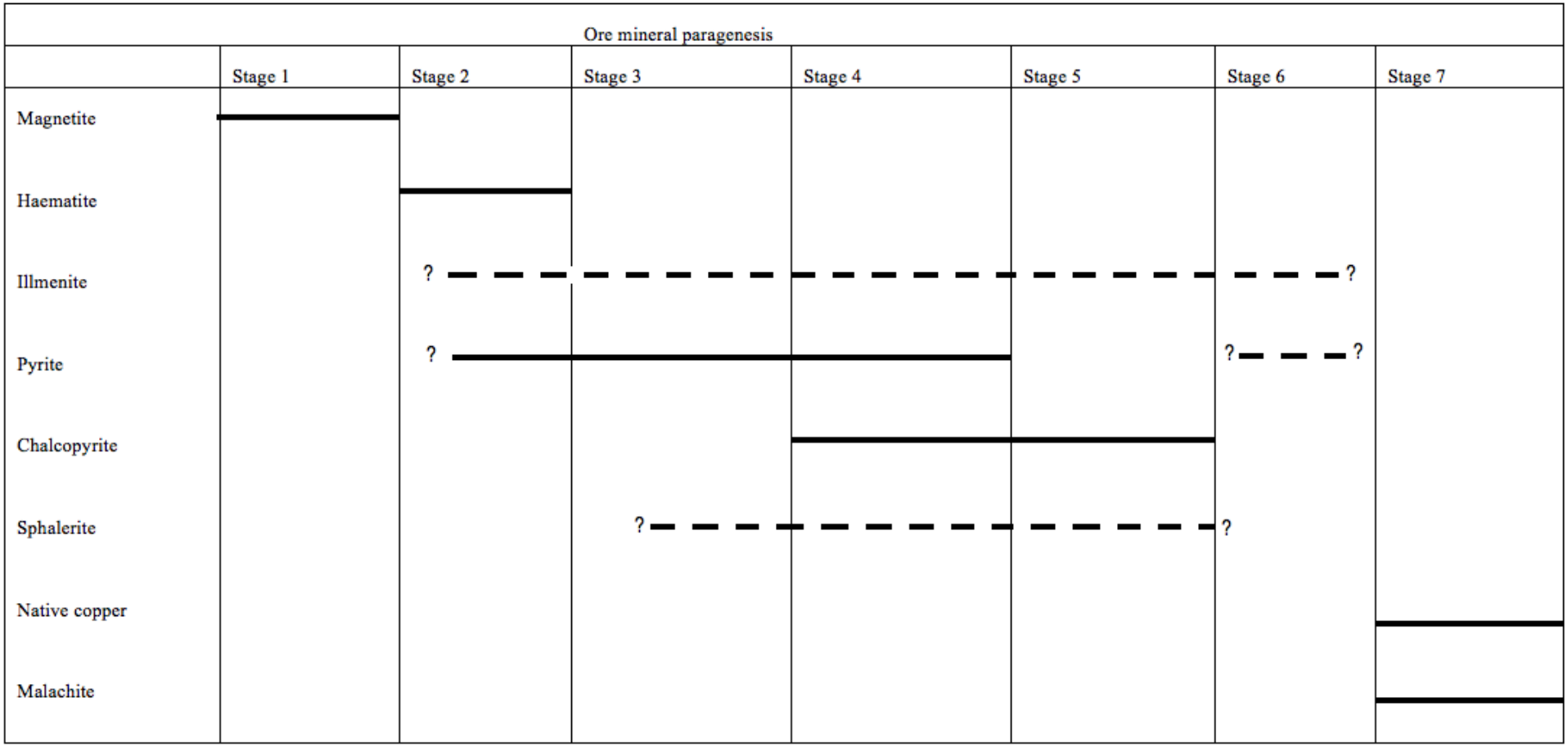

Figure 23: Paragenic sequence of opaque minerals.

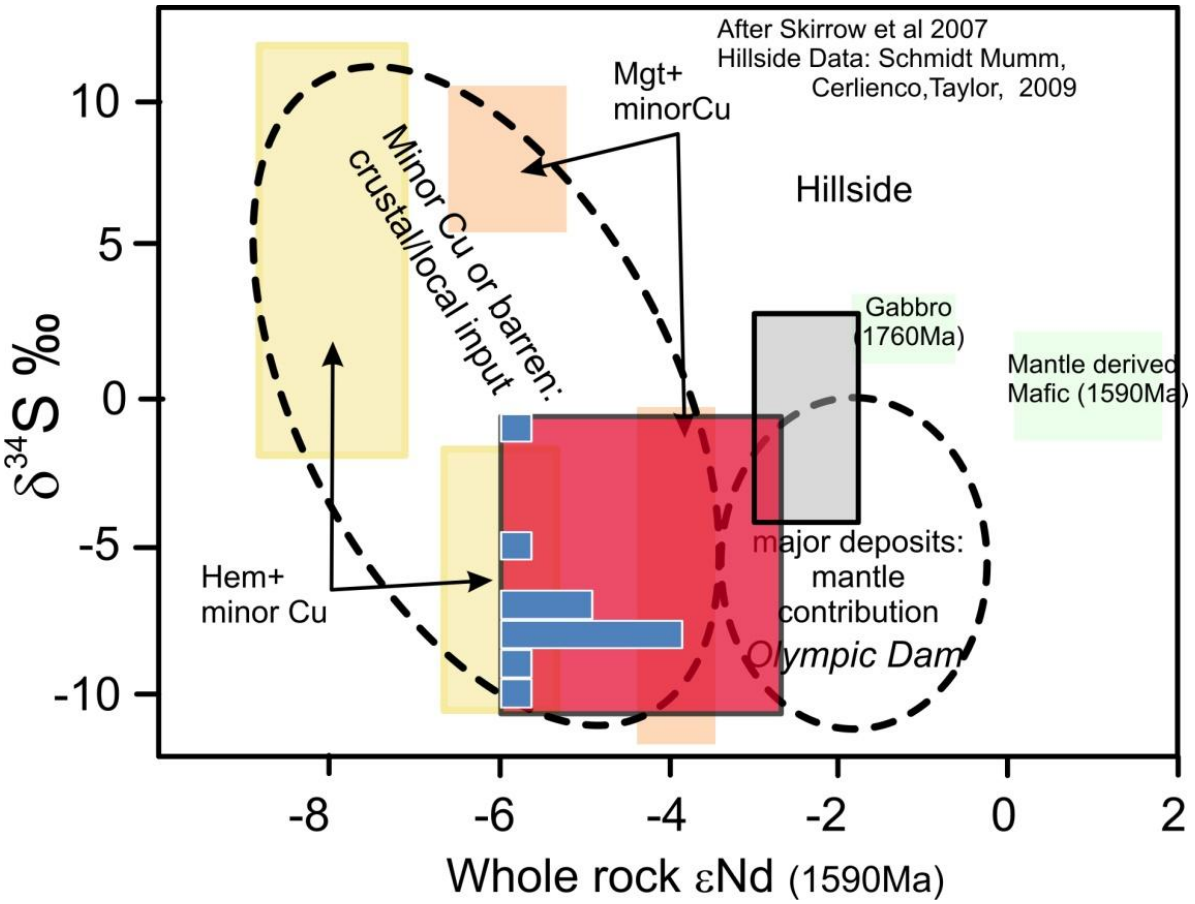

Figure 24: εNd interpretation of the Sm/Nd analysis of Moola Prospect mineralised rock samples (red square), grey rectangle represents Hillside εNd values from Johnson & McCulloch, 1995, hatched rectangle are data from Skirrow et al (2006) of sub-economic IOCG occurrences of the Gawler Craton.

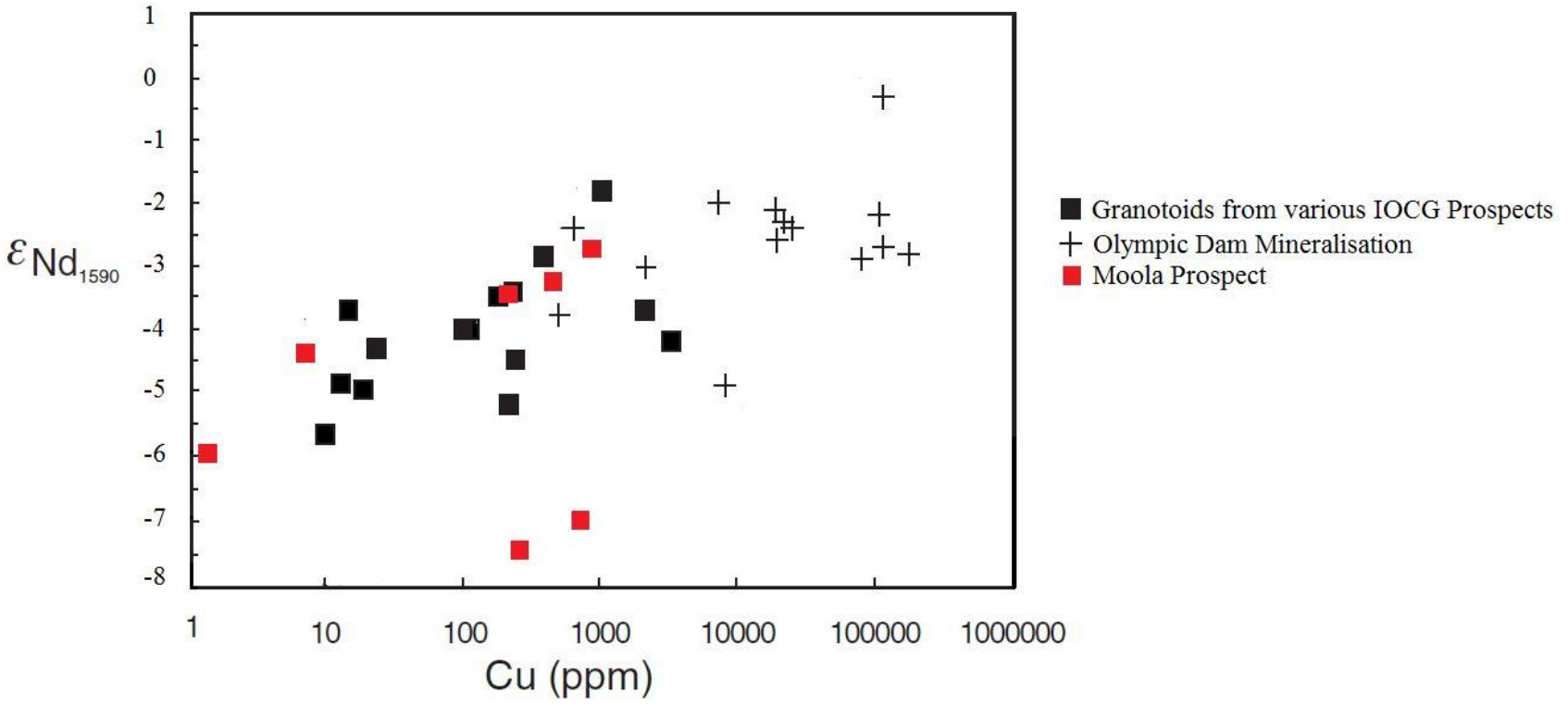

Figure 25: Bianary plot of εNd(1590ma) v's Cu concentration.Modified from Skirrow et al (2007)

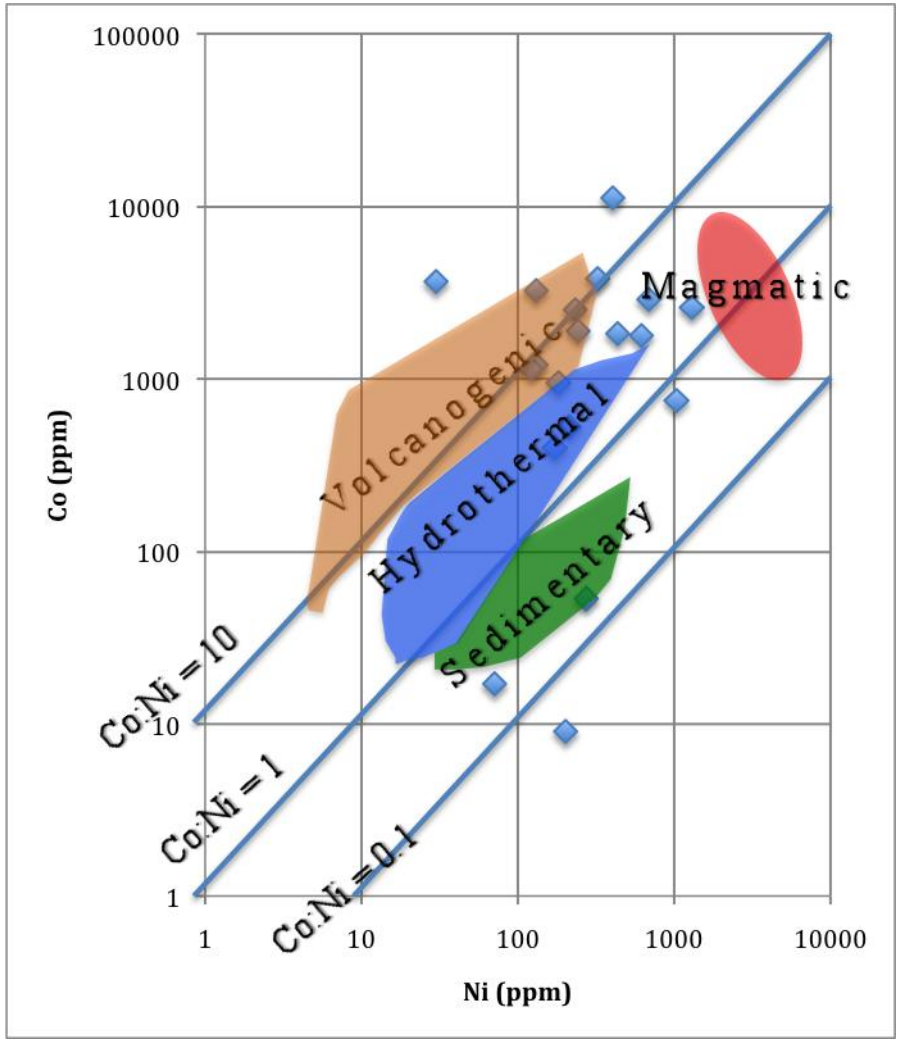

Figure 26: Co: Ni ratio diagram modified from Monterio et al. (2008) Co:Ni diagram, with pyrite Co and Ni concentrations from the Moola Prospect plotted on to the diagram

Tables

Sample	Locality	Petrology	SiO2 %	Al2O3 %	Fe2O3 %	MnO %	MgO %	CaO %	Na2O %	K2O %	TiO2 %	P2O5 %	SO3 %
MC003	ML001 (core)	Altered Granite	75.23	13.66	0.98	0.01	0.33	0.22	2.85	5.73	0.05	0.06	0.00
MC008	ML001 (core)	Altered Rhy	62.72	14.74	1.18	0.20	0.49	5.12	4.16	5.69	0.15	0.07	0.30
MC005	ML001 (core)	Altered AMP	45.87	12.52	16.09	0.28	5.89	8.08	1.40	1.38	2.26	0.42	0.35
MC001	ML001 (core)	Altered QFHGNS	49.89	15.45	16.37	0.19	5.55	0.44	0.51	2.81	2.71	0.27	0.01
MC004	ML001 (core)	Altered QFGNS	80.83	9.11	1.71	0.03	0.46	0.76	2.35	3.25	0.30	0.10	0.02
MC009	ML001 (core)	Altered QFGNS	79.25	9.97	1.33	0.21	0.42	0.93	1.98	3.49	0.17	0.08	0.10
MC012	ML001 (core)	Altered RHY DAC	47.42	13.82	16.05	0.23	7.20	2.85	2.99	0.11	2.70	0.35	0.02
MC013	ML001 (core)	Altered RHY DAC	56.90	16.55	9.39	0.13	4.14	1.11	3.86	2.85	0.84	0.16	0.01
MV001	Myola hills	RHY	71.95	12.92	3.91	0.01	0.04	0.09	4.28	4.81	0.46	0.04	0.00
MV003	Myola hills	RHY	71.92	12.80	4.06	0.04	0.10	0.57	3.53	5.59	0.35	0.03	0.01
18879	Myola hills	RHY	69.74	12.75	4.88	0.05	0.11	1.36	3.37	5.76	0.44	0.04	0.04
MV004	Myola hills	RHY	70.25	13.01	5.11	0.06	0.07	0.78	4.90	3.84	0.47	0.07	0.03
18858	Myola hills	AMP	46.93	13.80	14.41	0.36	6.21	7.56	2.61	2.32	2.42	0.86	0.01
18780	Myola hills	QFGNS	71.91	12.61	4.27	0.05	0.11	1.61	3.21	4.83	0.37	0.07	0.00
18781	Myola hills	QFGNS	72.21	13.06	3.08	0.05	0.27	6.69	3.15	0.23	0.48	0.07	0.00

Table 1: Major element, XRF analyses of selected samples of Moola Prospect core (ML001) and Myola Volcanics (Myola hills) (oxides %)

Sample	Locality	Petrology	Li	Be	B	Sc	V	Cr	Mn	Ni	Cu	Zn	Ga	As	Rb	Sr	Y	Cd	Cs	Ba	Re	Pb	Bi	Th	U	Zr	Nb
MC003	Core	Alt granite	6.97	4.74	688.16	5.03	10.90	3.79	172.19	3.47	6.47	50.67	128.13	1.09	565.72	83.42	24.71	0.00	38.53	374.48	0.00	110.57	0.23	14.89	5.25	33.20	12.40
MC008	Core	Alt rhyolite	6.30	2.97	14.73	2.46	7.02	4.55	2554.06	5.47	1421.14	6.99	170.95	0.83	375.46	83.66	11.47	0.00	7.76	675.83	0.00	118.35	1.39	14.06	36.23	123.60	15.70
MC005	Core	Alt amphibolite	41.47	2.52	10.48	55.54	772.53	137.14	3232.75	107.31	261.07	411.01	375.53	3.57	81.56	235.89	58.87	0.00	1.53	1556.35	0.00	110.35	0.98	7.66	2.85	210.40	15.50
MC001	Core	Alt Q-F-H gneiss	78.70	5.85	25.02	15.30	877.63	9.18	1951.83	56.50	185.05	371.24	60.20	1.29	5.10	15.14	19.77	0.00	5.93	36.51	0.00	10.92	1.90	5.65	5.34	187.70	14.50
MC004	Core	Alt Q-F gneiss	11.54	1.13	10.72	5.17	31.49	22.04	244.38	8.67	307.70	57.18	125.98	0.98	134.15	61.54	13.70	0.00	2.49	474.96	0.00	30.23	0.03	10.49	7.95	133.60	5.30
MC009	Core	Alt Q-F gneiss	3.00	1.80	12.90	2.61	17.08	32.44	1635.91	16.19	641.41	10.69	98.38	0.66	254.11	37.88	11.71	0.00	6.36	338.19	0.00	33.08	0.06	7.19	8.50	81.80	7.20
MC012	Core	Alt rhyodacite	64.97	2.23	1.60	19.31	559.30	121.29	2280.04	68.59	473.04	938.88	61.31	3.13	9.22	38.42	57.60	0.00	2.78	18.78	0.00	111.08	0.03	8.07	6.01	261.10	16.50
MC013	Core	Alt rhyodacite	35.78	2.43	12.20	7.20	134.17	83.01	726.57	35.97	1.17	111.06	68.45	5.57	95.25	45.94	21.39	0.00	3.27	106.16	0.00	11.17	0.00	17.42	6.55	169.80	13.40
MV001	Myola hills	Rhyolite	0.81	3.39	0.94	11.71	3.13	4.03	73.88	2.69	14.90	49.49	869.05	5.97	192.83	121.30	103.76	0.00	4.26	3248.59	0.00	54.49	0.09	29.76	7.54	621.90	33.70
MV003	Myola hills	Rhyolite	2.91	1.96	1.44	6.13	1.29	1.54	348.10	1.37	25.00	68.24	463.06	2.85	201.77	75.60	44.40	0.00	3.99	1624.34	0.00	40.63	0.00	17.75	7.62	557.80	35.10
18879	Myola hills	Rhyolite	1.86	4.31	0.38	7.25	0.60	1.47	488.47	1.03	7.66	129.93	540.93	1.41	197.70	98.16	21.65	0.00	1.15	1978.61	0.00	91.80	0.00	9.50	9.50	612.60	33.70
MV004	Myola hills	Rhyolite	1.10	3.85	1.58	11.94	1.56	3.01	536.90	5.08	31.21	29.81	657.30	4.79	144.56	130.85	88.14	0.00	2.24	2368.49	0.00	44.59	0.00	26.34	7.55	612.40	34.10
18858	Myola hills	Amphibolite	21.09	2.47	19.75	38.66	341.75	196.86	3186.32	118.54	12.09	241.44	284.57	3.69	103.52	194.01	43.63	0.00	2.58	1131.07	0.00	21.39	0.00	7.76	1.09	218.10	19.10
18780	Myola hills	Q-F gneiss	1.79	3.25	1.18	6.20	0.53	6.71	419.52	3.44	20.09	85.41	460.76	2.94	197.72	137.92	51.97	0.00	2.85	1601.24	0.00	63.92	0.08	19.90	7.97	591.00	35.30
18781	Myola hills	Q-F gneiss	7.75	6.29	12.33	17.91	0.70	1.35	656.53	1.09	1.07	47.09	109.11	6.55	28.27	557.86	115.28	0.00	2.66	132.26	0.00	39.04	0.92	27.28	12.86	576.50	33.60

Table 2: Trace element, XRF and solution ICP-MS analyses of selected samples of Moola Prospect core (ML001) and Myola Volcanics (Myola hills) (ppm)

Sample	Locality	Petrology	La	Ce	Pr	Nd	Sm	Eu	Gd	Tb	Dy	Ho	Er	Yb	Lu
MC003	Core	Alt granite	7.89	15.18	1.76	6.74	1.57	0.34	2.13	0.29	3.45	0.62	2.52	3.46	0.37
MC008	Core	Alt rhyolite	4.62	5.50	1.12	4.88	1.21	0.18	1.52	0.14	2.20	0.31	1.40	1.76	0.12
MC005	Core	Alt amphibolite	46.69	97.96	10.90	44.86	9.94	2.79	10.95	1.57	10.85	2.08	6.41	5.81	0.69
MC001	Core	Alt Q-F-H gneiss	7.19	40.27	2.62	12.17	2.98	0.65	3.47	0.41	3.84	0.68	2.48	2.58	0.22
MC004	Core	Alt Q-F gneiss	17.95	37.49	3.75	14.05	2.58	0.44	2.40	0.19	2.15	0.28	1.19	1.24	0.03
MC009	Core	Alt Q-F gneiss	10.13	20.12	2.18	8.61	1.60	0.24	1.67	0.11	1.67	0.21	1.00	1.08	0.02
MC012	Core	Alt rhyodacite	47.23	107.31	10.77	42.29	9.35	2.21	10.71	1.81	13.53	2.68	8.07	7.12	0.83
MC013	Core	Alt rhyodacite	40.82	100.42	8.76	32.47	5.53	0.89	4.34	0.42	3.38	0.54	2.04	2.08	0.13
MV001	Myola hills	Rhyolite	118.04	220.34	25.67	91.69	17.79	4.08	18.73	2.62	16.92	3.38	10.37	9.92	1.36
MV003	Myola hills	Rhyolite	27.52	123.03	9.08	35.65	7.50	1.31	7.84	1.23	9.59	1.97	6.47	6.41	0.81
18879	Myola hills	Rhyolite	11.37	43.25	3.48	14.78	3.39	0.76	3.62	0.58	5.45	1.08	3.98	4.47	0.53
MV004	Myola hills	Rhyolite	90.78	204.24	19.18	70.23	13.47	3.04	13.42	1.99	13.47	2.72	8.70	8.51	1.14
18858	Myola hills	Amphibolite	45.62	128.85	11.94	48.08	9.82	2.66	9.65	1.20	8.06	1.45	4.44	3.86	0.41
18780	Myola hills	Q-F gneiss	55.22	136.00	13.30	50.41	10.31	1.74	10.18	1.53	10.65	2.10	6.65	6.53	0.84
18781	Myola hills	Q-F gneiss	131.80	289.63	29.93	101.23	19.39	3.60	18.69	2.76	18.00	3.66	11.36	11.08	1.52

Table 3: Rare Earth Element, solution ICP-MS analyses of selected samples of Moola Prospect core (ML001) and Myola Volcanics (Myola hills) (ppm)

Sample ID	Mineral	$\delta^{34}S$ Value	std. dev.
OO4	Chalcopyrite	-10.5	0.2
6	Chalcopyrite	-8.9	0
#18	Chalcopyrite	-8.9	0.1
#9	Chalcopyrite	-5.4	0.1
#17	Chalcopyrite	-8.8	0.1
#19	Chalcopyrite	-9.4	0.2
#21	Chalcopyrite	-7.3	0.1
#A18	Chalcopyrite	-8.6	0.1
PBS	Chalcopyrite	-8.5	0
#11	Chalcopyrite	-7.8	0
#1	Pyrite	-7.9	0.1
#A11	Pyrite	-8	
OO5	Pyrite	-1.2	0.1

Table 5: Sulphur isotope data of selected sulphides

Sample	Nd (ppm)	Sm (ppm)	143Nd/ 144Nd	147Sm/ 144Nd	ENd (T0)
MC001	20.39114478	4.602384919	0.511839777	0.136435564	-15.57088935
MC003	5.816664272	1.303084316	0.511779648	0.135439798	-16.74381497
MC005	69.10626559	16.76382457	0.511744583	0.146636946	-17.42783349
MC008	4.640847771	1.086697223	0.511928829	0.141582641	-13.83375775
MC009	10.58222774	1.828993735	0.511345192	0.104498317	-25.21872655
MC0012	39.49061561	8.572366349	0.51178365	0.131235687	-16.66575888
MC0013	41.48103117	7.462491278	0.511414729	0.108760466	-23.86228208

Table 6: Results of the Sm and Nd isotopic analysis.

Sample	Lithology	Sr ppm	87Sr/86Sr	1 SD
MC001	Granite	83	1.5859817	0.0001981
MC003	Rhyolite	83	1.1669414	0.0001768
MC005	Amphibolite	235	1.1698976	0.0001545
MC008	Q-F Gniess	15	0.750298	0.0000791
MC009	Q-F Gniess	38	1.1542254	0.0001663
MC012	Rhyodacite	38	1.0951296	0.0002749
MC013	Rhyodacite	46	0.9377624	0.0001394

Table 7: Sr content and (87Sr/86Sr) variation in altered samples

Sample	Petrolography	Age of Rock (Ma)	*143Nd/144Nd (T)*	*ENd (T)*	*TDM (Ma)*	*TCHUR (Ma)*
MC001	Q-F Gniess	1590	0.510413636	-3.316462671	2545.04166	2015.308095
MC003	Granite	1590	0.510363916	-4.29025195	2627.601028	2131.025638
MC005	Amphibolite	1590	0.510211809	-7.269347377	3134.262325	2710.024193
MC008	Rhyolite	1590	0.510448886	-2.626068977	2539.547207	1958.345786

MC009	Q-F Gniess	1590	0.510252887	-6.464813532	2488.371586	2131.367166
MC0012	Rhyodactite	1590	0.510411862	-3.351199788	2488.777873	1985.612671
MC0013	Rhyodactite	1590	0.510277872	-5.97547336	2488.930682	2114.698055

Table 8: Interpretation of Sm and Nd isotopic analysis results

Sample	Petrology	S	P	V	Mn	Co	Ni	As	Mo	Ag	Cd	Sb	Pb	Bi
1	Chalcopyrite	W%	ppm	ppm	ppm	ppm	ppm	ppm	ppm	ppm	ppm	ppm	ppm	ppm
2	Chalcopyrite	34.6897	311	206	10<	10<	20<	10<	416	5<	175	382	1106	802
3	Chalcopyrite	34.809	132	301	10<	10<	339	10<	694	5<	1312	5<	1415	1942
4	Chalcopyrite	34.6252	198	95	221	10<	20<	637	361	469	5<	5<	1460	2365
5	Chalcopyrite	34.8526	378	32	10<	10<	20<	802	5<	5<	5<	5<	1062	1014
6	Chalcopyrite	34.7213	246	47	242	10<	47	1120	139	5<	5<	350	1152	1649
7	Chalcopyrite	34.5357	47	32	116	10<	537	10<	28	5<	350	5<	620	550
8	Chalcopyrite	35.4583	395	5<	10<	10<	20<	1207	5<	565	5<	5<	30<	886
9	Chalcopyrite	34.717	246	190	10<	10<	20<	193	5<	31	5<	175	1062	2324
10	Chalcopyrite	34.8597	274	5<	11	10<	20<	864	5<	407	5<	941	1549	1183
11	Chalcopyrite	34.527	236	16	168	10<	38	222	1195	5<	5<	5<	797	50<
12	Chalcopyrite	34.6695	330	47	231	10<	20<	627	5<	188	350	5<	354	972
13	Chalcopyrite	34.6036	331	5<	63	255	301	694	5<	5<	5<	590	30<	127
14	Chalcopyrite	34.635	255	5<	21	10<	160	856	5<	5<	5<	335	30<	3002
15	Chalcopyrite	34.5268	76	348	200	10<	273	10<	5<	5<	657	175	2568	888

16	Chalcopyrite	34.58	170	159	10<	187	395	247	806	251	5<	5<	443	1057
17	Chalcopyrite	34.2424	302	158	10<	10<	20<	10<	5<	5<	5<	5<	1152	888
18	Chalcopyrite	34.3438	104	32	10<	10<	20<	362	5<	5<	88	5<	1063	1395
19	Chalcopyrite	33.5187	378	5<	10<	10<	254	34	5<	5<	5<	5<	30<	50<
20	Chalcopyrite	33.9154	406	63	84	10<	20<	902	806	5<	175	223	30<	677
21	Chalcopyrite	34.7903	208	270	295	10<	151	534	5<	5<	614	5<	1151	1944
22	Chalcopyrite	34.5633	226	5<	10<	10<	20<	203	5<	471	176	256	2345	634
23	Chalcopyrite	34.5351	330	64	126	280	20<	820	5<	5<	703	5<	708	2578
24	Chalcopyrite	34.9996	273	5<	137	48	20<	265	111	5<	5<	608	752	1013
25	Chalcopyrite	34.7735	123	429	200	11	20<	560	805	5<	308	144	1769	50<
26	Chalcopyrite	32.5905	169	175	275	10<	28	283	5<	5<	5<	256	926	547
27	Chalcopyrite	34.7097	132	127	74	10<	20<	130	194	597	5<	752	795	759
28	Chalcopyrite	35.2826	235	5<	222	10<	20<	343	5<	5<	881	5<	30<	169
29	Chalcopyrite	34.7334	179	5<	169	16	670	521	5<	5<	5<	336	30<	633
30	Chalcopyrite	34.8664	328	64	74	10<	565	142	55	157	397	594	1588	2233
31	Chalcopyrite	34.6279	396	5<	10<	10<	20<	10<	5<	5<	5<	5<	531	1351
32	Chalcopyrite	34.386	30<	5<	95	10<	20<	185	888	565	5<	5<	265	1815

33	Chalcopyrite	34.553	188	5<	116	194	20<	1052	5<	5<	5<	384	1105	1393
34	Chalcopyrite	34.6164	85	5<	242	10<	28	501	5<	63	1537	48	663	2026
35	Chalcopyrite	34.6393	141	5<	10<	45	20<	682	5<	5<	264	128	265	50<
36	Chalcopyrite	34.6507	301	446	10<	10<	20<	987	5<	284	44	5<	795	1856
37	Chalcopyrite	34.1932	263	5<	95	10<	188	854	5<	786	264	256	1060	506
38	Chalcopyrite	34.5324	394	191	10<	10<	20<	96	582	693	5<	5<	88	1602
39	Chalcopyrite	34.4984	197	175	10<	142	56	184	5<	882	5<	674	1368	1012
40	Chalcopyrite	34.3222	141	143	10<	51	47	266	1412	566	749	5<	1412	1475
41	Chalcopyrite	34.7095	272	5<	105	10<	20<	330	305	5<	5<	5<	795	211
42	Chalcopyrite	34.7136	301	5<	10<	10<	20<	271	5<	189	5<	5<	1325	50<
43	Chalcopyrite	34.7753	441	5<	190	10<	94	55	609	32	44	225	1015	1264
44	Chalcopyrite	34.8187	338	5<	10<	10<	20<	426	1468	5<	5<	192	662	674
45	Chalcopyrite	34.6667	319	5<	105	10<	20<	438	5<	157	44	5<	1545	2361
46	Chalcopyrite	34.3804	75	5<	10<	10<	433	78	111	5<	132	336	707	1857
47	Chalcopyrite	34.4469	207	32	158	10<	20<	65	5<	283	5<	176	751	2404
48	Chalcopyrite	34.321	263	95	10<	10<	20<	365	277	5<	88	944	1944	50<
49	Chalcopyrite	34.3048	263	286	10<	10<	20<	996	5<	5<	176	1009	1723	717

50	Chalcopyrite	34.347	56	5<	158	10<	207	552	277	252	5<	433	3177	50<
51	Chalcopyrite	34.3152	150	5<	10<	10<	20<	1244	444	5<	749	5<	221	1266
52	Chalcopyrite	33.1358	245	175	10<	10<	20<	698	1638	5<	264	5<	1327	507
53	Chalcopyrite	34.2569	338	5<	11	10<	20<	10<	637	5<	618	5<	1369	1940
54	Chalcopyrite	34.145	225	5<	116	10<	20<	186	1024	5<	795	5<	1190	1348
55	Chalcopyrite	34.1861	169	5<	116	78	19	10<	5<	284	5<	530	30<	1053
56	Chalcopyrite	34.3765	231	403	10<	10<	20<	477	357	989	5<	5<	1618	1296
57	Chalcopyrite	34.2308	405	5<	43	10<	227	390	5<	32	5<	5<	437	1253
58	Chalcopyrite	34.4118	166	65	10<	76	20<	10<	5<	96	5<	211	612	459
59	Chalcopyrite	34.2823	423	5<	10<	10<	180	614	5<	160	5<	5<	1309	918
60	Chalcopyrite	34.3406	111	5<	128	10<	19	509	5<	768	5<	5<	829	1336
61	Chalcopyrite	34.3034	55	5<	10<	278	246	130	5<	5<	5<	310	30<	708
62	Chalcopyrite	34.2509	247	113	54	10<	20<	10<	5<	5<	5<	620	1217	50<
63	Chalcopyrite	34.4016	219	81	118	63	20<	300	5<	515	5<	5<	1259	706
64	Chalcopyrite	34.3421	355	162	10<	62	20<	443	5<	5<	5<	425	2992	1992
65	Chalcopyrite	34.5408	382	292	268	10<	133	1013	5<	5<	5<	278	43	1162
66	Chalcopyrite	34.164	328	5<	10<	84	484	10<	1281	32	90	5<	1431	830

67	Chalcopyrite	34.5141	127	33	11	69	256	84	815	129	5<	541	1038	2690
68	Chalcopyrite	36.8779	190	5<	10<	10<	134	121	398	708	141	5<	1560	1416
69	Chalcopyrite	34.9905	117	82	367	10<	20<	722	162	716	5<	5<	1679	2185
70	Chalcopyrite	33.1016	254	342	258	185	29	260	326	129	362	820	476	455
71	Chalcopyrite	34.9524	234	5<	10<	10<	400	10<	1056	292	91	5<	603	1691
72	Chalcopyrite	34.7354	216	131	313	10<	459	209	1299	292	454	5<	1679	50<
73	Chalcopyrite	34.8682	323	5<	259	10<	20<	690	325	5<	5<	148	688	1236
74	Chalcopyrite	34.6915	232	5<	10<	10<	86	133	512	847	364	5<	558	452
75	Chalcopyrite	34.976	134	164	10<	10<	441	1143	1213	5<	821	5<	772	986
76	Chalcopyrite	35.2026	250	98	152	10<	163	638	566	5<	5<	198	429	246
77	Chalcopyrite	34.1089	303	180	10<	10<	20<	10<	781	229	5<	231	1328	1272
78	Chalcopyrite	34.5975	232	5<	10<	10<	20<	10<	5<	196	91	908	1115	1068
79	Chalcopyrite	34.7264	63	5<	97	10<	20<	511	5<	294	5<	446	1930	329
80	Chalcopyrite	33.9176	357	98	10<	10<	163	329	5<	5<	320	347	814	369
81	Chalcopyrite	35.0253	143	5<	10<	10<	1	396	5<	98	5<	297	1330	699
82	Chalcopyrite	34.3734	30<	5<	152	10<	459	10<	5<	5<	5<	5<	1115	822
83	Chalcopyrite	34.7186	170	5<	206	10<	20<	620	5<	391	5<	149	730	82

84	Chalcopyrite	35.0196	286	164	10<	41	86	294	5<	848	5<	5<	1458	904
85	Chalcopyrite	36.2124	247	49	251	10<	441	10<	295	5<	92	5<	30<	1103
86	Chalcopyrite	34.6234	268	5<	10<	142	163	10<	5<	522	410	462	771	287
87	Chalcopyrite	34.8125	267	5<	10<	41	297	357	943	5<	5<	5<	514	1806
88	Chalcopyrite	35.0106	374	5<	10<	59	20<	502	5<	5<	5<	5<	1242	205
89	Chalcopyrite	34.3399	232	5<	173	10<	497	306	1213	685	1094	5<	729	1560
90	Chalcopyrite	34.8661	214	16	10<	325	163	369	5<	5<	5<	5<	815	1849
91	Chalcopyrite	35.0386	249	5<	163	10<	20<	1012	969	915	5<	5<	985	1436
92	Chalcopyrite	34.561	402	5<	336	10<	20<	432	5<	5<	182	1007	472	452
93	Chalcopyrite	34.6481	267	5<	119	76	172	622	2233	1667	5<	596	30<	1517
94	Chalcopyrite	34.288	330	213	10<	10<	20<	205	620	196	410	5<	814	698
95	Chalcopyrite	34.4534	330	5<	10<	10<	20<	39	1375	5<	5<	5<	214	575
96	Chalcopyrite	33.861	401	5<	303	10<	20<	10<	1105	5<	5<	5<	900	2586
97	Chalcopyrite	35.0548	159	181	10<	10<	20<	436	322	33	460	5<	1364	50<
98	Chalcopyrite	34.9469	309	247	10<	10<	268	273	536	5<	321	5<	1236	817
99	Chalcopyrite	34.9055	380	5<	65	47	20<	10<	5<	1083	5<	5<	1237	1185
100	Chalcopyrite	34.4993	246	5<	10<	10<	106	10<	5<	165	5<	5<	1318	1793

101	Chalcopyrite	34.4647	309	5<	10<	191	422	210	5<	5<	5<	5<	2088	3022
102	Chalcopyrite	34.6197	238	5<	207	10<	422	10<	5<	559	321	216	724	1511
103	Chalcopyrite	34.4608	229	5<	33	10<	106	10<	5<	5<	5<	5<	893	408
104	Chalcopyrite	34.539	290	231	98	184	20<	43	5<	494	5<	5<	1148	50<
105	Chalcopyrite	33.9901	123	83	109	398	20<	10<	668	826	5<	667	382	2402
106	Chalcopyrite	34.6752	61	5<	10<	10<	182	187	5<	5<	5<	283	1317	1873
107	Chalcopyrite	34.7957	316	5<	10<	10<	20<	10<	214	659	783	167	637	1955
108	Chalcopyrite	34.804	255	298	175	10<	20<	377	267	99	5<	717	1359	81
109	Chalcopyrite	35.0162	88	5<	10<	10<	20<	63	5<	330	5<	5<	1273	651
110	Chalcopyrite	34.5817	368	5<	273	10<	144	374	27	198	230	5<	85	2970
111	Chalcopyrite	34.2831	53	5<	10<	234	499	174	800	826	138	5<	1611	2480
112	Chalcopyrite	34.4484	132	5<	10<	308	20<	620	53	33	276	5<	30<	326
113	Chalcopyrite	34.5415	210	5<	10<	10<	20<	321	160	5<	5<	651	1188	1627
114	Chalcopyrite	34.7509	183	5<	427	10<	337	119	906	5<	5<	5<	931	203
115	Chalcopyrite	34.4238	314	33	10<	10<	20<	694	5<	5<	971	50	973	2030
116	Chalcopyrite	34.5596	227	397	10<	105	183	10<	53	199	601	468	1525	569
117	Chalcopyrite	34.8096	331	116	10<	42	394	10	53	99	463	5<	1312	934

118	Chalcopyrite	34.5738	200	5<	10<	10<	20<	34	692	232	648	5<	1986	2797
119	Chalcopyrite	34.5091	243	332	10<	10<	20<	10<	558	399	5<	5<	2619	1175
120	Chalcopyrite	35.1126	348	33	10<	10<	86	651	319	166	5<	5<	1184	2190
121	Chalcopyrite	37.161	146	84	232	107	19	198	5<	504	5<	5<	30<	1289
122	Chalcopyrite	34.9121	192	5<	230	10<	154	216	5<	5<	695	151	1057	1217
123	Chalcopyrite	35.0234	226	149	10<	10<	20<	847	5<	5<	232	5<	2157	771
124	Sphalerite	35.0513	139	365	10<	41	20<	650	5<	5<	232	5<	887	50<
125	Sphalerite	32.1841	225	264	10<	648	20<	304	2029	623	5<	5<	30<	1429
126	Sphalerite	32.0608	113	5<	10<	128	82	282	5<	5<	1190	5<	1694	1209
127	Sphalerite	32.2458	30<	5<	10<	128	613	312	5<	164	1054	5<	705	671
128	Sphalerite	32.3851	142	313	10<	456	20<	10<	1231	656	5<	5<	30<	579
129	Sphalerite	32.4741	30<	5<	303	350	20<	10<	2257	5<	595	297	1498	1559
130	Sphalerite	32.3943	132	281	10<	247	30	10<	440	5<	46	415	1217	1515
131	Pyrite	32.2917	30<	33	53	10<	20<	220	756	132	5<	5<	30<	1458
132	Pyrite	53.0042	30<	5<	10<	3237	131	2136	726	5<	5<	557	2616	1339
133	Pyrite	53.2628	30<	5<	115	1838	20<	1693	5<	5<	5<	5<	2573	2981
134	Pyrite	53.7289	30<	51	173	2876	688	2247	5<	139	5<	5<	1584	2026

135	Pyrite	53.0899	30<	5<	10<	10<	202	1074	5<	104	5<	5<	1543	4086
136	Pyrite	53.9689	31	5<	10<	10<	20<	978	550	452	5<	5<	1028	1870
137	Pyrite	54.0347	62	5<	10<	1202	131	904	1175	5<	194	17	2531	2634
138	Pyrite	53.7484	46	5<	10<	2506	233	85	325	139	5<	5<	910	458
139	Pyrite	53.6712	30<	5<	10<	11170	405	799	49	428	5<	36	1443	1395
140	Pyrite	53.8487	30<	5<	140	53	274	269	5<	643	5<	445	1750	1505
141	Pyrite	53.6701	45	17	140	10<	20<	563	123	5<	99	5<	2414	1883
142	Pyrite	53.6095	30<	5<	10<	10<	20<	669	5<	5<	5<	5<	1678	1736
143	Pyrite	53.6279	38	5<	10<	17	71	394	5<	5<	396	319	1914	2379
144	Pyrite	51.4242	68	5<	187	524	213	878	124	427	149	5<	1835	1547
145	Pyrite	53.0938	30<	5<	10<	397	172	444	5<	926	347	533	1716	113
146	Pyrite	53.9716	60	70	23	2584	1297	10<	173	5<	99	5<	1560	2412
147	Pyrite	53.9336	112	122	10<	746	1034	268	346	5<	99	284	2145	603
148	Pyrite	53.8509	39	5<	10<	1776	617	2835	525	279	5<	331	910	50<
149	Pyrite	53.4177	46	17	10<	1824	435	3161	5<	139	5<	611	1543	2636
150	Pyrite	53.6312	30<	188	10<	926	20<	2639	5<	453	5<	70	1186	2977
151	Pyrite	54.08	77	5<	10<	557	20<	2131	674	5<	5<	210	1658	1563

152	Pyrite	53.5224	92	5<	127	945	182	1741	424	802	5<	87	1264	877
153	Pyrite	53.8419	23	17	10<	2226	20<	1929	5<	315	5<	5<	1025	799
154	Pyrite	53.7399	200	5<	10<	1140	121	2552	823	559	243	5<	1696	1371
155	Pyrite	53.3185	30<	137	127	7039	20<	5159	5<	1115	5<	5<	712	1298
156	Pyrite	53.3064	30<	171	10<	1887	243	1999	673	35	5<	5<	986	50<
157	Pyrite	53.6787	30<	5<	10<	3802	324	2364	5<	5<	5<	5<	79	1258
158	Pyrite	53.2758	30<	5<	92	3655	30	2520	798	105	5<	175	1617	1866
159	Pyrite	53.3735	84	103	197	4706	20<	2050	1568	175	5<	648	1417	2319

Table 9.1: EMA data for sulphide species (Cu, Zn and Fe excluded due to analytical errors)

Sample	Petrology	S W(%)	Fe W(%)	Cu W(%)	Zn W(%)	Cu (ppm)	Zn (ppm)
Rj004 - 001	Chalcopyrite	33.9241	29.1717	33.6469	0.0001		<20
Rj004 - 2	Chalcopyrite	34.772	29.988	33.6003	0.0253		253
Rj004 - 3	Chalcopyrite	35.121	29.4067	33.2849	0.0001		<20
Rj004 - 5	Chalcopyrite	35.0746	30.6456	34.1804	0.0001		<20
Rj004 - 6	Chalcopyrite	35.1529	30.0346	33.6935	0.0001		<20
Rj004 - 10	Chalcopyrite	35.2447	29.3434	33.5316	0.0291		291
Rj004 - 20	Chalcopyrite	35.0613	30.2457	33.9952	0.0001		<20
Rj004 - 25	Chalcopyrite	34.9994	30.0681	34.1965	0.0531		531
Rj008 - 2	Chalcopyrite	34.8967	30.1487	34.6213	0.0303		303
Rj008 - 3	Chalcopyrite	34.9133	30.167	34.1204	0.0089		89
Rj008 - 4	Chalcopyrite	34.7644	29.8964	33.6454	0.0001		<20
Rj008 - 5	Chalcopyrite	35.0356	30.0086	34.3688	0.0001		<20
Rj008 - 6	Chalcopyrite	33.7345	29.0819	32.8471	0.0001		<20
Rj008 - 7	Chalcopyrite	35.2449	30.109	34.0767	0.0001		<20
Rj008 - 8	Chalcopyrite	34.8993	30.8533	34.6412	0.0215		215

Rj008 - 9	Chalcopyrite	34.7758	30.7065	34.493	0.0001		<20
Rj0012 - 2	Chalcopyrite	34.8895	30.2303	34.3097	0.0001		<20
Rj0012 - 3	Chalcopyrite	34.9218	30.7373	34.781	0.0001		<20
Rj0012 - 4	Chalcopyrite	34.9115	30.4133	34.2673	0.0013		13
Rj0012 - 5	Chalcopyrite	34.8792	30.2189	34.1247	0.0001		<20
Rj0012 - 6	Chalcopyrite	35.207	30.2597	34.1396	0.0001		<20
Rj0012 - 7	Chalcopyrite	33.3423	30.0123	31.952	0.0051		51
Rj0012 - 8	Chalcopyrite	34.8738	30.4028	34.1323	0.0001		<20
Rj0012 - 9	Chalcopyrite	34.9656	29.948	34.2166	0.0001		<20
Rj0012 - 10	Chalcopyrite	35.0134	30.3315	33.8679	0.0177		177
Rj0012 - 11	Chalcopyrite	35.5788	30.6086	34.201	0.0342		342
Rj0012 - 12	Chalcopyrite	35.262	30.4275	34.4981	0.0001		<20
Rj0012 - 13	Chalcopyrite	34.927	30.2502	34.0716	0.0001		<20
Rj015 - 2	Chalcopyrite	35.0795	30.1601	33.9456	0.0001		<20
Rj015 - 3	Chalcopyrite	34.6719	30.5677	34.1228	0.0001		<20
Rj015 - 4	Chalcopyrite	34.5997	30.3666	34.1841	0.0493		493
Rj015 - 6	Chalcopyrite	31.2797	35.5022	27.4182	0.0102		102

Rj006 - 2	Chalcopyrite	35.3138	30.1647	33.5458	0.0089		89
Rj006 - 3	Chalcopyrite	34.659	29.4913	33.8009	0.0657		657
Rj006 - 4	Chalcopyrite	34.7429	29.9348	34.0827	0.0001		<20
Rj006 - 5	Chalcopyrite	34.8014	29.8407	33.6076	0.0025		25
Rj006 - 6	Chalcopyrite	34.9871	30.3202	34.0478	0.0001		<20
Rj006 - 7	Chalcopyrite	35.3569	30.3853	34.4532	0.0001		<20
Rj006 - 8	Chalcopyrite	35.0941	30.1489	34.0672	0.0001		<20
Rj006 - 10	Chalcopyrite	35.2139	30.6392	33.9525	0.0001		<20
Rj006 - 11	Chalcopyrite	35.0312	30.1462	34.2265	0.0001		<20
Rj006 - 12	Chalcopyrite	34.8427	30.5007	34.2043	0.0001		<20
RJ004 point_2	Chalcopyrite	34.6897	30.233	35.3969	0.0001		<20
RJ004 point_3	Chalcopyrite	34.809	30.6939	35.6507	0.0158		158
RJ004 point_4	Chalcopyrite	34.6252	29.4233	35.7232	0.0001		<20
RJ004 point_5	Chalcopyrite	34.8526	29.8295	35.7206	0.0171		171
RJ004 point_6	Chalcopyrite	34.7213	29.9876	36.1226	0.0012		<20
RJ004 point_7	Chalcopyrite	34.5357	29.8186	35.7166	0.0001		<20
RJ004 point_8	Chalcopyrite	35.4583	29.3491	35.0861	0.033		330

RJ004 point_9	Chalcopyrite	34.717	30.1538	36.0334	0.0001		<20
RJ004 point_10	Chalcopyrite	34.8597	29.829	35.6283	0.0012		<20
RJ004 point_11	Chalcopyrite	34.527	29.7591	35.5634	0.0001		<20
RJ004 point_12	Chalcopyrite	34.6695	29.8478	35.498	0.0085		85
RJ004 point_13	Chalcopyrite	34.6036	29.1661	35.7002	0.0001		<20
RJ004 point_14	Chalcopyrite	34.635	29.1514	35.6742	0.011		110
RJ004 point_15	Chalcopyrite	34.5268	29.4844	35.8807	0.0001		<20
RJ004 point_16	Chalcopyrite	34.58	28.4305	36.0164	0.0001		<20
RJ004 point_18	Chalcopyrite	34.2424	29.1518	35.5598	0.0012		<20
RJ004 point_20	Chalcopyrite	34.3438	29.0863	35.6353	0.0001		<20
RJ004 point_21	Chalcopyrite	33.5187	28.9799	34.7813	0.0012		<20
RJ004 point_22	Chalcopyrite	33.9154	28.5901	34.7108	0.0354		354
RJ004 point_23	Chalcopyrite	34.7903	28.9152	35.9006	0.0001		<20
RJ004 point_24	Chalcopyrite	34.5633	27.884	35.5982	0.05		500
RJ004 point_25	Chalcopyrite	34.5351	27.6276	35.6911	0.0244		244
RJ004 point_26	Chalcopyrite	34.9996	27.7502	35.4621	0.0001		<20
RJ004 point_28	Chalcopyrite	34.7735	27.6201	35.485	0.0439		439

RJ004 point_30	Chalcopyrite	34.7097	27.8666	34.8858	0.0001		<20
RJ004 point_31	Chalcopyrite	35.2826	27.4906	35.0353	0.0001		<20
RJ004 point_32	Chalcopyrite	34.7334	28.0783	34.3344	0.0001		<20
RJ004 point_33	Chalcopyrite	34.8664	27.4159	34.1627	0.0001		<20
RJ004 line 1__3	Chalcopyrite	34.6279	28.0007	35.1947	0.0061		61
RJ004 line 1__4	Chalcopyrite	34.386	28.2837	34.8367	0.0001		<20
RJ004 line 1__5	Chalcopyrite	34.553	28.1655	34.8213	0.022		220
RJ004 line 1__6	Chalcopyrite	34.6164	27.8966	35.4224	0.0037		37
RJ004 line 1__7	Chalcopyrite	34.6393	28.0702	34.7316	0.0001		<20
RJ012 (inside cp) point_11	Chalcopyrite	34.8319	29.2095	36.1384	0.0001		<20
RJ012 (inside cp) point_12	Chalcopyrite	34.8113	29.1867	36.3877	0.0001		<20
RJ012 (inside cp) point_13	Chalcopyrite	34.5671	29.3138	35.9836	0.0001		<20
RJ012 (inside cp) point_14	Chalcopyrite	34.706	29.2998	36.8243	0.0001		<20
Rj010 - 1	Pyrite	54.2838	46.3252	0.0543	0.036	543	360
Rj010 - 2	Pyrite	54.013	47.5082	0.0104	0.0001	104	<20
Rj010 - 3	Pyrite	53.1171	46.2091	0.0323	0.0146	323	146
Rj010 - 4	Pyrite	53.8137	46.5082	0.0081	0.0493	81	493

Rj010 - 5	Pyrite	53.1255	45.1631	0.262	0.0001	2620	<20
Rj010 - 6	Pyrite	53.4548	46.7411	0.0635	0.0426	635	426
Rj010 - 7	Pyrite	51.7376	46.9998	0.0727	0.0001	727	<20
Rj010 - 8	Pyrite	52.9402	45.6278	2.0091	0.0093	20091	93
Rj010 - 9	Pyrite	52.1802	45.2415	0.0005	0.0001	20<	<20
Rj010 - 10	Pyrite	53.5397	45.7248	0.0635	0.0479	635	479
Rj010 - 11	Pyrite	54.0294	46.6169	0.0092	0.0253	92	253
Rj010 - 13	Pyrite	53.7022	46.7518	0.0058	0.0001	58	<20
Rj010 - 14	Pyrite	53.7011	45.8898	0.0392	0.0599	392	599
Rj010 - 15	Pyrite	53.2944	46.655	0.0173	0.0413	173	413
Rj010 - 16	Pyrite	53.7342	46.5702	0.0005	0.0001	20<	<20
Rj008 - 1	Pyrite	54.0428	46.9449	0.0358	0.028	358	280
Rj008 - 10	Pyrite	53.4058	46.7798	0.1385	0.0001	1385	<20
Rj008 - 11	Pyrite	53.9954	46.8566	0.0392	0.0001	392	<20
Rj008 - 12	Pyrite	54.1603	47.1209	0.0069	0.0506	69	506
Rj008 - 13	Pyrite	53.3056	46.0924	0.7491	0.105	7491	1050
Rj0012 - 1	Pyrite	53.5677	46.8567	0.784	0.0558	7840	558

Rj008 - 14	Sphalerite	33.2301	0.9486	0.6226	65.8795	6226	
Rj008 - 15	Sphalerite	33.3173	1.076	0.6884	65.5013	6884	
Rj008 - 16	Sphalerite	33.2347	4.6223	5.203	56.2029	52030	
Rj008 - 18	Sphalerite	32.8408	3.1612	2.7558	61.5783	27558	
Rj008 - 19	Sphalerite	33.4807	3.4024	2.4437	55.1947	24437	
Rj008 - 20	Sphalerite	33.3725	2.3921	2.0119	62.3625	20119	
Rj015 - 1	Sphalerite	33.2905	2.3926	2.0133	62.5953	20133	

Table 9.2: EMA data for sulphide species major elements Cu, Fe, S and Zn (re-run)

Sample	Petrology	Ti W%	Fe W%	O W%	Mg ppm	S ppm	Ti ppm	V ppm	Cr ppm	Mn ppm	Co ppm	Ni ppm	Cu ppm	Zn ppm	As ppm	Ce ppm	Pb ppm	Bi ppm
1	Illmenite	28.6979	35.102	34.3165	20<	20<	286979	10<	306	264	20<	20<	20<	1632	20<	2<	20<	1914
2	Illmenite	31.6639	28.4737	33.4272	534	177	316639	826	10<	146	20<	20<	20<	20<	874	2<	20<	477
3	Illmenite	27.9196	36.5051	34.3632	84	20<	279196	10<	10<	384	20<	20<	20<	358	158	2<	554	50<
4	Illmenite	23.6895	40.6875	33.3293	20<	20<	236895	1730	386	71	382	20<	458	20<	20<	2<	20<	781
5	Illmenite	41.0538	16.463	34.5321	20<	20<	410538	720	569	124	20<	20<	461	120	20<	2<	20<	708
6	Illmenite	37.9473	23.3176	35.4262	185	66	379473	1301	226	368	209	51	362	960	129	2<	670	712
7	Illmenite	41.0538	16.463	34.5321	20<	20<	410538	720	569	124	20<	20<	461	120	20<	2<	20<	708
8	Illmenite	37.9473	23.3176	35.4262	185	66	379473	1301	226	368	209	51	362	960	129	2<	670	712
9	Illmenite	28.2625	33.8246	33.4552	84	20<	282625	484	192	890	20<	101	131	20<	298	2<	184	897
10	Illmenite	26.1951	35.0265	32.6368	1144	20<	261951	10<	10<	384	20<	582	590	20<	20<	2<	985	779
11	Illmenite	41.8266	16.9256	35.2367	20<	20<	418266	1064	10<	668	20<	203	296	120	670	2<	60	1003
12	magnetite	0.0361	70.1057	30.1752	141	196	361	190	10<	156	20<	579	227	472	20<	2<	20<	983
13	magnetite	0.1216	69.5849	30.0058	225	20<	1216	10<	10<	201	20<	20<	20<	79	38	2<	20<	1413
14	magnetite	0.1212	69.0569	29.7739	20<	196	1212	10<	10<	45	20<	20<	390	669	758	2<	20<	50<
15	magnetite	0.0532	69.1206	29.7588	187	115	532	10<	183	10<	20<	20<	20<	20<	619	2<	127	50<
16	magnetite	0.0617	67.4379	29.0385	20<	20<	617	434	10<	446	86	277	65	197	1035	2<	20<	50<
17	magnetite	0.1577	67.0743	28.9614	66	20<	1577	543	430	201	719	20<	162	118	99	2<	20<	1044
18	magnetite	0.0171	69.5042	29.9125	244	104	171	10<	71	10<	20<	579	20<	591	777	2<	253	50<

19	magnetite	0.1775	69.5626	30.0112	20<	20<	1775	10<	10<	10<	20<	226	292	20<	367	2<	380	430
20	magnetite	1.5064	68.0995	30.3465	1155	69	15064	328	10	10<	20<	126	227	20<	712	2<	20<	184
21	Haematite	0.0202	66.6758	28.6675	20<	219	202	298	10<	67	20<	20<	747	20<	378	2<	20<	983
22	Haematite	0.0202	66.6758	28.6675	20<	219	202	298	10<	67	20<	20<	747	20<	378	2<	20<	983
23	Haematite	0.7757	63.1289	27.879	3404	20<	7757	1637	197	10<	20<	101	20<	20<	20<	2<	190	50<
24	Haematite	0.8271	66.5961	29.2584	1120	46	8271	2292	259	90	20<	20<	20<	20<	410	2<	20<	675
25	Haematite	0.3958	66.81	29.0278	487	20<	3958	2884	10<	156	20<	20<	20<	709	553	2<	20<	50<
26	Haematite	0.2717	67.7132	29.3326	468	23	2717	1712	82	647	46	20<	20<	20<	875	2<	506	50<
27	Haematite	0.5126	67.57	29.4112	20<	92	5126	2314	319	10<	20<	20<	20<	709	183	2<	20<	50<
28	Haematite	0.2467	65.9469	28.6074	1413	20<	2467	2283	133	134	20<	20<	682	39	445	2<	20<	50<
29	Haematite	0.2708	64.7615	28.157	2160	35	2708	1739	103	10<	111	50	32	20<	20<	2<	20<	61
30	Haematite	0.7119	66.3843	29.0291	206	184	7119	3273	290	10<	20<	20<	1007	20<	198	2<	20<	307
31	Haematite	0.6485	67.0894	29.2734	150	20<	6485	1715	10<	22	20<	151	292	20<	20<	2<	20<	61
32	Haematite	0.6285	66.1158	28.9477	1474	20<	6285	2892	10<	671	20<	428	20<	20<	20<	2<	20<	1964
33	Haematite	0.8189	66.0104	28.9614	728	172	8189	2374	10	10<	20<	20<	909	20<	106	2<	20<	798
34	Haematite	0.0021	68.5797	29.4864	20<	20<	21	10<	92	10<	20<	20<	325	433	73	2<	253	860
35	Haematite	0.0021	68.5797	29.4864	20<	20<	21	10<	92	10<	20<	20<	325	433	73	2<	253	860
36	Haematite	4.9662	65.3421	31.4253	20<	126	49662	10<	239	612	20<	630	20<	20<	462	2<	20<	367
37	Haematite	0.4999	66.8465	29.0887	243	34	4999	2019	10<	10<	329	126	454	551	253	2<	1834	1596

Table 10: EMA data for Iron oxide species

APPENDIX A

Hole ID: ML001 **Sample Number:** RJ001(Thin Section) **Depth:** 64.5m **Reason for Sampling:** Representative sample of the top of the hole and amphibole, investigating the style of alteration present which is forming the large red/brown veins and assess in impact of weathering on this rock. **Hand specimen Description:** Blue/green well foliated dense rock, with bands of plagioclase + quartz and red pink alteration bands (haematite dusted feldspars or albite?) Amphibolite?	

Transmitted Microscopy

This thin section is a representative sample of the highly weathered and altered section, which is prevalent at the top of the hole and appears to contain two distinct domains of simular mineralogy but different characteristics.

This rock's matrix is dominated by chlorite with lesser quartz and sericite. In this section the serecite is highly prevalent replacing feldspartoids, this alteration is so prevailing that the felspathoid end member cannot be distinguished.

Chlorite occurs as medium grained, platy, dark green minerals (dark blue purple in cross polars. The chlorite appears to wrap around the oxides and serecite (pseudomorphed feldspartoids), with no observed chlorite wrapping around the quartz grains.

Quartz occurs as a recrystalised aphatic groundmass and as subhedral to anhedral porphryritic phenocrysts ≈ 0.2 mm in size.

Minor occurrences of opaque minerals, most likely haematite, and are disseminate throughout the fabric they are generally fine to medium grained anhedral and share the same preferred orientation as the host rock which clearly defines the parallel linear banding as the primary fabric of the rock.

Trace amounts of zircon and monazite occur in the slide as fine grained euhedral to subhedral grains.

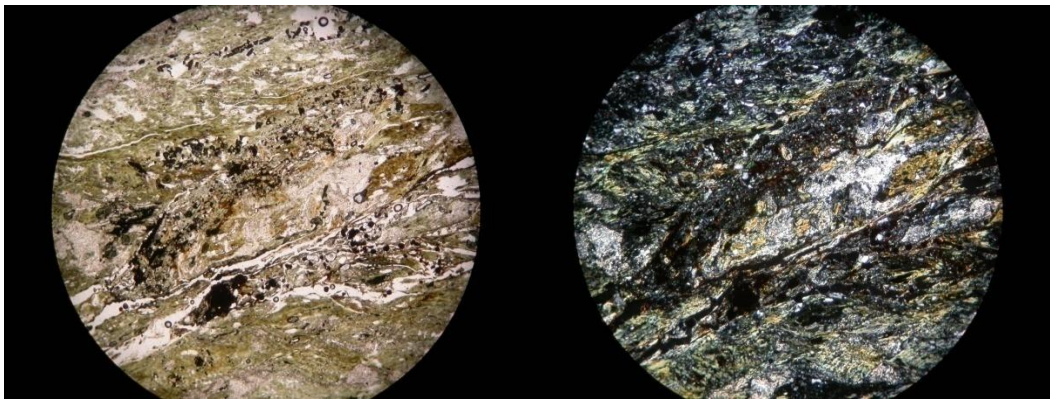

Interpretation

This fine grained rock is a highly serecite, chlorite altered amphibolite. The matrix is dominated by chlorite, which wraps around serecite and oxides.

Hole ID: ML001 **Sample Number:** RJ002 (Thin Section) **Depth:** 107.0m **Reason for Sampling:** Representative sample of the small amphibolite unit, which is strongly magnetic. The sample also contains haematite and carbonate veining within the minor brecciation present. **Hand specimen Description:** Dark blue/ black dense rock with multiple stages of carbonate veining, with haematite veining. Chlorite alteration is also visible on joints. Amphibolite?	

Transmitted Microscopy

This thin section is a representative sample of the amphibolite unit present within the core. The matrix of this fine grained rocks is dominated by chlorite, chlorite occurs as, .02-4mm euhedral to subhedral, elongated platy grains, and are from its dark-blue/ purple appearance in cross polarised light is interpreted as being an iron rich chlorite. The chlorite wraps around the oxides and feldspars (now altered to sericite) and aligns in a preferential orientation, to define a foliation.

Sericite occurs as pseudomorphs of plagioclase, of which it has completely replaced. The sericite occurs as subhedral to anhedral grains approximately ≈0.1mm in size. As previously stated sericite represents the complete replacement of plagioclase by sericite.

Quartz makes up the fabric in the amphibolites along with plagioclase (serecite), chlorite. Quartz occurs as fine-grained subhedral to anhedral grains ≈0.1 mm in size, the quartz exhibits undulosed extinction.

Amphibole is a green to dark green variety and is assumed to be hornblende and occurs as 0.1-0.3mm anhedral grains. The hornblende is observed being replaced by the chlorite.

Carbonate veining is observed in alignment, as well as cutting the foliation. The carbonate species was not determined.

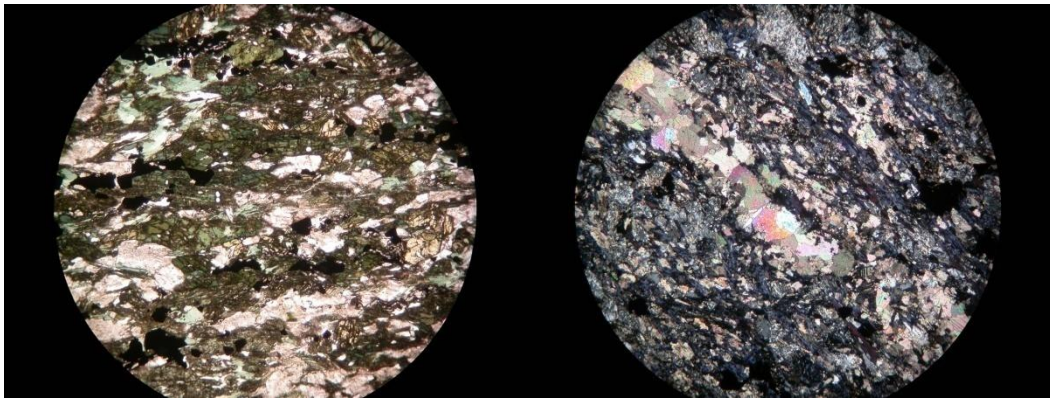

Interpretation

This fine-grained rock is a highly serecite, chlorite altered amphibolite, with carbonate veining observed cutting the fabric. The matrix is dominated by chlorite and quartz, which wraps around serecite and oxides. Hornblende is observed being replaced by an iron rich chlorite.

Hole ID: ML001 **Sample Number:** RJ002 (Polished Block) **Depth:** 107.0m **Reason for Sampling:** High magnetic susceptibility reading, likely due to magnetite, also possible haematite veining. **Hand specimen Description:** Massive fine-grained amphibolite unit composed of hornblende-Biotite- Plagioclase. It is strongly magnetic (possible magnetite) and contains varying sized carbonate veins with evident haematite present (Red Dusting)	

Reflected Microscopy

Magnetite

Magnetite is observed in abundant quantities in RJ002 and forms fine 0.01 to 2 mm sized euhedral to subhedral, equigranular crystals to elongated lathes that display an alignment parallel to the fabric of the rock.

Magnetite in RJ0002 is observed dark grey crystals, and displays a degree of martititsation along veins, fractures and the rim to haematite. The martititsation is mild to pervasive, with degree of martititsation increasing towards thin haematite veins

Haematite

Haematite occurs in two different forms in RJ002.

One type is martititsed haematite, which is a psedumorph of the predating magnetite minerals and subsequently display the same crystallographic features i.e. .01 to 2mm sized euhedral to subhedral equigranular crystals to elongated lathes that display an alignment parallel to the fabric of the rock. The martititsed haematite is light green/green in colour; with martititsation ranging from mild to pervasive.

The other type is thin 0.2-0.5mm wide veins of gangue, with tiny .01-.02mm grains of mint green haematite. Martititsation of magnetite increases in intensity towards these veins.

Chalcopyrite

Chalcopyrite forms fine .01 to massive <3cm sized euhedral to anhedral equigranular crystals.

Chalcopyrite mineralization is confined within quartz/ quartz- carbonate veins, and is yellow-gold in colour. The chalcopyrite in RJ002 commonly displays a moderate degree of fracturing, along this fracturing alteration of the chalcopyrite is observed with the alteration characterised by its dark yellow brown colour. Chalcopyrite also displays moderate to high degree of pitting (0.01-0.1mm pits).

Martitised haematite forms from the replacement of the predating magnetite, and the intensity of replacement increases towards the haematite veining suggesting these two haematite types were precipitated coevally.

Chalcopyrite relationship with magnetite and haematites is unclear.

Hole ID: ML001 **Sample Number:** RJ004 (Polished Block) **Depth:** 136.93-137.03m **Reason for Sampling:** Chalcopyrite precipitation in quartz- carbonate vein, hosted in micro granite. **Hand specimen Description:** Pinkish- brown medium to coarse-grained micro granite, containing overprinting sets of quartz-carbonate veins with possible offset of earlier set. Quartz-carbonate veins mineralised with chalcopyrite.	

Reflected Microscopy

Haematite

Haematite forms 0.01 to 2mm sized euhedral to subhedral equigranular crystals to elongated lathes that display an alignment parallel to the fabric of the rock, and is mint green in colour.

Chalcopyrite

Chalcopyrite forms fine .01 to massive <3cm sized euhedral to anhedral crystals.

Chalcopyrite mineralization is confined within quartz/ quartz- carbonate veins, and is yellow-gold in colour. The chalcopyrite in RJ004 commonly displays a moderate degree of fracturing, along this fracturing alteration of the chalcopyrite is observed with the alteration characterised by its dark yellow brown colour. Chalcopyrite also displays moderate to high degree of pitting (0.01-0.1mm pits).

Pyrite

Pyrite forms fine 0.01 to 1 mm sized euhedral to subhedral equigranular crystals.

Pyrite is commonly found in a close relationship with chalcopyrite, and like chalcopyrite, pyrite mineralization is confined within quartz/ quartz-carbonate / veins. Pyrite is observed as a cream colour. Pyrite crystals commonly display a mild degree of fractured with minor pitting.

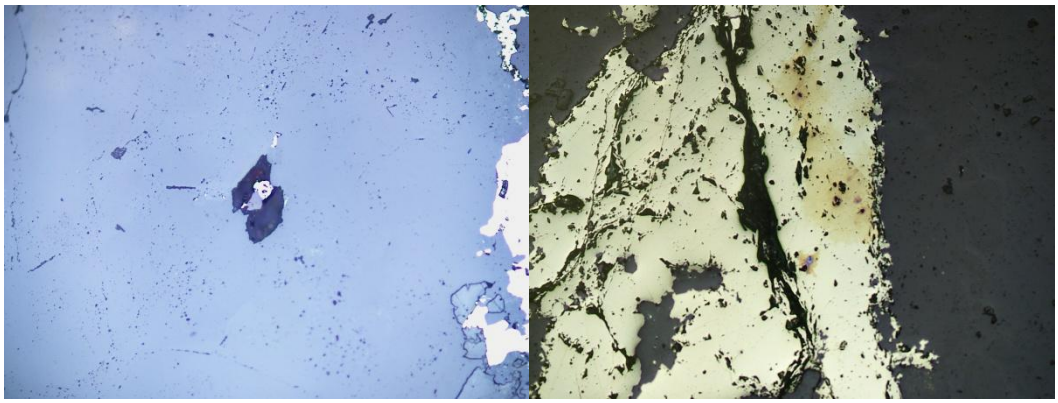

Interpretation

Chalcopyrite shows a slight degree of alteration, with alteration being focussed along fractures within the chalcopyrite. Chalcopyrite formed after to coeval with pyrite.

Hole ID: ML001 **Sample Number:** RJ006 (Thin Section) **Depth:** 162.7-162.8m **Reason for Sampling:** Representative sample of highly altered, felsic volcanic unit (rhyolite), targeting apparent sericite alteration and visual amounts of disseminated pyrite and chalcopyrite. **Hand specimen Description:** Medium to fine grained pink to green, highly sericite altered micro granite with multiple stages of quartz veining with chalcopyrite and bornite? present.	

Transmitted Microscopy

The granite matrix is dominated by aphatic quartz and plagioclase, with large ≈ 5-20 mm subhedral to anhedral crystals of K-feldspar and plagioclase and at a lesser extent muscovite. Amphibole, in the form of a sodic amphibole, is also present within the granite, but is relatively rare.

Plagioclase occurs as subhedral to anhedral grains ranging in size from the aphatic groundmass to 20 mm in size. The phenocrysts of plagioclase are characterised by a varying degree of sericite alteration, from crystals exhibiting minor alteration to crystals almost entirely pseudomorphed by serecite. The phenocrysts of plagioclase often exhibit polysynthetic twinning (albite) as well as containing inclusions of magmatic muscovite.

Quartz occurs in the granites along with plagioclase as the aphatic groundmass.

K-Feldspar occurs as approximately 1-12mm subhedral to anhedral grains. The K-Feldspar is relatively unaltered (some minor sericite alteration observed) and commonly exhibits tartan twinning (microcline), some grains contain inclusions of the sericite altered plagioclase and quartz.

Muscovite occurs as euhedral to subhedral strongly deformed, locally kinked lathes approximately 0.1-4mm in size. The muscovite is deflected around the highly sericite altered plagioclase. The muscovite is magmatic in origin.

The amphibole occurs as 0.4-1.5mm euhedral to subhedral grains that exhibit a pleochroism from pink to dark green and is assumed as being a sodic amphibole.

A large vein transects the sample consisting of course, subhedral interlocking recrystallised quartz along with some occurrence of coarse-grained carbonate. This vein cross cuts the apparent fabric of the host rock which is created by the preferred orientation of the ground mass and the larger phenocrysts.

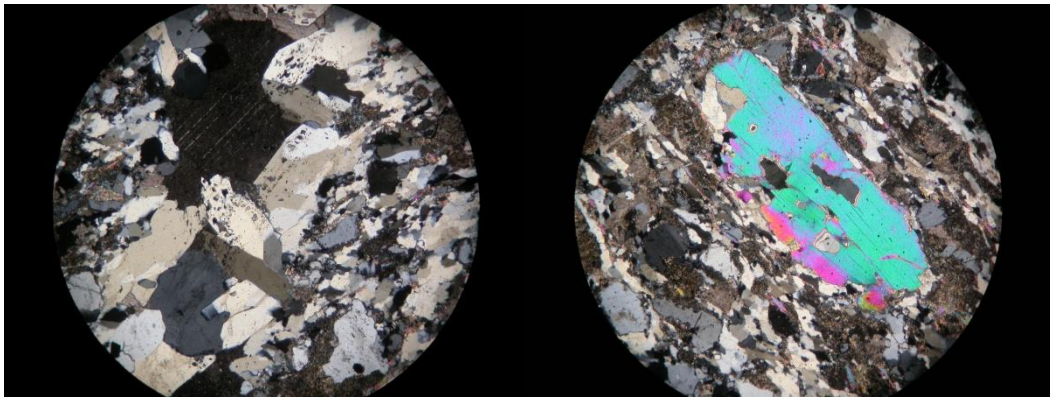

Interpretation

This medium to fine grained, to green rock is a rhyolite. Which is extensively altered by chlorite, sericite, Na-Ca and quartz-carbonate styles of alteration.

Hole ID: ML001 **Sample Number:** RJ006 (Polished Block) **Depth:** 162.7-162.8m **Reason for Sampling:** Targeting possible bornite mineralisation within a carbonate± quartz vein housed within highly altered felsic volcanic. **Hand specimen Description:** Medium to fine grained pink to green, highly sericite altered volcanic rock rhyolite? with multiple stages of quartz veining with chalcopyrite and bornite? present.	

Reflected Microscopy

Haematite

Haematite occurs in two different forms in RJ006.

One type haematite forms 0.01 to 2mm sized euhedral to subhedral equigranular crystals to elongated lathes that display an alignment parallel to the fabric of the rock, and is mint green in colour.

The other type occurs as thin .01 to 1mm mint green radiating needles of haematite, these needles show no affinity for alignment and dominate the composition (50%) of a 0.7mm wide quartz ± carbonate vein.

Chalcopyrite

Chalcopyrite forms fine .01 to massive <3cm sized euhedral to anhedral equigranular crystals to lathes.

Chalcopyrite mineralization is confined within quartz/ quartz- carbonate veins, and is deep metallic yellow-gold in colour. The chalcopyrite in RJ006 commonly displays a moderate degree of fracturing, with moderate pitting (0.01mm pits).

Pyrite

Pyrite forms fine 0.1 to 0.4 mm sized euhedral to subhedral equigranular crystals.

Pyrite is commonly found in a relationship with chalcopyrite and radiating haematite, and is confined within quartz/ quartz-carbonate. Pyrite is cream white in appearance in RJ006 and has been observed growing around/ into radiating needles of haematite.

Bornite

No bornite was observed in the polished section.

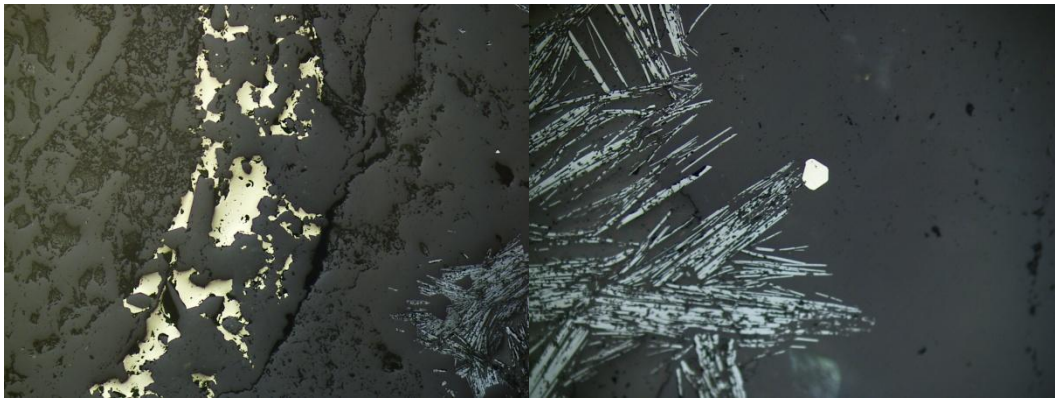

Interpretation

Radiating haematite and other haematite relationship unclear but both have similar colouration. Pyrite forming coeval or after precipitation of radiating haematite.

Hole ID: ML001 **Sample Number:** RJ007 (Polished Block) **Depth:** 163.6-163.9m **Reason for Sampling:** Targeting minor quartz veins which crosscut breccia infill, both of which contain mineralisation. **Hand specimen Description:** Pinkish red, fine grained moderately to strongly serecite altered rhyolite, major feature is the large quartz-carbonate brecciation complex with minor chalcopyrite mineralisation	

Reflected Microscopy

Haematite

Haematite forms 01 to 2mm sized euhedral to subhedral equigranular crystals to elongated lathes that display an alignment parallel to the fabric of the rock, and is mint green in colour.

Chalcopyrite

Chalcopyrite forms fine .01 to massive <3cm sized euhedral to anhedral equigranular crystals.

Chalcopyrite mineralization is in a close relationship with pyrite, with small pyrite crystal being encases in chalcopyrite. Chalcopyrite is confined within quartz/ quartz- carbonate/ carbonate breccia, and is cream yellow to deep yellow-gold in colour. The chalcopyrite in RJ007 commonly displays a moderate degree of fracturing, along this fracturing alteration of the chalcopyrite is observed with the alteration characterised by its blue white colour. Chalcopyrite also displays moderate pitting (0.01mm pits).

Pyrite

Pyrite forms fine 0.01 to 1 mm sized euhedral to subhedral equigranular crystals.

Pyrite is commonly found in a close relationship with chalcopyrite, and like chalcopyrite, pyrite mineralization is confined within quartz/ quartz-carbonate / veins. Pyrite is observed as a cream colour and crystals are often intergrown with other pyrite crystals. Pyrite crystals commonly display a mild degree of fracturing with minor pitting.

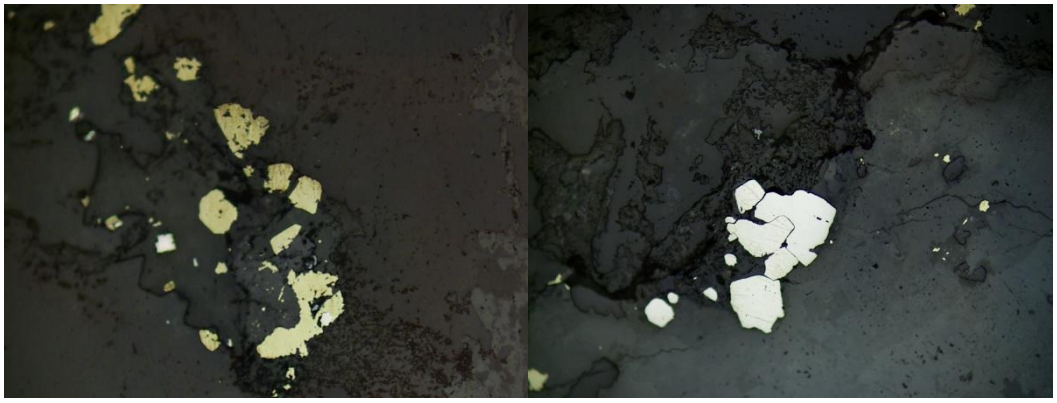

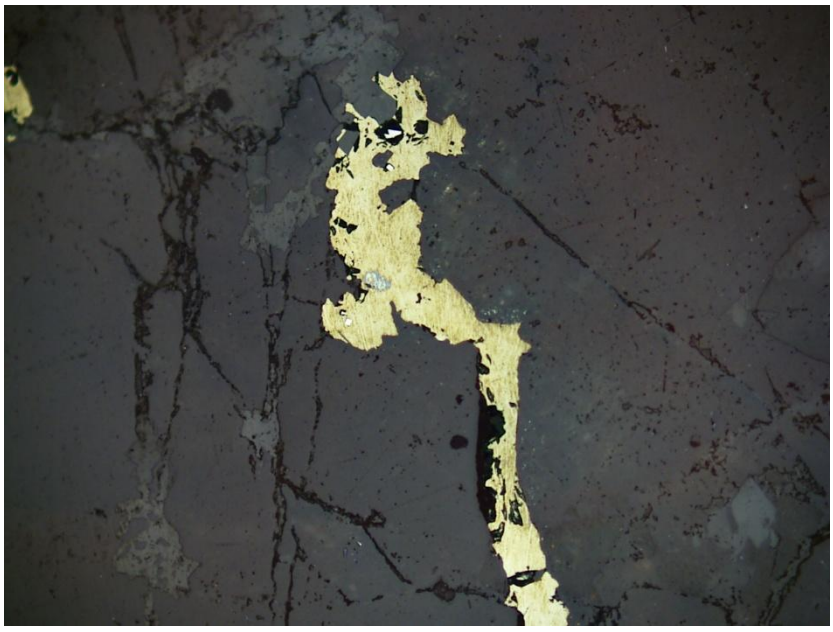

Interpretation

Pyrite formed before to coeval with chalcopyrite, chalcopyrite shows a minor alteration.

Hole ID: ML001 **Sample Number:** RJ008-Vein (Thin Section) **Depth:** 170.3-170.5m **Reason for Sampling:** Quartz vein hosting significant amount of mineralization, both pyrite and chalcopyrite, housed within felsic volcanic unit. **Hand specimen Description:** Large quartz -carbonate vein containing chalcopyrite cutting fabric of highly altered (sericite, carbonate, quartz) rhyolite.	

Transmitted Microscopy

This thin section is dominated by a large quartz vein that contains significant amounts of chalcopyrite. The vein is hosted within a highly silious section of the rhyolite unit which is predominantly composed of medium to coarse-grained anhedral quartz and along with coarse-grained subhedral feldspars. The latter of which shows evidence of being replaced via sericite alteration, with some occurrences ranging from intact to almost fully replaced. Sericite also occurs within the extensive thin vein network, prominent in this sample, and as very fine-grained infill around grains.

The vein housing the opaque ore minerals is dominated by medium to coarse grained interlocking quartz crystals of varying crystal habits (tabular, equant, subhedral), which both surround and are included within the opaques, with those crystals in direct contact having a highly anhedral shape. Fine grain quartz groundmass is also present in places, which supports the coarse crystals.

Minor occurrences of carbonate are also present throughout the vein and within the mineralisation in the form of fine to medium-grained subhedral crystals, though one section of the vein does indicate a higher amount of carbonates at the centre of the vein, however this cannot be further identified due to the orientation of the sample within the vein.

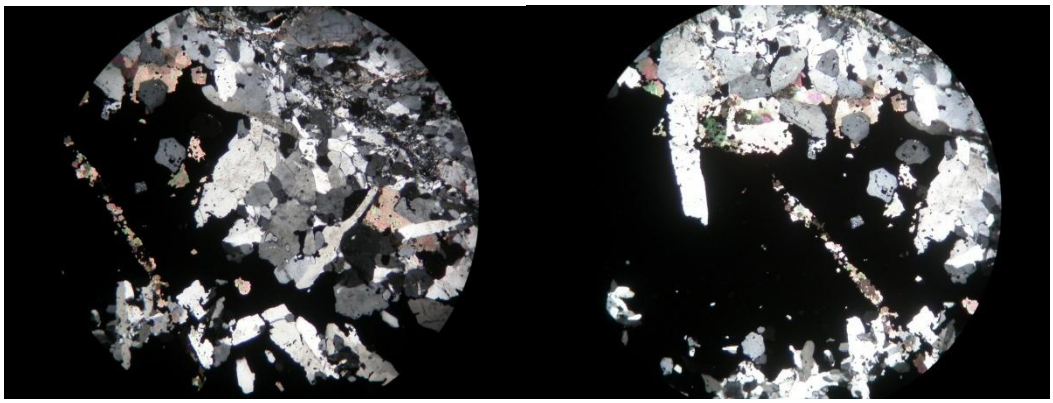

Interpretation

This vein is dominated by quartz with minor carbonate. Chalcopyrite mineralisation is present in significant amounts and has quartz inclusions.

Hole ID: ML001

Sample Number: RJ008 (Polished Block)

Depth: 170.3-170.5m

Reason for Sampling:

Quartz vein hosting significant amount of mineralization, both pyrite and chalcopyrite, housed within felsic volcanic unit.

Hand specimen Description:

Fine to medium grained, highly sericite and chlorite altered reddish to pink rock volcanic rock, with prominent multiple generations of quartz ± carbonate with chalcopyrite mineralisation.

Reflected Microscopy

Opaque minerals observed in RJ008 are haematite, pyrite, chalcopyrite and sphalerite.

Haematite

Haematite forms fine 0.01 to 2 mm sized mint green euhedral to subhedral, equigranular crystals to elongated lathes that display an alignment parallel to the fabric of the rock, haematite also occurs as small growths of mint green haematite occurs on the rims of a few pyrite crystals, and occurs as small .01-.05mm anhedral crystals

Pyrite

Pyrite forms fine 0.01 to 2 mm sized euhedral to subhedral equigranular crystals.

Pyrite is commonly found in a close relationship with chalcopyrite, and like chalcopyrite, pyrite mineralization is confined within the carbonate veins. Pyrite colour varies within this polished block from cream to yellow crystals. Pyrite crystals are often intergrown with other pyrite crystals, with pyrite crystal commonly being mildly fractured with minor pitting.

Chalcopyrite

Chalcopyrite forms fine .01 to massive <3cm sized largely anhedral crystals, chalcopyrite mineralization is in a close relationship with pyrite, and is confined within quartz/ quartz- carbonate/ carbonate veins, and display quite variability in colour from a cream yellow to yellow-gold.

Chalcopyrite commonly contains inclusions of haematite, haematite rim growth pyrite, magnetite, pyrite, sphalerite and gangue.

Along with containing abundant inclusions the chalcopyrite commonly displays a moderate degree of fracturing; with chalcopyrite cut by fine veins 0.1 to 1 mm of gangue exhibits a higher level of fracturing. Chalcopyrite is also characterised by moderate small 0.01mm pits.

Chalcopyrite is observed encasing pyrite, haematite and forms infill textures in pyrite fractures.

Sphalerite

Sphalerite occurs as small subhedral to anhedral equigranular 0.1 to 0.2mm dark grey crystals, enclosed exclusive within chalcopyrite crystals. The sphalerite exhibits chalcopyrite emulsion textures, precipitating chalcopyrite within itself as small ≈0.01mm crystals.

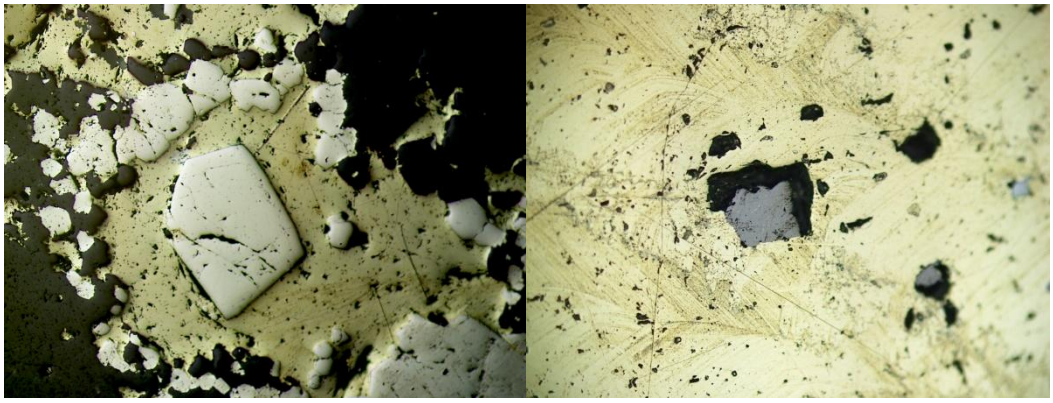

Interpretation

Pyrite formed coeval or prior to chalcopyrite and chalcopyrite formed prior to haematite. Haematite is thought to have formed coeval or prior to pyrite. Sphalerite formed coeval to prior to chalcopyrite mineralisation.

Hole ID: ML001 **Sample Number:** RJ008-Host Rock (Thin Section) **Depth:** 170.3-170.5m **Reason for Sampling:** Larger representation of the host rock housing the mineralisation bearing quartz vein, typical highly altered felsic volcanic, definite sericite alteration present. **Hand specimen Description:** Fine to medium grained, highly sericite and chlorite altered reddish to pink rock volcanic rock, with prominent multiple generations of quartz ± carbonate with chalcopyrite mineralisation.	

Transmitted Microscopy

This thin section displays a gradational change in the composition of the sample. Going from one extent, which consists of large coarse grain, subhedral feldspars phenocrysts, displaying simple twinning, hosted within medium grained, subhedral quartz. Sericite infill is present to a moderate degree found around grains and within phenocrysts via complete and partial replacement of the feldspar crystals.

Further, across the thin section there is a distinct increase in the amount of sericite infill between grains and replacement experience by the large phenocrysts, which has lead to the complete replacement of a large percentage of them.

Quartz occurs in the rhyolite along with plagioclase as a recrystalised aphatic groundmass, and as subhedral to anhedral porphryritic phenocrysts 0.2 mm in size.

K-Feldspar, in the rhyolites occurs as approximately 1-5 mm subhedral to anhedral porphryritic phenocrysts. The K-Feldspar is pervasively sericite altered to the degree from mildly altered to completely replaced, the milder altered crystals of K-feldspar often exhibit tartan twinning (microcline).

Muscovite occurs as euhedral to subhedral strongly deformed, locally kinked lathes approximately 0.05- 0.2 mm in size, intergrown with chlorite. The kinked lathes of muscovite are magmatic in origin with the muscovite intergrowth much finer in grain size and intergrown with chlorite to form a fabric in a preferred orientation.

Chlorite is assumed as being an iron rich variety, due to its deep blue colour in some samples. The chlorite occurs as 0.05- 0.2 mm euhedral to subhedral, elongated platy grains, which intergrows with muscovite, opaques and quartz to form a fabric in a preferred orientation. Chlorite and the non-magmatic muscovite wrap around phenocrysts of highly sericite altered plagioclase and K-feldspar.

Small (≈.01mm) veins of sericite are observed cutting plagioclase grains.

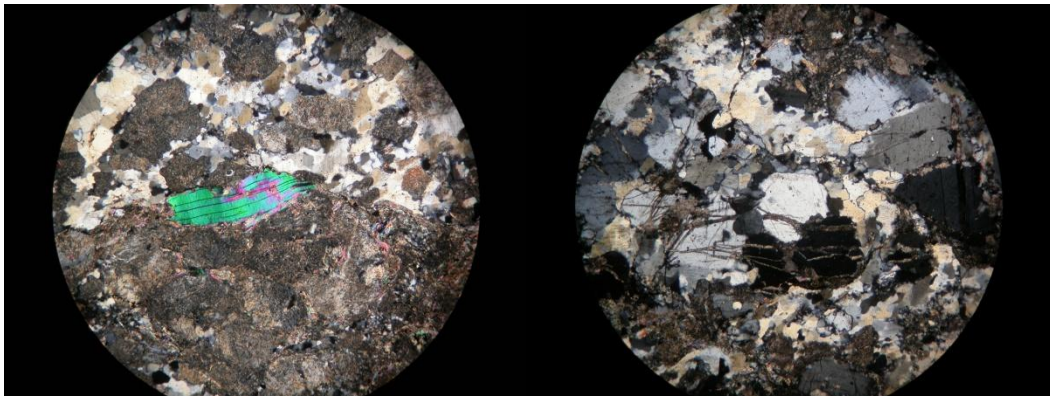

Interpretation

This medium grained rock is a highly serecite, chlorite altered rhyolite, with carbonate-quartz and fine sericite veining observed cutting the fabric. The matrix is dominated by chlorite and quartz, which wraps around serecite and oxides. Hornblende is observed being replaced by an iron rich chlorite.

Hole ID: ML001 **Sample Number:** RJ009 (Polished Block) **Depth:** 189.5-186.6m **Reason for Sampling:** Sample of the highly weathered felsic volcaniclastic section, the sample also contains minor occurrences of native copper. **Hand specimen Description:** Light green/white to grey/green moderate to highly weathered felsic volcaniclastic containing native copper occurrences, void spaces with minor quartz crystal regrowth, moderate brecciation	

Reflected Microscopy

Opaque minerals observed in RJ009 are haematite, pyrite, chalcopyrite and native copper, of these only native copper was present in a large enough size of abundance to gain information about mineralisation other than there presence.

Native copper

Native copper was observed as fine 0.1- 0.5mm subhedral to anhedral equigranular crystals, and native copper precipitation is coincidental with quartz/ quartz- carbonate/ carbonate veins, in addition to forming an infill texture in vuggs.

Interpretation

Native copper formed from the supergene alteration of copper sulphide minerals (chalcopyrite) and represents a secondary ore precipitation stage.

Hole ID: ML001 **Sample Number:** RJ009 (Thin Section) **Depth:** 189.5-186.6m **Reason for Sampling:** Sample of the highly weathered felsic volcaniclastic section, the sample also contains minor occurrences of native copper. (Thin and Polished section) **Hand specimen Description:** Light green/white to grey/green moderate to highly weathered felsic volcaniclastic containing native copper occurrences, void spaces with minor quartz crystal regrowth, moderate brecciation	

Transmitted Microscopy

This thin section is a sample of the highly weathered "volcaniclastic" unit, this zone contains supergene alteration with native copper and malachite, though due to the unconsolidated state of a majority of unit this sample was chosen for its stability not that its is a representative sample.

This sample is comprised predominantly of a fine-grained quartz and sericite and very fine-grained chlorite that is highly weathered and does not match the chlorite found elsewhere in the hole. The quartz present also appears to have fine-grained sericite inclusions.

Quartz veins ranging and form a cross cutting network across the sample which is comprised of medium to course grained quartz.

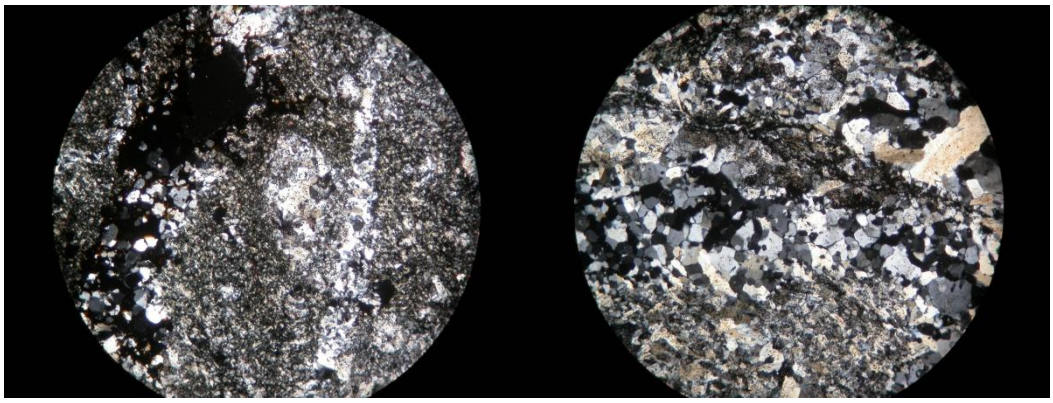

Interpretation

This fine-grained rock is highly sericite and chlorite altered volcaniclastic unit. This volcaniclastic unit is cut by fine quartz and sericite veins.

Hole ID: ML001 **Sample Number:** RJ010 (Thin Section) **Depth:** 202.0-202.2m **Reason for Sampling:** Representative sample of the rhyodacite unit, which contains? disseminated mineralisation, chalcopyrite. **Hand specimen Description:** Black/ blue fine grained rhyodacite with fine quartz veins with chalcopyrite. Some chalcopyrite mineralisation appears disseminate.	

Transmitted Microscopy

This rock is fine-grained, holocrystalline rocks, commonly displaying a gneissic texture, these bands, are dominated by, quartz with lesser chlorite, and iron oxides with lesser quartz.

Plagioclase occurs both in the groundmass along with quartz, in the quartz plagioclase bands, and as phenocyrsts. The groundmass plagioclase occurs as subhedral to euhedral grains ranging in size from the aphatic groundmass plagioclase to 0.1mm in size. The plagioclase phenocyrsts display mild to pervasive sericite alteration, with some of the phenocyrsts being completely pseudomorphed by sericite. Some of the more mildly sericite altered plagioclase's exhibit polysynthetic twinning (albite).

Quartz occurs in the rhyodactite along with the quartz plagioclase banding and oxide quartz banding, The quartz occurs as fine euhedral to subhedral grains groundmass ≈0.01-0.05mm in size.

Chlorite occurs as, 0.01-1.0mm euhedral to subhedral, elongated platy grains, and from thin section, as being an iron rich variety, due to its deep blue to purple colour. The chlorite wraps around the highly sericite altered plagioclase feldspars and along with oxides aligns in a preferential orientation, to define a foliation.

Opaques occurs as anhedral elongated grains, and from reflected light microscopy is composed of magnetite with haematite alteration, like the chlorite the oxides aligns in a preferred orientation, to define a foliation.

Small veins are present throughout the slide and are composed of fine to medium grained sudhedral? carbonate along with varying amounts of fine grained subhedral to anhedral quartz.

Also present within the carbonate vein is occurrences of coarse grain subhedral to anhedral opaques, most likely chalcopyrite.

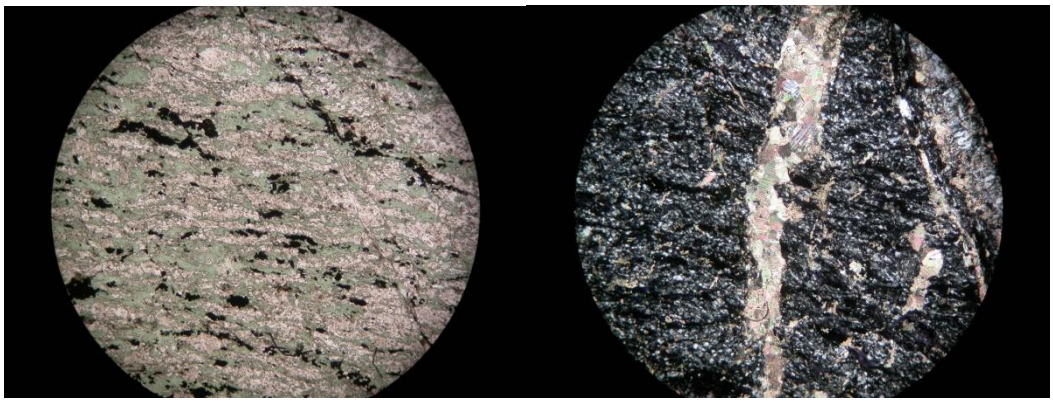

Interpretation

This fine-grained, chlorite sericite altered holocrystalline rocks is a rhyodacite. Small carbonate veins containing chalcopyrite cut the fabric of the rock, no disseminate chalcopyrite mineralisation was observed.

Hole ID: ML001 **Sample Number:** RJ010 (Polished Block) **Depth:** 202.0-202.2m **Reason for Sampling:** Chalcopyrite and pyrite mineralisation in carbonate vein. **Hand specimen Description:** Black/ blue fine grained rhyodacite with fine quartz veins with chalcopyrite. Some chalcopyrite mineralisation appears	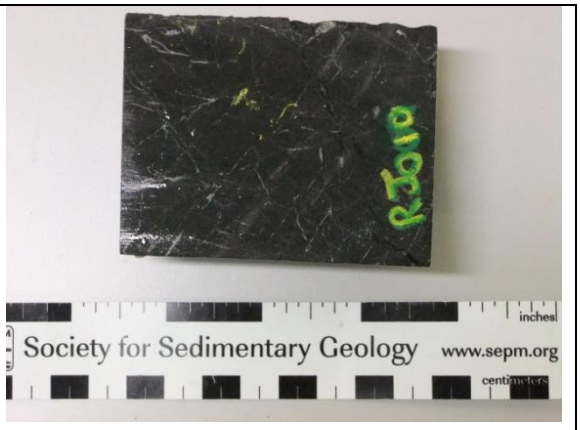

Reflected Microscopy

Opaque minerals observed in RJ010 are haematite, pyrite and chalcopyrite.

Haematite

Haematite forms fine 0.01 to 2 mm sized euhedral to subhedral, equigranular crystals to elongated lathes that display an alignment parallel to the fabric of the rock and appear to increase in size and amount when in the proximity of both the primary and secondary carbonate veins. Often haematite will form along the boundary of these veins and cross cut the fabric of the host rock as they follow the vein. Minor occurrence of haematite is found within the chalcopyrite mineralisation these appear as very small anhedral crystals.

Chalcopyrite

Chalcopyrite occurs in relationship with fractured host rock, pyrite and carbonate veining, with the carbonate veins hosting mineralisation.

Chalcopyrite forms fine .01 to massive <3cm sized deep yellow-gold euhedral to anhedral crystals. The chalcopyrite commonly contains inclusions of haematite and gangue, along with displaying a moderate degree of fracturation. Chalcopyrite also appears to have a close relationship with pyrite in this slide growing on the crystals faces of some as well as infill textures in pyrite.

Pyrite

Pyrite forms fine 0.01 to 2 mm sized euhedral to subhedral equigranular crystals.

Pyrite is commonly found in a close relationship with chalcopyrite, and like chalcopyrite, pyrite mineralization is confined within the carbonate veins. Pyrite colour varies within this polished block from cream to yellow crystals. Pyrite crystals are often intergrown with other pyrite crystals, with pyrite crystal commonly being mildly fractured with minor pitting

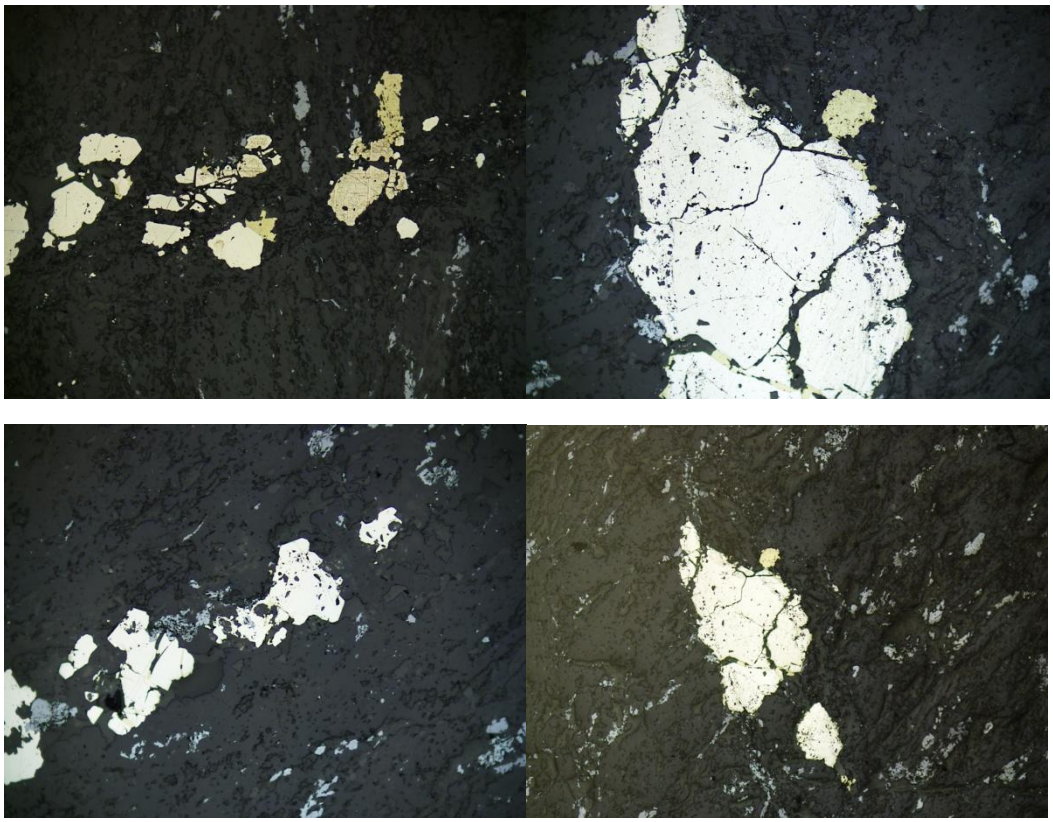

Interpretation

Pyrite formed coeval or prior to chalcopyrite and chalcopyrite formed prior to haematite. Haematite pyrite relationship not clear from this polished block.

Hole ID: ML001 **Sample Number:** RJ012 (Thin Section) **Depth:** 206.6-206.8m **Reason for Sampling:** Large carbonate vein hosting a significant amount of mineralisation, only chalcopyrite, hosted in the rhyodactite unit. **Hand specimen Description:** Black/ blue fine grained rhyodacite with a large carbonate vein (3-4cm) containing chalcopyrite cutting the fabric.	

Transmitted Microscopy

This thin section is dominated by a large carbonate vein, which contains significant occurrence of chalcopyrite. The vein is hosted within the rhyodacite unit which is comprised of fine grained quartz and sericite matrix which houses anhedral opaque ore minerals, most likely haematite, along with extensive fine grained platy chlorite, ranging up to course grained in areas.

This slide displays a gneissic texture these bands, are dominated by quartz with lesser chlorite, and iron oxides with lesser quartz.

Carbonate veins commonly cross cut the host rock fabric, these veins form a network throughout the slide. This cross cutting along with compositional variances in the veins indicates multiple generations of carbonate veining. Most veins are composed of both coarse and fine grained carbonate, which are primarily anhedral, with minor fine to medium grained, anhedral quartz.

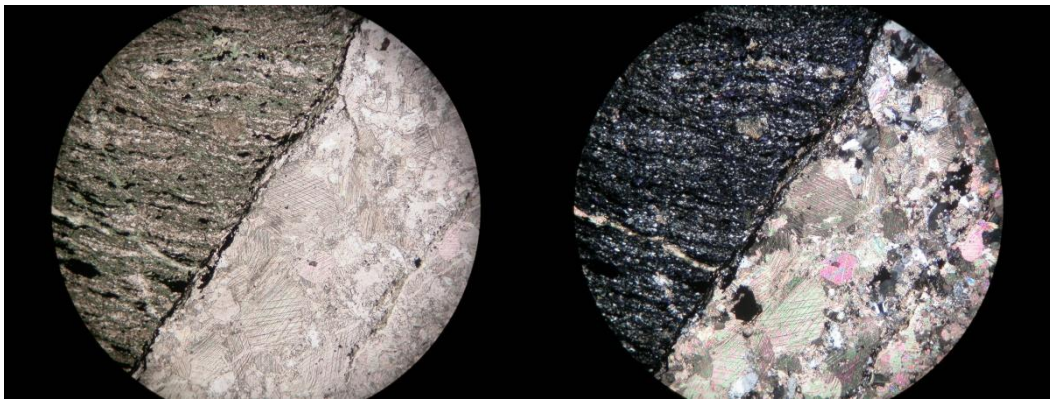

Interpretation

This fine-grained, chlorite sericite altered holocrystalline rocks is a rhyodacite. Small carbonate veins containing chalcopyrite cut the fabric of the rock, no disseminate chalcopyrite mineralisation was observed.

Hole ID: ML001 **Sample Number:** RJ012 (Polished Block) **Depth:** 206.6-206.8m **Reason for Sampling:** Large carbonate vein hosting a significant amount of mineralisation, only chalcopyrite, which is housed within rhyodactite volcanic. **Hand specimen Description:** Black/ blue fine grained rhyodacite with a large carbonate vein (3-4cm) containing chalcopyrite cutting the fabric.	

Reflected Microscopy

Opaque minerals observed in RJ012 are haematite and chalcopyrite.

Haematite

Haematite forms fine 0.01 to 2 mm sized euhedral to subhedral, equigranular crystals to elongated lathes that display an alignment parallel to the fabric of the rock and appear to increase in size and amount when in the proximity of both the primary and secondary carbonate veins. Often haematite will form along the boundary of these veins and cross cut the fabric of the host rock as they follow the vein. Minor occurrence of haematite is found within the chalcopyrite mineralisation these appear as very small anhedral crystals.

Chalcopyrite

Chalcopyrite occurs in relationship with fractured host rock and the carbonate vein, the carbonate veins host mineralisation. Calcite± dolomite is often incorporated within the chalcopyrite, along fractures or as individual crystals trapped within it.

Chalcopyrite forms fine .01 to massive <3cm sized euhedral to anhedral equigranular deep metallic yellow-gold crystals. The chalcopyrite commonly contains inclusions of haematite, sphalerite and gangue, along with displaying a moderate degree of fracturation;

Interpretation

Chalcopyrite was precipitated after haematite.

Hole ID: ML001 **Sample Number:** RJ013 (Thin Section) **Depth:** 214.6-214.7m **Reason for Sampling:** Another representative sample of the rhyodacite unit, this time targeting a highly deformed and vein rich section. **Hand specimen Description:** Black/ blue fine grained highly deformed rhyodacite with abundant carbonate veining.	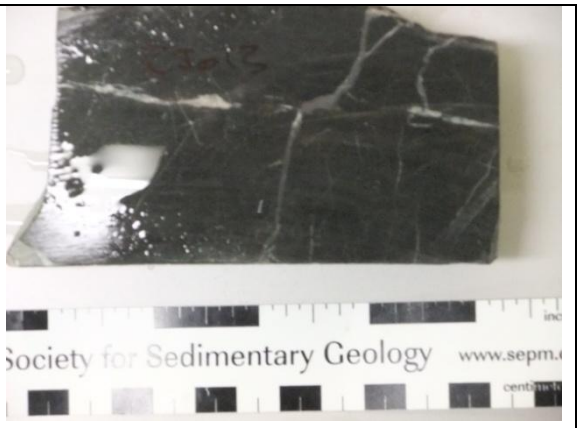

Transmitted Microscopy

This thin section is a representative sample of a highly deformed section of the rhyodacite unit. Similar to the rest of the unit this slide displays a gneissic texture, these bands, are dominated by, quartz with lesser chlorite, and iron oxides with lesser quartz

These minerals all appear to have a preferred orientation, which forms the primary fabric of the rock, which for a majority of the sample is a parallel linear banding, which are defined predominantly by the opaques present.

Due to the extensive veining and deformation experienced by the sample the fabric is not homogeneous throughout, often diverting around large veins forming localised, parallel sweeping bands.

The extensive vein network present in this slide and are predominantly composed of course to fine grained, subhedral, tabular carbonates with the size of the crystals being correlated to the size of the vein they are hosted within. Fine to medium grained anhedral quartz is often associated within the veins, with some places appearing to have it as the dominant component of the vein. A higher percentage of anhedral opaques, most likely haematite is found concentrated around the edges of the large veins.

Cross cutting veins are very common throughout, along with the offsetting of once continuous veins which records the variant deformation history of this sample.

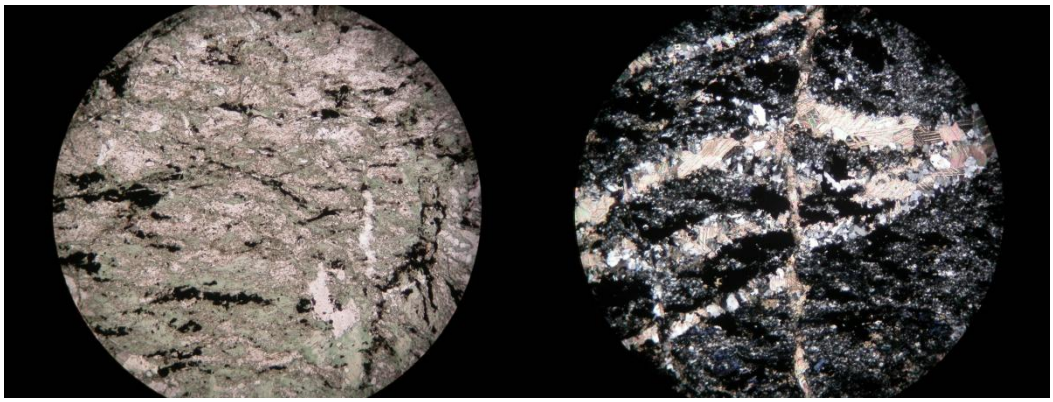

Interpretation

This rock is a highly deformed rhyodacite that is cut by multiple carbonate and quartz veins with some of these veins displaying offset

Hole ID: ML001 **Sample Number:** RJ014 (Thin Section) **Depth:** 238.8-238.9m **Reason for Sampling:** Targeting highly heterogeneous swirling layered section, which is similar in appearance to the rhyodactite units seen elsewhere but appears to have a different composition. **Hand specimen Description:** Black blue rhyodacite, interbanded with brown-red (rhyolite)	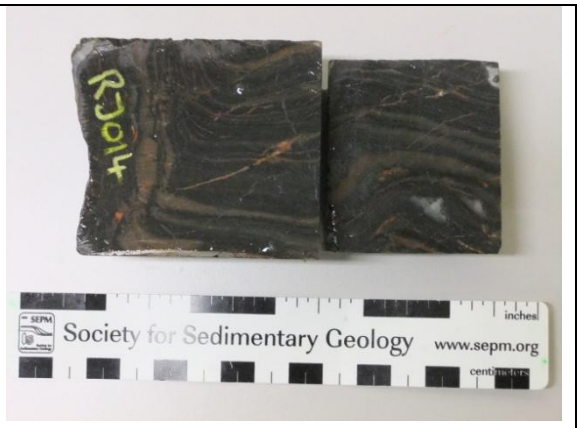

Transmitted Microscopy

This sample is highly heterogeneous, even differing vast amounts within its two major components, the first of which is dominated by fine grained tightly spaced, speckley opaque minerals, most likely haematite, which is supported within two differing fine grain groundmasses. The other major component of this sample is the large quartz and feldspar layering which transect the sample in a curved and sweeping pattern forming a layering texture along with the opaque dominant component.

The opaque dominated portions are supported by two distinct matrixes, fine grained quarts and fine grained sericite respectably. The quartz supported regions are more tightly packed, meaning less spacing between opaque grain, then there counterpart and the quarts crystals are very fine, beyond the optical capabilities of these microscopes, and are most probably anhedral. Within this portion, the opaques are fine grained, bladed and appear to have a preferred orientation, which forms a, acute angle to the laying within the sample.

The sericite supported regions have greater spacing between the opaque minerals and there still appears to be the same preferred orientation within the fine grained, opaques but they have been deformed, becoming wavy and variable, seeming to follow the sericite grains. The sericite matrix is composed of fine grained anhedral occurrences but retains some enclaves of semi altered quartz regions.

The other major component, the quartz-feldspar layering, is dominated by fine→medium grained anhedral quartz, with some larger coarse grained recrystallised sections present within. The feldspar components present are medium grain sudhedral occurrences and occur in lower quantities. Fine grained, anhedral opaques are also present within these layers, scattered throughout in trace amounts.

Other minor components within the sample include small to medium sized crosscutting veins of varying composition including chlorite, quartz, carbonates and feldspars. Chlorite is also founded as coarse →medium grained occurrences localised along the boundary of the quartz-feldspar layers.

There are also signs of deformation with the sample through the offsetting of veins and compositional layers.

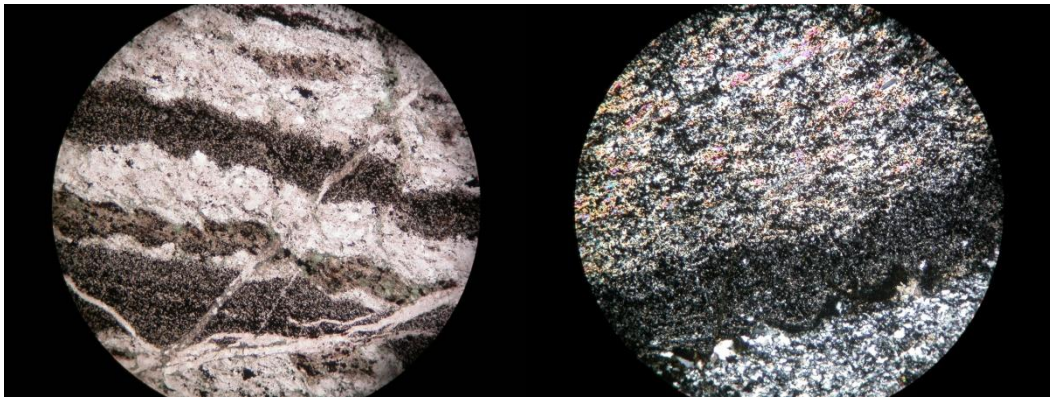

Interpretation

This rock is a compositional layered rhyodacite, and is cut by multiple carbonate and quartz veins with some of these veins displaying offset

Hole ID: ML001 **Sample Number:** RJ015 (Thin Section) **Depth:** 248.9-249.0m **Reason for Sampling:** Representative sample of the bottom of whole unit, clearly unique to units seen elsewhere in the whole, strange red phenocrysts/components within a rhyodacite like ground mass. **Hand specimen Description:** Black blue interbanded with red orange rhyodacite/ rhyolite large 2-3cm wide quartz vein sheared by a white (opaque) carbonate vein.	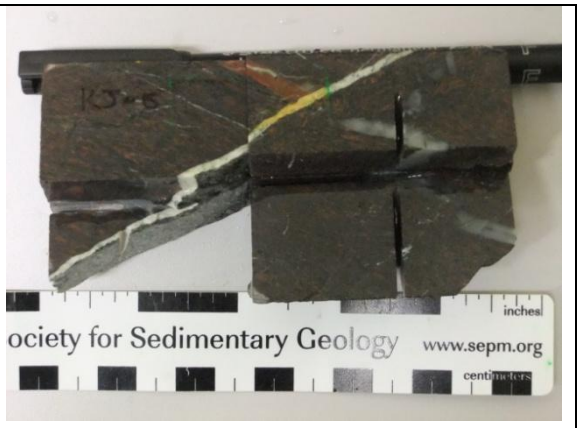

Transmitted Microscopy

This thin section is a representative sample of the bottom of the hole, which is comprised of a fine grained quarts and sericite matrix, which houses extensive fine→medium grained platy chlorite, anhedral opaques, mostly likely haematite and phenocrysts of feldspars, which have undergone varying extents of sericite replacement, but still exhibit the characteristic simple twinning.

Most minerals, excluding the feldspar phenocrysts, appear to have a preferred orientation defined by the opaques and chlorite that form a rough undulating banding throughout the sample and which seem to deflect around areas of heavy sericite alteration of feldspars.

Small fractures transect the sample, with some forming into minor veins in places, which are comprised of fine grained carbonate. These fractures/veins often cross cut each other forming offsets of once continuous features. Chlorite appears to have an affinity to these fractures/veins forming around the edges or appearing in greater concentrations in proximity to them.

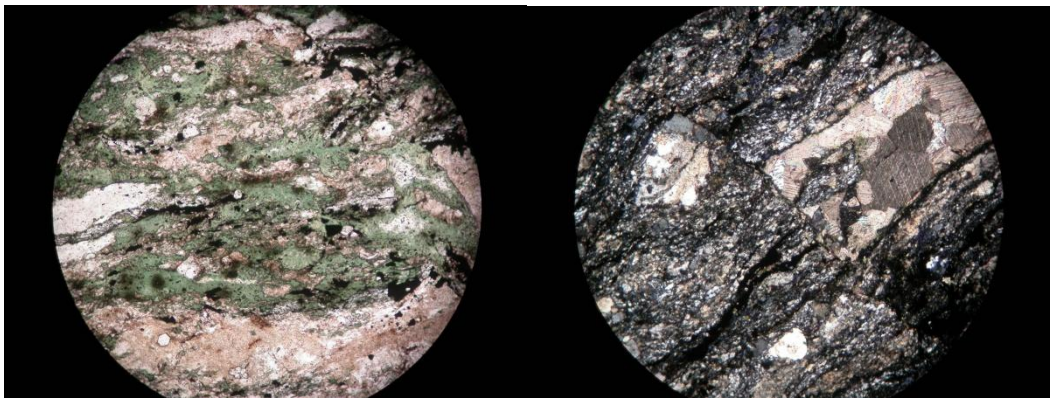

Interpretation

This rock is a compositional layered rhyodacite, and is cut by multiple carbonate and quartz veins with some of these veins displaying offset

Hole ID: ML001 **Sample Number:** RJ015 (Polished Block) **Depth:** 248.9-249.0m **Reason for Sampling:** \ **Hand specimen Description:** Black blue interbanded with red orange rhyodacite/ rhyolite large 2-3cm wide quartz vein sheared by a white (opaque) carbonate vein.	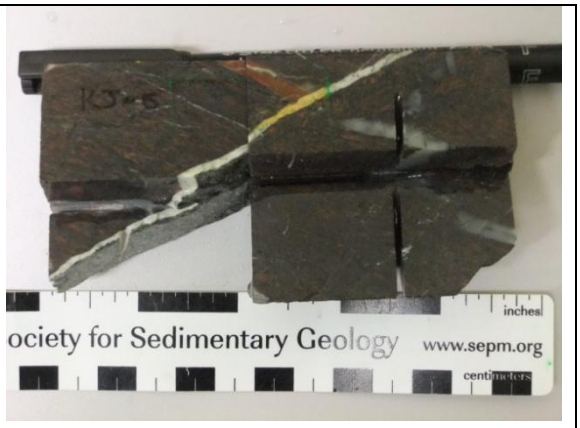

Reflected Microscopy

Opaque minerals observed in RJ015 are haematite, magnetite and chalcopyrite.

Magnetite

Magnetite is observed in abundant quantities in RJ015 and forms fine 0.01 to 2 mm sized euhedral to subhedral, equigranular crystals to elongated lathes that display an alignment parallel to the fabric of the rock.

Magnetite is observed as dark grey crystals, and displays a degree of martititsation along veins, fractures and the rim to haematite. The martititsation is mild to pervasive, with degree of martititsation increasing towards thin haematite veins

Haematite

Martitised haematite, is a psedumorph of the predating magnetite minerals and subsequently display the same crystallographic features i.e. .01 to 2mm sized euhedral to subhedral equigranular crystals to elongated lathes that display an alignment parallel to the fabric of the rock. The martititsed haematite is light green/green in colour; with martititsation ranging from mild to pervasive.

Chalcopyrite

Chalcopyrite is forms fine .01 euhedral equigranular crystals in RJ015, with mineralisation being confined within carbonate-quartz / carbonate veins, and are cream yellow in colour.

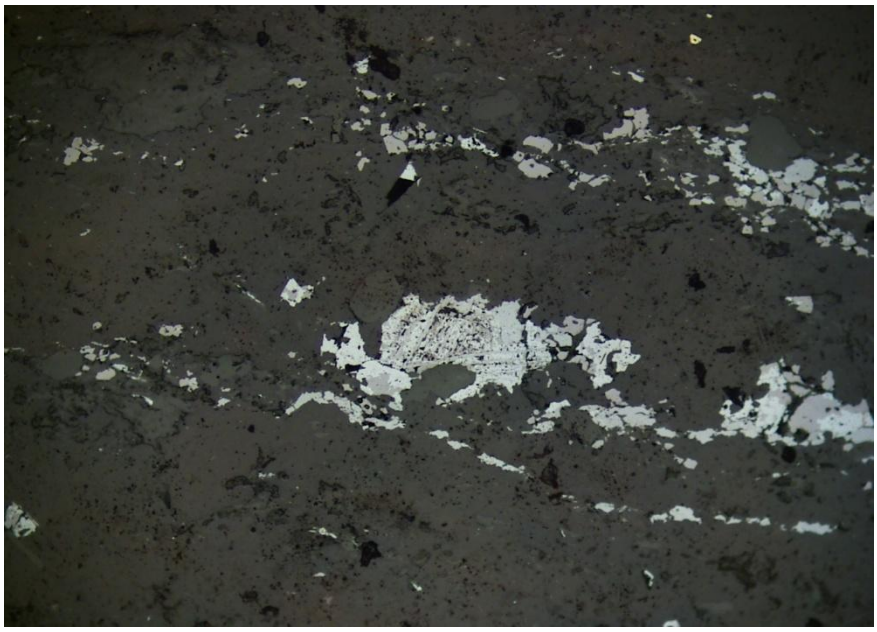

Interpretation

Haematite is formed by the martititsation of magnetite

Hole ID: ML001 **Sample Number:** OS001(Thin Section) **Depth:** 212.44-212.51m **Reason for Sampling:** Representative sample of the banded rhyodacite, targeting all major lithology components for identification and classification. **Hand specimen Description:** Fine grained grey foliated rhyodacite, moderately carbonate altered with multiple sets of carbonate veins throughout	

Transmitted Microscopy

This thin section is a representative sample of the banded rhyodacite unit that is characterized by three major domains, which repeat throughout the sample creating the banding.

The first domain is comprised of the remanent large interlocking feldspar phenocrysts, which have undergone intense brecciation and varying degrees of sericite alteration, ranging from sleight to complete replacement. These phenocrysts are hosted within fine to medium grained, anhedral, interlocking quartz, forming wide bands that are repeated throughout the thin section. This section shows characteristic red staining of the sericite present, which is typical throughout the hole.

The second domain is comprised of medium grained, anhedral, quartz, accompanied by minor fine grained sericite as infill around grains. Hosted within this groundmass is a considerable amount of remanent medium→coarse, anhedral feldspar, which is evenly spaced throughout the domain and has been partially or completely replaced by sericite, to form pseudomorphs. Some of these feldspars are still identifiable as being plagioclase as these occurrences still retain the characteristic simple twinning. The preferred orientation of crystals within this domain coincides with the layering of the sample, running parallel to the fabric identified in other domains.

The third domain is primarily composed of fine→medium grained anhedral quartz and medium grained anhedral feldspars showing varying extents of sericite replacement, which are accompanied by a large amount of fine grained sericite infill around and between grains. Though the composition is predominantly the same there is some variability in the abundance of sericite present that in places can become the dominant mineral. The third domain is significantly finer grained then its counterparts and contains a trace amounts of fine grain chlorite with the sericite matrix.

A large quartz vein also transects the thin section, which is common throughout the sample. It is comprised of fine to medium grained, interlocking anhedral quartz, which hosts solitary occurrences of fractured

coarse grained anhedral feldspar, identified as both microcline and plagioclase via characteristic cross hatched and simple twinning respectably. In addition, present within the vein is an isolated occurrence of coarse grained platy muscovite, which records evidence of deformation experienced by the sample in the offset between its two halves, which has been sheared apart.

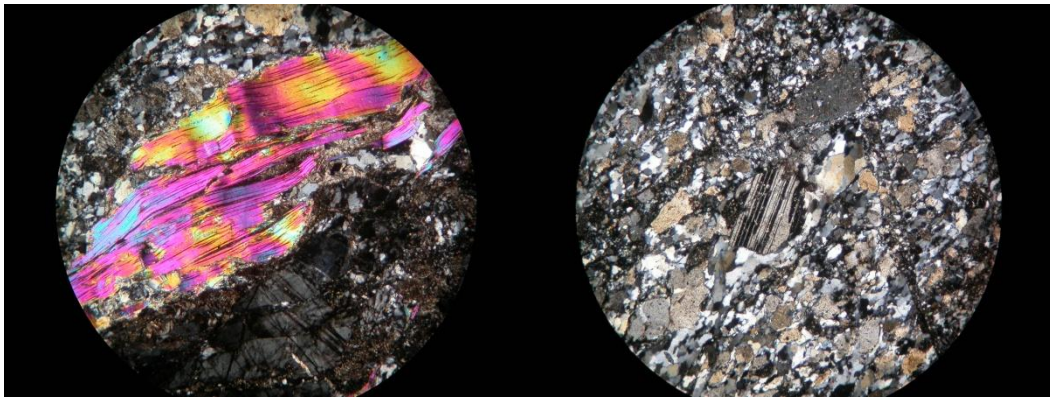

Interpretation

This fine grained grey rock is a Rhyodacite, with primary muscovite is observed within thin sections.

Hole ID: ML001

Sample Number: OS003 (Thin Section)

Depth: 166.94m

Reason for Sampling:

Representative sample of felsic volcanic unit, which appears to have banding of highly sericite alteration areas.

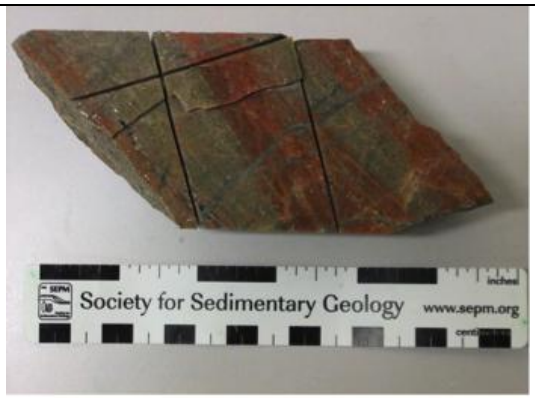

Hand specimen Description:

Fine grained sericite and chlorite altered, interlayered grey-pink felsic gneiss.

Transmitted Microscopy

This thin section is comprised of fine to medium grained groundmass consisting of anhedral interlocking quartz and a high percentage of fine grained sericite infill, which occurs between grains. Supported within the matrix is remanent coarse grain, anhedral feldspars phenocrysts, which have undergone intense sericite alteration with a high percentage having achieved complete replacement, forming pseudomorphs. Some of the phenocrysts can be identified as plagioclase as they display its characteristic simple twinning.

Both the ground mass and the larger phenocrysts appear to have a preferred orientation forming a fabric across the sample, also present is distinct zonation in some areas of the sample highlighted by a red discolouration of sericite in plain polar light even though the mineralogy is the same.

A large vein transects the sample consisting of fine grained quartz and sericite matrix, which supports medium grained elongate, rectangular quartz, which appears to have no preferred orientation. This vein completely cross cuts the fabric of the host rock.

Other minor components present include medium grained platy muscovite which occur scattered throughout the sample, scattered disseminated opaques, most probably sulphides, and trace occurrences of dark green, anhedral amphiboles.

The amphibole and muscovite present in the sample do not appear to have a preferred orientation and seem to exist independent of the fabric formed by the other minerals in the sample.

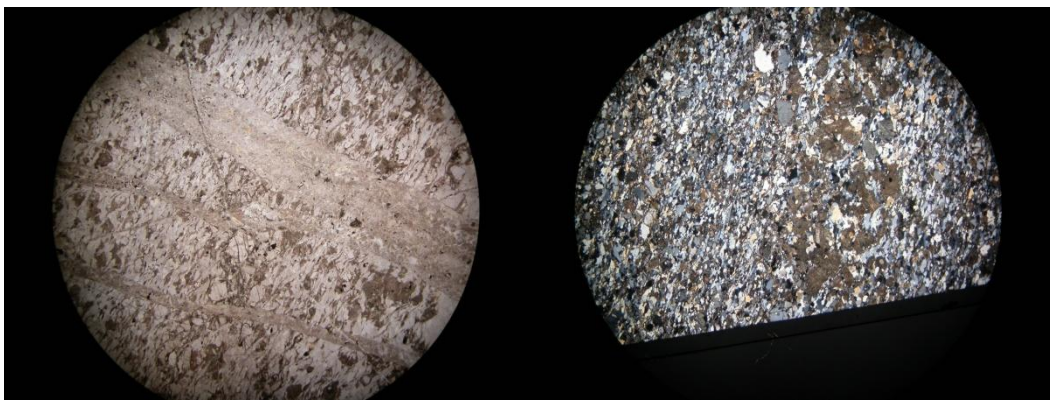

Hole ID: ML001 **Sample Number:** OS004 (Thin Section) **Depth:** 82.98-83.10m **Reason for Sampling:** Representative sample of the intrusive granite unit, targeted to get composition. **Hand specimen Description:** Medium grained porphryritic pinkish microgranite.	

Transmitted Microscopy

This thin section is a representative sample of the microgranite present within the drill core. It is composed of large medium grained subhedral to anhedral feldspar phenocrysts, which form a porphryritic texture. Both plagioclase and microcline comprise the phenocrysts, displaying their characteristic simple and cross hatched twinning respectively, they are effected by varying stages of fine grained sericite alteration, ranging from none to fully replaced pseudomorphs. Perthite exsolution patterns are also found within some phenocrysts, formed via the intergrowth of potassium rich and sodium rich feldspars.

Fine grained sericite is also found within the surrounding groundmass, which is predominantly comprised of anhedral, medium grained, and interlocking quartz.

Other minor components present include subhedral and tabular, dark green amphiboles along with coarse grained magmatic muscovite, which occur as large isolated tabular grains, infill and some as inclusions within the feldspar phenocrysts.

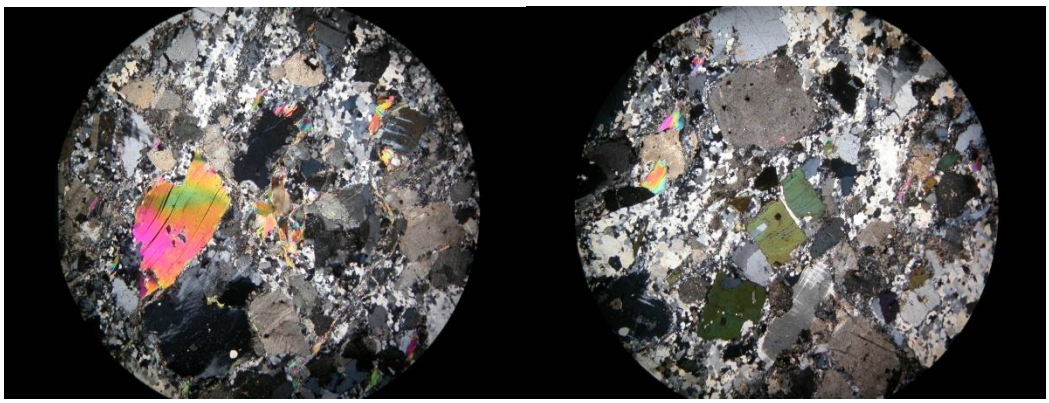

Interpretation

This fine to medium grained rock is a chlorite, sericite, Na-Ca altered quartz-plagioclase-sodic amphibole microgranite that contains magmatic muscovite.

Sample Location: ML001 (Core) **Sample Number:** MC009 **Lithology:** quartz-feldspar gneiss **Depth:** 166.84-166.94m **Analytical techniques subjected to:** Whole rock (major, trace, REE) Radiogenic isotopes Sm, Nd and Sr **Hand specimen Description:** Fine grained sericite and chlorite altered, interlayered grey-pink quartz-plagioclase-K-feldspar gneiss, contains mineralised (chalcopyrite) Quartz carbonate vein. **Alteration:** Chlorite, sericite, Na-Ca-Fe, quartz-carbonate	

Sample Location: ML001 (Core) **Sample Number:** MC001 **Lithology:** quartz-feldspar-Hornblende gneiss **Depth:** 65.35-65.47m **Analytical techniques subjected to:** Whole rock (major, trace, REE) Radiogenic isotopes Sm, Nd and Sr **Hand specimen Description:** Fine grained sericite and chlorite altered, interlayered grey-pink quartz-plagioclase-K-feldspar gneiss, contains mineralised (chalcopyrite) Quartz carbonate vein. **Alteration:** Chlorite, sericite, Na-Ca-Fe, quartz-carbonate	

Sample Location: ML001 (Core) **Sample Number:** MC004 **Lithology:** quartz-feldspar gneiss **Depth:** 99.27-99.39m **Analytical techniques subjected to:** Whole rock (major, trace, REE) Radiogenic isotopes Sm, Nd and Sr **Hand specimen Description:** Fine grained sericite and chlorite altered, interlayered grey-pink quartz-plagioclase-K-feldspar gneiss, contains mineralised (chalcopyrite) Quartz carbonate vein. **Alteration:** Chlorite, sericite, Na-Ca-Fe, quartz-carbonate	

Sample Location: ML001 (Core) **Sample Number:** MC005 **Lithology:** Amphibolite **Depth:** 106.24-106.32m **Analytical techniques subjected to:** Whole rock (major, trace, REE) Radiogenic isotopes Sm, Nd and Sr **Hand specimen Description:** Dark blue/ black dense rock with multiple stages of carbonate veining, with haematite veining. Chlorite alteration is also visible on joints **Alteration:** Chlorite, sericite, Na-Ca-Fe, quartz-carbonate	

Sample Location: ML001 (Core) **Sample Number:** MC008 **Lithology:** Rhyolite **Depth:** 145.22-145.32m **Analytical techniques subjected to:** Whole rock (major, trace, REE) Radiogenic isotopes Sm, Nd and Sr **Hand specimen Description:** Fine grained pink foliated porphryritic rhyolite; phenocrysts are dominantly plagioclase and K-feldspar, with the fine grained groundmass consisting of quartz, plagioclase and K-feldspar. Contains mineralised (chalcopyrite) Quartz carbonate veins **Alteration:** Highly potassic altered, Chlorite, sericite	

Sample Location: ML001 (Core) **Sample Number:** MC012 **Lithology:** Rhyodacite **Depth:** 212.4-212.51m **Analytical techniques subjected to:** Whole rock (major, trace, REE) Radiogenic isotopes Sm, Nd and Sr **Hand specimen Description:** Fine grained black-blue rhyodacite with extensive cross cutting mineralised (chalcopyrite) fine-medium carbonate veins. **Alteration:** Highly Carbonate altered quartz, chlorite, and sericite? Na-Ca-Fe?	

Sample Location: ML001 (Core) **Sample Number:** MC013 **Lithology:** Rhyodacite **Depth:** 225.1-225.25m **Analytical techniques subjected to:** Whole rock (major, trace, REE) Radiogenic isotopes Sm, Nd and Sr **Hand specimen Description:** Fine grained black-blue banded rhyodacite. **Alteration:** Chlorite, Na-Ca-Fe, sericite?	

Sample Location: Myola Hills **Sample Number:** 18879 **Lithology:** Rhyolite **Analytical techniques subjected to:** Whole rock (major, trace, REE) **Hand specimen Description:** Fine grained pink-brown foliated porphryritic rhyolite; phenocrysts are dominantly plagioclase and K-feldspar, with the fine grained groundmass consisting of quartz, plagioclase and K-feldspar. **Alteration:** Na-Ca-Fe and Sericite	

Sample Location: Myola Hills **Sample Number:** 18780 **Lithology:** Quartz-feldspar gneiss **Analytical techniques subjected to:** Whole rock (major, trace, REE **Hand specimen Description:** Fine grained pink-brown rock, comprised of quartz, plagioclase, K-feldspar and abundant oxides **Alteration:** Na-Ca-Fe and Sericite?	

Sample Location: Myola Hills **Sample Number:** 18781 **Lithology:** Quartz-feldspar-Hornblende gneiss **Analytical techniques subjected to:** Whole rock (major, trace, REE **Hand specimen Description:** White/green speckled gneissic dense rock, comprised of quartz, plagioclase, K-feldspar?, Hornblende **Alteration:** Na-Ca-Fe?	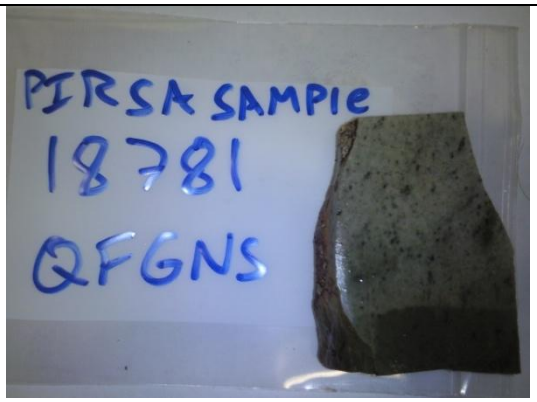
Sample Location: Myola Hills **Sample Number:** 18858 **Lithology:** Amphibolite **Analytical techniques subjected to:** Whole rock (major, trace, REE **Hand specimen Description:** Black/green well foliated dense rock, with bands of white minerals plagioclase? and quartz? **Alteration:** Na-Ca-Fe?	

Sample Location: Myola Hills **Sample Number:** MV004 **Lithology:** Rhyolite **Analytical techniques subjected to:** Whole rock (major, trace, REE) **Hand specimen Description:** Fine grained pink-brown foliated porphryritic rhyolite, phenocrysts are dominantly plagioclase and K-feldspar, with the fine grained groundmass consisting of quartz, plagioclase and K-feldspar. **Alteration:** Na-Ca-Fe and Sericite	

Sample Location: Myola Hills **Sample Number:** MV003 **Lithology:** Rhyolite **Analytical techniques subjected to:** Whole rock (major, trace, REE) **Hand specimen Description:** Fine grained pink-brown foliated porphryritic rhyolite, phenocrysts are dominantly plagioclase and K-feldspar, with the fine grained groundmass consisting of quartz, plagioclase and K-feldspar. **Alteration:** Na-Ca-Fe and Sericite	

Sample Location: Myola Hills **Sample Number:** MV001 **Lithology:** Rhyolite **Analytical techniques subjected to:** Whole rock (major, trace, REE) **Hand specimen Description:** Fine grained pink-brown foliated porphryritic rhyolite, phenocrysts are dominantly plagioclase and K-feldspar, with the fine grained groundmass consisting of quartz, plagioclase and K-feldspar. **Alteration:** Na-Ca-Fe and Sericite	

APPENDIX B

MYOLA VOLCANICS PETROGRAPHY

By A.J Parker

R Number	TS Number
18776	41819
18777	41820
18778	41821
18780	42862
18781	42863
18783	42865
18784	42866
18786	42868
18787	42869
18788	42870
18799	42881
18852	44321
18853	44322
18855	44324
18857	44326
18858	44327

Sample: 6331 RS74; TS41819

Applicant's Number: 2086/063-1C

Descriptive Information: Middleback; Broadview Station (?Myola volcanics).

Hand Specimen:

A fine-grained, reddish rock with some evidence of fine banding.

Thin Section:

A visual estimate of the minerals is as follows:

	%
Potash feldspar	50
Quartz	40
Opaques	9
Chlorite	1
Plagioclase	Trace

This is a sedimentary rock composed of sub-rounded, sub-angular and angular grains of potash feldspar and irregular grains of opaques cemented by a network of finely crystalline quartz. The potash feldspar is fresh and generally untwinned, although some grains show microcline twinning; the grain size is 0.05-0.2 mm and where elongate, the grains tend to be oriented sub-parallel. The grains of opaques range from 0.01 to 0.4 mm in size, with most being smaller than 0.1 mm. They are widely disseminated throughout the rock and in places occur in elongate concentrations parallel to the orientation of the elongate porash feldspar grains.

The matrix to these detrital grains of potash feldspar and opaques consists of finely crystalline chert-like quartz in which individual quartz crystals are generally less than 0.05 mm in size. The quartz fills in interstices between the potash feldspar and opaque grains and forms a ribbon-like network. Locally, traces of chlorite are intergrown with the quartz.

Conclusion:

This is a feldspathic (potash-feldspar-rich) sandstone. Detrital potash feldspar grains occur in a matrix of cherty quartz which may have originated as a chemical precipitate during or after sedimentation.

Sample: 6331 RS75; TS41020

Applicant's Number: 2134/035-1

Descriptive Information: Middleback; Broadview Station

Hand Specimen:
A pinkish, banded metasandstone.

Thin Section:
A visual estimate of the minerals is as follows:

	%
Potash feldspar	50
Quartz	30
Plagioclase	15
Opaques	4
Biotite and altered biotite	1

This rock consists predominantly of a granoblastic intergrowth of potash feldspar, quartz and plagioclase with minor opaques and fresh and altered biotite. The crystal size is mainly 0.05-0.2 mm, but locally crystals up to 0.6 mm are present. The potash feldspar is fresh, untwinned and rarely perthitic, whereas the plagioclase is generally incipiently sericitized and has a brownish colour. A vague banding is defined by elongate aggregates of potash feldspar and plagioclase and by the sub-parallel orientation of some of the biotite flakes.

Opaques occur as irregular crystals commonly 0.01-0.1 mm in size, but rarely up to 0.4 mm. Biotite forms irregular flakes up to 0.2 mm in size and commonly is bleached and/or chloritized.

Conclusion:
This is a metamorphosed feldspathic sandstone.

Sample: 6331 RS76; TS41821

Applicant's Number: 2134/035-2

Descriptive Information: Middleback; Broadview Station

Hand Specimen:
A pinkish-grey, massive quartzite.

Thin Section:
A visual estimate of the minerals is as follows:

	%
Quartz	50
Potash feldspar	20
Plagioclase	20
Opaques	4
Blue-green amphibole	4
Zircon	1
Calcite	1
Biotite	Trace
Chlorite	Trace

This rock is a feldspathic quartzite consisting predominantly of a granoblastic intergrowth of quartz, potash feldspar and plagioclase with a crystal size of 0.05-0.2 mm. The potash feldspar is fresh but the plagioclase is commonly incipiently sericitized.

Minor to trace amounts of blue-green amphibole are present as irregular and prismatic crystals up to 0.1 mm in size. Traces of calcite are present but show no obvious association with the amphibole. Brown biotite, in places partially chloritized, forms irregular flakes up to 0.1 mm in size. Opaques occur as irregular crystals 0.01-0.1 mm in size.

Conclusion:
Feldspathic quartzite formed by the metamorphism of a slightly calcareous feldspathic sandstone. This rock is generally similar in composition and texture to RS75, both originating from the metamorphism of feldspathic sandstone. RS76, however, contains calcite and blue-green amphibole which are not present in RS75. Both RS75 and RS76 are much better crystallized than RS74, which still retains much of its sedimentary texture; however, all three rocks are rich in potash feldspar and represent original feldspathic sandstones. RS73 is quite different from RS74-76 in that it consists essentially of muscovite and quartz and lacks the abundant feldspathic components of the latter.

Sample: 6331 RS 78; TS42862

Applicant's No.: 2134/037-43A

Location: Middleback 1:100,000

Hand Specimen:

A greyish-pink, moderately fine-grained, massive rock with a smooth to slightly conchoidal fracture. In places it shows evidence of a very weak foliation visible mainly on weathered surfaces.

Staining with cobaltinitrite shows abundant potash feldspar.

Thin Section:

Mineral assemblage:

	%
Potash feldspar	50-55
Quartz	25-30
Plagioclase	15-20
Amphibole	3-5
Sphene	1-2
Epidote	Trace
Opaque oxide	Trace
Rutile	Trace
Apatite	Trace
Metamict mineral	Minute Trace

Quartz and feldspar minerals throughout much of the rock have a common grain size of 0.05-0.2 mm, but there are a few larger grains up to about 0.6 mm and in some of the larger feldspar grains twinning planes have been deformed. In general, quartz tends to be finer-grained than the feldspar and clearly some of it represents former larger grains which have been granulated and drawn out in the direction of weak foliation. The general texture therefore suggests a hornfels (?or granulite) which has been deformed by a later episode of metamorphism and a weak foliation developed. Small, ragged crystals of deeply-coloured amphibole (orange-brown to very dark, almost opaque green) are scattered throughout the rock and are generally of similar size to the quartz and feldspar grains but there are a few very irregularly-shaped aggregates in which amphibole is associated with small crystals of sphene with and without a little opaque oxide. There are also numerous isolated crystals of sphene up to 0.05 mm in size scattered throughout the rock.

There is a trace of epidote associated with some amphibole and there is also a small, discontinuous vein containing epidote. Accessory minerals include a few small crystals of apatite less than 0.05 mm in size and a few small orange grains of a metamict mineral.

Conclusion:

This could be classified either as a feldspathic schist or a weakly foliated hornfels. It has been subjected to at least two episodes of metamorphism and its origin cannot be determined from available evidence. The rock probably originally contained some calcareous material.

Applicant's No.: 2134/037-43B

Location: Middleback 1:100,000

Hand Specimen:
A pale greyish-green, fine-grained rock with a smooth to slightly conchoidal fracture similar to that in sample 43A and it also shows a similar very weak foliation. A freshly cut surface shows variations in colour and these are related to the presence of small, cross-cutting veins.

Thin Section:
As the composition varies in different zones an overall estimate would have little meaning.

Some zones are composed almost entirely of quartz and epidote in approximately equal proportions, with trace amounts of sphene, and other zones contain similar amounts of quartz with only 15-20% of epidote and the remainder is turbid, altered and sericitized feldspar.

In the epidote-rich zone the rock consists of elongated aggregates of quartz generally between about 0.2 and 0.4 mm in size intergrown with generally elongate crystals and aggregates of epidote and there are scattered crystals of pale, orange to brown sphene 0.1-0.2 mm in size. The texture of the quartz is similar to that in sample RS 78 (43A) but it is rather more abundant and clearly the elongate aggregates represent former grains which have been drawn out in the direction of weak foliation. The epidote crystals and aggregates show patchy turbidity and this is interpreted as indicating that the epidote has crystallized across pre-existing minerals but there are no clearly defined relict textures marked by this turbidity and therefore the identity of the former minerals cannot be determined. Some aggregates of epidote contain traces of chlorite, some contain small crystals of sphene and some have small, dark-stained zones. There are small, cross-cutting veins which contain concentrations of epidote and one of these forms a boundary between epidote-rich rock and a zone containing a much lower concentration of epidote.

In the zone containing a lower concentration of epidote the texture of the rock is very similar to that in the epidote-rich zone but the elongated grains or aggregates of quartz are intergrown with grains and aggregates of very turbid, partly sericitized, altered feldspar and there are scattered crystals and aggregates of epidote which appear to have partly replaced some of the feldspar. Traces of chlorite are associated with some of the epidote and crystals of sphene are similar to those in the zone containing a high concentration of epidote. In the area sectioned this zone contains a few larger aggregates of epidote 1-2 mm in size and most of these contain a few crystals of sphene. One of these larger aggregates of epidote contains minor chlorite and has faintly preserved relict textures suggesting that the epidote may have replaced a moderately large crystal of ?amphibole or ?pyroxene.

Conclusion:
Quartzo-feldspathic schist or gneiss which has been extensively replaced by epidote, particularly in some zones. It is probably related to sample 6331 RS 78 (43A).

R 1783

Sample: 6331 RS 81; TS42865

Applicant's No.: 2134/037-44

Location: Middleback 1:100,000

Hand Specimen:

A greyish-pink, moderately fine-grained rock with a distinct foliation. A freshly cut surface shows some slight variations in colour (disregarding that due to weathering) and these could indicate some compositional layering parallel to the foliation but there are no great variations in composition.

Staining with cobaltinitrite shows moderately abundant potash feldspar.

Thin Section:

Mineral assemblage:

	I
Potash feldspar	35-40
Plagioclase	30-35
Quartz	25-30
Amphibole	5-10
Sphene	1-2
Opaque oxide	Trace-1
Apatite	Trace

This is a medium-grained metamorphic rock which has been subjected to tectonic stress after the main episode of recrystallization. It contains crystals of potash feldspar and plagioclase 0.4-0.8 mm in size with a few up to 1 mm and these were very probably intergrown with quartz of similar grain size but most of the recent tectonic stress has been taken up by the quartz which has been strained, granulated and drawn out in the direction of foliation. Some of the potash feldspar crystals show undulose or strain extinction and patchy twinning (typical of microcline) indicating tectonic stress but, in general the plagioclase shows very little evidence of deformation. Ragged crystals and aggregates of dark green to yellowish-green amphibole similar to that in sample 6331 RS 78 (43A) occur throughout the rock and there is no apparent variation in concentration of this amphibole although, in places, there are some larger, elongate aggregates. Crystals of sphene are intergrown with some of the aggregates of amphibole and are also scattered throughout the rock. There are some elongate aggregates of opaque oxide up to 1 mm long which occur in interstices and along grain boundaries and some of this is intergrown with amphibole and with sphene. One zone or band in the thin section contains a higher concentration of this opaque oxide. There are a few small apatite grains generally included within or intergrown with amphibole and opaque oxide.

Conclusion:

Fine-grained, quartz-feldspar-amphibole gneiss which is similar to, and probably related to, sample 6331 RS 78 (43A) but it has a higher concentration of amphibole and a stronger foliation. There is no conclusive proof of origin but, as there is a faint suggestion of compositional layering, a metasediment is more likely than an igneous rock.

Sample: 6331 RS 82; TS42866

Applicant's No.: 2134/035-5A

Location: Middleback 1:100,000

Hand Specimen:

A greyish-pink, moderately fine-grained gneiss very similar in general appearance to sample 6331 RS 81 except that there are a few dark spots or aggregates of dark-coloured amphibole 1-3 mm in size. Staining with cobaltinitrite shows moderately abundant potash feldspar.

Thin Section:

Mineral assemblage:

	%
Potash feldspar	35-40
Quartz	20-25
Amphibole	20-25
Plagioclase	15-20
Sphene	2-3
Iron oxide	1-2
Apatite	Trace
Metamict mineral	Minute Trace

This is composed of intergrown feldspar and quartz with a common grain size of 0.3-0.6 mm and although some of the quartz has re-crystallized to finer-grained aggregates elongated parallel to the foliation this is not as conspicuous as in sample 6331 RS 81. There are a few crystals or remnants of coarser-grained feldspar up to 1 mm long and one larger plagioclase crystal 1.5 mm in size has been fractured and bent.

Dark bluish-green to brownish-green hornblende is present in higher concentrations than in the previous sample and there are a few larger, poikilitic crystals up to 1 mm in size containing inclusions of quartz and sphene. Traces of epidote are associated with some of the amphibole but there is very little of this in the area sectioned.

Sphene is very similar to that in the previous sample but is present in slightly higher concentrations and there are also a few small crystals of apatite generally less than 0.1 mm in size but there are a few larger grains up to 0.5 mm. Opaque iron oxide is also present in slightly higher concentrations than in the previous sample and this occurs as irregularly shaped crystals and aggregates up to 0.8 mm in size generally, but not invariably, associated with hornblende. Some is associated with sphene.

There are no obvious variations in composition in the area sectioned but the hand specimen shows a few thin, paler-coloured bands; however, this is no sufficient to suggest sedimentary layering. In the area sectioned there is one coarser-grained aggregate of hornblende and quartz 4 mm in size but whether or not this is the result of some local hydrothermal activity is uncertain.

Conclusion:

Quartz-feldspar-amphibole gneiss containing a higher concentration of amphibole than sample 6331 RS 81. It also has slightly more sphene, apatite and iron oxide.

Sample: 6331 RS 85; TS42869

Applicant's No.: 2134/035-!1

Location: Middelback 1:100,000

Hand Specimen:

A pale salmon-pink, moderately fine-grained gneiss with some diffuse banding suggested by variations in colour. The rock tends to split along some planes parallel to this banding.

Staining with cobaltinitrite shows a moderate amount of potash feldspar.

Thin Section:

Mineral assemblage:

	I
Quartz	55-60
Potash feldspar	20-25
Plagioclase	15-20
Iron oxide	1-2
Muscovite	1-2
Biotite	1-2
Apatite	Trace
Zircon	Trace

A medium-grained metamorphic rock containing feldspar crystals 0.5-1 mm in size, and textures suggest that these were once intergrown with quartz of similar grain size, but most of the quartz has been granulated and drawn out to form elongate aggregates parallel to the foliation. The few remaining quartz grains which are of similar size to the feldspar grains show evidence of strain between crossed nicols and in this respect the texture is similar to that in most of the other samples of gneiss. There are a few muscovite and partly altered biotite flakes generally parallel to the foliation and there are small, irregularly shaped iron oxide grains averaging 0.1 mm in size which are present mainly in interstices. Other accessory minerals include small grains of zircon averaging 0.05 mm in size and some of these appear very well rounded. There are also a few grains of apatite 0.05-0.1 mm long. Most of the plagioclase has been partly altered to sericite but the potash feldspar (including some microcline) is relatively fresh.

Conclusion:

Quartz-feldspar gneiss containing a higher proportion of quartz than the previous samples. It is probably a metasediment.

Sample: 6331 RS 86; TS42870

Applicant's No.: 2134/ S-118

Location: Middleback 1:100,000

Hand Specimen:

A moderately fine-grained, grey gneiss with a few pale pink bands 2-5 mm thick. Staining with cobaltinitrite shows moderately abundant potash feldspar and there are concentrations of potash feldspar in at least some of the pink bands.

Thin Section:

Mineral assemblage:

	%
Quartz	50-55
Potash feldspar (microcline)	25-30
Plagioclase	15-20
Biotite	2-3
Iron oxide	Trace-1
Zircon	Trace
Muscovite	Trace

This is very similar to sample RS 85 and it differs mainly in that there is a slightly higher proportion of biotite flakes, most of which are parallel to the foliation. Quartz and feldspar once had a common grain size of 0.5-1 mm but, as in the other specimens, most of the quartz has recrystallized to finer-grained aggregates which tend to be elongated in the direction of foliation. There are a few small patches of very fine myrmekitic intergrowths between some plagioclase and potash feldspar crystals and also invading some potash feldspar, indicating some reaction along grain boundaries, but these are not very conspicuous.

Accessory minerals include small grains of opaque iron oxide 0.1-0.3 mm long, most of which are parallel to the foliation, and a few very small grains of zircon generally less than 0.05 mm in size. There are also a few very small grains now composed of a very fine-grained mineral with high refractive index and birefringence which may be a jarosite mineral but there is insufficient of this for it to be positively identified. The presence of jarosite would suggest that the rock may once have contained a little pyrite.

Compositional layering noted in the hand specimen is not apparent in the thin section.

Conclusion:

Quartz-feldspar-biotite gneiss similar to sample 6331 RS 85, but it contains a slightly higher proportion of biotite.

Sample: 6331 RS 97; TS42881

Applicant's No.: 2086/065-13

Location: Middleback 1:100,000

Hand Specimen:

A salmon-pink to slightly greyish-pink, predominantly fine-grained rock with a few diffuse and/or poorly defined dark streaks or layers 2-3 mm thick.

Staining with cobaltinitrite shows abundant potash feldspar, most of it very fine-grained, but there are some scattered patches and aggregates which are slightly coarser-grained. The staining also shows up a few parallel, very thin layers which contain plagioclase.

Thin Section:

Mineral assemblage:

	%
Potash feldspar	50-55
Quartz	30-35
Plagioclase	3-5
Opaque iron oxide	3-5
Hornblende	2-3
Sphene	Trace-1
Apatite	Trace
Carbonate	Trace

Much of the rock consists of intergrown, fine-grained orthoclase and quartz with a common grain size of 0.05-0.2 mm, and these fine-grained zones also contain numerous small iron oxide crystals generally less than 0.05 mm in size and a few very small crystals of sphene and dark green hornblende. Some of the hornblende forms very thin streaks or elongate aggregates less than 0.05 mm thick and up to 1.5 mm long. There are some lenticular patches and bands containing coarser-grained potash feldspar with a few crystals 1-1.5 mm in size which could be remnants of once more abundant, coarser-grained rock, as these do not appear to be porphyroblasts.

In the area sectioned there are a few thin layers 0.5-1 mm thick which contain concentrations of partly sericitized plagioclase intergrown with quartz, iron oxide, hornblende and sphene, and these contain little or no potash feldspar. In general, they tend to be slightly coarser-grained than most of the rock and locally have hornblende and opaque oxide crystals up to 0.5 mm in size. Sphene and quartz are also coarser-grained in some of these plagioclase-bearing bands.

The rock contains a few small crystals of apatite generally less than 0.1 mm in size and there are a few interstitial patches of secondary carbonate in some of the coarser-grained zones.

Conclusion:

Quartz-feldspar-hornblende gneiss with some very poorly defined layering.

PETROGRAPHIC DESCRIPTIONS OF SAMPLES FROM EYRE PENINSULA

Sample: 6331 RS 150; TS44321

Hand Specimen:
A medium to pale grey, blastoporphyritic, quartzo-feldspathic schist that displays a gneissose texture defined by some of the coarser-grained potash feldspar crystals whose boundaries have been modified during metamorphism so that they are elongate in one preferred orientation.

Staining of the sample using hydrofluoric acid and sodium cobaltinitrite indicates that the blastophenocrysts and much of the groundmass comprise potash feldspar.

Thin Section:
A visual estimate of the constituents gives the following:

	%
Quartz	30-35
Potash feldspar	40
Plagioclase	5-6
Opaque iron-titanium oxide	10-12
Sphene	3
Epidote	2-3
Hornblende and biotite	1-3
Chlorite	1
Apatite	minute trace
Calcite	2
Dolomite	trace

This rock comprises mainly a slightly lepidoblastic, but almost granoblastic mosaic of quartz and potash feldspar crystals, throughout which some coarser, potash feldspar blastophenocrysts are randomly distributed. Some of the blastophenocrysts appear randomly oriented, but most of the coarser crystals have been modified during metamorphism so that they now comprise composite crystals oriented elongate parallel to the foliation. There are a few plagioclase blastophenocrysts, but the potash feldspar blastophenocrysts are predominate and they average approximately 3 × 1 mm in size, although they are mostly made up of aggregates of crystals which are between 0.05 and 1.5 mm in size. Many of the potash feldspar crystals show partial alteration to clay and carbonate (mainly calcite, but some dolomite is also present) and hornblende. Crystals of opaque oxide which are generally coarser than those distributed throughout the finely crystalline groundmass of the rock are also associated with some of the more-altered feldspar blastophenocrysts and many of these opaques are, in turn, associated with finely crystalline sphene which is an alteration product surrounding the opaque oxides. Epidote is another mineral present which occurs with the hornblende and calcite; and biotite, another alteration product, occurs in association with hornblende and/or the opaque oxide crystals.

The crystals of the groundmass are generally equigranular and mainly 0.01 to 0.03 mm in size. They are mostly anhedral and give a recrystallised, granoblastic texture. As mentioned previously, quartz and feldspar are the dominant minerals of the groundmass, but abundant euhedra and subhedra of opaque oxides and anhedra of epidote are disseminated throughout. The

quartz and feldspar of the groundmass are difficult to distinguish from each other; however, the potash feldspar appears slightly dusty, although it is much less altered than that of the blastophenocrysts.

Conclusion:

This is a hornblende, epidote, quartzo-feldspathic schist that is considered to be a product of metamorphism of an acid volcanic rock as phenocrysts of feldspar remain within the rock.

Sample: 6331 RS 150; TS44322 R12253

Hand Specimen:

A medium to pale grey, blastoporphyritic, quartzo-feldspathic schist that displays a well-defined gneissose texture and segregation banding. It contains relict igneous phenocrysts of potash feldspar which have been modified during metamorphism of the rock so that they are elongate parallel to a foliation in the sample.

The gneissose texture is much better-defined than in sample 6331 RS 150. The potash feldspar was identified by microchemical tests.

Thin Section:

A visual estimate of the constituents gives the following:

	%
Quartz	45-50
Potash feldspar	30-35
Plagioclase	2-4
Opaque oxides	10
Biotite	1-2
Muscovite	1-2
Chlorite	1
Calcite	minute trace
Epidote	trace

This rock comprises thin layers of microcrystalline quartz which alternate with thin layers of mainly finely crystalline, potash feldspar which contain blastophenocrysts of potash feldspar. The segregational banding in this sample is much stricter than that in the previously described sample. The quartz-rich layers comprise mainly anhedral crystals of quartz that average 0.02 mm in size. There are possibly some small crystals of potash feldspar disseminated throughout throughout the quartz-rich layers; however, these are difficult to distinguish. Small anhedral crystals of opaque oxides averaging 0.01 mm in size are disseminated throughout all of the fine-grained layers of the sample. The potash feldspar-rich layers are generally coarser-grained, than the quartz layers and they comprise anhedral crystals of feldspar which range in size from 0.03 up to 1.5 mm. The larger crystals display prominent cleavage, but they are generally much more altered than the finer crystals. The banding in the sample is considered to be an original feature of the acid volcanic rock from which this slightly metamorphosed is derived.

Opaque iron oxides are relatively abundant throughout the sample as they occur in both the coarser-grained and the finer-grained layers. The more coarsely crystalline iron oxides and iron-titanium oxides are generally fairly euhedral, but there are anhedral crystals which are generally associated with micaceous minerals or with minute traces of sphene. The crystals of opaque oxides in the more coarsely crystalline, potash feldspar-rich layers of the sample show a large variation in grain size from minute up to 0.5 mm. The micaceous minerals (muscovite and biotite) associated with the opaques are generally about 0.1 to 0.3 mm in size, although finer crystals are present. Trace epidote and chlorite is associated with the very altered blastophenocrysts of potash feldspar which appear brown in colour because of their abundant inclusions.

Red limonite occurs along many of the boundaries between crystals and in fractures within some of the larger potash feldspar crystals, as well as in association with the opaque oxides and biotite. The biotite generally

appears more red in colour than is usual.

Conclusion:

This is a slightly metamorphosed, banded, potash rhyolite in which opaque oxides are abundant.

R 1263

Sample: 6331 TS 153; TS44324

Hand Specimen:

A banded, pink and grey, finely crystalline meta-acid volcanic rock. Microchemical tests involving staining of the rock with sodium cobaltinitrite indicate that potash feldspar is abundant.

Thin Section:

A visual estimate of the constituents gives the following:

	%
Potash feldspar	40-35
Quartz	35-40
Plagioclase	1-2
Biotite and (?) hornblende	3-5
Opaque and semi-opaque iron oxides	5-10
Sericite	1-2
Epidote	minute trace

This is a holocrystalline, metamorphic rock which displays small-scale segregational banding and comprises mainly fine crystals of potash feldspar and quartz forming a granoblastic mosaic with small flakes of lepidoblastic metamorphic biotite and (?)hornblende in the interstices between the felsic crystals. The obvious banding of the rock is caused by variations in concentrations of opaques and other mafic minerals, quartz and potash feldspar, as well as variations in average crystal sizes from band to band within the sample. The more felsic bands are mainly 1 to 3 mm thick while the more mafic and generally slightly coarser-grained bands are generally only about 0.1 to 0.2 mm thick.

Some of the more coarsely crystalline bands comprise almost entirely equigranular, slightly sericitized, dusty potash feldspar crystals that average 0.1 to 0.15 mm in size. Any quartz crystals in these layers are easily distinguished as they are colourless and free of inclusions, but quartz is generally more abundant in the bands of finely crystalline material, although it is more difficult to distinguish in these layers as the finely crystalline potash feldspar is apparently less-altered than the coarser feldspar. The small crystals of quartz and potash feldspar forming the granoblastic mosaic that makes up most of the bands of the sample are generally equigranular and 0.01 to 0.03 mm in size, while the small biotite flakes occurring in the interstices between the felsic crystals are generally 0.005 to 0.01 mm in size.

There are thin bands in the rock that have high concentrations of brown biotite and perhaps a little hornblende or green biotite, and opaque and semi-opaque iron oxides, and these are generally associated with the bands in which potash feldspar shows the greatest degree of alteration. The biotite flakes in the mafic-rich bands are generally coarser than those occurring interstitially in the felsic-rich layers and the coarser flakes are mainly 0.05 to 0.1 mm in length and 0.02 mm in thickness. Small euhedral crystals of opaque iron oxides averaging 0.01 mm in size are disseminated throughout the sample, but there are also coarser, elongate crystals of iron oxides up to 0.3 mm in length, which are generally more anhedral and associated with semi-opaque limonite and biotite in the mafic-rich bands. Rare crystals of yellow epidote, mainly about 0.05 mm in size are also associated with the mafic-rich bands. Anhedral crystals of relatively fresh plagioclase are present within the sample and generally in association with the slightly

Sample: 6331 RS 155; TS44326

Hand Specimen:
A mauve, slightly metamorphosed, porphyritic, acid volcanic rock. Treatment of the sample with hydrofluoric acid and sodium cobaltinitrite identified the phenocrysts or blastophenocrysts in the volcanic as potash feldspar. The groundmass also contains potash feldspar, but it mainly comprises finely crystalline quartz

The sample is cut by many fine fractures along which some carbonate and mafic minerals have crystallised.

Thin Section:
A visual estimate of the constituents gives the following:

	%
Potash feldspar	40
Quartz	42-45
Plagioclase	2-3
Opaque oxides and limonite	7-8
Sphene	trace
Hornblende and chlorite	3-5
Biotite	2
Calcite	3-5
(?)Dolomite	minute trace
Epidote	minute trace

The sample comprises mainly a groundmass of finely crystalline quartz and potash feldspar, throughout which some blastophenocrysts of potash feldspar and some fine crystals of opaque iron and iron-titanium oxides are disseminated. Fine fractures throughout the sample are lined with anhedral crystals of hornblende, chlorite, calcite, biotite, limonite and opaque oxides.

The quartz and potash feldspar crystals forming the groundmass of the volcanic are equigranular anhedra, mainly 0.02 to 0.06 mm in size, that display a granoblastic texture. The fine crystals of opaque oxides disseminated throughout the groundmass are subhedral to anhedral and mainly 0.01 to 0.05 mm in size.

The blastophenocrysts make up about 15 to 20% of the rock and they average about 0.4 to 0.5 mm in size, although their original size is difficult to estimate as they now comprise aggregates of feldspar crystals which are only slightly larger than those of the groundmass, and their boundaries are fairly indistinct. It is the more extensive weathering of most of the blastophenocrysts that distinguishes them most easily from the rest of the sample. There are rare blastophenocrysts of quartz and plagioclase which are distinguished because of their lack of alteration and their multiple twinning respectively. The potash feldspar phenocrysts are generally associated with opaque oxides, chlorite, hornblende, calcite and biotite all of which are similar to those found within the fine fractures in the sample, although the opaque oxides associated with the potash feldspar are generally more coarsely crystalline and may be up to 0.3 mm in size. Most of the opaque oxides are associated with red limonite, although there are some which are surrounded by finely crystalline brownish-coloured, sphene anhedra. The crystals of ferromagnesian minerals throughout the sample are all extremely anhedral and their shape is governed by the crystals of quartz and feldspar

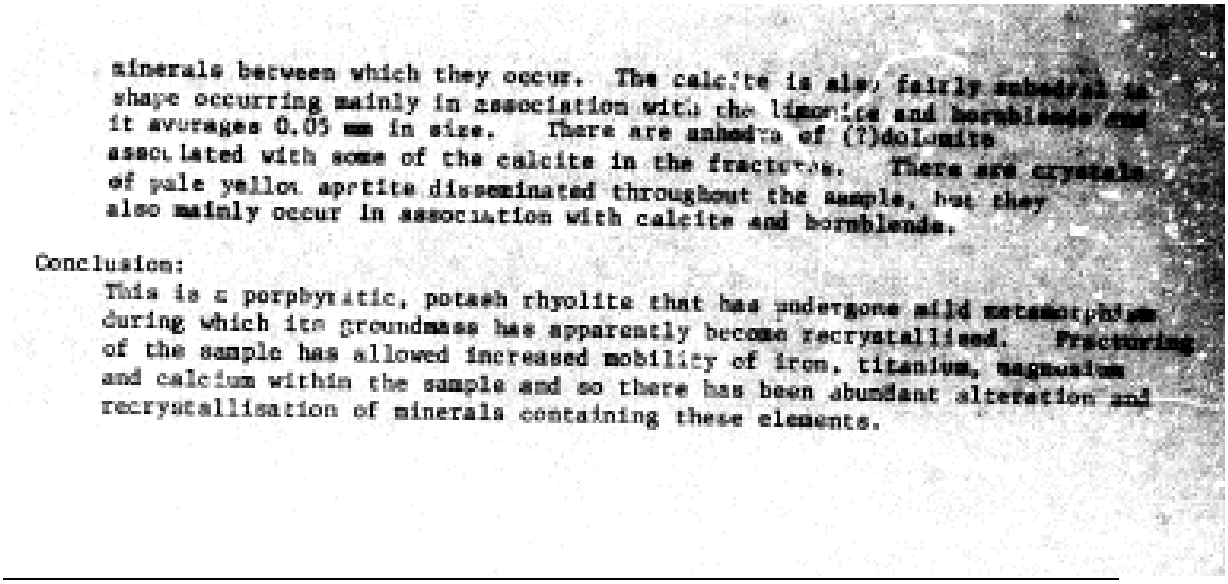

minerals between which they occur. The calcite is also fairly anhedral in shape occurring mainly in association with the limonite and hornblende and it averages 0.05 mm in size. There are anhedra of (?)dolomite associated with some of the calcite in the fractures. There are crystals of pale yellow apatite disseminated throughout the sample, but they also mainly occur in association with calcite and hornblende.

Conclusion:

This is a porphyritic, potash rhyolite that has undergone mild metamorphism during which its groundmass has apparently become recrystallised. Fracturing of the sample has allowed increased mobility of iron, titanium, magnesium and calcium within the sample and so there has been abundant alteration and recrystallisation of minerals containing these elements.

Sample: 6331 RS 156; TS44327

Hand Specimen:

A medium-crystalline, holocrystalline, metamorphic rock in which a foliation is defined by segregated layers of preferentially oriented hornblende and feldspar crystals.

Thin Section:

A visual estimate of the constituents gives the following:

	%
Amphibole (hornblende or riebeckite)	50-55
Plagioclase	30
Potash feldspar	5
Quartz	2-3
Sphene	5-10
Opaque oxides + limonite	trace
Biotite	minute trace
Calcite	minute trace
Apatite	minute trace

This holocrystalline, medium-crystalline, metamorphic rock comprises predominantly green/blue-green/yellow, pleochroic amphibole which may be riebeckite or blue-green hornblende. Most of the amphibole crystals are oriented so that they are elongate parallel to a foliation defined by segregational banding of amphibole and feldspar minerals; however, there are some basal sections of amphibole visible. The amphibole crystals are mainly 0.5 to 2 mm in size, although there are rare finer crystals within some of the feldspar layers. Most of the amphibole crystals are xenoblastic; however, there are some idioblastic crystals also present.

Most of the feldspar in the sample occurs in thin layers and lenses between bands of amphibole. Most of the feldspar is considered to be plagioclase as there are some fairly fresh crystals which display a characteristic multiple twinning; however, most of the feldspar is extensively altered to clay and sericite and so its original identity is difficult to determine. Microchemical tests carried out on the hand specimen showed that only a very small amount of the feldspar was potassic and this also supports an identification of plagioclase. The crystals of plagioclase, including the fresher ones, are all anhedral in shape and mainly 0.1 to 0.3 mm in size.

Sphene in the sample generally occurs in association with amphibole crystals, although there are some sphene crystals within the layers of plagioclase. The crystals of sphene are mainly 0.05 to 0.2 mm in size and they mainly occur in aggregates up to 1 mm in length. The sphene in association with amphibole is generally more euhedral in shape (showing characteristic diamond-shaped sections), than the anhedral crystals found within the feldspar laths. There is a small amount of epidote within the sample which is easily distinguished from the more brownish sphene because of its pale yellow colour and its lower relief. The epidote is mostly associated with feldspar and occurs in single crystals averaging 0.1 mm in size. There are some smaller, elongate crystals of apatite also associated with the plagioclase and these average about 0.07 mm in size.

A minute trace of calcite occurring as minute, anhedral crystals averaging

0.01 mm in size, occur in association with amphibole. There are also a small number of opaque oxides and some concentrations of limonite associated with the amphibole. Many of the opaques are surrounded by small crystals of sphene. Limonite generally occurs in thin fractures throughout the sample and it is more abundant than any opaque oxides.

Apart from the very thin fractures lined by films of limonite, the sample is cut by some pegmatitic veins averaging 0.15 mm in thickness, that are filled with finely crystalline quartz and plagioclase crystals which are equigranular and average 0.1 mm in size.

Conclusion:

This is an amphibolite or a glaucophane schist which was probably derived from metamorphism of an intrusive, basic igneous rock.